Res Electricae Magdeburgenses

MAgdeburger FOrum zur Elektrotechnik

Muhammad Tayyab

Holistic approach for microgrid planning and operation for e-mobility infrastructure under consideration of multi-type uncertainties

Integrating renewable energy sources in sectors such as electricity, heat, and transportation must be structured in an economic, technological, and emission-efficient manner to address global environmental issues. Microgrids appear to be the solution for large-scale renewable energy integration in these sectors. The microgrid components must be optimally planned and operated to prevent high costs, technical issues, and emissions. Existing approaches for optimal microgrid planning and operation in the literature do not include a solution for e-mobility infrastructure. As a consequence, a compact e-mobility infrastructure methodology is provided. The development of e-mobility infrastructure has associated uncertainties (short and long-term). As a result, a new stochastic method referred to as IGDM-DRO is proposed in this dissertation. The proposed method provides a risk-averse strategy for microgrid planning and operation by including long-term and short-term uncertainty related to e-mobility. The multi-cut bender decomposition is applied for IGDM-DRO to prevent the suggested method's intractability. Finally, the deterministic and stochastic methodologies are combined in a novel holistic approach for microgrid design and operation in terms of cost and robustness. The proposed method is tested on a new settlement area in Magdeburg, Germany, under three different EV development scenarios (negative, trend, and positive). The share for the number of electric vehicles reached 31 percent of conventional vehicles by the end of the planned horizon. As a result, the microgrid's overall cost has been increased by 2.3 to 2.9 percent per electric vehicle. Three public electric vehicle charging stations will be required in the investigated settlement area in trend 2031. The investigated settlement area will require a total cost of 127,029 € in the trend scenario. To achieve full robustness against long-term uncertainties, the cost of the microgrid needs to be increased by 80 percent.

ISSN 1612-2526
ISBN 978-3-948749-25-5
DOI 10.24352/UB.OVGU–2022-084

Muhammad Tayyab: Ph.D. Dissertation

MAFO 92

Magdeburg 2022

MAFO
Band 92

Res Electricae Magdeburgenses

Magdeburger **Fo**rum zur Elektrotechnik

Muhammad Tayyab

Holistic approach for microgrid planning and operation for e-mobility infrastructure under consideration of multi-type uncertainties

Otto-von-Guericke-Universität Magdeburg
Magdeburg 2022

Res Electricae Magdeburgenses

Magdeburger Forum zur Elektrotechnik, Jg. 2022, Band 92, 2022

www.mafo.ovgu.de

Impressum

Herausgeber:

- Prof. Dr.-Ing. Andreas Lindemann, Lehrstuhl für Leistungselektronik, Institut für Elektrische Energiesysteme
- Prof. Dr.-Ing. habil. Martin Wolter, Lehrstuhl für Elektrische Netze und Erneuerbare Energie, Institut für Elektrische Energiesysteme
- Prof. Dr. rer. nat. Georg Rose, Lehrstuhl für Medizinische Telematik/Medizintechnik, Institut für Medizintechnik
- Prof. Dr.-Ing. Ralf Vick, Lehrstuhl für Elektromagnetische Verträglichkeit, Institut für Medizintechnik

Gründungsherausgeber:

- Prof. Dr. rer. nat. habil. Jürgen Nitsch
- Prof. Dr.-Ing. habil. Zbigniew Antoni Styczynski

alle: Otto-von-Guericke-Universität Magdeburg

V.i.S.d.P.:

Muhammad Tayyab
Otto-von-Guericke-Universität, Institut für Elektrische Energiesysteme, Universitätsplatz 2, 39106 Magdeburg

1. Auflage, Magdeburg, Otto-von-Guericke-Universität, 2022
Zugl.: Magdeburg, Univ., Diss., 2022

Auflage: 30

Redaktionsschluss: 2022

ISSN: 1612-2526
ISBN: 978-3-948749-25-5

DOI: 10.24352/UB.OVGU-2022-084

Bezug über die Herausgeber

Druck: docupoint GmbH Otto-von-Guericke-Allee 14, 39179 Barleben

Holistic approach for microgrid planning and operation for e-mobility infrastructure under consideration of multi-type uncertainties

Dissertation

zur Erlangung des akademischen Grades

Doktoringenieur

(Dr.-Ing.)

von M. Sc. Tayyab, Muhammad
geb. am 04.04.1987 in Kech

genehmigt durch die Fakultät für Elektrotechnik und Informationstechnik
der Otto-von-Guericke-Universität Magdeburg

Gutachter: Jun.-Prof. Dr.-Ing. Ines Hauer
Prof. Dr.-Ing. habil. Martin Wolter
Prof. Dr. Luciane Neves Canha

Promotionskolloquium am 31. August 2022

Acknowledgment

This dissertation is the outcome of extensive and time-consuming work done in the chair of Electric Power Networks and Renewable Energy at Otto von Guericke University in Magdeburg, Germany. Many people supported me during this time, to whom i am incredibly grateful.

I would like to thank Prof. Dr.-ing. Ines Hauer, who give me the opportunity to work under her supervision and availability to assist on the hardest time of this journey. The incredible support received from her was the cause that motivated me to finish what has been started. I also appreciated the freedom in the working environment and the backing in research directions and ideas.

I am especially grateful to Prof. Dr.-Ing. habil. Martin Wolter for welcoming and supporting me in the chair. Furthermore, i am greatfull to him for his interest in this topic and willingness to review and examine my dissertation. I am grateful to Prof. Dr. Luciane Neves Canha from the Federal University of Santa Maria brazil for her time and efforts as the third examiner.

I am thankful to Sebastian Helm for his support in research direction and organizational matters. Without him, the finished dissertation would have hardly been possible. Special thanks to all of my current and former colleagues of the chair for the friendly working environment and diversity. Due to them, i was never short of advice. Finally, I am also grateful to Jonte Dancker and Leonardo Nogueira Fontoura Silva for helping with my research questions and proofing respectively.

I would like to dedicate this work to my family who inspired me always. It is quite an honor to come from an underdeveloped area, lacking basic education, and have a doctorate from a well-reputed university in Germany. For this, i am grateful to DAAD Germany and HEC pakistan collaborative funding programs.

Magdeburg, August 31, 2022 Muhammad Tayyab

Abstract

Integrating renewable energy sources in sectors such as electricity, heat, and transportation must be structured in an economic, technological, and emission-efficient manner to address global environmental issues. Microgrids appear to be the solution for large-scale renewable energy integration in these sectors. The microgrid components must be optimally planned and operated to prevent high costs, technical issues, and emissions. Existing approaches for optimal microgrid planning and operation in the literature do not include a solution for e-mobility infrastructure. As a consequence, a compact e-mobility infrastructure methodology is provided. A retropolation approach for planning the rise in the number of electric vehicles, Monte-Carlo simulation for EV-behaviors, electric vehicle charging station (EVCS) numbers based on occupancy time, and public EVCS placement based on Monte-Carlo simulation are all included in the proposed method. Distributed energy resources and e-mobility infrastructure cause technical concerns in microgrid planning and operation, such as voltage issues. The above-mentioned methods and technical issues are used to develop a deterministic approach for microgrid planning and operation for e-mobility infrastructure. Flat and flexible tariffs are used to evaluate deterministic microgrid planning and operation. Furthermore, the development of e-mobility infrastructure has associated uncertainties (short and long-term). As a result, a new stochastic method referred to as IGDM-DRO is proposed in this dissertation. The proposed method provides a risk-averse strategy for microgrid planning and operation by including long-term and short-term uncertainty related to e-mobility. The multi-cut bender decomposition is applied for IGDM-DRO to prevent the suggested method's intractability. Finally, the deterministic and stochastic methodologies are combined in a novel holistic approach for microgrid design and operation in terms of cost and robustness.

The proposed method is tested on a new settlement area in Magdeburg, Germany, under three different EV development scenarios (negative, trend, and positive). The share for the number of electric vehicles reached 31 percent of conventional vehicles by the end of the planned horizon. As a result, the microgrid's overall cost has been increased by 2.3 to 2.9 percent per electric vehicle. Three public electric vehicle charging stations will be required in the investigated settlement area in trend 2031. The investigated settlement area will require a total cost of 127,029 € in the trend scenario. To achieve full robustness against long-term uncertainties, the cost of the microgrid needs to be increased by 80 percent. If the confidence level is reduced to 96 percent by including short-term uncertainty, the robustness of around 60 percent will be obtained. With the robustness of the allowable budget of 80 percent and confidence level of 96 percent, 66.7 percent of the cost has been increased as compared deterministic approach in the trend scenario in 2031.

Kurzfassung

Die Integration erneuerbarer Energiequellen in Sektoren wie Strom, Wärme und Verkehr muss auf wirtschaftliche, technologische und emissionsarme Weise strukturiert werden, um globale Umweltprobleme anzugehen. Micro Grids scheinen die Lösung für eine groß angelegte Integration erneuerbarer Energien in diesen Sektoren zu sein. Die Microgrid-Komponenten müssen optimal geplant und betrieben werden, um hohe Kosten, technische Probleme und Emissionen zu vermeiden. Bestehende Ansätze für optimale Planung und Betrieb in der Literatur beinhalten keine Lösung für E-Mobilitätsinfrastrukturen. Daher wird eine kompakte E-Mobilitätsinfrastruktur-Methodik vorgestellt. Die vorgeschlagene Methode umfasst einen Retropolationsansatz für die Planung der stetig steigenden Anzahl von Elektrofahrzeugen, eine Monte-Carlo-Simulation für das Verhalten von Elektrofahrzeugen, die Anzahl von öffentlicher Ladeinfrastrukture auf basis der Belegungszeit und die Platzierung öffentlicher Ladeinfrastrukture auf der Grundlage einer Monte-Carlo-Simulation. Dezentrale Erzeugungsanlagen und E-Mobilitätsinfrastruktur verursachen technische Probleme bei der Planung und dem Betrieb von Micro Grids, wie z.B. Spannungsprobleme. Die oben genannten technischen Methoden und Parameter werden verwendet, um einen deterministischen Ansatz für die Planung und den Betrieb von Micro Grids für E-Mobilitätsinfrastruktur zu entwickeln. Fest und flexible Tarife werden verwendet, um die deterministische Mikronetzplanung und den Betrieb zu bewerten. Darüber hinaus ist die Entwicklung der E-Mobilitätsinfrastruktur mit Unsicherheiten (kurz- und langfristig) behaftet. Aus diesem Grund wird in dieser Dissertation eine neue stochastische Methode namens IGDM-DRO vorgeschlagen. Die vorgeschlagene Methode bietet eine risikoaverse Strategie für die Planung und den Betrieb von Micro Grids, indem sie langfristige und kurzfristige Unsicherheiten im Zusammenhang mit der E-Mobilität berücksichtigt. Die Multi-Cut-Bender-Zerlegung wird für IGDM-DRO angewandt, um die Unlösbarkeit der vorgeschlagenen Methode zu verhindern. Schließlich werden die deterministischen und stochastischen Methoden in einem neuartigen ganzheitlichen Ansatz für die Planung und den Betrieb von Micro Grids in Bezug auf Kosten und Robustheit kombiniert.

Die vorgeschlagene Methode wird in einem neuen Siedlungsgebiet in Magdeburg, Deutschland, unter drei verschiedenen EV-Entwicklungsszenarien (negativ, Trend und positiv) getestet. Die Anzahl der Elektrofahrzeuge erreichte bis zum Ende des Planungshorizonts 31 % der konventionellen Fahrzeuge. Infolgedessen sind die Gesamtkosten des Micro Grids um 2,3 bis 2,9 Prozent pro Elektrofahrzeug gestiegen. Im Trend 2031 werden im untersuchten Siedlungsgebiet drei öffentliche Ladeinfrastrukture für Elektrofahrzeuge benötigt.

Für das untersuchte Siedlungsgebiet werden im Trendszenario Gesamtkosten von 127.029 € berechnet. Um die volle Robustheit gegenüber langfristigen Unsicherheiten zu erreichen, müssen die Kosten für das Microgrid um 80 Prozent erhöht werden. Wird das Konfidenzniveau durch Einbeziehung der kurzfristigen Unsicherheit auf 96 % gesenkt, ergibt sich eine Robustheit von etwa 60 %. Bei einer Robustheit des zulässigen Budgets von 80 % und einem Konfidenzniveau von 96 % sind die Kosten um 66,7 % im Vergleich zum deterministischen Ansatz im Trendszenario 2031 erhöht.

Table of Contents

1 Introduction

The integration of renewable energy sources in the heat, electricity, gas, and mobility sectors has huge potential for reducing greenhouse gases (GHG). The smooth energy transition needs the interconnection between these sectors using sector coupling technologies such as heat pumps, electrolyzers, and fuel cells. Due to the coupling of these sectors, technologies such as heat pumps will increase renewable energy sources by converting electrical energy into heat energy. Furthermore, the production from renewable energy sources can be stored in the form of heat in a thermal energy storage system to be used later. The GHG emissions by different sectors in Germany are shown in Figure 1.1.

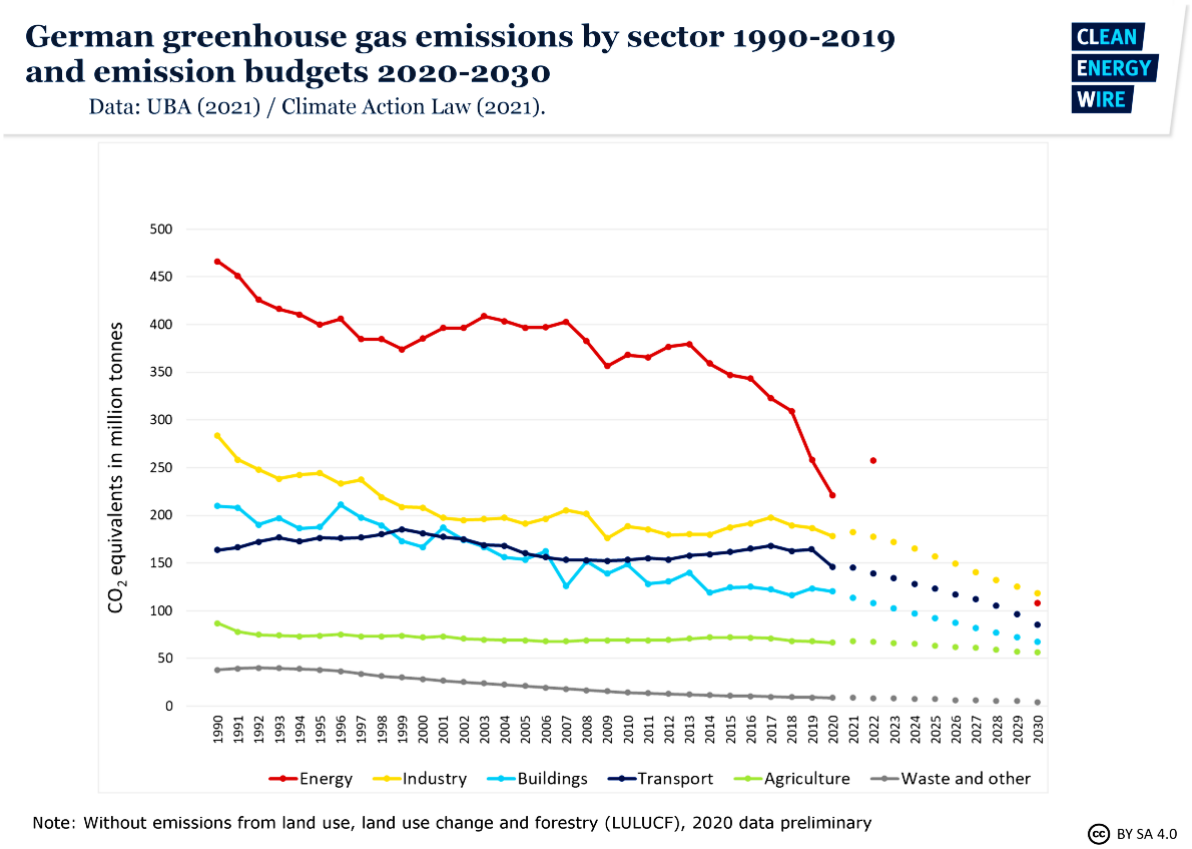

Figure 1.1 German greenhouse gas emissions by sector [1]

Germany aims to be an emission-free country by 2045 [1]. GHG reductions are targeted to be reduced by at least 65 percent by 2030 and 88 percent by 2040 compared to 1990 levels [2]. To achieve these targets, renewable energy sources must replace fossil fuels in all sectors. The transformation of electrical energy into heat and fuel is termed Power to X. As the need for fuel in all sectors is enormous, an immense installation and production of renewable energy sources will be necessary. As a result, traditional grids will comprise a diverse range of renewable energy sources (RES).

Consequently, the operation of these grids will be changed [3]. With the change in operation, many challenges arise from the perspective of grid operators, end-user, and markets. The challenges include system stability, planning, control, reliability, and sustainability. Due to stability issues, e.g. congestion and voltage problems, the integration of RES is limited. The local use of the produced renewable energy is one way to avoid some stability problems. Due to this, the conventional grid will be transformed from traditional centralized grids into a distributed system.

The concept of distributed grids can be effective in cost and technical constraints [4]. Some of these distributed grids can be designed and emerge as microgrids. The microgrid's purpose is to offer public and private consumers electricity and heat that is reliable, economical, and clean, with a high proportion of renewable energy sources. A microgrid is assumed to be a single structural entity operated with interconnected generation, storage, and load, as shown in Figure 1.2 [5]. Microgrids have been the focus of attention in the energy sector over the past decade as a crucial component of the future smart grid. A microgrid consists of renewable energy resources, energy storage systems, and controllable and uncontrollable loads. It can be either operated in grid-connected mode or islanded mode. Furthermore, AC and DC microgrids are also quantified in the field of research [6].

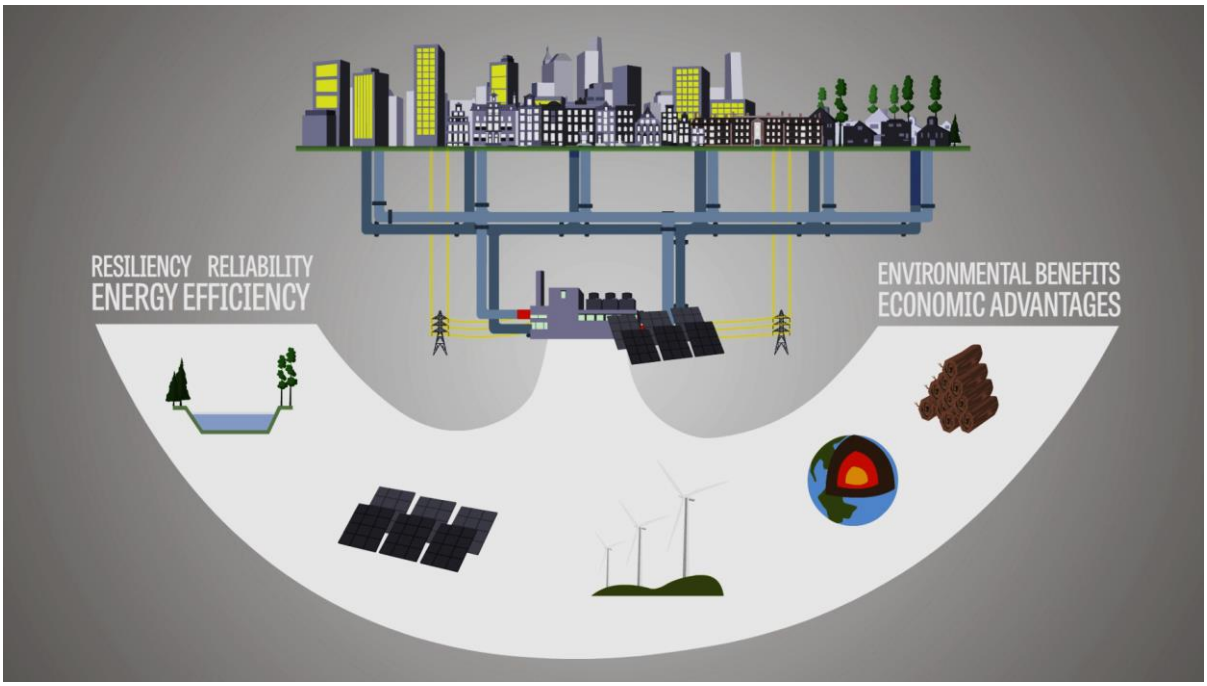

Figure 1.2 Microgrid structure [5]

The microgrid's load might be of several types, such as residential, commercial, industrial, or mixed load. Similarly, the generation consists of combined heat and power (CHP), backup generators, and renewable energy sources such as photovoltaic (PV) and wind power.

Different types of energy storage can also be integrated into microgrids for numerous advantages. For instance, electrical energy storage systems (EESS), thermal energy storage (TESS), and hydrogen energy storage systems (HESS) can participate in load balancing and other services such as peak shaving demand response and ancillary services. The goal of the microgrid should be the large-scale integration of renewable energy sources. If the integration is unplanned, the grid's secure and safe functioning will be jeopardized. This is caused by the intermittent nature of renewable energy sources. Due to this, the improvement in the integration of RES in the microgrid got hype in the field of research. Apart from the electrical supply system, the heat supply and the gas system can also be part of the microgrid at a community level. These types of microgrids are often called multi-energy microgrids [7].

1.1 Motivation and goal

The primary GHG emissions in the transport sector are caused by internal combustion engines (ICE). The use of ICE facilitates the carbon dioxide emissions that cause global warming and the depletion of fossil fuels. To mitigate the emissions frm the transport sector, electric vehicles, replacing the ICEs, have been the technology that provides economic and environmental benefits by integrating the transport and energy sector. At the same time, there are calls for a license ban for combustion engines from 2030. In the long-term, these will be replaced by lower-emission or zero-emission vehicles, such as hybrid and electric vehicles or fuel cell vehicles [8]. Even if the number of the electric vehicle increased as per requirements, the high amount of use for these electric vehicles is still hampered by the acquisition costs, the range, and, in particular, the lack of charging infrastructure. A high amount of electric vehicles require a significant quantity of charging energy. For that reason, a substantial proportion of renewable energy sources have to be used to power the e-mobility infrastructure. To secure their local renewable supply, electrical vehicles (EV) and electric vehicle charging stations (EVCS) must be forecasted, and the amount for renewable power supply should be planned.

The low-voltage grid usually powers the EVCS and EV. Furthermore, installed renewables such as PV are mostly integrated into the middle and low voltage grid [9]. However, the existing power grid will not always be able to handle the additional power and adverse impacts due to the large-scale deployment. A microgrid can be a solution for integrating a high amount of renewables and e-mobility infrastructure in a low-voltage grid. Nevertheless, the components need to be optimally planned to avoid high costs, technical problems, and high emissions. Motivated by the alternatives to power the sustainable e-mobility infrastructure alongside other demands, optimal microgrid planning and operation are needed.

The best planning and operation can be realized for a new settlement area where sustainable energy and power supply may be developed for a green, efficient, and smart infrastructure-based community. However, the statistic (number of people, house, house types, etc.), generation, and consumption need to be planned based on ground realities from scratch. As a result, complex analytical and numerical solutions are required in order to ensure well-handled decision-making for the new settlement area.

A microgrid's decision-making must be planned for the future, considering affecting variables. Furthermore, the investment in the microgrid needs to be backed up by confidence in smooth and secure operation. An overestimated microgrid is a waste of money, whereas underestimated one has issues such as a high amount of energy imported from the conventional grid. Optimization algorithms solve these problems with optimal planning and optimal operation of the microgrid. Uncertain or unavailable data that are needed to estimate the future effect of microgrids for decision-making are the major hurdles in efficient microgrid planning and operation. Significantly, the development of e-mobility infrastructure has been fraught with short and long-term uncertainties in nature. The following points address the risks associated with the e-mobility infrastructure:

- Short-term uncertainty: The arrival of electric vehicles for charging is unpredictable. As a result, reliable forecasting is impossible.
- Long-term uncertainty: The increase in the number of EVCS is influenced by direct and indirect factors. Some of the determining elements are listed below.
    - Direct factor
        - The rise in the number of EV
    - Indirect factors
        - Development of EV battery technology
        - Development of charging point technology
        - Developments in the government regulation
        - Development of public infrastructure
        - Announcements of electric vehicle subsidies
        - Political infrastructure goals
        - Development of other alternative transport technologies, such as synthetic fuels and fuel cell vehicles

Due to these factors, microgrid planning and operation need to consider multi-type uncertainties regarding e-mobility infrastructure. Figure 1.3 shows different rise rates for the number of EVCS in Germany.

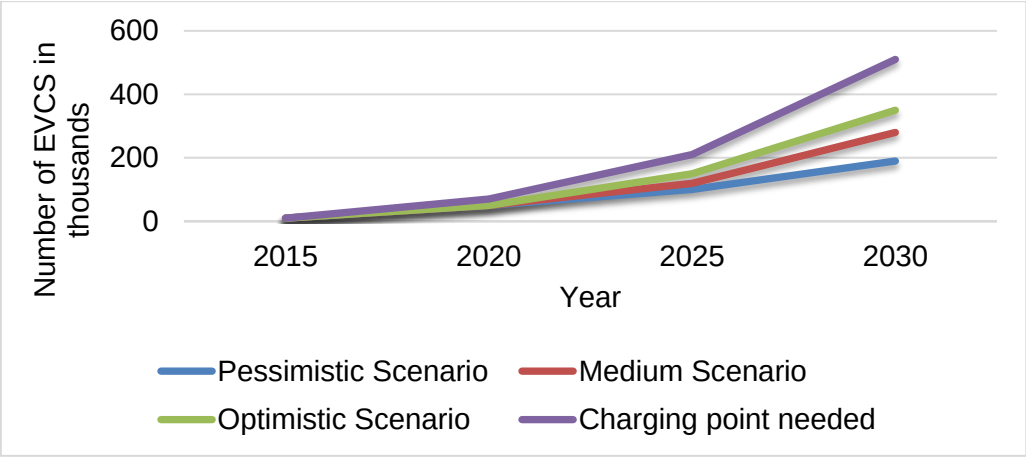

Figure 1.3 Development scenarios of EVCS forecasted [10]

The different scenarios show that the forecasts are based on past experiences. However, the number of EVCS can be triggered toward positive or negative due to the direct and indirect influencing factors. For that reason, the forecast has a long-term uncertainty that needs to be modeled for a risk-averse situation in microgrid decision-making. Furthermore, the necessity of risk-free decision-making is essential for optimal microgrid planning and operation in the face of short-term and long-term uncertainty. The long-term uncertainty is more important for the planning problem, while the short-term uncertainty has a higher impact on the operation problem.

1.2 State-of-the-art and research gaps

Microgrids are being studied in terms of technical, technological, organizational, legal, and economic benefits. These main issues are summarized in Table 1.1 [11].

Table 1.1 Main issues concerned the implementation of Microgrid [11]

Issues	Challenges
Technical	Appropriate work coordination between generators, and protection systems, maintaining the stability of voltage and frequency in grids
Technological	Acceptable equipment for energy generation (solar panels, wind turbines, cogeneration equipment)
Organizational	Developed coordination and operation between all participants of the energy sector
Legal	The legal opportunity to sell the excesses of electrical energy to the centralized grid
Economic	The developed market for electrical energy and economic benefits for users (usage and transit tariffs)
Environmental	Planning and operation with as low as possible emissions

Table 1.1 points out some of the challenges in the implementation of microgrids. However, the challenges regarding microgrids are subject to demography, types, planning periods, target for the installation, and so on. In the current study, the grid-connected microgrid is designed, planned, and operated for German conditions using the following methods:

- Deterministic optimal microgrid planning and operation from scratch
- Development in the e-mobility sector
- Information gap decision method based distributional robust optimization
- Microgrid planning and operation under the white tariff system

1.2.1 Deterministic microgrid planning and operation from scratch

The optimal microgrid planning and operation have been studied vastly. Microgrid planning and operation considering loads, renewables, and energy storage are proposed in [12,13]. For the promotion of renewables and cost reduction, energy storage and demand responses are included in these studies. Furthermore, the multi-energy microgrid with the aim of optimizing the portfolio mix for the components is proposed in [14,15]. In this study, generation units such as Combined Heat and Power (CHP), PV, and wind systems are alongside the energy storage units such as EESS and TESS to satisfy the demand. The Power to Heat (P2H) sector coupling complements the analysis. Renewable energy-based P2H technology uses RES power to generate useful heat energy for consumers with the aim of decreasing curtailments [16]. The study claimed that heat pumps are more efficient than other forms of P2H technologies. Electric boilers have low investment expenditures, operating profitably with only a few full load hours, but the heat pumps can allow heating and cooling [17]. However, a low-temperature heating grid needed to be modeled to supply the heating for a community using effective technologies such as heat pumps or fuel cells. The different case studies based on the low-temperature heating grid are given in Annex B.3. The distributed cogeneration of heat and power has been admitted as an efficient decentralization of the power systems that have decreased the maintenance cost of the networks and nonrational losses of energy [18]. The P2H can be categorized as centralized and decentralized [19]. The centralized heating grid outperforms distributed heating in terms of the cost and efficiency of the generating units [20]. The distributed heating system would be ideal for preventing heat losses if the houses in the settlement area were spread out across a vast region. The TESS can be used in a district heating system with a hydrogen system to increase the system efficiency and reduce the cost by increasing self-consumption [21]. Furthermore, the TESS construction is more logical as a centralized unit. Further information about the categorization of P2H can be seen in Annex A. A multi-energy microgrid considering the P2H sector coupling is shown in Figure 1.4.

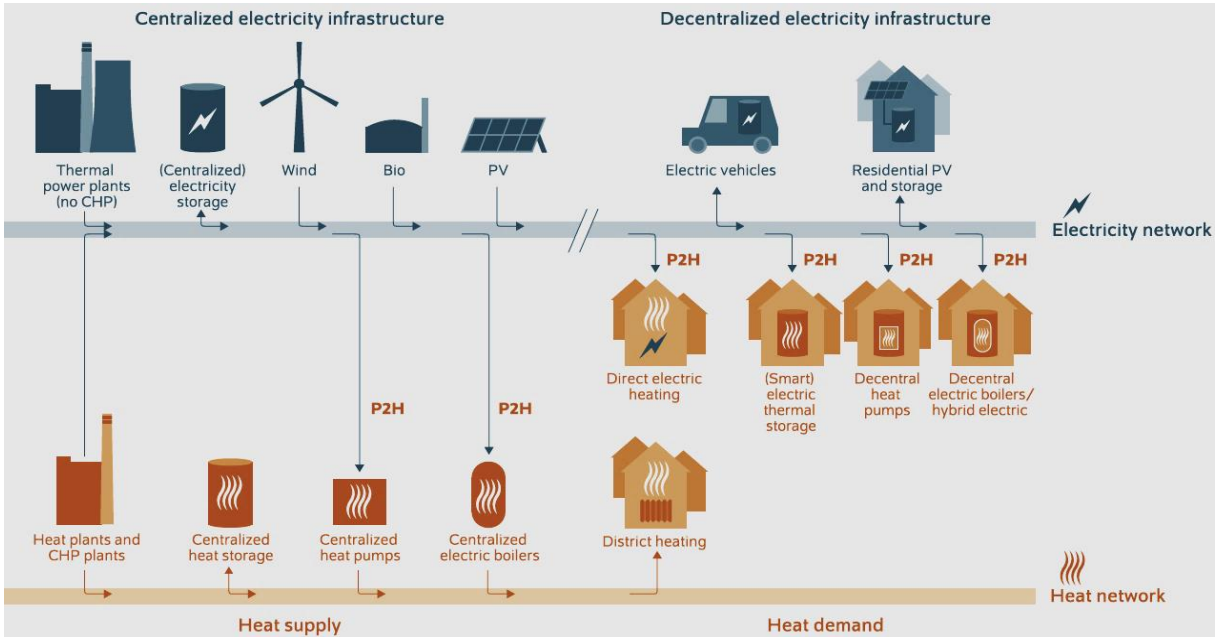

Figure 1.4 Interconnections of P2H with electricity and district heating networks [19]

In [22], the authors show that P2H systems have delivered a surplus of renewable energy sources (RES) above the self-consumption level with a 35 percent reduction in curtailments. In these publications, optimal planning and operation are usually solved in two stages. The first stage identifies the optimal sizes and capacities of the components, and the second stage solves the operation problem [23]. Mostly, the heat and power sectors are considered in these studies. Combined cooling, heating, and electricity are considered in [24]. However, technical constraints such as losses in the heating grid and voltage limits in the electricity grid are lacking. This issue has been solved by introducing linear equations for the grids in [25]. Formulating a second-order cone for the optimal power flow for energy storage planning with transformers is another attempt to incorporate grid technical constraints [24]. A few pieces of literature have considered the combined technical constraints of heat and power grid. The following methods are proposed for a new settlement area based on the above-stated literature.

- A microgrid from scratch is proposed based on the following methodologies
    - Number of people and house types (Single-family houses,multi-family houses)
    - The heating load (space heating and district water heating (DHW)) and Seasonal Coefficient of performance (SCOP) for the heat pump are calculated based on
        - House types and number of the person
        - Outside temperature and day types
    - The PV plan is based on the available area for the settlement

- ❖ Combined microgrid planning and operation for heat, power, and e-mobility sectors
    - The deterministic optimization method for microgrid planning and operation uses mixed-integer nonlinear programming (MINP) with the consideration of capital cost, operation cost, and penalty cost for emission minimization.
        - Consideration of changing cost for the emission certificates
        - low-temperature district heating grid model with central heating sources
        - Consideration of low voltage power grid model

1.2.2 Development in the e-mobility sector

The studies neglect the e-mobility sector, especially the inclusion of EVCS as an additional electrical load in the planning and operation horizon. However, in [26–28], the electrical vehicle charging load is generally shown by a probability distribution and has been included in considering a unified aggregator. This will lead to an unreal realization of EVCS planning as the EV load and the number of EVCS is interdependently independent. This raises the question of how many EVCS are sufficient for how many EVs. Hence, the number of EVCS in a community is an important problem for planning and operation. Apart from the number of EVCS, the placement of EVCS is also important due to the high load associated. The authors of [29] present an optimization process for optimal siting and sizing with road networks using graph theory. A genetic optimization-based algorithm considering cost, EV energy losses, and power system losses has been presented [30]. An EVCS placement algorithm has been shown for under-construction traffic networks by minimizing transportation waste costs using queuing theory [31]. A heuristic planning method considering the EV charging demand rather than the traffic model has been present in [32]. The authors of [33] developed a location model considering an EV driver's existing activities. While a colony optimization has been presented for optimal placement considering cost, real power loss, voltage instability, and traffic flow constraints in [34,35]. A particle swarm optimization (PSO) has shown a better and faster convergence for this problem in [36–38]. Algorithms such as genetic algorithms (GA) and Teaching-learning based algorithms have also been used for this problem [39–46]. In addition to heuristic techniques, the primal-dual interior-point algorithm has been used to find the optimal location depending on coverage and environmental factors [47]. Greedy algorithms and linear programming have also been used for this issue in [48,49]. In the above-stated methods, the multi-period planning for the development in the e-mobility sector, e.g., the rise in the number of EVs and EVCS, the realistic random behavior of EV depending on the traffic model is still lacking the best of the author’s knowledge.

Furthermore, in a planning problem, the placement for EVCS is probabilistic due to the high number of impacting factors, such as the electrical grid structure, space, accessibility, and the quantity of EVs expected to be charged. To consider these different influences, Monte-Carlo simulation-based placement strategy is useful. In this dissertation, the following methods are contributed to the field of e-mobility development.

- Model for e-mobility infrastructure
    - Forecast method for the number of EVs based on retropolation and extrapolation
    - Monte-Carlo simulation for EV behavior
    - The determination of the number of EVCS based on the occupancy time
    - EVCS placement algorithm based on Monte-Carlo simulation

It is necessary that the e-mobility infrastructure must be planned in conjunction with the electrical and heat grid to be powered by high renewables.

For that reason, a new microgrid planning and operation strategy have been developed for the rise of e-mobility infrastructure based on cost and changing policies on emissions. The proposed method considers the linking between traffic, low voltage grid, low-temperature heat grid, technical constraints, and operational strategies of the components.

1.2.3 Information gap decision method - distributional robust optimization

In addition to uncertainties related to e-mobility in the planning problem, the uncertainties might have huge impacts. To consider the effect of the uncertainty, the methods used in the literature are summarized in Figure 1.5.

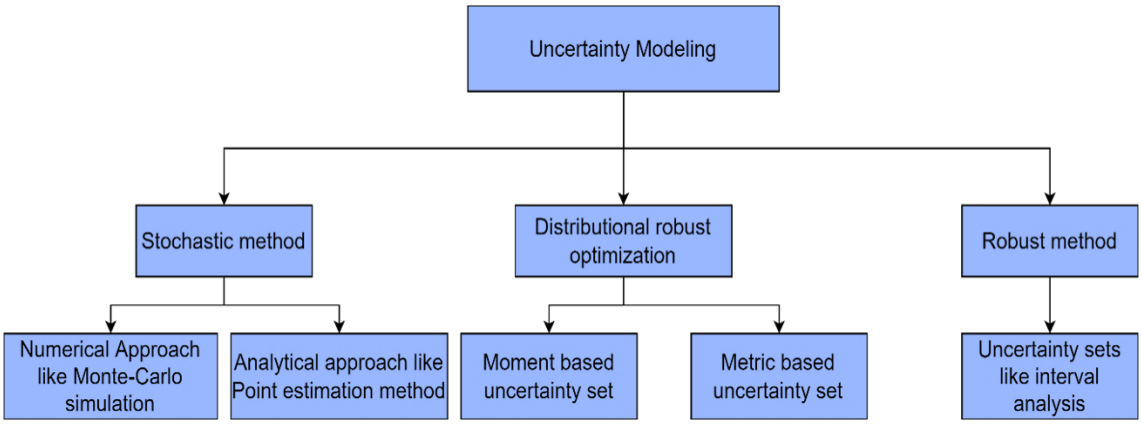

Figure 1.5 Available uncertainty modeling techniques [50]

The randomness associated with renewable generation is considered for sizing multi-energy microgrids using the interval optimization method in [51]. The load is considered as an

uncertain parameter in [52]. Microgrid planning and operation have mainly been studied using stochastic programming and robust optimization to tackle uncertainties. Stochastic programming is used for generating output uncertainty in [53]. However, stochastic programming needs high computational time [54]. The planning and operation problem has been solved with robust optimization [55]. However, the robust optimization resulted in a conservative solution due to the worst-case consideration. The disadvantages of stochastic programming and robust optimization are overcome by distribution robust optimization (DRO) in [56]. In this modeling method, the unknown distribution of the uncertain variable is believed to be in an ambiguity set that comprises all possible distributions of the uncertain variable. An extensive dataset is not required to build a probability distribution function (PDF), as is the case with probabilistic modeling, because the probability distribution is created based on the partial information provided. In the ambiguity set, DRO optimizes the system for the worst-case distribution. Moment-based, distance-based, structural, hypothesis test-based, and likelihood-based ambiguity sets can all be categorized in DRO. Moment-based ambiguity sets, in which the distributions exchange moment information, and distance-based ambiguity sets, in which distributions near a reference distribution with a preset probability discrepancy metric are chosen. The most widely employed metrics are Wasserstein-distance, phi-divergence, KL-divergence, and Prokhorov-metric.

Wasserstein-based DRO was used to model the wind power uncertainty for a rural microgrid to adjust economy and robustness [54]. For the energy management of an islanded microgrid, the wind power uncertainty was modeled using a moment-based ambiguity set in this study. Although these strategies are regarded as short-term uncertainties, there is a lack of modeling short-term uncertainties in EVs optimal planning and operation problems. The EV traffic is considered uncertain and solved the planning and operation using KL divergence for highways in [57]. As the EV traffic in the cities will be different, the short-term uncertainty regarding EVs must be considered in the planning and operation.

Although the above-stated method considers planning and operation for mix-portfolio for DERs, these are solved without any uncertainty or just short-term uncertainties. However, the long-term uncertainty has not been considered. A study that evaluated long-term uncertainties regarding the declining cost of the battery is solved with robust optimization [58]. The long-term uncertainties regarding the rise in the EVCS are still lacking. Due to this, there is a need for a method based on DRO considering short-term and long-term uncertainty regarding e-mobility infrastructure. This is because the growth of e-mobility

infrastructure and the risks that come with it are imminent. To reduce the financial, emission, and technical risk, novel approaches considering the rise in EVCS uncertainty are needed.

In the dissertation, a new robust decision-making method for microgrids in a new settlement area has been developed. The proposed method is a novel stochastic optimal microgrid planning and operation method considering the long and short-term uncertainty. The proposed method is claimed to be recommended as compared to deterministic microgrid planning and operation, as the risk-averse level can be realized when uncertainties occur. The risk-averse levels then enable the decision-makers to decide on the microgrid planning and operation based on robustness for multi-type uncertainty. Especially, consideration of the multi-type uncertainties enables a better realization of a robust microgrid than the consideration of only short-term uncertainties. The contributed methods developed for the stochastic microgrid planning and operation are as follows:

- Information gap decision method (IGDM) - distributional robust optimization (DRO) is developed for optimal planning and operation of the microgrid under the rise in the EV and EVCS uncertainty.
- The proposition of scalability of IGDM-DRO using the multi-cut bender decomposition method

Finally, a holistic approach that combines the deterministic and stochastic optimization approach under consideration of multi-type uncertainties enables optimally planning and operating of a microgrid. The proposed combined approach is claimed to be beneficial for decision-makers to increase the local use of renewables when the e-mobility developed with associated

1.2.4 Microgrid planning and operation under the flexible tariff system

The application of battery storage systems in a microgrid application poses several advantages. Since the high amount of intermittent generation of renewable energy sources can be managed using battery storage systems. An analysis should be performed under different conditions, such as the use of different energy tariffs, since smart meters allow the application of flexible energy prices [59]. The study presents incentives such as feed-in and energy tariffs as important input terms for maximizing self-consumption. Such flexible tariffs are often referred to as off-peak and on-peak price levels, where the battery charges at off-peak price times and discharges at on-peak times. Introduced in Brazil, the white tariff realizes this principle [60]. It is an hourly tariff and can be applied efficiently to use storage and other distributed energy resources. Introducing the white tariff in Germany with different

production and load profiles can be beneficial. The maximization of self-consumption is another important interest factor in a microgrid application.

Local energy consumption from renewable energy sources is recommended, which reduces the grid supply. The use of the battery energy storage system for efficient energy use, such as peak shaving, voltage support, reliability, and integration of renewable energy sources, has been studied in [61]. The studies show the usage of storage management for power balancing by storing energy at off-peak hours and distributing it at on-peak hours. Furthermore, the support of the distribution grid by energy storage systems has been widely studied, e.g., in [62]. Grid-connected microgrids with battery energy storage systems (BESS) in a different configuration and under consideration of time-of-use tariffs got more attention [63,64]. The BESS studies in terms of self-consumption based on demand forecasting have been studied in [65–70]. Similarly, self-consumption with different electricity prices has been analyzed in [71]. It is still being studied how to combine multiple distributed energy resources with electrical energy storage systems (EESS) to generate technological and economic benefits [72]. Investigation of EESS coupled with PV to facilitate the consumer benefit from feed-in tariffs incentive has been done in [73]. The study uses mixed-integer linear programming (MILP) to solve the optimization problem. The studies [74,75] considered the optimization of different tariff structures. Furthermore, BESS with PV and time-varying tariffs to decrease the operational cost has been studied in [76–80]. However, an economical tariff system that benefits the microgrid owner and consumers need to be proposed to motivate the higher integration of renewables.

With the rise in EVs, the local use of renewable energy in microgrids should be supported by the implementation of ESS. The implementation of ESS can be cost-effective with a potentially optimistic tariff system.

- The microgrid's flexible tariff system is introduced to support local energy use compared with a typical flat tariff.

1.3 Outline, assumptions, and limitations of the thesis

The thesis is composed of seven parts. The first chapter provided general information about the background, motivation, state of the art, and the work's scientific contribution. In the second chapter, the components of the microgrid are modeled, including the DERs, load profiles, grids, and statistical models. The e-mobility infrastructure is presented in chapter 3, where the number of EVs is analyzed, followed by the EV behavior modeling. Furthermore,

Chapter 3 also consists of the methodologies for the number of public EVCS and the placement for the EVCS.

The optimization methodologies to optimally plan and operate the microgrid are presented in chapter 4. Chapter 4 is divided into deterministic and stochastic optimization methodologies. The stochastic methods presented in chapter 4 consist of the information gap decision method and Distributional robust optimization. The modeling of the flexible tariff system is also described in chapter 4. Chapter 5 provides the results and discussion for the e-mobility infrastructure, deterministic optimization approach, and stochastic optimization approach for microgrid planning and operation. Furthermore, Chapter 5 presents a sensitivity analysis on the DERs, the comparison between flexible and flat tariff systems, and the comparison between deterministic and the proposed stochastic method.

Finally, Chapter 6 concludes the entire study, and the thesis-based outlook is outlined. References, a list of symbols/abbreviations, a List of Tables, a List of Figures, and an Appendix make up the rest of the dissertation.

Several assumptions are made in light of the current dissertation. Firstly, the microgrid will usually be operated using a grid operator similar to a utility grid. However, in the present study, the role and functionality of a grid operator are neglected. However, the recommendation based on the current studies is not contrary to the role of the grid operators. Furthermore, the control issues related to microgrid operation are out of this dissertation's scope. Secondly, The regulatory framework for a completely integrated contemporary microgrid connected to the current low-voltage grids is mainly ignored. Thirdly, due to new settlement descriptions, some methods, such as the computation of heating loads, are limited to the condition of Germany. However, other modeling methodologies related to e-mobility deterministic and stochastic optimizations are transferable to a diverse amount of case studies. Finally, the load profiles in the second resolution are interpolated into hours resolution due to the high computation time required by the optimization algorithm. Due to this, the peaks that occur for a small amount of time is lost. This limitation must be considered in the future as some of the technical problems in the microgrid occurs in a small resolution and create a high impact.

2 Component Modeling

The microgrid can work islanded and grid-connected. The most important microgrid planning and operation parameters are cost and CO_2 emissions. Due to this, an economical and sustainable microgrid needs to be optimized for these parameters. The microgrid consists of PV systems, wind systems, heat pumps, EESS, TESS, Fuel cells, electrolyzers, HESS, and electric vehicle charging stations, as shown in Figure 2.1. Renewable energy sources, energy storage systems, and sector coupling technologies are referred to DERs in the microgrid.

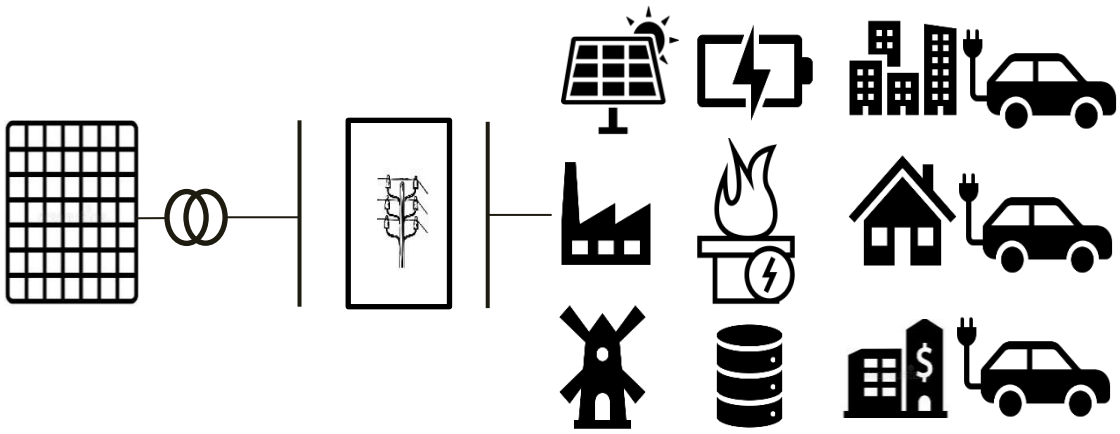

Figure 2.1 Microgrid Model

2.1 Statistical model for a new settlement area planning

The microgrid planning and operation for new settlement areas need planning from scratch. The planning from scratch included the statistic regarding the settlement area. The house types are distinguished into single-family houses (SFH), multifamily houses (MFH), and commercial real estate (CRE). An SFH comprises one to five people, whereas an MFH is made up of 12 or 16 flats [81]. For a single-family house, the area is assumed to be 140 $m^{2,}$ whereas the multi-family house with 12 dwellings and 16 dwellings is considered 950 m^2 and 1170 m^2 respectively [81]. Commercial real estate is estimated to be equal to a medium-sized office and is regarded as 400 m^2 [81]. All the buildings, carports, and commercial real estate are equipped with PV. The roofs of the SFH are mostly at the slope with a 30-degree south exposure. Similarly, the dwelling in the MFH has the same ratio of people. The distribution of persons over the SFH and dwellings in the MFH is random.

2.2 Electrical load modeling

The load profile is a curve form that shows how the load changes over time [82]. The load will vary depending on the type of selection (residential or commercial), season, weather, entity

dispersion, size, and location at any given time. The load profiles are used in planninggeneration and accounting for energy derived from renewable energy sources. The conventional way of creating load profiles is to record consumption per time unit [82]. In the absence of a real load profile, synthetic load profiles have been developed for research purposes. Synthetic load profiles have been developed to depict the energy consumption for various building types. Standard load profiles are usually available for planning and operation [83]. However, because the total load of the houses in the microgrid adds up, true microgrid planning behavior is impossible to achieve. Furthermore, the high peak of EV load aggravates the situation. As a result, the larger capacity of the microgrid component can be seen, perhaps leading to an increase in unplanned costs. As a result, the recorded load profiles reveal the greater potential for microgrid planning and operation, which was used in the current study for the electrical load profile.

The identification of a practical approach to the planning of sector coupling technologies for settlement relies heavily on load profiles. Heating and electricity loads in Germany are governed by the type of building, the number of people in single-family homes or the number of flats in multi-family homes, and the country's climate zone. In Germany, the annual energy for a residential building is determined according to EnEV (energy saving ordinance) using DIN V 4701-10 and DIN EN 832 standards [84]. Based on the number of persons, the household load profiles are assigned. The electrical load profiles for this work have been taken from the database of HTW Berlin- University of Applied Sciences. The data for the electric load profiles were taken from the field test experiment 'Moderne Energiesparsysteme in Haushalten by the "Institut für ZunkunftsEnergieSysteme" (IZES) in the years 2008 through 2011 using smart meters for 497 households. Of the 497 household profiles, 74 were chosen from a single grid to have proximity to each other. The annual electricity consumption is between 1.4 MWh and 8.6 MWh [85]. The electricity consumption depends on the number of the person in the household. Under consideration of the annual electricity consumption, the load profiles were picked from the database. The annual electricity consumption for different households is given in Table 2.1.

Table 2.1 Annual electricity consumption for different household sizes [86] [87]

Household size	**Annual electricity consumption for SFH in MWh**	**Annual electricity consumption for MFH in MWh**
1	2.3	1.4
2	3	2
3	3.6	2.6
4	4	3
5	5	3.6

The available database in the resolution of seconds. By averaging the data points, the second resolution is turned into an hour resolution for a span of 1 year time period for the current study. The comparison of a second and hour resolution load profile for a day is given in Annex B.1. For the single-family houses, five different types of load profiles are selected from the database under the consideration of Table 2.1. For the SFH, the load profiles are available in a variety. The MFH, on the other hand, is larger than a 5-person household. A combination of load profiles is employed for the load profile assignment for an MFH with more than 5 persons. A publicly available profile was also utilized to mimic energy demand in commercial real estate [88]. Figure 2.2 depicts the load profiles for a single day. The electrical load profile is then assigned to the houses of the settlement area for 365 days of the year in a 1-hour resolution.

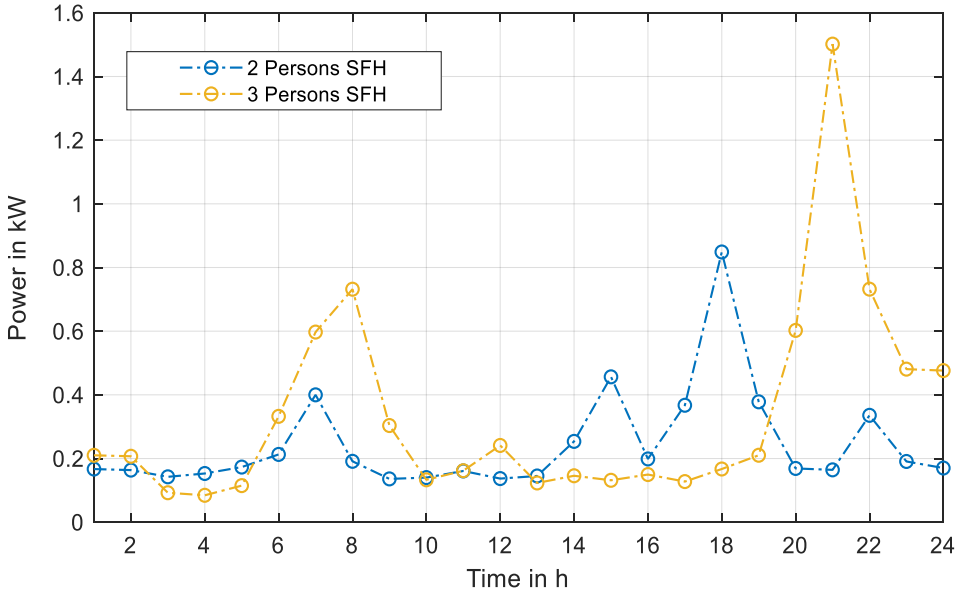

Figure 2.2 Electrical load profiles

2.3 Heating load modeling

The houses in the settlement are considered low-energy passive houses according to DIN V 4701-10 and DIN EN 832 standards. The houses are categorized by the amount of annual heating energy required in kWh/m²a to maintain a specific indoor temperature of 19 °C. Passive houses need annual heating and cooling load of 10 kWh/m²a to 15 kWh/m²a, whereas an old building without insulation requires around 400 kWh/m²a [81]. The thermal transmittance (also known as U-value) of these buildings with better-insulated windows can be as low as 0.7 W/m²K [81]. The heating load is defined as the amount of energy in the form of heat that needs to be added to a building to maintain a specified temperature. The indoor temperature that should be maintained is assumed as 19 °C for the settlement area. Heating load profiles are classified into space heating and domestic hot water (DHW). In the present

study, the heating load is determined by using VDI 4655 standard. The set of 10-day type categories is shown in Table 2.2. Sundays and public holidays are classified as holidays, whereas the rest of the days are classified as workdays [89].

Table 2.2 Typical day categories [89]

Season	**Workday (W)**		**Holiday (S)**	
	Fine (H)	**Cloudy (B)**	**Fine (H)**	**Cloudy (B)**
Transition (U)	UWH	UWB	USH	USB
Summer (S)	SWX		SSX	
Winter (W)	WWH	WWB	WSH	WSB

The average cloud amount (B) is recorded from 1 to 8. If the average cloud amount is less than 5, the day is considered as Fine (H), otherwise, cloudy is considered [88]. A distinction has not been made for cloudy/fine in summer (S) because the space heating demand is the same for both days. If the average per-day temperature (T_{m}) is between 5 °C and 15 °C, and the day is defined as a transition day (U). If the average per day temperature is greater than 15 °C, the day is categorized as a summer day, and alternatively, if T_{m} is below 5 °C the day is considered winter day (W). As a result, the days from 1st January to 15th March and 1st November to 31st December are categorized as winter days. From 1st June to 28th August, the days are classed as Summer, and the remaining days are classified as a transition. Every seventh day has been treated as a holiday. The cloudy days are randomly chosen and assumed. The data are generated using German weather seasonal conditions of DWD [89]. The temperature has been measured 2 meters above the ground level on a 24-hour based.

The heating load has been calculated by using the heating energy factor F_{DT} The heating energy factor is defined as given in (2.1) [89].

$$F_{\mathrm{DT}} = \frac{(T_{\mathrm{o}} - T_{\mathrm{m}})\ \phi_{\mathrm{h,DT}}}{\sum\left[(T_{\mathrm{o}} - T_{\mathrm{m}})\ N_{\mathrm{DT}}\ \phi_{\mathrm{h,DT}}\right]} \tag{2.1}$$

where, T_{o} is the defined temperature above which no heating is required and $\phi_{\mathrm{h,DT}}$ is the factor for deviation of each day type category. It includes special influences such as solar radiation in the investigated zones. $\phi_{\mathrm{h,DT}}$ also depend on the type of house, as SFH has a different heating factor than MFH for the everyday type category. N_{DT} is the number of days in the day type. In addition, the average per-day temperature (T_{m}) is calculated per day and will be assumed to be a constant value.

2.3.1 Computation of the day-type space heating load

The annual space heating load can be calculated according to standard DIN EN 832 at the European level [89]. This document has been updated and replaced with DIN EN ISO 13790:2008-09. The annual heating energy demand $Q_{\mathrm{h,a}}$ in kWh/a is determined by (2.2).

$$Q_{\mathrm{h,a}} = \mathrm{A_h} Q_{\mathrm{Sh,a}} \tag{2.2}$$

where A_{h} is the total area of the specific building as described in section 2.1. $Q_{\mathrm{Sh,a}}$ is the specific annual space heating demand. The value of $Q_{\mathrm{Sh,a}}$ for passive dwellings built after EnEV 2009 is between 10 and 15 kWh/m^{2}a [90]. In the present work, 15 kWh/m^{2}a has been considered for the calculation. The daily space heating energy demand for a particular day type is given by (2.3) [89].

$$Q_{\mathrm{h,DT}} = Q_{\mathrm{h,a}} F_{\mathrm{DT}} \tag{2.3}$$

The daily heating energy demand has been calculated for a minute of each day type with the assumption that it will be consistent for each minute in the same day category. The heating energy demand per minute $Q_{\mathrm{h,DT,Min}}$ is determined by (2.4).

$$Q_{\mathrm{h,DT,Min}} = \frac{Q_{\mathrm{h,DT}}}{1440} \tag{2.4}$$

2.3.2 Computation of the day-type domestic hot water (DHW) load

The DHW demand for typical day categories is defined by using VDI 4655. The DHW load is not dependent on the outside air temperature and is defined as 500 kWh per person for a single-family house and 1000 kWh per dwelling for a multi-family house. The annual DHW demand $Q_{\mathrm{D,a}}$ can be calculated as follows [89],

$$Q_{\mathrm{D.a}} = Q_{\mathrm{SD,a}}\, N_{\mathrm{h}} \tag{2.5}$$

where N_{h} is the number of persons or number of dwellings depends on the type of building and $Q_{\mathrm{SD,a}}$ is the specific DHW heating energy demand. A ratio of people to the basement area is taken into account when calculating the CRE's annual DHW heating energy consumption. A medium-sized office with a basement area of 450 m^2 and a people design level of 18 m^2 per person is considered. For the CRE, it is assumed that there are 26 persons and that each person consumes 1000 kWh [85]. The DHW energy demand for a particular day-type category ($Q_{\mathrm{D,DT}}$) can be determined by (2.6) [89,91].

$$Q_{\mathrm{D,DT}} = Q_{\mathrm{D,a}} \left(\frac{1}{365} + N_{\mathrm{h}}\, F_{\mathrm{D,DT}} \right) \tag{2.6}$$

Where, $F_{\mathrm{D,DT}}$ is the DHW heating energy factor extracted from VDI 4655. The DHW energy demand per minute in kWh/min has been calculated by (2.7).

$$Q_{\mathrm{D,DT,Min}} = \frac{Q_{\mathrm{D,DT}}}{1440} \tag{2.7}$$

The load profiles for heating (space and DHW) are formed by multiplying the day-type heating energy demand (equations 2.3 and 2.6) with a normalized time series given in VDI 4655 for the computation of the heating load profiles. The normalized heating energy factor is multiplied by the calculated daily heating energy demand for the particular day type to form a one-day space heating in a one-minute resolution for single-family houses and a 15-minute resolution for multi-family houses. By averaging the data points, the 1-minute and 15-minutes resolutions are turned into an hour resolution for a span of 1 year time period for the current study.

2.4 Electric grid modeling

The electrical grid is commonly divided into three categories based on voltage: high, middle, and low voltage grids. Low-voltage grid structures are often classified as radial, ring, or mesh grid structures [92]. European low-voltage grids are typically radial structures where the consumers are connected to the feeders [93].

The microgrid is assumed to be a radial low-voltage grid consisting of connection nodes, lines, and loads. Different types of loads are considered, such as single-family houses, multi-family houses, and commercial real estate. The voltage and power losses in the electric grid have been considered in this study. Line losses are proportional to the line resistance and square of the current. The parameter of nodes is the nominal voltage and node type (i.e., slack bus, load bus). In the line modeling, the length, status of the lines, and parameters of the cable types (resistance, capacitance, and reactance) have been considered. The nominal line-to-line voltage for the electric low-voltage grid is 400 V [96]. The voltage must be in the range of $\pm$10 percent of the nominal voltage according to DIN-EN-50160 [97] during the total planning period, maintaining the microgrid's secure operation and customer satisfaction. The line parameters are modeled as NAVY 4x 35-150 mm², while the house connections are depicted as NAVY 4x 16-50 mm² as summarized in Table 2.3. Power flow analysis is frequently employed in the operation and design of power systems [98]. The power flow is created by

combining data from the network, load, and generation. The voltage at various buses, line currents, and power losses are the outputs of the power flow calculation.

Table 2.3 Line Parameters [94,95]

Cable Profile	Resistance (R) in Ω / km	Reactance (X) in Ω / km	Capacitance in nF / km	Maximum Current in kA
150 mm²	0.64	0.08	540	0.275
120 mm²	0.25	0.07	530	0.232
70 mm²	0.53	0.07	670	0.195
50 mm²	0.64	0.08	670	0.141
35 mm²	0.87	0.09	380	0.092
25 mm²	0.64	0.08	400	0.076
16 mm²	1.15	0.3	300	0.060

Nodal power balancing equations are used to solve these load flow analyses. Due to the nonlinear nature of these equations, iterative methods such as Newton-raphson, Gauss-seidel, and the fast decoupling method are used. The Newton-raphson (NR) power flow is chosen in this investigation since it is more accurate and common for the placement problem described in section 3.4 [99]. The detailed model of NR power flow can be seen in Annex B.2.

The expansion planning of the distribution grid of the microgrid is assumed to be out of the scope of the work. The voltage at the nodes and thermal limits of the cables of the microgrid are constraints in order to avoid technical power grid problems in the span of the planning horizon. To determine the voltage, power losses, and other technical aspects, power flow equations are used. However, the ordinary power flow equation consists of trigonometric functions. Although in the present study, the power equations needed to be used as constraints only, integrating them into the optimization problem is challenging due to the non-convexity of these equations. However, different methods exist to convexify power flow equations, such as semidefinite programming (SDP) and second-order cone programming (SOCP) [100]. DC power flow can also be used on the cost-oversimplified optimal power flow, which is not suitable for this type of application [101]. The SOCP is solved more efficiently as compared to SDP [102]. Due to this, the SOCP is used in the present study. As the aim is to avoid optimizing the power grid for a particular objective but to use the power flow equation as a constraint and the grid structure used is a radial distribution grid, the DistFlow approach is well suited. Distflow is proposed with linearization for efficient computation of the power flow and voltage drop from the slack bus toward the end of the branch [103,104]. This is most commonly used in conjunction with the radial grid structure [101]. Concluded from the above studies, the DistFlow model turns out to be

significantly more numerically stable than the bus injection model, and its linearization provides simple analytical solutions. The branch flow is given in (2.10) and (2.11).

$$P_{\text{in}} = \boldsymbol{A}(P_{\text{s}}) - \boldsymbol{A}\left(I_{\text{ij}}R_{\text{ij}}\right) + \boldsymbol{B}(P_{\text{s}}) \tag{2.10}$$

$$Q_{\text{in}} = \boldsymbol{A}(Q_{\text{s}}) - \boldsymbol{A}\left(I_{\text{ij}}X_{\text{ij}}\right) + \boldsymbol{B}(Q_{\text{s}}) \tag{2.11}$$

Here R_{ij} and X_{ij} are the resistance and reactance of the branch from node i to node j, respectively. The power injected P_{in} at a node must be equal to transfer to other nodes through branches P_{s}. The incident matrix $\boldsymbol{A}$ is the connecting matrix that contains the information of the branch connection going away from the node, while $\boldsymbol{B}$ is the connecting matrix containing the information of the branch coming into the node. A grid with four nodes, including a slack node and three lines, is shown in Figure 2.3.

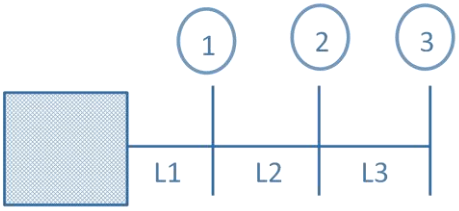

Figure 2.3 Grid with four nodes, including slack node

The incident matrices A and B for the grid shown in Figure 2.3 are as follows,

$$\boldsymbol{A} = \begin{bmatrix} 1 & 0 & 0 \\ 0 & 1 & 0 \\ 0 & 0 & 1 \\ 0 & 0 & 0 \end{bmatrix} \boldsymbol{B} = \begin{bmatrix} 0 & 0 & 0 \\ 1 & 0 & 0 \\ 0 & 1 & 0 \\ 0 & 0 & 1 \end{bmatrix}$$

Here, the row shows the number of nodes, while the columns show the number of lines. Node 0, also called a slack node, has one outgoing line without any incoming line. Due to this, matrix ***A*** has 1 in the first row while matrix ***B*** is zero. Similarly, node 2 has an incoming from line 1 and an outgoing to line 2. Due to this, matrix A has 1 at $A_{22,}$ and matrix B has 1 at B_{21}. The voltage U at node i in DistFlow is given in (2.12) [104], and the approximation of the power equation can be seen in Annex B.2.2 in accordance with the linear relaxation method described in references [104,105].

$$U_{\text{i}} = U_{\text{j}} - 2\left(R_{\text{ij}}P_{\text{s}} + X_{\text{ij}}Q_{\text{s}}\right) + \left(R_{\text{ij}}^2 + X_{\text{ij}}^2\right)I_{\text{ij}} \tag{2.12}$$

The current I passes through the line and is limited by the current-carrying capacity given in Table 2.4 is shown in (2.13).

$$I_{\mathrm{ij}}^2 \leq I_{\max} \tag{2.13}$$

The active power P_{s} and reactive power Q_{s} of the branch, flow is also limited to a maximum allowable limit as given (2.14) and (2.15).

$$P_{\mathrm{s,min}} \leq P_{\mathrm{s}} \leq P_{\mathrm{s,max}} \tag{2.14}$$

$$Q_{\mathrm{s,min}} \leq Q_{\mathrm{s}} \leq Q_{\mathrm{s,max}} \tag{2.15}$$

$P_{\mathrm{s,min}}$ and $Q_{\mathrm{s,min}}$ are the lower allowable bounds for active and reactive power of the branches, whereas, $P_{\mathrm{s,max}}$ and $Q_{\mathrm{s,max}}$ are the highest allowable bounds for active and reactive power in the lines. The voltage drops through a line due to the connected load and adds up due to generation, such as PV. The voltage security constraint is given in (2.16)

$$U_{\min} \leq U_{\mathrm{k}} \leq U_{\max} \qquad \forall k \in ij \tag{2.16}$$

Here, the $U_{\min}$ is the minimum allowed voltage of a node and $U_{\max}$ is the maximum allowed voltage. The voltage at the slack bus is given as,

$$U_{\mathrm{k}} = U_{\mathrm{n}} \qquad \forall k \in ij \;\; \forall n \in ij \tag{2.17}$$

Note that the above Distflow is still non-convex and is hard to be solved for commercial solvers. Due to this, a second-order cone programming (SOCP) approach is taken for this study to transform it into convex [100,106,107]. To convexify, the equation (2.16) and (2.17) are transformed into (2.18),(2.19), and (2.20).

$$U_{\mathrm{k}} = U_{\mathrm{n}}^2 \qquad \forall k \in ij \tag{2.18}$$

$$U_{\mathrm{min}}^2 \leq U_{\mathrm{n}}^2 \leq U_{\mathrm{max}}^2 \qquad \forall n \in ij \tag{2.19}$$

$$I_{\mathrm{ij}}^2 = \frac{P_{\mathrm{S}}^2 + Q_{\mathrm{S}}^2}{U_{\mathrm{k}}^2} \qquad \forall k \in ij \tag{2.20}$$

The above transforms a cone programming with second-order as given in (2.21).

$$\left\| \begin{matrix} 2P_{\mathrm{S}} \\ 2Q_{\mathrm{S}} \\ I_{\mathrm{ij}} - U_{\mathrm{k}} \end{matrix} \right\|_2 \leq I_{\mathrm{ij}} + U_{\mathrm{k}} \qquad \forall k \in ij \tag{2.21}$$

2.5 Heating grid model

The considered heating grid can provide space and water heating using a low-temperature district heating grid. It consists of heating nodes (HN) and heating branches (HB). The heating branches are pipes, and the heating loads are assigned to connected heating nodes. The heat is extracted in terms of heating load from the nodes, fulfilling the water and space heating demand. In this planning study, the space and water heating have been modeled for the household of the microgrids. The heating grid consists of a source that generates heat and pumps responsible for the flow of water. The pump model is out of the scope of this work. Due to this, the effect of the pump is ignored in the present study. The total heating load Q_{H} for a household is given in (2.22).

$$Q_{\mathrm{H}} = Q_{\mathrm{h,DT,Min}} + Q_{\mathrm{D,DT,Min}} \tag{2.22}$$

After the heating load profile is created, the loads are assigned to the houses of the microgrid. The heating grid is characterized by n heating nodes and m heating branches. The source of the heating is connected to a source node, and loads are connected to other nodes. A mass flow $\dot{m}$ of the heating substance, such as water or steam, is pumped through the branches of the grid in the positive direction. The required heating is extracted from the nodes, and the heating substance mass flow returns in the negative direction by losing heat, as shown in Figure 2.4. The current study takes the value of mass flow rates from [108].

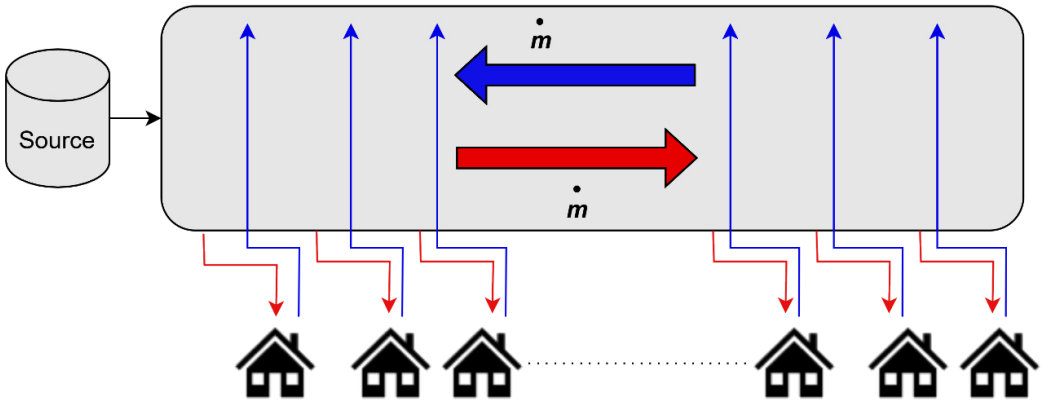

Figure 2.4 Heating grid model

Considering a low-temperature heating grid, a supply temperature of 50 °C to 60 °C is enough, considering the losses and heating loads of the passive houses in the settlement areas [109]. There are case studies of low-temperature heating grids. The list of low-temperature district heating grids can be seen in Annex B.3. Due to this, the temperature at the nodes in the positive direction TN_{pos} must be maintained between 50 °C to 60 °C. Similarly, the node

temperature in the negative direction TN_{neg} is assumed to be above 40 °C considering the available case studies as given in (2.23-2.26). Figure 2.5 shows the heating structure of a node, with $TB_{\text{in, pos}}$ representing the temperature that goes into a heating node in the positive direction and $TB_{\text{in,neg}}$ representing the temperature that goes into the bus in the negative direction. Similarly, $TB_{\text{out, pos}}$ and $TB_{\text{out,neg}}$ are the temperature out of the heating nodes in positive and negative direction respectively.

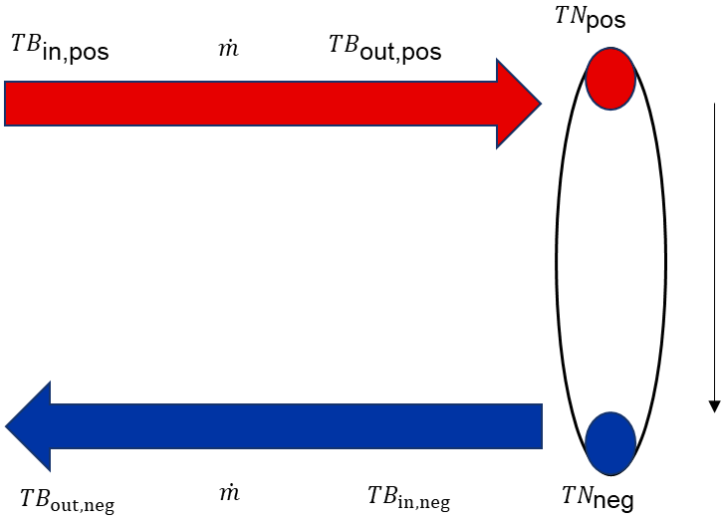

Figure 2.5 Heat node structure

$$50 \leq TB_{\text{in,pos}} \leq 60 \tag{2.23}$$

$$50 \leq TB_{\text{out,pos}} \leq 60 \tag{2.24}$$

$$40 \leq TB_{\text{in,neg}} \tag{2.25}$$

$$40 \leq TB_{\text{out,neg}} \tag{2.26}$$

The mass flow and temperature at a particular node must equal the temperature and mass flow to all branches connected to the node, as given in (2.27).

$$\sum_{N} \dot{m}\, TN_{\text{pos}} = TB_{\text{in,pos}} \sum_{B} \dot{m} \qquad \forall N \in HN \qquad \forall B \in HB \tag{2.27}$$

Similarly, the temperature and mass flow are given in (2.28) in the negative direction.

$$\sum_{N} \dot{m}\ TN_{\text{neg}} = TB_{\text{in,neg}} \sum_{B} \dot{m} \qquad \forall N \in HN \qquad \forall B \in HB \tag{2.28}$$

If the heating losses through the branches are neglected, the temperature at the beginning of the branches and the temperature at the end of the branches will be the same, as shown in (2.29) and (2.30).

$$TB_{\text{out,neg}} = TB_{\text{in,neg}} \tag{2.29}$$

$$TB_{\text{in,pos}} = TB_{\text{out,pos}} \tag{2.30}$$

The heating load calculated in sections 2.3.1 and 2.3.2 is extracted from the connected node of the heating grid as given in (2.31). The equation is also called specific heat in thermodynamics and is given in (2.31) [110,111].

$$Q_{\text{H}} = Q_{\text{p}} \dot{m}_{\text{in}} \left(TB_{\text{pos}} - TB_{\text{neg}}\right) \tag{2.31}$$

where Q_{p} is called specific heating capacity. It is equal to 4200 J/kg °C if water is used as a heating substance and $\dot{m}_{\text{in}}$ is the mass flow rate of the heating substance into the load nodes. $\dot{m}_{\text{in}}$ should be equal to $\sum_N \dot{m}$. Similarly, the heating source Q_{N} is given by (2.32).

$$Q_{\text{N}} = Q_{\text{p}} \dot{m}_{\text{out}} \left(TB_{\text{pos}} - TB_{\text{neg}}\right) \tag{2.32}$$

Here, $\dot{m}_{\text{out}}$ is the mass flow rate of the heating substance out of the source nodes. $\dot{m}_{\text{out}}$ should be equal to $\sum_B \dot{m}$. The detailed heating grid is important in the planning and operation to consider the losses that occur during the heating grid operation. The heat losses through the branches are subject to the length of the pipe L_{p}, the conductivity of pipe λ_{p}, specific heating capacity Q_{p}, mass flow rate $\dot{m}$ and outside temperature T_{outside}. Other parameters, such as time delay, have been neglected in the current study. The temperature in terms of heat losses through a branch is given as (2.33) [110].

$$TB_{\text{out,pos}} = \left(TB_{\text{out, pos}} - T_{\text{outside}}\right) e^{-\frac{\lambda_{\text{p}} L_{\text{p}}}{Q_{\text{p}} \dot{m}}} + T_{\text{outside}} \tag{2.33}$$

2.6 Heat pump Model

Heat pumps are used to provide the part of the above-mentioned heat required. There are several types of the heat pumps, such as groundwater, ground source, and air to provide the heat demand of the residential building. The electric energy required for the heat pumps for compressor drives, controls, and other drives in a year can be calculated using combined space and DHW heating consumption. The electric power requirement for heat pumps to provide

annual heating energy for the settlement heating grid depends on the Seasonal coefficient of performance (*SCOP*) as given (2.34).

$$Q_{\mathrm{HP,out}} = SCOP_{\mathrm{WPA}} P_{\mathrm{HP,in}} \tag{2.34}$$

The SCOP for the heat pump to fulfill the space and DHW heating requirement is defined by VDI 4650. A single heat pump covers space and DHW heating demand, but SCOP is calculated separately for both, and then the proportion of weight is inserted in the annual energy demand. The outdoor source heat pump is used. The SCOP for the air source heat pump for space heating is calculated by (2.35) [112].

$$SCOP_{\mathrm{H}} = \frac{F_{\Delta\vartheta}}{\frac{F_{\vartheta 1}}{COP_{\mathrm{N1}}} + \frac{F_{\vartheta 2}}{COP_{\mathrm{N2}}} + \frac{F_{\vartheta 3}}{COP_{\mathrm{N3}}}} \tag{2.35}$$

where, $F_{\Delta\vartheta}$ is the correction factor for the deviating temperature difference in the condenser during operation. For under-floor heating, the correction factor is assumed 5 °K to 7 °K, and for calculation purposes, 6 °K is assumed. $F_{\vartheta 1}, F_{\vartheta 2}, F_{\vartheta 3}$ are the correction factor for different operating conditions. It will vary with heating limit, outdoor, maximum supply, and fixed/variable speed compressor types. For calculation purposes of settlement, a variable speed heat pump is assumed. The COP_{N1}, COP_{N2}, COP_{N3} are the coefficient of performance determined by standard DIN EN 14511. COP_{N1} is the coefficient of performance as per DIN EN 14511 at A-10/W60, where A-10 stands for the Air source heat pump as a heat source at the air temperature of -10 °C and W60 stands for the water as the heat pump sink medium at a supply temperature of 60 °C. COP_{N2} is the coefficient of performance for A2 / W60, taking defrost into account and COP_{N3} is the coefficient of performance as per DIN EN 14511 at A10/W60. The SCOP of the heat pump to cover the demand of the DHW is calculated as per equation (2.36) [112].

$$SCOP_{\mathrm{W}} = COP_{\mathrm{N3}} F_{\Delta\vartheta} F_1 F_2 \tag{2.36}$$

Where $F_{\Delta\vartheta}$ is the same as described for space heating with a temperature difference of 6 °K during the operation. Whereas F_1 is the correction factor for deviating design temperature and F_2 is the correction factor for DHW heating at 50 °C. The value of F_2 is 0.716 for the heat pump type with storage tank plus internal heating water pipe coil and 0.644 for all other types [112]. The total SCOP can be determined by using the share of space and DHW weightage. The weightage of total SCOP is given by (2.37) [112].

$$SCOP_{\mathrm{WPA}} = \frac{1}{(1-\partial)\frac{\gamma_1}{SCOP_{\mathrm{H}}} + \mathrm{y}\frac{\gamma_1}{SCOP_{\mathrm{W}}} + (1-\gamma_1)} \tag{2.37}$$

where ∂ is the proportion of DHW demand in the total heating demand and γ_1 is the coverage of monoenergetic operation in terms of space and DHW heating demand. The share of DHW heating for the whole settlement is approximately 28 percent of the total energy consumption. It is assumed to be a monovalent operation for the calculation, and α is considered to be 1 [112]. The properties of the selected heat pump can be seen in Table 2.4.

Table 2.4 Properties of the heat pump [112,113]

Space heating	**Vitocal 300-A AWO-AC 302.B60**
COP_{N1}	2.940
COP_{N2}	3.660
COP_{N3}	4.420
$F_{\Delta\vartheta}$	0.990
$F_{\vartheta 1}$	0.038
$F_{\vartheta 2}$	0.525
$F_{\vartheta 3}$	0.340

The properties of specifications for the specified heat pumps to supply DHW are shown in Table 2.5.

Table 2.5 Properties of specific heat pumps for the DHW supply [112,113]

DHW	**Heat pump**
F_1	1.000
F_2	0.644

Based on equation (2.34), the electrical input of the heat pump should be bounded by the capacity constraint of the heat pump. The heat pump input should be operated below the rated capacity as given in (2.38). Furthermore, the heat pump capacity constraint for the optimization model is given in (2.39).

$$0 \leq P_{\mathrm{HP,in}} \leq P_{\mathrm{HP,cap}} \tag{2.38}$$

$$0 \leq P_{\mathrm{HP,cap}} \leq P_{\mathrm{HP,max}} \tag{2.39}$$

2.7 Fuel cell, hydrogen storage, and electrolyzer model

Peak demand occurs largely in the evening because of the integration of electric vehicles. As a result, some generation sources (PV, wind) cannot satisfy this demand. Due to the emission

target, the increased demand from the grid must be limited. On the other hand, PV power at the on-peak time could be higher than the demand. One possibility is to store this energy in hydrogen for later use. For that issue, an electrolyzer-hydrogen storage-fuel cell system is taken into account. The electrolyzer will use electricity to break the water into hydrogen and oxygen. Neglecting the dynamics of the electrolyzer for simplicity, the hydrogen produced by the electrolyzer $H_{2,\,\mathrm{out}}$ is given in (2.40) [114].

$$H_{2,\,\mathrm{out}} = \frac{P_{\mathrm{elec}}}{H_{\mathrm{low}}}\eta_{\mathrm{elec}} \tag{2.40}$$

Here P_{elec} is the electrical power required to operate the electrolyzer. η_{elec} is the efficiency of the electrolyzer and is assumed to be 70 percent [114]. H_{low} is the low heating value of hydrogen used as fuel (33.33 kWh/kg) [115]. The amount of heating released by the combustion of a specific amount of a substance is referred to as the heating value [116]. The chemical energy will be converted into electrical energy in the fuel cell. Electrolyzed hydrogen is injected into a fuel cell, which turns the hydrogen fuel into electrical and thermal energy. Fuel cells come in a variety of forms, including polymer electrolyte membrane fuel cells (PEM), solid oxide fuel cells (SOFC), alkaline fuel cells, and so on [117]. PEM is chosen in this investigation because of its capacity to operate flexibly at low temperatures. The fuel cell in the present study will act as micro combined heat and power (CHP) unit. The output power of the fuel cell P_{FC} is dependent on the hydrogen consumption, low heating value, and efficiency of the fuel cell η_{FC} as given in (2.41) [114]. Note that the stoichiometry factor is assumed to be 1.1 considering the standard conditions (T°=20 °C, p° =1,01325 bar) [118].

$$P_{\mathrm{FC}} = H_{\mathrm{low}}\, H_{2,\mathrm{FC}}\, \eta_{\mathrm{FC}} \tag{2.41}$$

The efficiency of the fuel cell is assumed to be 60 percent [114]. The efficiency assumes that peripheral losses concerning fuel cells are included in the efficiency. The heat produced by the micro-CHP is used to fulfill the heating demands alongside other sources. The produced and recovered fuel cell heat Q_{FC} used for the heating purpose is given by (2.42).

$$Q_{\mathrm{FC}} = P_{\mathrm{FC}}\left(\frac{1-\eta_{\mathrm{FC}}-\Theta_{\mathrm{FC}}}{\eta_{\mathrm{FC}}}\right) \tag{2.42}$$

The heating efficiency is represented by the Θ_{FC}. The electrolyzer's output hydrogen will be stored in the hydrogen storage and fed to the fuel cell when needed. As a result, hydrogen should be bound with the electrolyzer hydrogen output when charging the hydrogen storage $H_{2,\,\mathrm{HC}}$. In the same way, the hydrogen discharge $H_{2,\,\mathrm{HD}}$ should not exceed the

hydrogen delivered to the fuel cell. Hydrogen charge and discharge affect the energy content in terms of hydrogen storage E_{HESS}.

$$0 \leq \gamma_{\mathrm{H},2} H_{2,\,\mathrm{HC}}(t) \leq P_{\mathrm{elec,cap}} \tag{2.44}$$

$$0 \leq \gamma_{\mathrm{H},1} H_{2,\,\mathrm{HD}}(t) \leq P_{\mathrm{FC,cap}} \tag{2.45}$$

$$\gamma_{\mathrm{H},1} + \gamma_{\mathrm{H},2} \leq 1 \tag{2.46}$$

$$0 \leq E_{\mathrm{HESS}}(t) \leq E_{\mathrm{HESS,\,cap}} \tag{2.47}$$

$$0 \leq E_{\mathrm{HESS,\,cap}} \leq E_{\mathrm{HESS,\,max}} \tag{2.48}$$

$$E_{\mathrm{HESS}}(t+1) = E_{\mathrm{HESS}}(t) + (H_{2,\mathrm{HC}}(t) - H_{2,\mathrm{HD}}(t)) \tag{2.49}$$

γ_{H} is introduced as a binary variable to avoid hydrogen energy storage charging ($H_{2,\mathrm{HC}}$) and discharging $H_{2,\,\mathrm{HD}}$ at the same time. The hydrogen produced by the electrolyzer must be equal to the hydrogen consumed by the fuel cell $H_{2,\mathrm{FC}}$ and hydrogen energy storage system as given in (2.50). The hydrogen losses in hydrogen storage are neglected in the current study.

$$H_{2,\,\mathrm{HC}} + H_{2,\mathrm{FC}} - H_{2,\,\mathrm{out}} = 0 \tag{2.50}$$

The fuel cell and electrolyzer are bounded with a rated power capacity of the component as given by (2.51)-(2.54).

$$0 \leq P_{\mathrm{FC}}(t) \leq P_{\mathrm{FC,cap}} \tag{2.51}$$

$$0 \leq P_{\mathrm{elec}}(t) \leq P_{\mathrm{elec,cap}} \tag{2.52}$$

$$0 \leq P_{\mathrm{FC,cap}} \leq P_{\mathrm{FC,max}} \tag{2.53}$$

$$0 \leq P_{\mathrm{elec,cap}} \leq P_{\mathrm{elec,max}} \tag{2.54}$$

Here, the $P_{\mathrm{FC,cap}}$ and $P_{\mathrm{elec,cap}}$ are the rated power capacity of the fuel cell and electrolyzer, respectively.

2.8 Electrical energy storage model (EESS)

The EESS transfers energy from periods of firm renewable energy generation to periods of energy scarcity, allowing the Microgrid to operate under a wide range of operational conditions. The EESS operation should ensure that consumers are adequately supplied. The charged or discharged condition at a specific time defines the EESS operation. More detailed

types of available electrical energy storage systems are given in Annex B.4. A stationary lithium-ion battery is considered as electrical energy storage for the microgrid due to the benefits given in Annex B.4. The capacity of the battery capacity $E_{\text{EESS, cap}}$ in kWh is given by the constraint (2.55) and (2.56).

$$0 \leq E_{\text{EESS}}(t) \leq E_{\text{EESS, cap}} \tag{2.55}$$

$$0 \leq E_{\text{EESS, cap}} \leq E_{\text{EESS, max}} \tag{2.56}$$

where, E_{EESS} is the energy content of the battery. The energy content of the battery depends on the battery charging P_{BC} and discharging P_{BD} in the current time step *t*. Furthermore, the amount of energy from the previous time step *t*-1 needs to be considered. The energy content of the battery is given in (2.57).

$$E_{\text{EESS}}(t+1) = E_{\text{EESS}}(t) + \eta_{\text{BC}} P_{\text{BC}}(t) - \frac{P_{\text{BD}}(t)}{\eta_{\text{BD}}} \tag{2.57}$$

where, η_{BC} and η_{BD} are the efficiency of the energy storage system during charging and discharging respectively. The charging and discharging must be constraint by the rated power of the battery inverter $P_{\text{EESS,cap}}$ as given in (2.58) and (2.59).

$$0 \leq \gamma_{\text{B,2}} P_{\text{BC}}(t) \leq P_{\text{EESS,cap}} \tag{2.58}$$

$$0 \leq \gamma_{\text{B,1}} P_{\text{BD}}(t) \leq P_{\text{EESS,cap}} \tag{2.59}$$

γ is introduced as a binary variable to avoid energy storage charging and discharging simultaneously as given in (2.60).

$$\gamma_{\text{B,1}} + \gamma_{\text{B,2}} \leq 1 \tag{2.60}$$

The rated power capacity of the inverter is bunded with the maximum allowed inverter capacity $P_{\text{ESS, max}}$ as given in (2.61).

$$0 \leq P_{\text{EESS,cap}} \leq P_{\text{EESS, max}} \tag{2.61}$$

The state of charge SOC of the battery energy storage at any time step *t* is given by (2.62).

$$SOC(t) = \frac{E_{\text{EESS}}(t)}{E_{\text{EESS, cap}}} \tag{2.62}$$

2.9 Thermal energy storage model

Thermal energy storage systems are classified as sensible heat storage, latent heat storage, and thermochemical heat storage. The hot water tank, which is based on the sensible heat of water, is one of the most frequent energy storage technologies. Further information on the available thermal energy storage technologies can be seen in Annex B.5. A heating device heats water outside or within an insulated tank, where it is held for a limited duration. The amount of energy stored is determined by the temperature of the hot water and the size of the tank. The tank insulation determines the heat losses and storage time. A general model for thermal energy storage is used for the microgrid. It is assumed that thermal energy storage can provide the required temperature described in section 2.6. The capacity of the thermal energy storage capacity $E_{\text{TESS, cap}}$ in kWh is given by the constraint (2.63),(2.64), and (2.65).

$$0 \leq \gamma_{\text{T,2}} E_{\text{TESS}}(t) \leq E_{\text{TESS, cap}} \tag{2.63}$$

$$0 \leq \gamma_{\text{T,1}} E_{\text{TESS, cap}} \leq E_{\text{TESS, max}} \tag{2.64}$$

$$\gamma_{\text{T,1}} + \gamma_{\text{T,2}} \leq 1 \tag{2.65}$$

Where E_{TESS} is the energy content of thermal energy storage. γ_{T} is the binary variable to avoid charging and discharging at the same time. The thermal storage is connected to the heat grid of the microgrid. Due to this, the source for the thermal charging Q_{TC} and discharging Q_{TD} is possible by the heat pump and fuel cell. The charging and discharging from thermal energy storage are given in (2.65) and (2.66).

$$0 \leq Q_{\text{TC}}(t) \leq Q_{\text{TESS}} \tag{2.65}$$

$$0 \leq Q_{\text{TD}}(t) \leq Q_{\text{TESS}} \tag{2.66}$$

Here the Q_{TESS} is the input heat from the heating sources of the microgrid. The energy content of the thermal energy storage is given by (2.67).

$$E_{\text{TESS}}(t+1) = E_{\text{TESS}}(t) + \eta_{\text{QC}} Q_{\text{TC}}(t) - \frac{Q_{\text{TD}}(t)}{\eta_{\text{QD}}} \tag{2.67}$$

2.10 Wind generation modeling

The power production from the wind energy system is highly dependent on the wind speed v in m/s. Due to this, proximity must be considered in the process of input data selection. The capacity constraint for wind generation is given in (2.68).

$$0 \leq P_{\mathrm{w}}(t) \leq P_{\mathrm{w,n}}(t) P_{\mathrm{wind,cap}} \tag{2.68}$$

Here, P_{W} is the normalized available electrical power that can be extracted from the wind. The constraint makes sure that the production is only available if the wind is blowing. The active power output of the turbine P_{w} is calculated based on the wind speed recorded data of DWD [119]. P_{w} is calculated as given in (2.69) and then normalized by min-max normalization [120]. Which is the most frequent approach for data normalization. The smallest value of the characteristics is turned into a zero, while the highest value is turned into a one using this procedure. The normalized wind power is given in (2.69) [121].

$$P_{\mathrm{w,n}}(t) = 0.5 \rho_{\mathrm{w}} A_{\mathrm{w}} C_{\mathrm{p}} (v(t))^3 \tag{2.69}$$

Here ρ_{w} is the density of the air in kg/m^3, C_{p} is the Betz value, and A_{w} is the rotor area. The capacity limit constraints related to the wind generation model are given by (2.70).

$$0 \leq P_{\mathrm{wind,cap,}} \leq P_{\mathrm{wind,max}} \tag{2.70}$$

2.11 PV system

The PV system capacity depends on the Ground Coverage Ratio (GCR) and the roof area. The GCR is the total PV area divided by the total system area. The PV area is the surface area of all PV modules, and the total system area is the area of the system on the roof, including space between modules. The system size is limited to the available roof area. The tilt angle and GCR are related to each other as an increase in the tilt angle required more distance between two modules to avoid the shading effect. So, increasing the tilt angle results in decreasing GCR. The optimal tilted angle for the PV module is 30$^{\mathrm{o}}$ south oriented with a GCR of 50 percent [122]. The output of the PV production depends on the solar irradiance, tilted surface, the ambient temperature. The total irradiance of Germany from 1980 to 2010 was approximately 1055 kWh/m^2 per year. To get complete coverage, the building's roof with slope should be inclined North-south with an inclination of 30$^{\mathrm{o}}$ to 40$^{\mathrm{o}}$. This mechanism will increase production by 15 percent compared to the horizontal surface [122]. The rated PV production is calculated based on pre-establish methods in (2.71) [123].

$$P_{\mathrm{PV,max}} = G \eta_{\mathrm{M}} P_{\mathrm{R}} A_{\mathrm{PV}} \tag{2.71}$$

where G represents the horizontal irradiance in W/m^2, η_{M} refers to the solar module efficiency, P_{R} shows the complete system performance ratio and A_{PV} is the total PV area. Solar irradiance depends on the solar modules' location, azimuth, and inclination. The SunPower module efficiency of solar panels is higher in today's market. The module efficiency of

SunPower solar panels is from 19.1 percent to 22.2 percent. A module efficiency of 19.1 percent is assumed with the standard test conditions, which is defined as a horizontal irradiance of 1000 W/m^2 for a module temperature of 25 °C [124]. A performance ratio of 85 percent is assumed, with an inverter efficiency of 97 percent for a transformer-less inverter [65]. The total PV area for the areas described in section 2.1 is given by (2.72) [110].

$$A_{\mathrm{PV}} = A_{\mathrm{R}}\, GCR \tag{2.72}$$

where A_{R} is the total roof area. GCR is the ground coverage ratio, and it is assumed as 75 percent. The optimal capacity of the PV system is constrained as given in (2.74). The PV generation in a time step must not be greater than the allowed limit and respect the irradiance profile as given in (2.73).

$$0 \leq P_{\mathrm{PV}}(t) \leq P_{\mathrm{Irr}}(t) P_{\mathrm{PV,cap}} \tag{2.73}$$

$$0 \leq P_{\mathrm{PV,cap}} \leq P_{\mathrm{PV,\,max}} \tag{2.74}$$

3 E-mobility infrastructure

The planning of e-mobility for the microgrid planning and operation is performed in three steps. First of all, the rise in the number of EVs is forecasted for different scenarios. Considering the occupancy time, the number of EVCS is modeled based on the rise in the number of EVs and charging behavior. Finally, a placement algorithm is incorporated to find the best place for the number of EVCS. The structure of this section is presented in Figure 3.1.

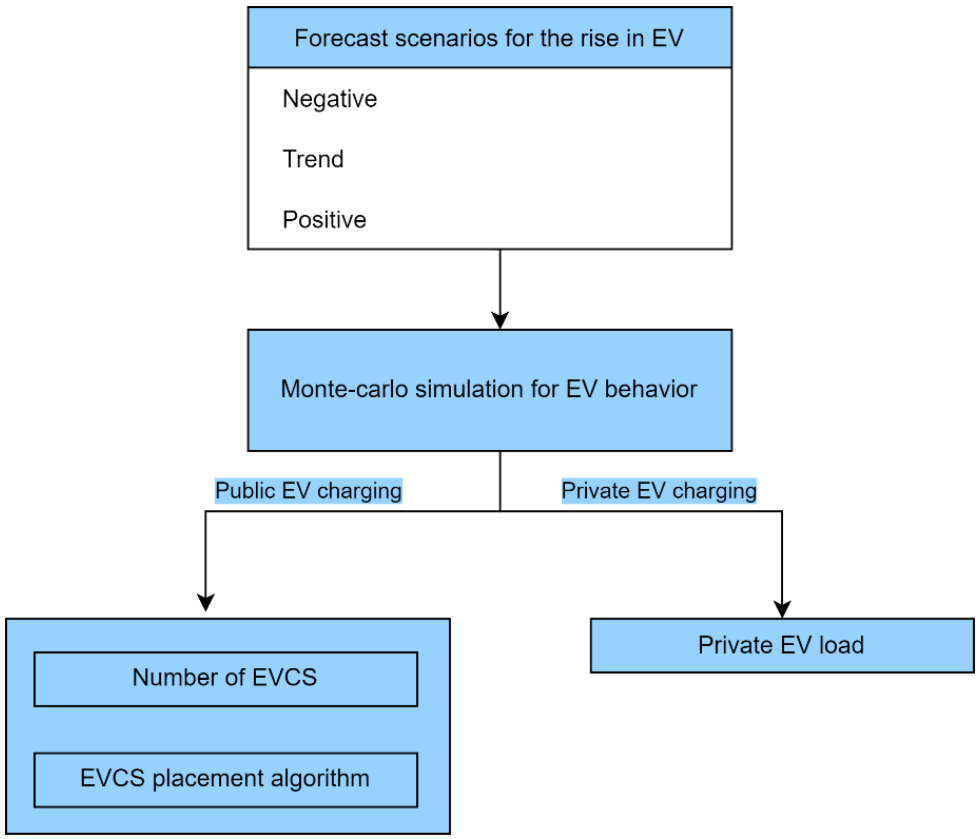

Figure 3.1 Proposed methodology for e-mobility infrastructure

3.1 Forecast for the rise in the number of EVs based on retropolation

The first step is to develop a future scenario for the number of EVs for e-mobility infrastructure planning. The number of EVs is essential to deciding the number of EVCS. To analyze the rising EVs, a scenario-based method is used. To distinguish the rise of EVs, the following three scenarios have been developed:

- Positive
- Trend
- Negative

The key factor is to define the realization of these scenarios consistently and completely. It is assumed that the development of EVs over the conventional vehicle is dependent on the following factors:

- Investment cost
- Operational cost
- Driving benefit
- Additional benefits

The development of scenarios based on key factors is given in Table 3.1.

Table 3.1 Development of EV based on key factors

Key factor	Negative	Trend	Positive
Investment cost	Cost targets do not reach until later. In 2026, electric vehicles will be even more expensive. The federal government did not extend the funding (poor costs/benefits; more investments in public transport or other technologies)	Production costs fall through technology improvements, learning, and economies of scale, especially battery prices. It is expected that cost parity will be reached by 2026. Around 300,000 vehicles are to be subsidized	Cost targets reach much earlier (e.g., 2023). Therefore, cost advantages in 2026. The federal government continues to subsidize vehicles to accelerate the turnaround in traffic
Operational cost	Energy costs rise, CO_2 tax rises moderately, and vehicle tax is levied. Insurance and repairs are a little more expensive as compared to combustion engines	Energy costs rise despite lower production costs for renewables, and vehicle tax remains exempt for ten years. The advantage of CO_2 tax increases (higher CO_2 prices with a simultaneous reduction in CO_2 intensity of electricity). Insurance, wear and tear, and repairs are also not so expensive	Energy costs decrease. CO_2 tax rises dynamically, and vehicle tax exemption remains. Insurance and repairs become cheaper based on empirical values
Driving benefits	For reasons of efficiency, acceleration and driving experience	There are no significant developments in acceleration. The driving range is increasing continuously, more and more fast-	Acceleration and driving experience increase to a more precise distance

Key factor	Negative	Trend	Positive
	are not further developed. Driving range, mileage, and charging time remains lower	charging stations are being set up, and charging time is approaching a vehicle tank duration.	than combustion engines. Excellent driving range than combustion engines. Charging (e.g., by induction) takes place without additional effort
Other benefits	Space is only slightly better in EVs. Similar features to ICE´internm of storage. The number of variants remains lower than combustion engines	Space is increasing moderately through further optimizations. Equipment is becoming more extensive and growing in importance for bi-directional charging. A variety of variants is developed as compared to combustion engines	Significantly more space and better equipment in all EVs. EV is far better in terms of storage. The variety of variants exceeds combustion engines

A trend is identified through literature for each of these factors, and the development of trend scenarios is estimated. The positive and negative scenarios are then computed by shifting the value of the key parameters. Based on the key factors, the scenario development compared to the conventional vehicle is shown in Table 3.2 [125].

Table 3.2 assessment of the key factor to generate scenario for 2026

Key factors	Positive	Trends	Negative
Investment cost	EV better	EV neutral	EV worse
Operational cost	EV much better	EV better	EV marginal better
Driving benefit	EV better	EV neutral	EV worse
Another benefit	EV better	EV neutral	EV marginal better
Assumed EV share	55%	40%	20%

Table 3.2 illustrates how the EV outperforms the traditional vehicle. These assumptions rebased on the EV registered. If the EV is better in these factors, it will be bought and registered more. The assumed EV share is assumed based on the hypothesis. Due to this, these shares can be flexible to be changed.

To implement retropolation for the next five years, the share of EVs must be assumed in 2026. The share of EVs compared to conventional vehicles in 2026 is known from Table 3.2. Once the number of EVs in 2026 is known, the number of EVs from 2022 to 2026 is developed through retropolation. Retropolation is the technique to connect the future with the current scenarios shown in Figure 3.2 [126]. The meaningful trend analysis leads to planning the future through retropolation.

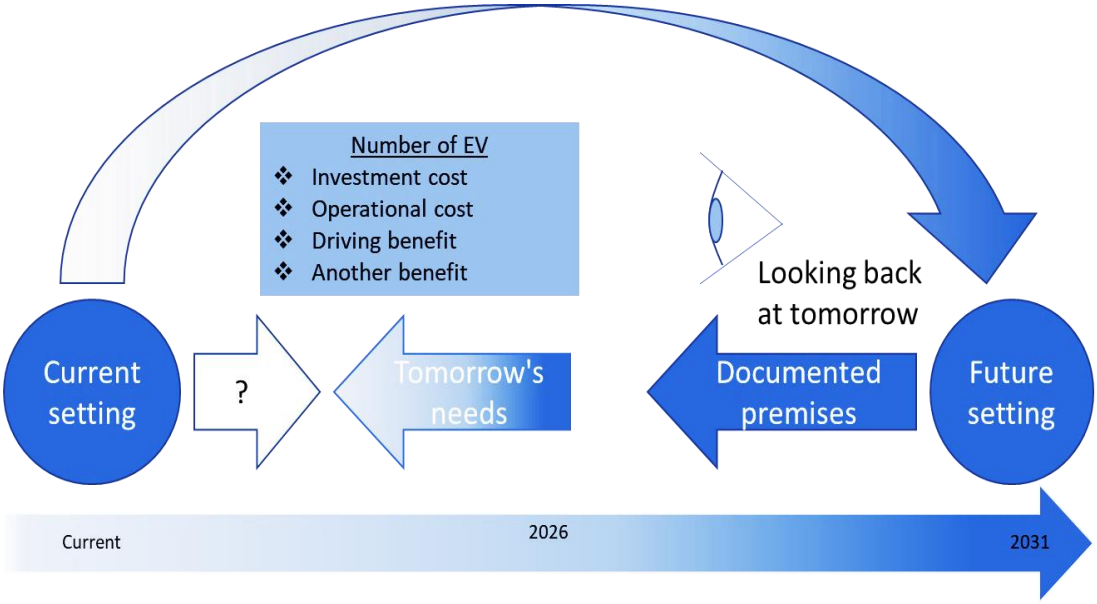

Figure 3.2 Retropolation method

The basis for these calculations is the new registrations and stock figures from the Federal Motor Transport Authority Germany. It is initially assumed that the new registrations and stock figures will remain constant (2020: 2.9 million new registrations with 47.7 million cars in stock) [127]. The forecast for the number of EVs is considered to grow exponentially due to user adoption. Due to this, the exponential growth function for the rise in the number of EVs (N_{EV}) in a year (y) in the planning horizon is shown in (3.1).

$$N_{\mathrm{EV}} = X_{\mathrm{o}}(\mathcal{M})^{\tau} \tag{3.1}$$

where X_{o} is the number of EVs in the initial year. τ is the difference between the current year y_{current} and the initial year y_{initial}. The initial year is considered to be 2020 in the present study, and the current year will be changing on the planning horizon. $\mathcal{M}$ is the rate at which the rise of the EV can reach 20 percent for negative, 40 percent for trend, and 55 percent for the positive scenario. The value of $\mathcal{M}$ can be calculated by rearranging equation (3.1) and solving it with the base value of 2020 for N_{EV} and X_{o}. The value of $\mathcal{M}$ is 1.067, 1.198, and 1.263 for the negative, trend, and positive, respectively. The rising rate of the EV based on equation 3.1 and Figure 3.2 is shown in Figure 3.3.

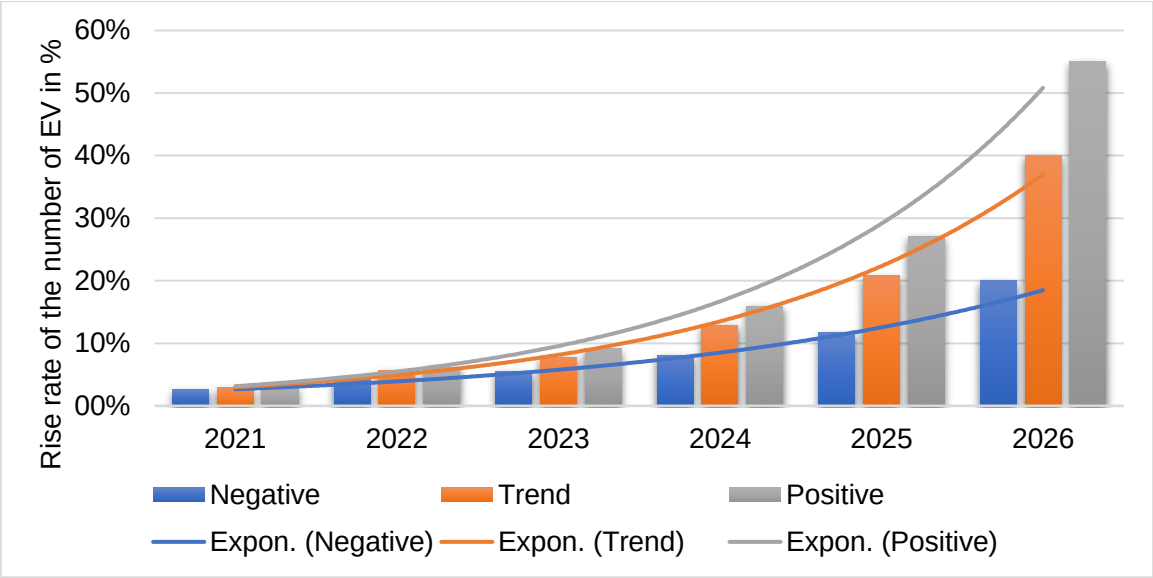

Figure 3.3 rise rate of the EVs in different scenarios based on retropolation

In addition to these scenarios, trend extrapolations from 2025 to 2030 were set up based on previous developments. By applying the above-described method, the rise in the number of new registration of EVs in Germany based on retropolation is shown in Figure 3.4.

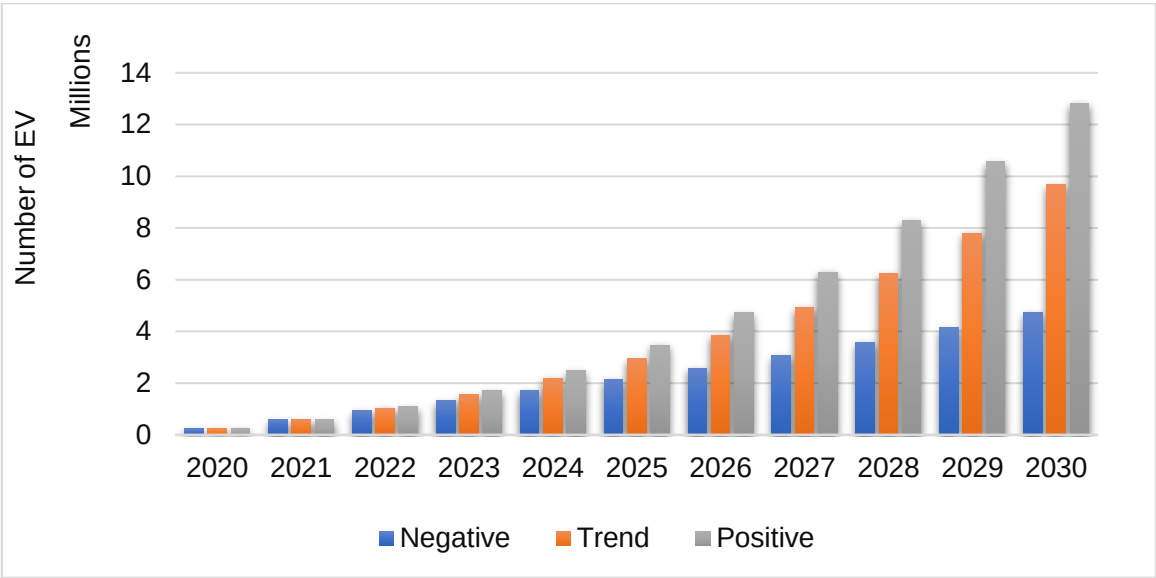

Figure 3.4 The rise of EVs in Germany based on retropolation and extrapolation

3.2 Electric vehicle behavior using Monte-Carlo simulation

The EV can be in three different states. It can be traveling, charging, or parked without charging. Due to the EV owner's random decision parameters, it is nearly impossible to predict these states at any given time step. Parameters such as the number of trips, arrival time, departure time, kilometers traveled in a trip, duration of a trip, and power consumption according to speed are some of the EV owner's random decisions. Due to this, these

parameters must be considered as random as much as possible. The Monte-Carlo simulation is used to model the EV behaviors to consider the randomness. A Monte-Carlo simulation is a stochastic method that generates a set of random numbers and handles the random number in a simulation for a series of repeated times. A detailed explanation of the Monte-Carlo simulation can be seen in Annex C.1.

Nonetheless, examining as many random variables as possible in terms of EV behaviors would be preferable. Still, some of them must be fixed to avoid high complexities. The characteristics such as the number of trips, power cost per kilometer, and EV battery state of charge socEV required to travel are regarded as fixed parameters in the current studies. Whereas the arrival times, kilometers traveled, and duration of travel are assumed to follow a distribution. The distribution has mostly resulted from a detailed traffic model of Burg city, located in Germany. To mimic the behavior of EV based on these distribution functions, a distribution fit that is formed with the existing probability distribution functions must be implemented. Annex C.1 shows the most common types of probability distribution functions. In the current study, the survey data from the traffic model is used for the probability distribution fit and Monte-Carlo simulation [128]. The traffic model has been developed together with Mr. J. Brinken, according to [125]. Based on the Burg traffic model, the EV arrival distribution is distinguished for district type. Annex C.2 shows the EV arrivals for various types of districts. The traffic data need to be fitted with the available probability distribution functions to simulate the EV load based on these parameters. For a settlement area classified as a residential area with a small number of shops and markets, the following distribution function and related distribution fit are displayed in Figure 3.5.

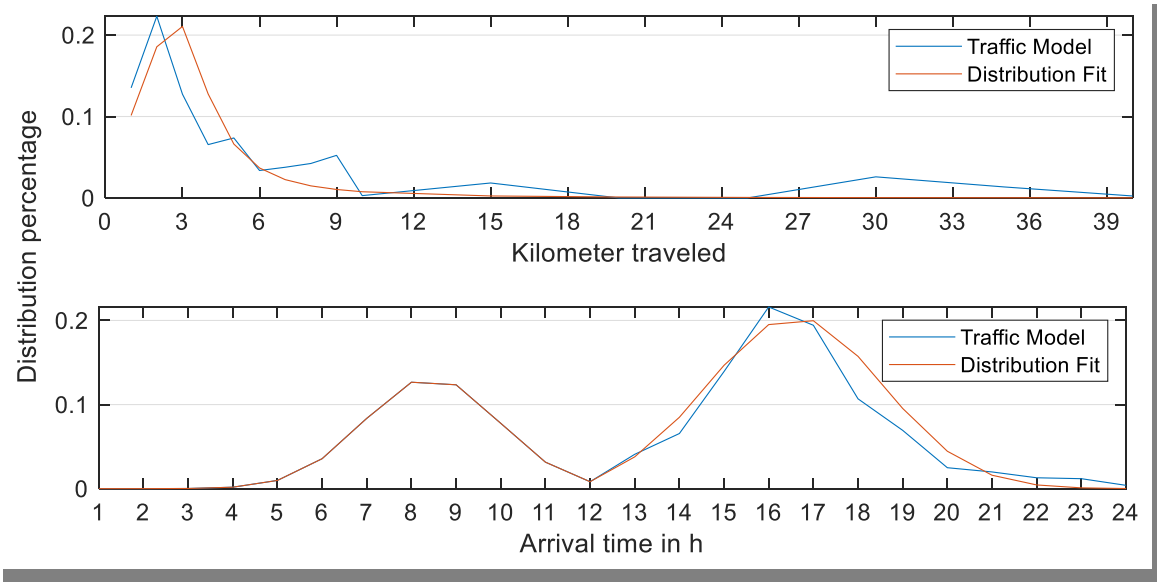

Figure 3.5 Traffic model and distribution fit for a residential area [125,128,129]

The kilometer traveled and duration of travel have heavier tails. Due to this, the t-Location-scale distribution fit is the most suitable fit with a high confidence level. The distribution fit for the duration of travel is shown in Annex C.2.

The arrival time is distributed with arrivals in the morning and arrivals in the evening. In both cases, the best fit is considered as the normal distribution. Note that Monte-Carlo simulation for EV behavior is assumed to be deterministic as it follows one true distribution and runs for a one-year scenario to make a charging behavior for the number of EVs known from section 3.1. The arrival of EVs is divided into the following two categories:

- Private charging: The EVs are charged from home
- Public charging: The EVs are charged from the EVCS

The EV behavior simulation method is given in Figure 3.6.

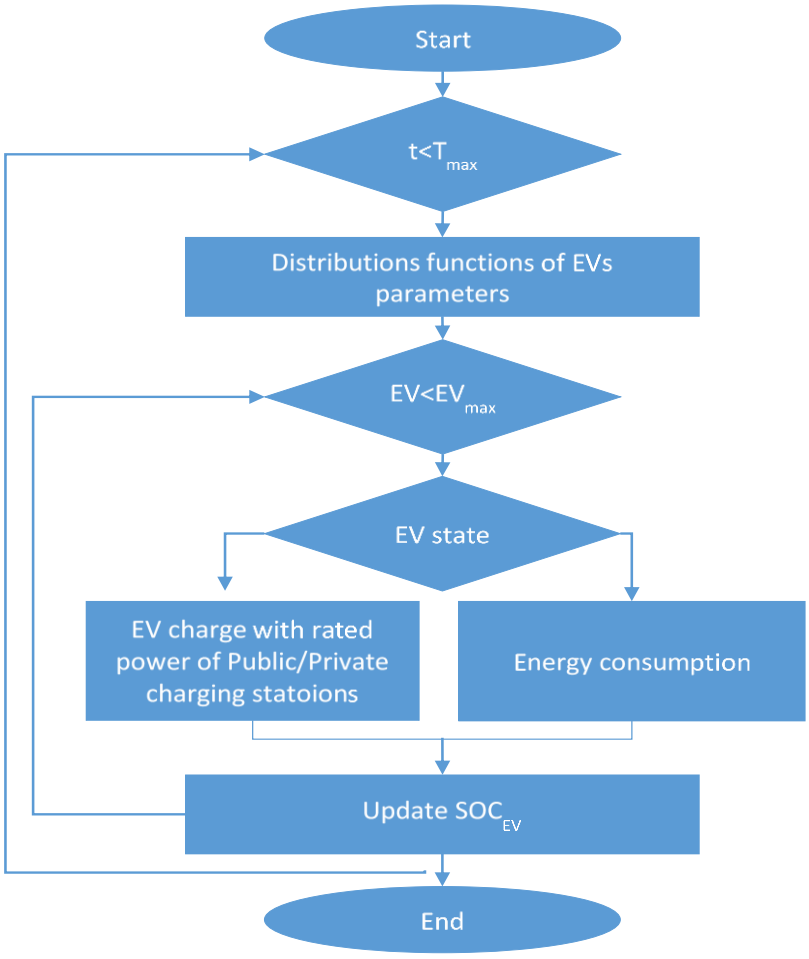

Figure 3.6 Method for EV behaviors

It is assumed that 15 percent of the time, the EV will charge from public EVCS [130]. According to this theory, 85 percent of EVs arriving at a time step will charge privately, while the

remaining 15 percent will charge publicly. The precise EVs that will charge from private and public charging stations are picked randomly. The distribution of private charging stations in the electrical network is linear and even, with a ratio determined by the total number of (anticipated) electric vehicles and network connection nodes. If the ratio is *n*, a private EV charging station with a rated power of 11 kW is placed in the n^{th} node of the grid. The nodes can have more than one private charging station depending on the number of EVs and the available nodes.

It is assumed that the EV charge with the rated charging power EVCS. From 3.6, once these parameters are defined, an EV can be categorized as either charging or traveling during these times. When traveling, the change in the State of Charge of the EV battery (soc_{EV}) is calculated as given in (3.2), where E_{cons} is the energy consumption of the EV during the time of travel (tr).

$$soc_{\mathrm{EV},t} = soc_{\mathrm{EV},t-1} - \frac{E_{\mathrm{cons},\,tr}}{E_{\mathrm{EV,bat}}} \tag{3.2}$$

Here, $E_{\mathrm{EV,bat}}$ is the rated capacity of the battery of the electric vehicle. The energy consumption of an EV is calculated by multiplying the consumption per kilometer and kilometer traveled. A value of 0.1922 kWh per kilometer has been used [131]. If the soc_{EV} during the charging state is smaller than 0.9, the EV is charged with a rated power of EVCS (P_{EVCS}). The EV is charged until the charging time (t_{ch}) or soc_{EV}=1 is reached. A 22 kW EVCS is assumed in the present study for public charging, and 11 kW is used for private charging. At the time of charging, the soc_{EV} is determined according to (3.3).

$$soc_{\mathrm{EV},t} = soc_{\mathrm{EV},\,t-1} + \frac{P_{\mathrm{EVCS}}\, t_{\mathrm{ch}}}{E_{\mathrm{EV,\,bat}}} \tag{3.3}$$

Aside from component modeling, the methodology for estimating the increase in the number of electric vehicles is offered. Based on the forecast methodology, the microgrid is planned deterministically and stochastically.

3.3 Model for the occupancy time for public electric vehicle charging station

The critical deciding factor for the number of public EVCS will be the number of EVs arriving at the charging station at a given time instant and how many of them can wait. A detailed model has been developed for charging stations based on occupancy. The number of EVCS is dependent on several parameters, such as location, usage, and budget, among others. In the current study, the usage of EVCS is highlighted as the most important parameter. The usage

of EVCS is highlighted in terms of the period when the EV occupies the EVCS. This period is referred to as occupancy time in the current study. The occupancy time is defined as the times in which EVs are already connected to EVCS, and another EV is expecting a time slot. The novelty of the proposed model is the relationship between the number of charging stations and the occupancy time.

The mathematical optimization models consist of an objective function that is either minimized or maximized, and constraints need to be satisfied. On the other hand, simulation studies the behavior of a real-world system by representing the system by a mathematical or theoretical approach. In some cases, optimization gives better results, while simulation has the upper hand in plans that have a complex structure. Since occupancy time is a function of multiple variables, modeling such processes is complex and unpredictable. A case is considered where the number of charging stations is decided by modeling it as an optimization problem. In that case, the objective is to minimize cost while the constraint will be limiting the occupancy time every hour. The optimizer would choose the charging station without considering the occupancy time because the best value for determining the acceptable occupancy time is ambiguous. The occupancy time for an EVCS should be calculated by an iterative process depending on the EV behaviors described in section 3.2. However, a change in the EV waiting profile is caused by the addition of a new charging station. The optimization will take high computational effort to solve the problem if the iterative method for calculating the occupancy time of EVCS is coupled. The occupancy time concerning three EVs for a single EVCS is shown in Figure 3.7.

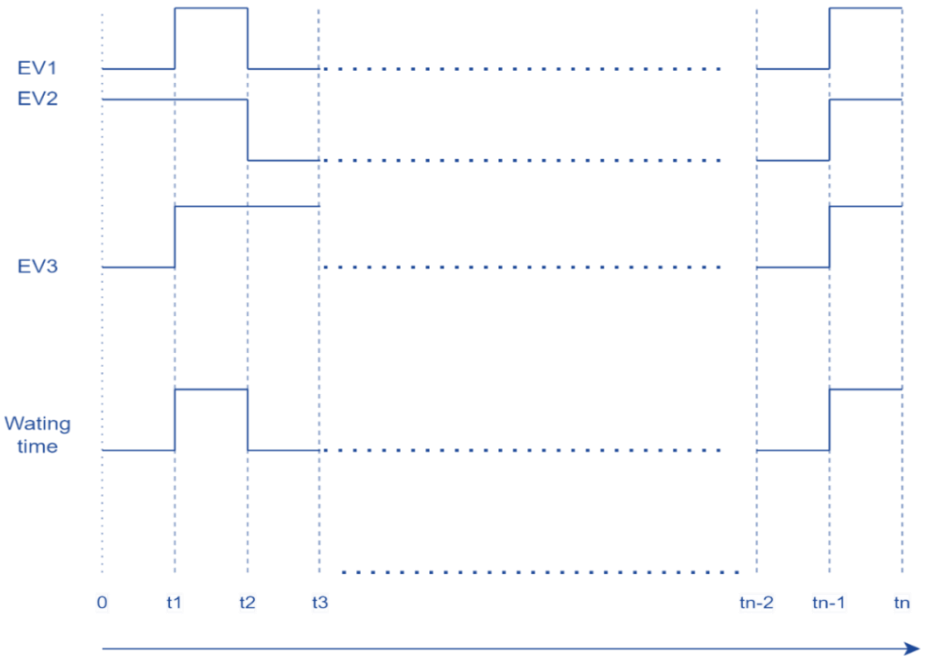

Figure 3.7 Waiting time for EV arriving to charge

If there is only one EVCS, and the number of EVs is high, there will be queues of EVs waiting. Otherwise, the EVCS will be overestimated. Hence the optimal number is needed to have a low investment cost and an acceptable occupancy time. In time step *t1*, three EVs arrive to charge simultaneously on the operation horizon. A single EVCS handles two EVs simultaneously, so the third EV must wait. This waiting time for EVs will determine the occupancy time of the EVCS. From time step t2, the EVCS becomes free and available to be occupied by the following EV. However, the occupancy time becomes zero during this period as there is no EV waiting. Similarly, at time step *tn-1*, three EVs arrived to charge, increasing the waiting time as one EV waited again. Finally, the total times when the EVCS is occupied are averaged per day, and the number of EVCS is determined based on the occupancy time. A detailed description of the model to determine the number of EVCS is given in Annex C.3.

3.4 Placement algorithm for Public EVCS with Monte-Carlo simulation

The next point is to optimally place the public charging infrastructure in the electrical network so that it can be supplied in the best possible way. The EVCS should be consistent and ready to power the EV with its rated power at all times without affecting the critical grid voltage. For that reason, the microgrid electrical power system without any infeed of the DERs is taken into account. This is a kind of worst-case consideration to take care of the critical under voltage is avoided after placement

Using the power flow as described in section 2.4, the sensitivity of the voltage to EVCS load is computed with the node voltage-sensitive index (NVSI). The Newton-Raphson method is used to calculate the power flow. A single EVCS station with a rated power of 22 kW is placed on a node of the grid. In addition, apart from the nodes where EVCS is connected, all other nodes of the grid have no associated EVCS. In the next step, the voltages for all nodes of the grid are calculated to find the NVSI of this node. The procedure has been repeated for every grid node. The NSVI has been used for optimal distributed generation (DG) placement and load-shedding algorithms in literature [131,132]. The calculation of NVSI for an EVCS-connected node (i) is stated in (3.4).

$$NVSI_i = \sqrt{\frac{\sum(U_{\mathrm{N}} - U_{\mathrm{j}})^2}{n}} \qquad \forall i \in j \;\; \forall j \in n \qquad (3.4)$$

Here, U_{j} is the matrix containing all the voltage for the nodes of the entire grid resulting after EVCS is placed at i^{th} node. In the next step, when the EVCS is placed on $i + 1^{\mathrm{th}}$ node, the

values of entire U_j will be changed. Due to this, different sensitive values can be realized from equation 3.4. n is the number of total nodes and U_N is the nominal voltage and n is the total number of nodes. The Monte-Carlo simulation is deployed to identify the best configurations, as shown in Figure 3.8.

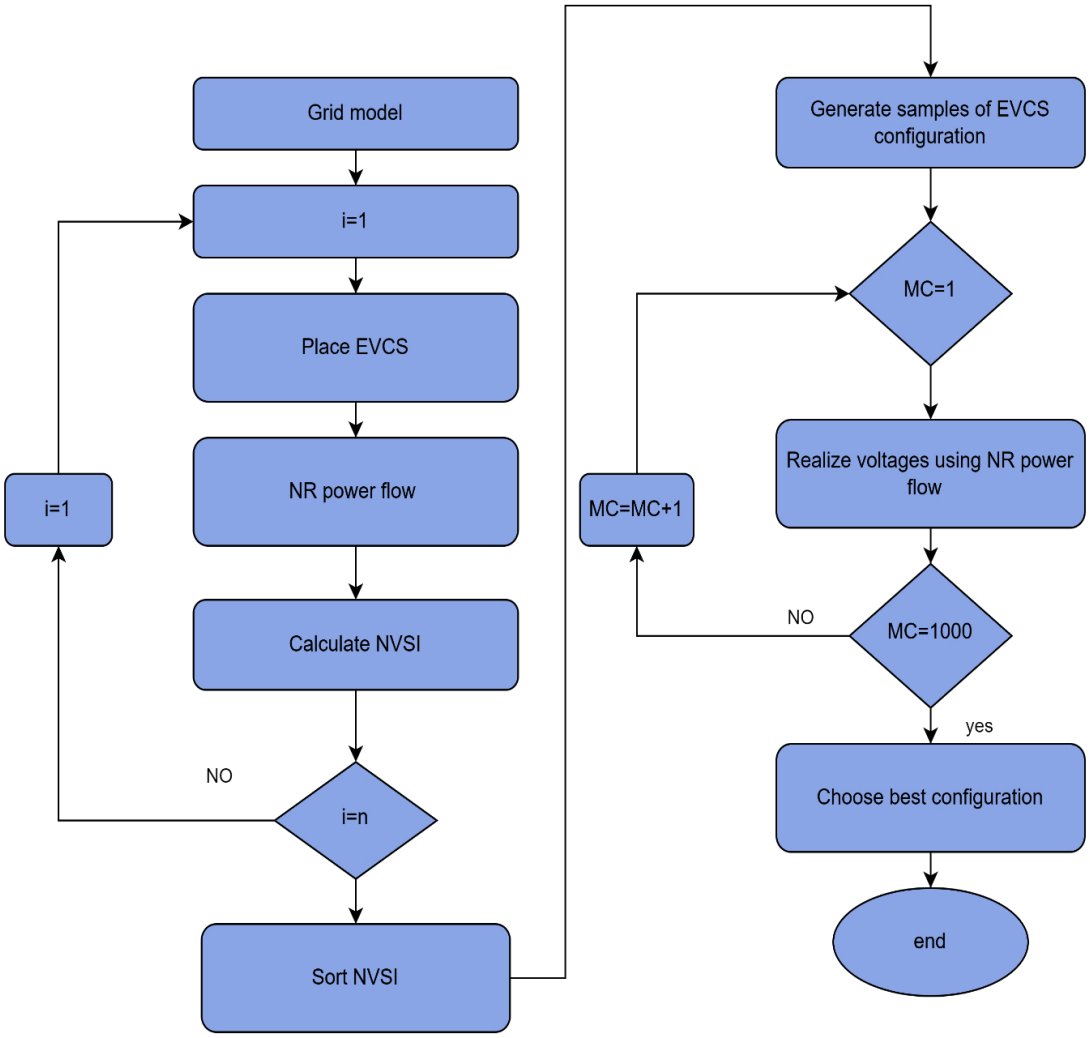

Figure 3.8 EVCS placement algorithm

The goal is to place the EVCS in the least sensitive nodes to the high load. Due to this, the node with the highest NVSI is the worst node, and the node with the least NVSI is the best node for the EVCS connection. The appropriate location for the EVCS is calculated after the best and worst nodes are found using NVSI. If there is just one EVCS, the node with the lowest NVSI is the optimal spot to deploy the EVCS. For two or more EVCS, however, the optimal node configuration must be determined. This is due to the fact that installing EVCS on some nodes, even those with low sensitivity, might result in a significant voltage drop across the string. The following are the reasons behind this:

- The EVCS-associated nodes may belong to the same string.
- The EVCS is deployed on a node that can only support the installation of EVCS in a certain configuration with other nodes.

The configuration is defined as the arrangement of the number of EVCS over the available nodes. First of all, the best nodes based on the sorted NVSI are taken. Then samples of configuration for the best nodes are generated for the number of EVCS known from section 3.3. The samples of possible configurations will be equal to the number of Monte-Carlo simulation runs. For each configuration, the voltage is recorded. The sample configuration resulted in the best possible voltage being treated as optimal. The configuration which gives the voltage below 380 V at any node is discarded. The best configuration of nodes for EVCS is decided based on the quantification of voltages. The EV load behavior described in section 3.2 is used as input to depict the EVCS load. The more Monte-Carlo iteration searches, the more configuration on the cost of higher computational time. For an EVCS placement, the installation of EVCS is subject to available places, e.g., parking places, and the use case, e.g., near markets or public transport. Due to this, there should be a variety of configuration results. Decision-makers will then use these methods to know the suitable area and the electrical power nodes to power the EVCS. In the present study, the placement of EVCS is proposed in the ten best configurations, and the first configuration is used to place the EVCS.

4 Optimization Methodology

The optimization for microgrid planning and operation is used to get an ultimate settlement area with minimum possible cost (Investment and operational) and CO_2 emissions. The optimization for microgrid planning and operation is performed in a deterministic and stochastic manner. In the current study, deterministic optimization is employed to propose a microgrid for a new settlement area where the aim is to handle the development of e-mobility with minimum cost and emission. However, it is expected that e-mobility will be developed with associated uncertainties. The use of uncertainties (randomness) in modeling the optimization approach is the major difference between stochastic and deterministic methods. The deterministic optimization, which is expected to be more cost-effective, can not realize these uncertainties resulting in an un-robust or semi-robust microgrid. Due to this, stochastic microgrid planning and operation are proposed for the decision-makers, where the aim is a robust settlement area. The robustness will increase the cost of handling more uncertainties which is not a good solution. Due to this, the combined optimization model is proposed to get high robustness with minimum cost for planning a new settlement area, as shown in Figure 4.1.

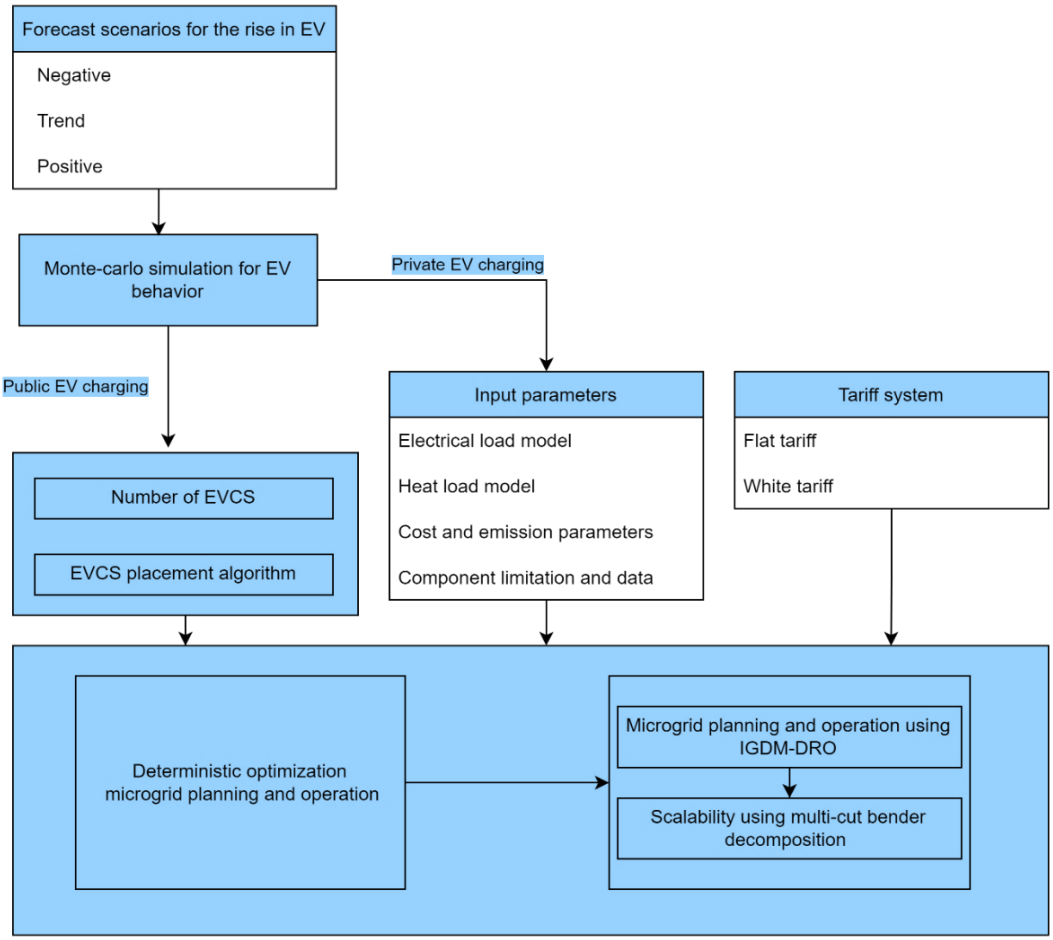

Figure 4.1 Proposed optimization methodology

Furthermore, both approaches (deterministic and stochastic) contain novel methods, as described in section 1.2. Microgrid planning and optimization are based on a novel concept for the growth of e-mobility infrastructure. The parameter value and the initial conditions define the model's output in deterministic models. The stochastic model has uncertainties, which means that the same set of parameter values and initial conditions will produce distinct outputs. After the input parameters, such as electrical and heat loads are modeled, the E-mobility infrastructure is determined as described in section 3. The microgrid planning and operation are performed with a planning horizon (Y) of 10 years and with an operation horizon of 1 year. The 1-hour time step is used. A multi-stage approach is used to tackle the planning challenge. Each choice is made based on the present operation horizon's problem, as shown in Figure 4.2.

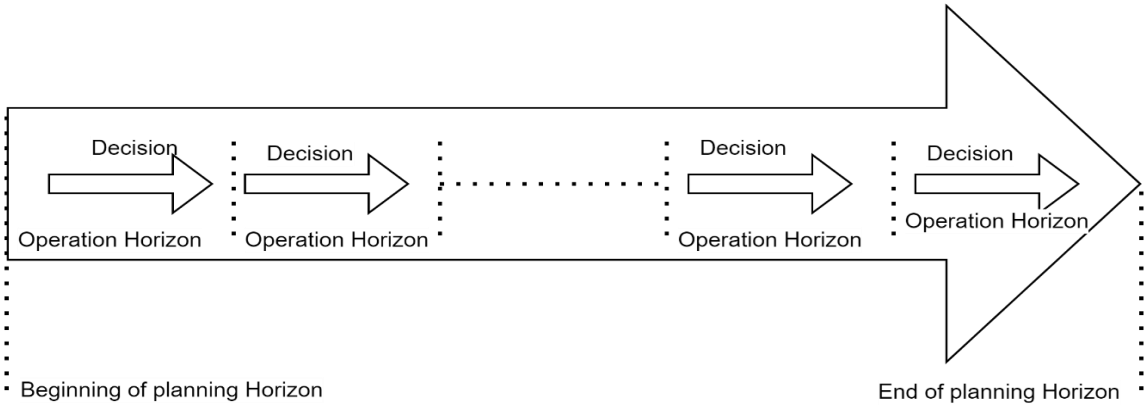

Figure 4.2 The planning method

The capacities for the DERs are optimally decided in each operation horizon, as shown in Figure 4.2. The operating horizon is then added to the planning horizon to produce the planning horizon. It is assumed that the capital and operational cost will not change in the planning horizon. Furthermore, it is assumed that the electrical and heating grid structure will not be changed for the planning horizon. For optimal planning and operation, the cost parameter of the DERs used in the present study is given in Table 4.1.

Table 4.1 Cost parameter of DERs

DERs	**Terms**	**Values**
PV	Capital cost	800 €/kW[133]
	life	20 years[134]
Wind	Capital cost	1460 €/kW [133]
	life	20 yeas [135]
BESS	Capital cost	528 €/kWh [136]
	life	8 years [136]
	Efficiency	95 % [136]
TESS	Capital cost	200 €/kWh [137]
	life	20 years [138]
	Efficiency	65%[139]

HESS	Capital cost life	150 €/m^3 [140] 10 years [139]
HP	Capital cost life	700 €/kW [141] 20 years [142]
Fuel cell	Capital cost life Efficiency	5738 €/kW[143] 60000 hours [144] 60 % [114]
Electrolyzer	Capital cost life Efficiency	238 €/kW[145] 60000 hours[145] 70 % [114]
EVCS	Capital cost life	10000 Euro/EVCS[146] 10 years[147]

The maintenance cost is assumed to be 1 percent of the capital cost [148]. The German government plans to increase the cost of CO_2 certificates [149]. The trend for the cost of CO_2 per tonne is given in Figure 4.3, and the emission intensity of the electrical grid is shown in Figure 4.4.

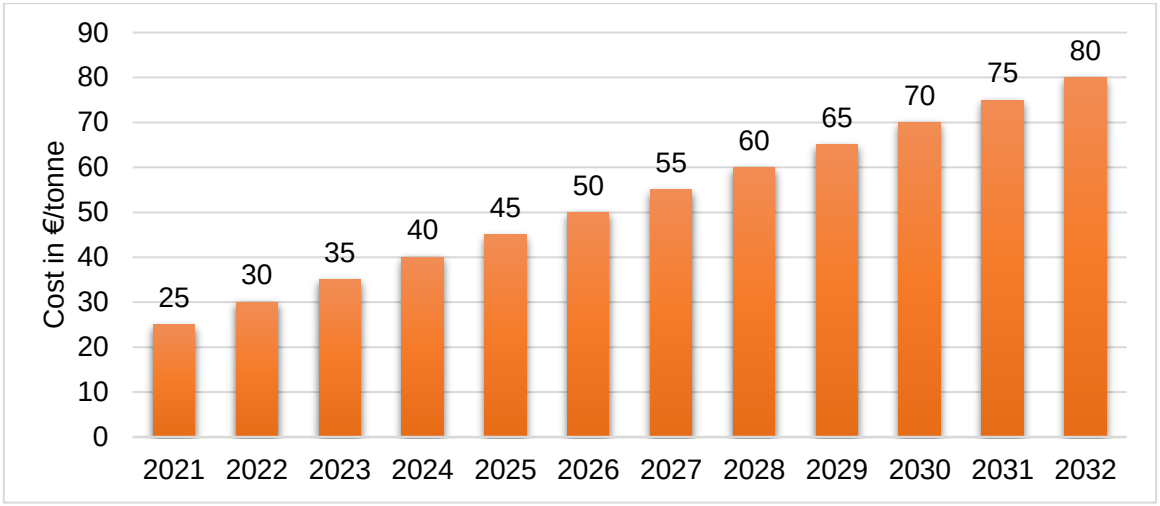

Figure 4.3 Trend for the cost of CO_2 certificates per tonne [149]

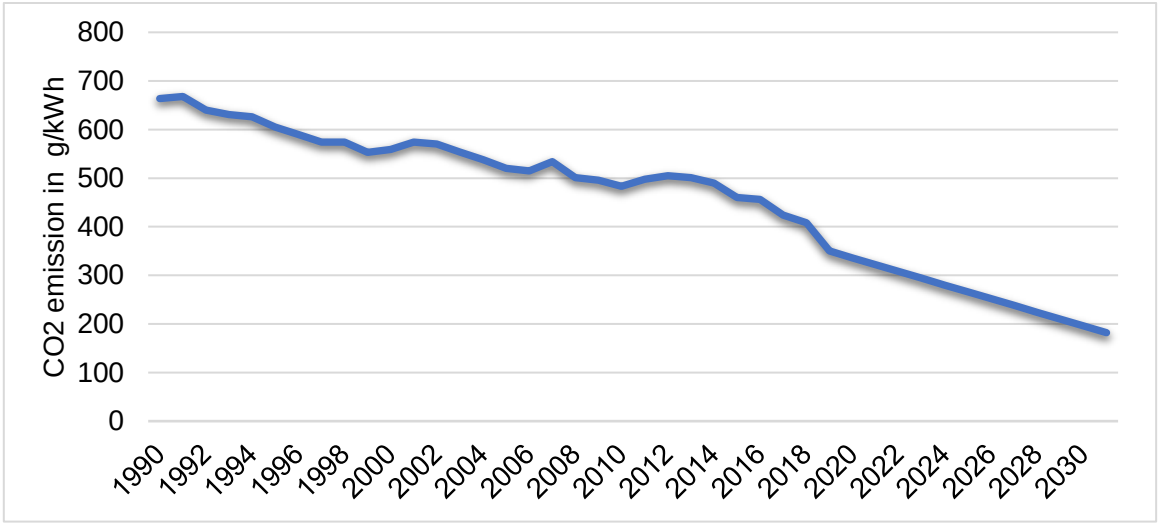

Figure 4.4 GHG emission by electricity grid based on [150]

In the present study, it is assumed, according to Figure 4.3, that CO_2 price will increase by 5 Euros per tonne per year throughout the planning horizon. CO_2 is assumed to be emitted from the electricity grid. The CO_2 is decreasing per year for the electricity grid, as shown in Figure 4.4. The average decrease in GHG was recorded as 4 percent per year from 1990 till 2021. Due to this, in the present study, it is assumed that this trend will continue to form the whole planning horizon. The penalty cost related to CO_2 emission for the microgrid is associated with all DERs especially CO_2 emitted during the manufacturing process. Moreover, the highest share is associated with the electricity grid. Due to this, the CO_2 emission associated with the manufacturing process of DERs is ignored in the present study.

4.1 Deterministic optimization method

Depending on the kind of problem, the deterministic optimization technique focuses on finding the global minimum or maximum. Deterministic optimization is classified as linear programming (LP), mixed-integer linear programming (MILP), non-linear programming (NLP), and mixed-integer nonlinear programming (MINLP). The optimization problem is made up of two parts: an objective function that defines the problem's goal and constraints that must be met. Constraints are depicted as component model restrictions in the microgrid planning and operation problem, as discussed in section 2. The objective of the deterministic model is to decrease the investment cost C_{inv}, operational cost C_{op} and the penalty cost per tonne of CO_2 emissions $C_{\text{penalty, CO}_2}$ for the microgrid as given in (4.1).

$$\text{Min} \sum_{y} \left(C_{\text{inv}} + C_{\text{op}} + C_{\text{penalty, CO}_2} \right) \qquad \forall y \in Y \qquad (4.1)$$

The investment cost of the DERs for each year (y) is the product of the annual capital cost and the capacity of the particular DERs as given in (4.2).

$$C_{\text{inv}} = C_{\text{PV}} P_{\text{PV,cap}} + C_{\text{w}} P_{\text{wind,cap}} + C_{\text{EESS}} E_{\text{EESS,cap}} + C_{\text{HP}} P_{\text{HP,cap}} + C_{\text{TESS}} E_{\text{TESS,cap}} + C_{\text{FC}} P_{\text{FC,cap}} + C_{\text{elec}} P_{\text{elec,cap}} + C_{\text{H}} E_{\text{HESS,cap}} \qquad (4.2)$$

The operation cost is subject to power import from the electricity grid (P_{grid}), and annual operational cost of DERs ($C_{\text{op, DERs}}$) given in (4.3).

$$C_{\text{op}} = \sum_{DERs} C_{\text{op,DERs}} P_{\text{DERs}} + \sum_{t} (C_{\text{grid}} P_{\text{grid}}) \qquad \forall t \in T \qquad (4.3)$$

$$DERs \in [PV, WIND, EESS, HP, TESS, FC, ELEC, HESS]$$

C_{grid} is the energy import cost from the electrical grid in €/kWh. The emission intensity parameter for the electricity grid (EM_{Grid}) is assumed from Figure 4.4. The emission objective is given in (4.4).

$$C_{\text{penalty,CO}_2} = C_{\text{EM}}\left(EM_{\text{grid}} \sum_{t} P_{\text{grid}}\right) \qquad \forall t \in T \qquad (4.4)$$

Where C_{EM} is the cost of CO_2 emission and determined by Figure 4.3. The deterministic optimization model is subjected to the constraint described in section 2. Based on the occupancy time, the number of EVCS is known from section 3.3, and the number of EVCS is incorporated in the energy balance constraint in the deterministic optimization model. For a fixed occupancy time, the capital cost of the already-known number EVCS is added to the final cost of the microgrid after the optimization is solved. The energy balance constraint is given in (4.5)

$$P_{\text{PV}}(t) + P_{\text{w}}(t) + P_{\text{grid}}(t) + P_{\text{BD}}(t) + P_{\text{FC}}(t) - P_{\text{Load}}(t) - P_{\text{BC}}(t) \qquad \forall t \in T \qquad (4.5)$$
$$- P_{\text{elec}}(t) - P_{\text{HP,in}}(t) - P_{\text{EVCS}}(t) = 0$$

The deterministic approach used in this study will give proper planning and operation for the microgrid e-mobility infrastructure. However, the uncertainties related to e-mobility can not be realized. To consider the uncertainties, the stochastic approach is used.

4.2 Stochastic optimization method

In the stochastic approach, the following two optimization techniques are often used:

- Stochastic programming (SP)
- Robust optimization (RO)

Stochastic programming uses a scenario-based approach such as Monte-Carlo simulation to incorporate the uncertainty. As a result, it depends on the number of scenario trials. Stochastic programming with a high number of stochastic trials becomes intractable. On the contrary, Robust optimization uses a worst-case analysis. Taking only the worst-case analysis is beneficial in terms of computational time but deficient in terms of better realization of uncertainty. To bridge the gap between stochastic programming and robust optimization, distributional robust optimization (DRO) has gained popularity in literature, with uncertainty based on ambiguity sets rather than scenarios. The following types of uncertainties are crucial in microgrid planning and operation:

- Long-term Uncertainty: As discussed in section 3, the increase in the number of EVCS is dependent on a variety of factors. As a result, a flawless forecast for the planning horizon is almost unattainable.
- Short-term Uncertainty: The number of electric vehicle arrivals for charging is largely unpredictable. As a result, predicting the EV charging profile is difficult.

The SP, RO, and DRO are tools for quantifying uncertainty based on historical data, such as a distribution function. As a result, these strategies are appropriate for dealing with short-term uncertainty. The best method to incorporate short-term uncertainty is said to be DRO. However, the essential information needed to create an uncertainty model is missing in the long-term Uncertainty section. The prior trend for the number of EVCS is provided. However, it cannot be guaranteed that the pattern will be continued. As a result, an approach like the information gap decision method (IGDM) has to be adapted to the long-term incorporation of uncertainty. The proposed methodology for stochastic microgrid planning and operation is shown in Figure 4.5.

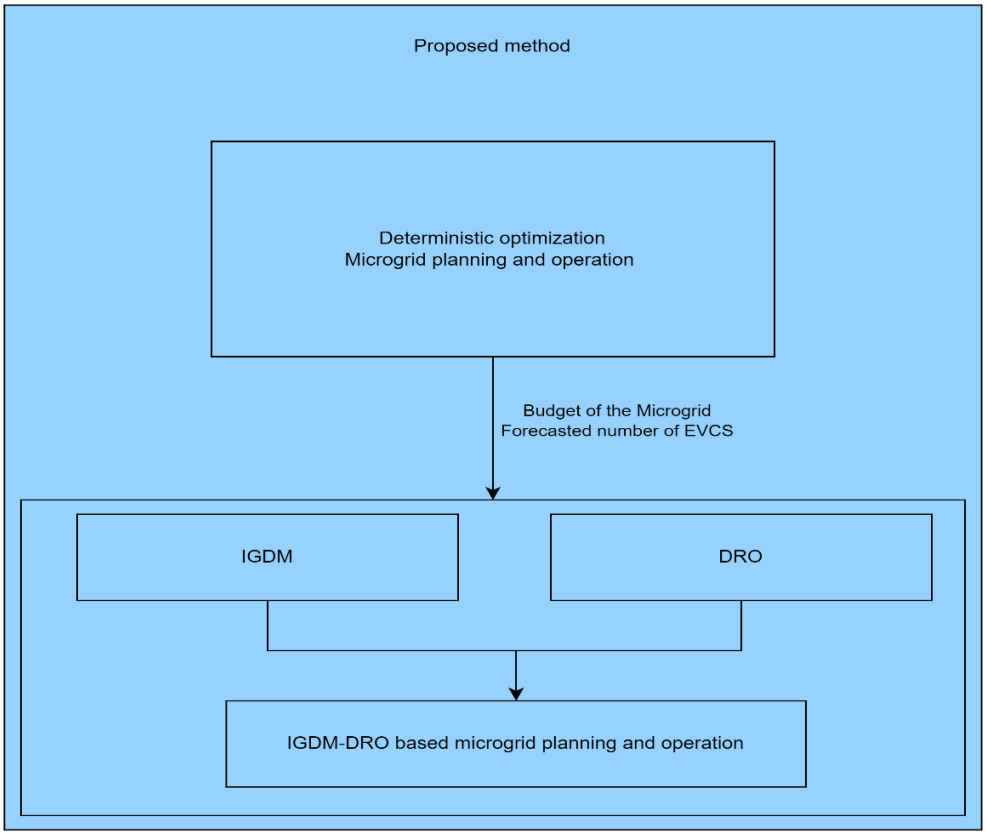

Figure 4.5 Proposed methodology for stochastic microgrid planning and operation

In this dissertation, a novel approach (IGMD-DRO) is proposed for microgrid planning and operation based on the idea that multi-type uncertainties (long and short-term) will have a significant impact on microgrids. If technical problems such as voltage problems owing to

uncertainties are neglected, the uncertainties are proportional to the cost of the microgrid in principle. Indirectly, it may be inferred that endless uncertainties can be handled as long as the cost budget is limitless. Due to this, it will be more efficient to consider the cost budget parameters, which is a result of the deterministic optimization model.

For EVCS-based optimal planning and operation of DERs, the model employs IGDM, which solely considers long-term uncertainty. Similarly, DRO-based optimal planning and operation for DERs have emerged from just considering short-term uncertainty about EV arrivals.

4.2.1 Long-term uncertainty modeling using IGDM

The IGDM is a non-probabilistic decision theory for sorting alternatives and making decisions and judgments in the face of extreme uncertainties [151]. Further information about the IGDM can be seen in Annex D.1. The key benefit of utilizing IGDT is that it allows the decision-maker to specify the values, which protects him from the risk of not meeting the minimal criteria due to uncontrolled parameter uncertainties. These criteria are assessed using the robustness function.

EVCS plays an important role in microgrid planning and operation. The number of EVCS is still low. However, the rise in the EVCS is inevitable. In the current study, it is assumed that the number of EVCS is subject to high uncertainty. If the uncertainty is considered too high, it will be assumed that no historical data, such as a probability distribution function, is available to generate an uncertainty set. The only available data is the forecasted number of EVCS, which can be taken from section 3.3. There is an information gap since there is a lack of historical beginning data to generate the uncertainty set for the growth in the EVCS. A limitation approach known as a bound method is necessary to determine the uncertainty region of information gaps uncertainty sets. In the current study, the envelope-bound method has been used to create the uncertainty set for the number of EVCS [58,152]. Unlike robust optimization, the uncertainty set has one unknown variable, the uncertainty region, or more accurately, the radius of the uncertainty zone. The radius of the uncertainty region for the number of EVCS is called α_{EVCS} in the present study. The α_{EVCS} will show the gap between the predicted number of EVCS (N_{EVCS}) and the uncertain number of EVCS ($\widehat{N}_{\mathrm{EVCS}}$). The radius of the uncertainty region needs to decrease or increase depending on the problem types (risk seeker or risk-averse). A detailed explanation of problem types is given in Annex D.1. The decision-makers in this study are supposed to prioritize the safe and secure planning and operation of microgrids over maximizing paybacks. As a result, the notion is referred to as the risk-averse approach, and it should be expressed as the maximum of the uncertainty region

(α_{EVCS}). The envelope-bound formulation to create the uncertainty set for the number of EVCS is given in (4.6).

$$\Gamma(\alpha_{\mathrm{EVCS}}, N_{\mathrm{EVCS}}) = \{\widehat{N}_{\mathrm{EVCS}}: |\frac{\widehat{N}_{\mathrm{EVCS}} - N_{\mathrm{EVCS}}}{N_{\mathrm{EVCS}}}| \leq \alpha_{\mathrm{EVCS}} \qquad \forall N_{\mathrm{EVCS}} \in \Gamma(\alpha_{\mathrm{EVCS}}, N_{\mathrm{EVCS}}) \tag{4.6}$$

Here Γ shows the uncertainty set and $\widehat{N}_{\mathrm{EVCS}}$ is the uncertain variable that shows the rising trend of the EVCS in the planning years. To define the region of uncertainty for the number of EVCS, α_{EVCS} is bounded as given in (4.7).

$$0 \leq \alpha_{\mathrm{EVCS}} \leq 1 \tag{4.7}$$

A zero-uncertainty region ($\alpha_{\mathrm{EVCS}} = 0$) means that there is no uncertainty, and the predicted number of EVCS is equal to the actual number of EVCS. While full-uncertainty region ($\alpha_{\mathrm{EVCS}} = 1$) means that there is severe uncertainty, and the predicted number of EVCS is equal to the upper bound of the uncertainty region. The upper and lower bounds of the uncertainty region are bounded by an envelope as shown in (4.8) [58]. All of the uncertainty associated with the number of EVCS is considered to have happened exclusively inside this region of the envelope.

$$(1 - \alpha_{\mathrm{EVCS}})N_{\mathrm{EVCS},} \leq \widehat{N}_{\mathrm{EVCS},} \leq (1 + \alpha_{\mathrm{EVCS}})N_{\mathrm{EVCS}} \tag{4.8}$$

When considering the uncertainty associated with the number of EVCS, the objective function for IGDM-based microgrid planning and operation is regarded as a risk-averse strategy and provided by (4.9).

$$\mathrm{Max}\, \alpha_{\mathrm{EVCS}} \tag{4.9}$$

The constraints of the optimization model are subject to component constraints given in section 2. The uncertainty region can be increased to any level as it is directly related to the number of EVCS installations. However, this resulted in high costs, which is not optimal. Finally, the robust region needs to be maximized while the cost needs to be minimized, which results in the two-level optimization problem. However, the cost objective can be transformed into a cost budget constraint which should be less than the allowed budget f_b of the microgrid as given in (4.10), (4.11), and (4.12).

$$\sum_{y} \left(\hat{C}_{\mathrm{inv,y}} + C_{\mathrm{op,y}} + C_{\mathrm{penalty,\ CO_2}}\right) \leq f_b \tag{4.10}$$

$$\hat{C}_{\text{inv}} = C_{\text{PV}}\, P_{\text{PV, cap}} + C_{\text{W}}\, P_{\text{wind,cap}} + C_{\text{EESS}}\, E_{\text{EESS, cap}} + C_{\text{HP}}\, P_{\text{HP,cap}} + C_{\text{TESS}}\, E_{\text{TESS,cap}} + C_{\text{FC}}\, P_{\text{FC,cap}} + C_{\text{elec}}\, P_{\text{elec,cap}} + C_{\text{H}}\, E_{\text{HESS,cap}} + C_{\text{EVCS}}(1 + \alpha_{\text{EVCS}})\, N_{\text{EVCS}} \quad (4.11)$$

$$\hat{C}_{\text{inv}} = C_{\text{PV}}\, P_{\text{PV, cap}} + C_{\text{W}}\, P_{\text{wind,cap}} + C_{\text{EESS}}\, E_{\text{EESS, cap}} + C_{\text{HP}}\, P_{\text{HP,cap}} + C_{\text{TESS}}\, E_{\text{TESS,cap}} + C_{\text{FC}}\, P_{\text{FC,cap}} + C_{\text{elec}}\, P_{\text{elec,cap}} + C_{\text{EVCS}} N_{\text{EVCS}} + C_{\text{EVCS}} \alpha_{\text{EVCS}} N_{\text{EVCS}} \quad (4.12)$$

$\hat{C}_{\text{inv}}$ is the investment cost after the consideration of uncertainty. The allowable budget is associated with the microgrid's deterministic cost, which is the objective function of the deterministic optimization model, as described in section 4.1. The allowable budget can also be tuned as per the requirement of the decision-makers. The minimum allowable budget is equal to the deterministic cost of the microgrid, while 100 percent is equal to two times the deterministic cost of the microgrid. In the stochastic optimization model, the number of EVCS is decided by the optimization according to the involved uncertainties. Due to this, from equation (4.12), the term $\alpha_{\text{EVCS}} N_{\text{EVCS}}$ are decision variables, due to which the optimization program becomes bilinear, resulting in mixed-integer nonlinear programming. The bilinear terms have been linearized by the McCormick method [58,153]. The linearization of bilinear terms is linearized in the same way as described in [58]. The term N_{EVCS} need to be converted to a series of binary variables E and a continuous integer i as given in (4.12). The variable i can take a value from one to the maximum number EVCS. The maximum number of EVCS may be deduced from the fact that the number of EVCS will always be fewer than this amount. The location of binary digit 1 is significant in determining N_{EVCS} in equation (4.13) because binary variables can only accept the binary digit 1 once in the array. As a result, there should only be one binary number 1 in the whole array, with the rest being 0 as given in (4.14). The number of EVCS will be *n* if the binary array's n^{th} position is 1.

$$N_{\text{EVCS,y}} = \sum_{\text{i=1}}^{N_{\text{EVCS,max}}} i E_{i,y} \qquad \forall\, E_{i,y} \in \{0,1\} \quad (4.13)$$

$$\sum_{\text{i=1}}^{N_{\text{EVCS,max}}} E_{i,y} = 1 \quad (4.14)$$

After the continuous integer $N_{\text{EVCS,y}}$ is transformed into continuous binary variables, the term $\alpha_{\text{EVCS}} N_{\text{EVCS}}$ is thus transformed as given in (4.15).

$$\alpha_{\mathrm{EVCS}} N_{\mathrm{EVCS,y}} = \sum_{\mathrm{i}=1}^{N_{\mathrm{EVCS,max}}} i\alpha_{\mathrm{EVCS}} E_{i,y} \qquad \forall E_{i,y} \in \{0,1\} \qquad (4.15)$$

Let say $\tilde{\alpha}_{\mathrm{EVCS}} = \alpha_{\mathrm{EVCS}} E_{i,y}$ then by using the McCormick linearization method [58], the linearized bilinear terms are as follows,

$$0 \leq \tilde{\alpha}_{\mathrm{EVCS}} \leq E_{i,y} \qquad \forall E_{i,y} \in N_{\mathrm{EVCS,max}} \qquad (4.16)$$

$$\alpha_{\mathrm{EVCS}} + E_{i,y} - 1 \leq \tilde{\alpha}_{\mathrm{EVCS}} \leq \alpha_{\mathrm{EVCS}} \qquad (4.17)$$

At this stage, considering the long-term uncertainty, the optimization problem for microgrid planning and operation is solved with the objective function described in equation (4.9). The IGDM-based microgrid planning and operation are subject to all the constraints related to the microgrid components described in section 2. Furthermore, the constraints described in this section need to be included.

4.2.2 Short-term uncertainty modeling based on DRO

To integrate short-term uncertainty related to the electric vehicle charging profile, a different method has been used, as stated in section (1.2.2). In stochastic programming, it is assumed that the decision-makers have complete knowledge of short-term uncertainties through a known PDF [154]. In the case of EV arrivals, the known PDFs can be seen in Figure 3.5 in section 3.2. On the contrary, in robust optimization, the decision-maker does not know the uncertainties, and the worst case is analyzed, due to which this method is conservative [155]. In the present study, the number of EV arrivals for charging is taken into account as short-term uncertainty. The DRO is employed over the RO to avoid conservative outcomes and to make use of the advantages of the available PDF stated in section 3.2. Furthermore, the DRO is employed instead of stochastic programming to save computational time and effort. It's worth noting that the nature of the uncertain parameter differs greatly between robust and stochastic perspectives. Nonetheless, by adopting a distributionally robust formulation instead of an adversarial or stochastic formulation, both views, adversarial and stochastic, may be united. It assumes that the uncertain parameter's distribution is ambiguous.

A stochastic perspective relates to an ambiguity set consisting of a singular distribution. The worst-case formulation can be captured by an ambiguity set consisting of all distributions. As a result, the worst-case distribution ambiguity set allows for simultaneous analysis of the robust and stochastic perspectives [156]. Further information regarding DRO can be seen in Annex D.2. Ambiguity sets can be classified as moment-based and metric-based, as described in Annex D.2 [157]. In the present study, the moment-based is used to model the ambiguity

set. The moment-based ambiguity set is defined as the family of all distributions that belong to the same moment, such as mean and standard deviation [158]. Two moments, mean and variance, have been used in the present study. When the mean and variance from the historical data are known, the ambiguity set for the arrivals of EVs can be expressed in (4.18)

$$\Omega^1_{\mathrm{EV,t}} = \left\{ \chi \in \Omega^0_{\mathrm{EV,t}}(EV^1_{\mathrm{t}}) \middle| \begin{matrix} \chi\{EV_{\mathrm{t}} \in EV^1_{\mathrm{t}}\} = 1 \\ E_\chi\{EV_{\mathrm{t}}\} = \mu_{\mathrm{t}} \\ E_\chi\{(EV_{\mathrm{t}} - \mu_t)^2\} = \sigma^2_{\mathrm{t}} \end{matrix} \right\} \tag{4.18}$$

Where μ_{t} is the mean and σ^2_{t} is the variance of the survey data for the arrivals of EVs, as described in section 3.2. $\Omega^0_{\mathrm{EV,t}}$ is the family of distribution for EV arrivals. The χ is the probability distribution of the EV arrivals survey EV_{t}. Inspired by the box type ambiguity [159], the moments are bounded with upper and lower bounds as given in (4.19) and (4.20).

$$\mu_{\min} \leq \mu_{\mathrm{t}} \leq \mu_{\max} \tag{4.19}$$

$$\sigma_{\min} \leq \sigma_{\mathrm{t}} \leq \sigma_{\max} \tag{4.20}$$

It is considered that the distribution from the ambiguity set with the highest mean and variance as the worst distribution will have resulted in conservative results. The conservative conclusions will account for all short-term uncertainty but at the cost of capital waste in the microgrid cost and emissions. The conservativeness of the results can be adjusted by introducing a type of constraint called chance constraints. The chance constraint defines the probability of meeting a constraint in the optimization model. The chance constraints are implemented in the power balance equation as the charging related to EV is associated with a type of load. In this case, at a specific degree of confidence $(1-\epsilon)$, the probability $(\mathrm{P_r})$ that the power balancing constraint is achievable where ϵ refers to the tolerance level of the microgrid. The chance constraint for the power balance is given by (4.21).

$$\begin{aligned} \mathrm{P_r}\big\{ & P_{\mathrm{PV}}(t) + P_{\mathrm{w}}(t) + P_{\mathrm{grid}}(t) + P_{\mathrm{BD}}(t) + P_{\mathrm{FC}}(t) - P_{\mathrm{Load}}(t) \\ & - P_{\mathrm{BC}}(t) - P_{\mathrm{elec}}(t) - P_{\mathrm{HP}}(t) - P_{\mathrm{EVCS}}(t) \big\} \geq 1 - \epsilon \end{aligned} \tag{4.21}$$

In the power balance, the arrival of the EV is uncertain, which will make the P_{Load} and P_{EVCS} uncertain. Due to this uncertain load, the power balance will not be met all the time. To avoid this, chance constraint allows the constraint to violate the solution with the probability specified. The chance constraints are considered to be difficult to solve in the optimization methods. The above chance constraint is a non-linear constraint that needs to be incorporated linearly. Furthermore, the chance constraint can be handled in different ways. The linear programing chance constraint (LPCC) is mostly used to handle the probabilistic constraint such

as equation (4.21) [160]. However, the LPCC is limited to cases where the uncertainty is mostly followed by Gaussian distribution [161]. In the current study, the uncertainties related to EV follow two normal distributions which have long tails. Due to this, the chance constraint in equation (4.21) needs to be linearized, convexified, and tractable. Hence, the equation (4.21) can be represented in an approximation in terms of value at risk (VAR) or conditional value at risk (CVAR) [162]. In the present study, the CVAR approach has been taken. The CVAR derivation of the constraint (4.20) is presented in Annex D2.1.

The IGDM-distributional robust optimization problem for the microgrid planning and operation considering multi-type uncertainty is solved with the objective function described in equation (4.8). The IGDM-DRO based microgrid planning and operation is subject to all the constraints related to the microgrid components described in section 2 and section 4.2.1. Furthermore, the constraints described in this section need to be included.

4.2.3 Scalability solution

On the one hand, the computational time in ordinary microgrid planning and operation problems is not significant. The optimization problem, on the other hand, should not be intractable. The computing time for microgrid planning and operation mentioned in section 4.1 is significantly high. Because the computational time grows exponentially with the number of equations and variables, resulting in a non-deterministic polynomial-time often known as an NP-hard problem. However, deterministic microgrid planning and optimization are tractable for a certain size of settlement area.

The problem becomes worse in the case of the stochastic optimization model. The stochastic microgrid planning and optimization model presented in section 4.2 is highly intractable even for small settlement areas. In general, robust optimization is more efficient in terms of computing, but stochastic programming optimization causes intractability. By bridging the gap between robust optimization and stochastic programming optimization, the DRO solves a portion of the problem. However, the implementation of DRO for the current study is still intractable due to the size of the settlement area and the nonlinear constraints. Due to this, a tractable solution is proposed for the stochastic microgrid planning and operation for e-mobility under multi-type uncertainties. Different methods have been used to improve the scalability of optimization models for microgrid planning and operation. The methods consist of model simplifications, fundamental changes in temporal resolution, reductions in solution space, mathematical reformulations, and combinations of these approaches [163]. In the present study, solution space reduction and mathematical reformulation are considered. The solution space reduction is considered by changing the operation horizon in a series of day-

type categories. As established in section 2.2, one investigation year was divided into 14-day types categories. PV, wind, electric vehicles, and loads are expected to fit into these categories. The mathematical reformulation is incorporated in sections 2 and 4.2, such as reformulation for second-order cone programming (SOCP). Furthermore, the optimization model is reformulated by the application of the decomposition method [163]. Decomposition is defined as splitting the mathematical problem into subproblems and then solving them in the iterative method [164].

The optimization problems are made up of some complicated variables and constraints, which add to the complexity of the problem in terms of computing time. These complicating variables and constraints are often called coupling variables and constraints in the literature [165]. The optimization problems are considered to be decomposable if complicating variables can be temporarily fixed or complicating constraints can be relaxed. Among others, the bender decomposition and Dantzig-Wolfe are mostly used for model reformulation. In general, the Dantzig-Wolfe method is appropriate for issues involving complicated constraints, whereas bender decomposition is appropriate for situations involving complicating variables [166]. For the current study, the objective function consists of coupling variables, due to which a bender decomposition is a suitable approach. Equation (4.1) consists of two types of cost, investment and operation (operation and CO_2 penalty cost). The investment costs, which depend on the capacities of the DERs, can be considered as the coupling variables, and the capacities of the DERs can be temporarily fixed. Due to this, the original problem can be decomposed into the investment cost (master problem) and operation cost (subproblem). Bender decomposition was first introduced by Jacques F. Benders in 1962 [167]. The bender decomposition method solves the master problem-based cuts from subproblems iteratively. Due to this, the number of cuts can be important in terms of computational time, as a single cut will result in a slow convergence [154]. The traditional bender decomposition might fail to achieve the required computational efficiency [168,169]. Due to this, acceleration methods are proposed for the bender decomposition [170–172]. Among others, so-called efficient cuts are added to the bender decomposition [173–175]. However, these methods are based on a single cut per iteration of bender decomposition. In the case of microgrid stochastic planning and operation, the problem type allows considering more than one cut per iteration [176]. There can be decomposition by a scenario that allows one cut for each scenario in a stochastic optimization problem which becomes multi-cut per bender iteration [177].

Pursuing the tractability in the current study, the proposed IGDM-DRO is decomposed by the day-type categories using multi-cut bender decomposition. The optimization problem itself

suits to be split up due to its bilevel nature. The operational part of the problem to minimize the operation cost is set to be a subproblem where the complicating variables related to investment cost are fixed, as given in (4.22).

$$\text{Min} \sum_{y} \left(C_{\text{op}} + C_{\text{penalty, CO}_2} \right) \qquad \forall y \in Y \;\; \forall t \in T \quad (4.22)$$

As the capacities of the DERs are complicating variables, the constraint for the subproblem related to capacities is fixed. In the present study, as the subproblem is solved first, the fixed capacities DERs can be achieved by the solution of the deterministic optimization model described in 4.1. The dual variables for the fixed capacities of DERs (ζ) are needed to generate a cut in the master problem. After the first time, when the master problem is solved, the fixed capacities of the DERs are updated for each bender decomposition. The capacities and dual constraints for the capacities of DERs are given as,

$$P_{\text{PV, cap}} = P^{\text{fixed}}_{\text{PV, cap}} \;\; : \;\; \zeta_{P_{\text{PV,cap}}} \quad (4.23)$$

$$P_{\text{wind,cap}} = P^{\text{fixed}}_{\text{wind,cap}} \;\; : \;\; \zeta_{P_{\text{wind,cap}}} \quad (4.24)$$

$$P_{\text{HP,cap}} = P^{\text{fixed}}_{\text{HP,cap}} \;\; : \;\; \zeta_{P_{\text{HP,cap}}} \quad (4.25)$$

$$E_{\text{EESS, cap}} = E^{\text{fixed}}_{\text{EESS,cap}} \;\; : \;\; \zeta_{E_{\text{EESS,cap}}} \quad (4.26)$$

$$E_{\text{TESS, cap}} = E^{\text{fixed}}_{\text{TESS,cap}} \;\; : \;\; \zeta_{E_{\text{TESS,cap}}} \quad (4.27)$$

$$E_{\text{HESS, cap}} = E^{\text{fixed}}_{\text{HESS,cap}} \;\; : \;\; \zeta_{E_{\text{HESS,cap}}} \quad (4.28)$$

$$P_{\text{FC,cap}} = P^{\text{fixed}}_{\text{FC,cap}} \;\; : \;\; \zeta_{P_{\text{FC,cap}}} \quad (4.29)$$

$$P_{\text{elec,cap}} = P^{\text{fixed}}_{\text{elec,cap}} \;\; : \;\; \zeta_{P_{\text{elec,cap}}} \quad (4.30)$$

Apart from the capacity constraint, all other constraints described in section 4.2.2 and the component constraints described in section 2 are part of the subproblem. The master problem still has to maximize the robust region as described in equation (4.9). Equation (4.10) is the relation between capital and operational costs. However, as the complicated variables are fixed, the operational cost terms ($C_{\text{op}} + C_{\text{penalty, CO}_2}$) need to be replaced by an auxiliary variable (λ_c).

$$\sum_{y}\left(\hat{C}_{\text{inv}}+\lambda_{\text{c}}\right)\leq f_{b} \tag{4.31}$$

The auxiliary variable is responsible for making the cuts in the master problem. Considering the multi-cut constraint of the bender decomposition over the bender iteration (*ii*), the auxiliary variable is defined as a constraint as given in (4.32).

$$\begin{aligned}\lambda_{\text{c}}^{\text{ii}} \geq \sum_{y} z_{\text{c}}^{\text{ii}} &+ \sum_{k}\zeta_{\text{PV}}^{\text{ii}}\left(P_{\text{PV, cap}}^{\text{jj}}-P_{\text{PV, cap}}^{\text{ii}}\right) \\ &+\sum_{k}\zeta_{\text{wind,cap}}^{\text{ii}}\left(P_{\text{wind,cap}}^{\text{jj}}-P_{\text{wind,cap}}^{\text{ii}}\right) \\ &+\sum_{k}\zeta_{\text{HP,cap}}^{\text{ii}}\left(P_{\text{HP,cap}}^{\text{jj}}-P_{\text{HP,cap}}^{\text{ii}}\right) \\ &+\sum_{k}\zeta_{\text{EESS,cap}}^{\text{ii}}\left(E_{\text{EESS,cap}}^{\text{jj}}-E_{\text{EESS,cap}}^{\text{ii}}\right) \\ &+\sum_{k}\zeta_{\text{TESS,cap}}^{\text{ii}}\left(E_{\text{TESS,cap}}^{\text{jj}}-PE_{\text{TESS,cap}}^{\text{ii}}\right) \\ &+\sum_{k}\zeta_{\text{HESS,cap}}^{\text{ii}}\left(E_{\text{HESS,cap}}^{\text{jj}}-PE_{\text{HESS,cap}}^{\text{ii}}\right) \\ &+\sum_{k}\zeta_{\text{FC,cap}}^{\text{ii}}\left(P_{\text{FC,cap}}^{\text{jj}}-P_{\text{FC,cap}}^{\text{ii}}\right) \\ &+\sum_{k}\zeta_{\text{elec,cap}}^{\text{ii}}\left(P_{\text{elec,cap}}^{\text{jj}}-P_{\text{elec,cap}}^{\text{ii}}\right)\end{aligned} \qquad \begin{aligned}&\forall\ \text{jj} \\ &=1\ldots\text{ii}-1\end{aligned} \tag{4.32}$$

The cuts constraints of the bender decomposition tighten the feasibility space of the master problem by using the sensitive values of dual variables (ζ). z_{c} is the objective function value of the subproblem over the planning horizon. Similar to binding every variable, the λ_{c} needs to be bound with an initially defined limit as given by (4.33).

$$\lambda_{\text{c}}^{\text{ii}} \geq \lambda_{\max} \tag{4.33}$$

In the present study, the value of $\lambda_{\max}$ is set to be -2500. Inspired by the study in [178], the convergence check for bender decomposition is given by (4.34)

$$\left|z_{\text{c}}^{\text{ii}}-z_{\text{s}}^{\text{ii}}\right| \leq Threshold \tag{3.34}$$

Where z_{s}^{ii} are the capital cost of the DERs and the value of λ_{c} defined in equation (4.37). Noted that at the first bender iteration, the value of λ_{c} is set to zero. If the set threshold level is achieved, the optimal solution is found otherwise, the next bender iteration will run for the next bender cut.

4.3 Flexible tariff system for microgrid

Finally, microgrid planning has been solved using different. In a traditional tariff, called a flat tariff, the user pays a fixed monthly rate, expressed in €/kWh, based on energy usage throughout the month, regardless of the time of day. Everyday consumption, on the other hand, is not consistent. It is higher in the late afternoon or evening in households and decreases around midnight. Due to this, a flexible tariff system called a time of use (TOU) is introduced. TOU tariffs are time-varying tariffs that encourage load adjustment. Customers may save money on their energy bills while supporting the system. For a renewable-powered future, demand-side flexibility is critical. Demand response is enabled through tariffs that fluctuate according to the time of consumption. The researchers estimate that TOU can save a home around 25 percent of carbon emissions and 50 percent of energy costs; however, these savings are only possible if the household has a varied variety of distributed energy resources [179]. Based on this study, flexible tariffs are categorized into the following types and defined by [179]:

Static pricing: A day is divided into two or more time sections under static pricing. The cost is fixed and changes based on the period. Static pricing is simply divided into day and night to represent peak and off-peak hours in its most basic form. Days, on the other hand, can be divided down into multiple chunks to better depict peak and off-peak periods.

Critical peak pricing: Prices are fixed here, however they may be raised during periods of exceptional peaks when a fixed surcharge is imposed. Customers are often given an early warning to move loads away from certain times.

Variable peak pricing: On-peak periods are known in advance, similar to static pricing. The premium, on the other hand, is determined by current wholesale pricing.

Real-time pricing: Real-time pricing reflects current wholesale power costs. As a result, prices are unknown in advance, and billing necessitates the use of high-resolution metering data to apply the relevant price.

From the definitions of the different types of tariff systems, real-time pricing has more potential for demand response due to flexibility throughout the day. The flexible tariff systems can also support the integration of renewable energy sources by a great amount if installed with storage systems [180]. The high load, such as EV adding to the peak load, makes the flexible tariff very charming to implement in terms of demand response and DERs integration. Due to this, an optimal tariff system based on real-time pricing is proposed in the present study.

The tariff introduced in this study is calculated based on the white tariff. It has been implemented in Brazil, where low-voltage consumers can choose between the white tariff and flat [60]. However, the difference between the proposed tariff and the white tariff is that the white tariff is a variable peak pricing type, and the proposed one is real-time pricing. The white tariff has been implemented in Brazil for low-voltage consumers and is shown in Figure 4.6.

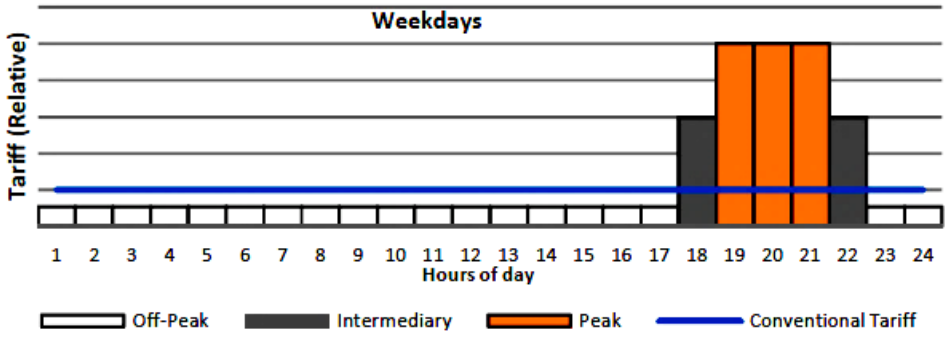

Figure 4.6 White tariff [60]

The white tariff (W_{T}) is calculated based on the peak (D_{p}), intermediary (D_{in}) and off-peak (D_{op}) demand on weekdays (WT_{wd}) as (4.35).

$$WT_{\mathrm{wd}} = kz\left(5D_{\mathrm{p}} + 3D_{\mathrm{in}} + D_{\mathrm{op}}\right) \tag{4.35}$$

$$W_{\mathrm{T}} = C_{\mathrm{GS}}\left(\sum_{1}^{p} WT_{\mathrm{wd}} + \sum_{1}^{q} kz \cdot D_{\mathrm{s}} + \sum_{1}^{r} kz \cdot D_{\mathrm{d}}\right) \tag{4.36}$$

kz is the relation between the price of conventional and white tariffs. It is defined by the utility and depends on the profile [60]. In the present study, it is assumed to be 0.18 to make the average price closest to the flat tariff in Germany. p, q, r is the number of weekdays, Saturdays, and Sundays in a month respectively. Due to a lack of knowledge in the load profiles, every 6th and 7th day has been considered as Saturday and Sunday. D_{s} is the demand on Saturday and D_{d} demand on Sunday. C_{GS} is the cost of electricity purchased from the grid at a flat rate. A flat rate of 30 Cents/kWh has been assumed [60]. In this paper, the peak time has been considered from 6 PM to 9 PM. Whereas 5 PM and 10 PM is intermediary peak time, the rest of the day has been regarded as off-peak time.

5 Results and discussion

5.1 Case Study

The proposed microgrid planning and operation strategy for e-mobility considering multi-type uncertainties has been applied to a settlement area planned in Magdeburg, Germany, named Alte-Zieglei, as shown in Figure 5.1. In the present study, the settlement is assumed to consist of twenty-five single-family houses (SFH) and six multi-family houses (MFH), with one commercial real estate (CRE).

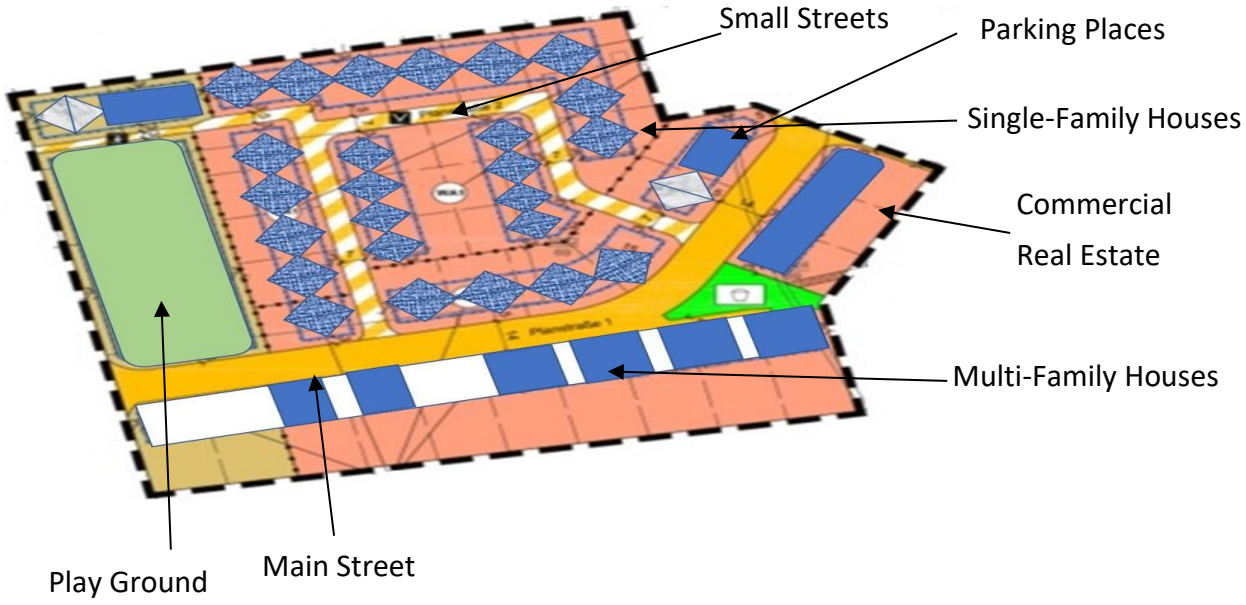

Figure 5.1 Investigated settlement area [181]

From the person distribution, the settlement area consists of 249 persons. The person distribution over the houses is given in Annex E.1. It is assumed that the settlement area is planned to be a grid-connected microgrid through a common coupling point (PCC) node. Microgrids may also be operated from a single node when linked to the local distribution network or transmission system [182]. As discussed in section 2, the DERs selected for this settlement area are shown in Table 5.1.

Table 5.1 DERs consideration for the settlement area

RES units	Storage units	Sector coupling units
PV	EESS	Fuel cell
Wind	TESS	HP
	HESS	Electrolyzer

The grid's topology for the settlement area is shown in Figure 5.2. There are 36 electrical and 36 heating grid nodes for this settlement area.

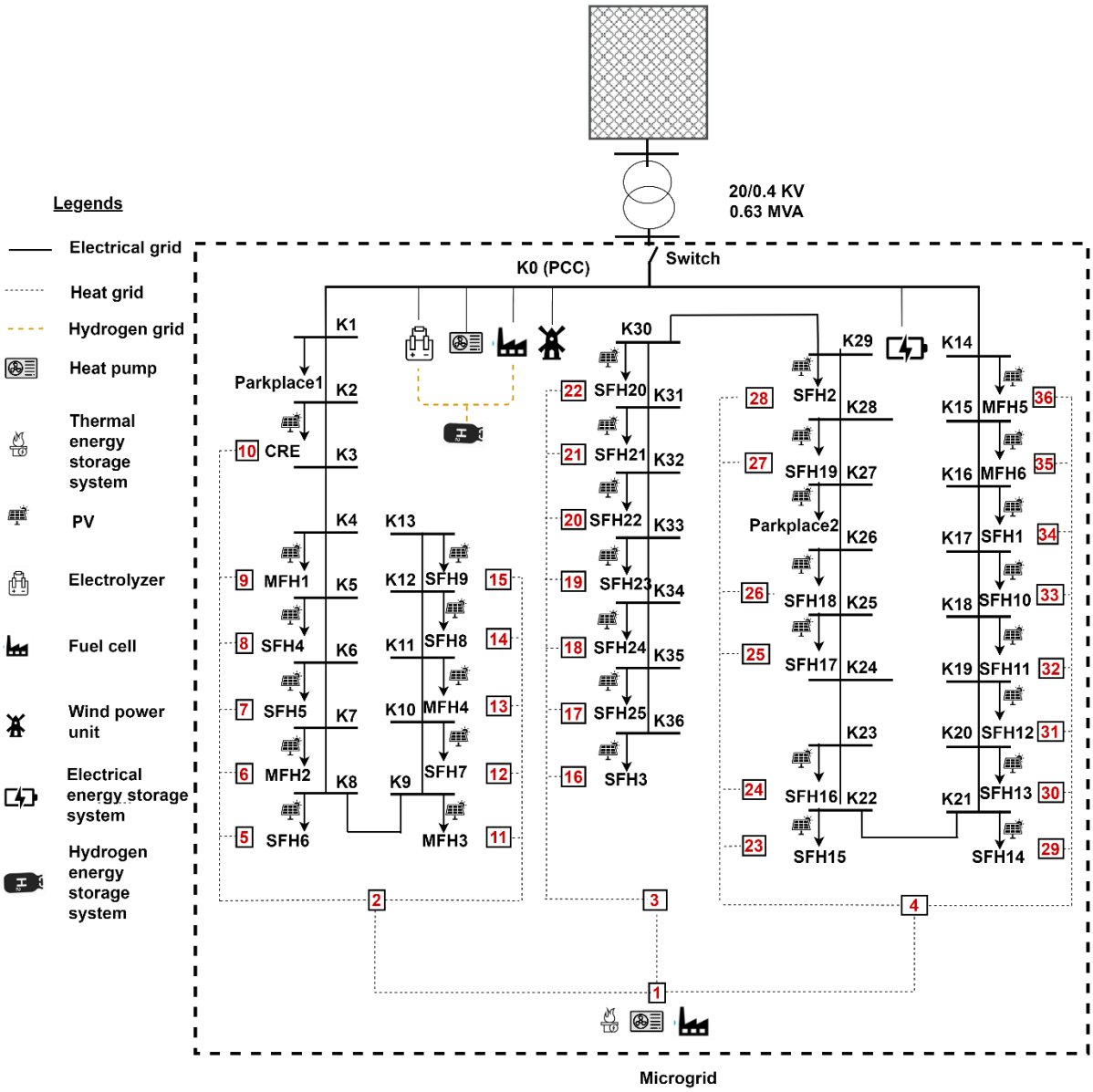

Figure 5.2 Grip Topology

The essential base data needed for the study are capital cost, operational cost, and CO_2 emissions related to the planning and operation of these DERs. The PV system is dispersed over the houses of the settlement area, as determined in section 2.11, to use available places such as roofs. Other DERs are assumed to operate in a microgrid as a centralized system and are connected to a node (K0). The EESS is considered centralized due to higher self-consumption and better energy utilization than decentralized [183]. The maximum rated power capacity of wind, fuel cell, and electrical energy storage systems is bound to 100 kW according to the eligibility for feed-in tariff set out in EEG 2017 [184,185]. Apart from the electricity grid, the heating grid is modeled for this settlement area and is connected to the electricity grid using sector coupling technologies. The settlement area's heating requirements are fulfilled by centralized heating.

5.1.1 Electrical load based on HTW berlin database

The sum of annual demand for the microgrid is 190.2 MWh. The microgrid's peak load is 79.2 kW, occurring on a winter day (December 12) without EV and heat demand. The electrical load profile employed in this study is an annual time series that varies depending on the kind of house. The daily electricity load profile for a single-family house consisting of three persons on the 16th of May is presented in Figure 5.3. The energy demand for the three-person SFH on the day is 13.6 kWh. There is a peak in the evening due to the activity time.

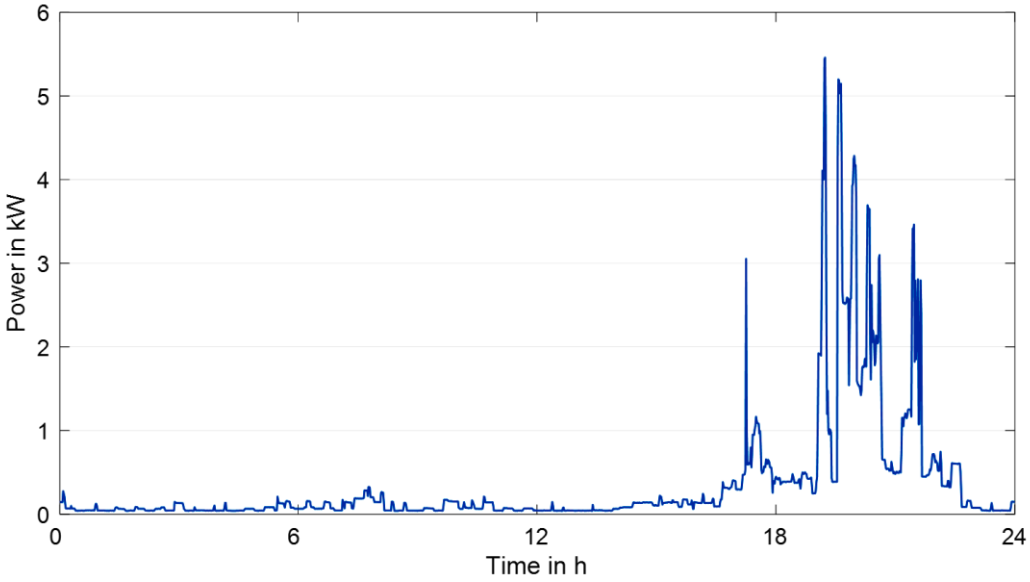

Figure 5.3 Electricity load profile on a transition workday (16th May)

5.1.2 Heating load profile

The settlement area is located in Magdeburg, and according to VDI 4655 [89], Magdeburg lies in German climate zone 4, specified as TRY04 (Test Reference Year 04). The total number of heating days per year is 274, and Table 5.2 summarizes their classification into day-type categories with corresponding average temperatures.

Table 5.2 Average number and temperature of typical day categories in TRY04

Type	UWH	UWB	USH	USB	SWX	SSX	WWH	WWB	WSH	WSB
Number of days	37	76	9	17	78	13	29	82	6	18
Average temperatures	11.1	10.2	10.6	9.5	17.5	17.4	-1.2	2	1.5	2.2

The heating energy factor for space heating based on VDI 4655 is shown in Table 5.3 for selected day-type categories. The yearly DHW heating energy computed using the heating energy factor can be found in Annex E.2. The annual space heating energy demand $(Q_{\mathrm{h,a}})$ computed for a single-family house, multi-family house with 12 dwellings, and multi-family

house with 16 dwellings, respectively, is 2,100 kWh/a, 14,250 kWh/a, and 17,550 kWh/a, according to section 2.3.

Table 5.3 Heating energy factor

Day types	Heating energy factor
UWH	0.001869
UWB	0.00227
USH	0.002547
USB	0.002546
SWX	0
SSX	0
WWH	0.005186
WWB	0.005203
WSH	0.005254
WSB	0.004699

The annual space heating demand for commercial real estate (CRE) is 36000 kWh/a. The space heating energy demand for the particular day has been calculated as described in section 2.3. The daily heating energy demand results in kWh per day type are shown in Table 5.4.

Table 5.4 Daily space heating energy demand per day type category in kWh

Type	UWH	UWB	USH	USB	SWX	SSX	WWH	WWB	WSH	WSB
SFH	3.93	4.74	5.35	5.35	0.00	0.00	10.89	10.93	11.03	9.87
MFHT1	26.63	31.43	26.36	28.84	0.00	0.00	86.87	70.04	77.49	60.49
MFHT2	32.75	38.71	32.46	35.52	0.00	0.00	106.98	86.73	95.43	74.50
CRE	67.27	79.41	66.58	72.86	0.00	0.00	219.45	177.90	195.75	152.81

The space heating depends on the temperature. The temperature in winter is low, so the space heating demand has been high, whereas, in the summer, the heating demand is zero due to the high outside temperature. During the transition period, the space heating requirement is 50 percent lower in winter. The peaks in Figure 5.4 indicate the single-family house's maximum heating demand day, WSH. In the winter, the WSB has the lowest heating requirement for space heating. The sum of heating energy demand for the microgrid is 349.8 MWh per year. The share of space heating is 72 percent, and DHW demand is 28 percent. The annual DHW energy demand for the different house types described in section 2.3 can be seen in Annex E.2. The DHW is dependent on the number of persons for single-family houses and the number of dwellings for multi-family houses. The annual heating demand for a single-family house consisting of three persons is shown in Figure 5.4.

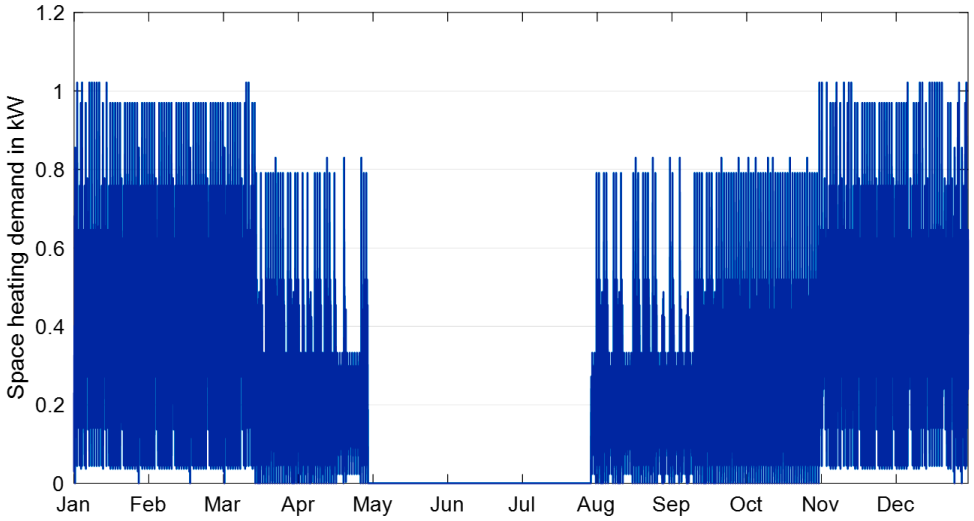

Figure 5.4 Annual space heating load for three persons SFH

5.2 E-mobility infrastructure

5.2.1 Development of electric vehicles

As described in section 3, three scenarios are created for the investigated settlement area. According to the “Mobilität in Deutschland” survey, the average number of cars in houses with one person, two persons, three persons, four persons, and five persons are 0.7, 1.3, 1.7, 1.8, and 1.9 respectively [186]. According to this study, there will be 133 conventional vehicles present in the settlement area. It is assumed that all vehicles are combustion engine-based in the settlement area in 2021.

According to the KBA (Germany's federal motor vehicle authority), Germany's total number of registered cars is 47,715,977, with 2,917,678 newly registered vehicles in 2020, including 394,632 electric vehicles [127]. The percentage of newly registered vehicles in total registered cars held by individuals was recorded as from 6.1 to percent 7.4 percent in the last ten years [187,188]. Consequently, the percentage of newly registered vehicles in total registered cars held by individuals is 6.1 percent, with EVs accounting for 13.53 percent of newly registered vehicles. Applying this methodology to the settlement area under study, in 2022, the number of newly registered vehicles in 2020 is expected to be 8, while the number of electric vehicles will be one. It is assumed that the number of newly registered vehicles will be eight constantly every year of the planning horizon. The newly registered vehicle is then replaced every year by EVs through retropolation in the planning horizon. The number of newly registered EVs from 2021 to 2030 replacing the newly registered conventional vehicles, as outlined in section 3.1, can be seen in Annex E.3. The number of EVs registered in the following year is added with the number of EVs present in the current year. The number of

EVs in 2021 is zero. However, one EV is registered in 2021, due to which the number of EVs in 2022 will be one. The number of EVs on the planning horizon is presented in Figure 5.5.

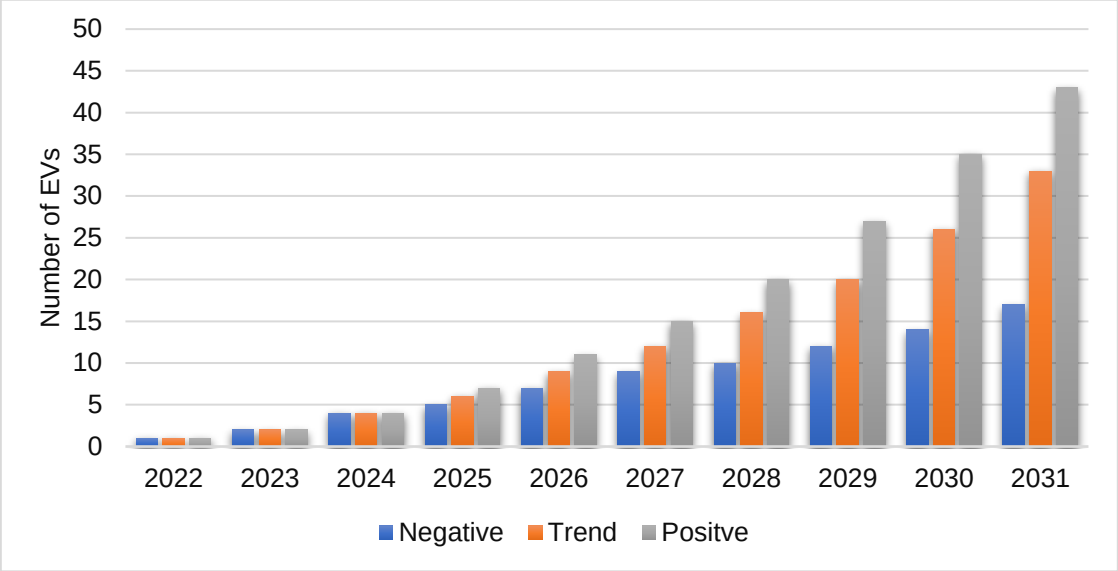

Figure 5.5 Number of newly EVsper in the investigated settlement area

The population of the settlement area is expected to remain constant over the planning horizon. In the negative scenario, the share of the EV in 2031 will reach 12.4 percent at the end of the planning horizon. The yearly rise rate in the EV from 2022 to 2031 varies between 1.1 and 2 percent in the negative, 4.6 to 23.4 percent in the trend, and 7 to 59 percent in the positive. The number of EVs reaches 24 percent of conventional vehicles in the trend and 32.7 in the positive scenario in 2031. The share of EVs in the settlement area compared to conventional vehicles can be seen in Annex E.3. The trend scenario has been used to show the results of the proposed methods.

5.2.2 Development of a private charging station

The number of electric vehicles is essential for the settlement area as the EVs are charged in the settlement area. From an economic perspective, as indicated in section 3.3, EVs will charge from private charging stations 85 percent of the time [130]. Once the number of EVs is known, the EV behavior is simulated as per section 3.2. As the settlement area is residential, the EV parameters shown in Figure 3.5 follow the residential attributes. The EV starts charging immediately after arriving with a rated power of 11 kW for a private charging station. The following statements are essential for the planning and operation of a microgrid:

- If a significant number of EVs are charged at the same time, the settlement load will become relatively high

- ❖ The voltage drop on the specific node and the subsequent node attached to the same string is caused by the EV charging

5.2.2.1 Simultaneous EV charging from private charging stations

In the trend scenario for EV development in 2031, the simultaneous arrival of EVs for charging in the settlement area and their influence on settlement load are depicted in Figure 5.6 for a particular day. Note that the number of EVs in the charging state on other days will look different due to the use of the Monte-Carlo simulation method.

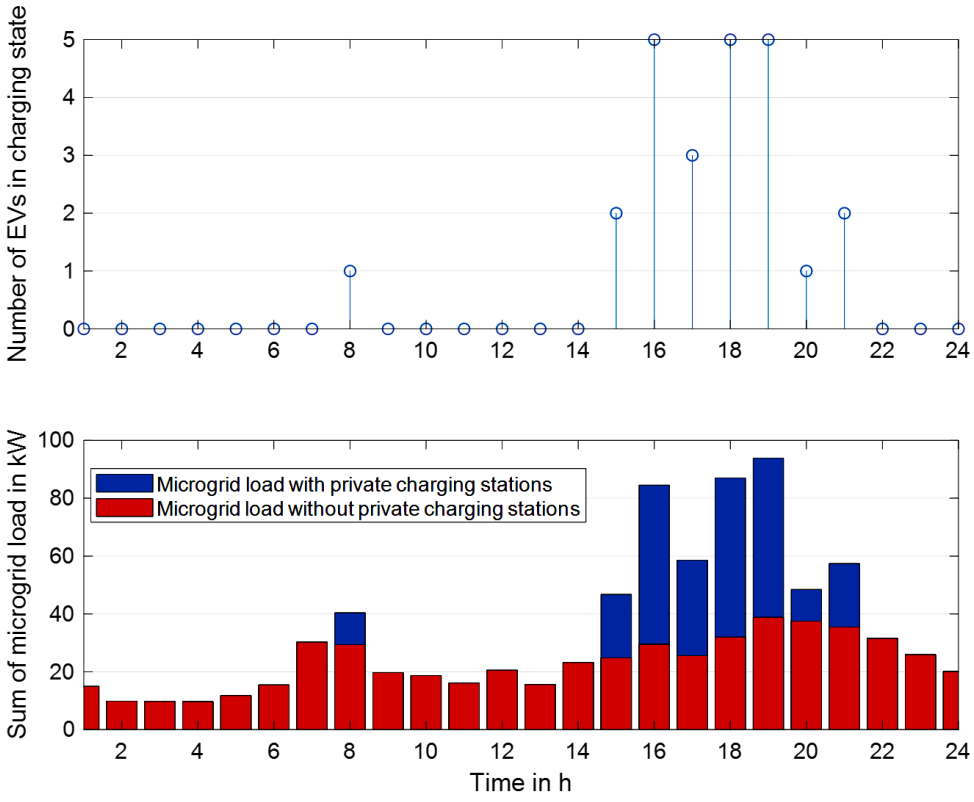

Figure 5.6 Number of EVs charging and their influence on the load of the settlement

On this day, 24 EVs out of 33 needed charging from the distributed private charging stations. From 4 PM to 7 PM, the settlement area had the most significant EVs charging simultaneously, approximately 75 percent of the total EV. Due to this, the settlement area load has increased roughly 48 percent on the day. Since consumers arrive at home mostly at the same time in the evening, the EV will connect and detach nearly at the same time. The expected simultaneous charging in the settlement area for a year in the trend scenario in 2031 is shown in Figure 5.7. Most of the time years, 3 percent of EVs are charged at the same time. The largest proportion of EV charging simultaneously is 34 percent, which rarely occurs twice a year. The load varies in a considerably smaller time step in actuality (e.g., Minutes/seconds resolution). Because EV arrivals would be more dispersed, it is expected that simultaneous EV charging will be significantly less in shorter time frames. The EVs coming at any moment within a one-hour

period are accumulated. The arrival of EVs is simulated at a 1-hour resolution because of a 1-hour resolution optimization hurdle. However, it is also believed that a 1-hour resolution for EV arrival is enough for the current study, as the highest percentage of simultaneous charging rarely occurs in the year, as shown in Figure 5.7.

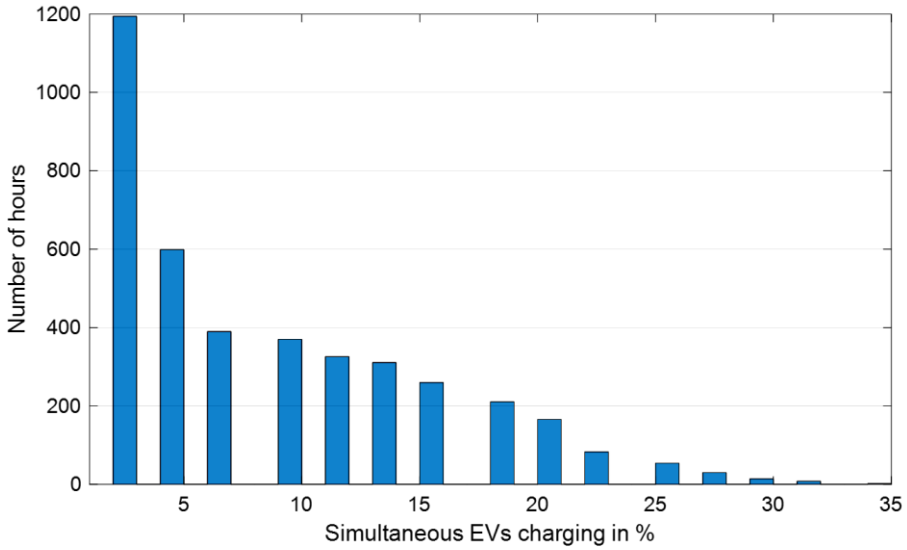

Figure 5.7 Expected percentage of EVs in simultaneous charging state in trend scenario

5.2.2.2 Impact of the private charging stations on the voltage

The placement of private charging stations described in section 3 can be seen in Annex E.3. The load for a single-family house equipped with a charging station at K8 and the voltage profile for a specific day is shown in Figure 5.8.

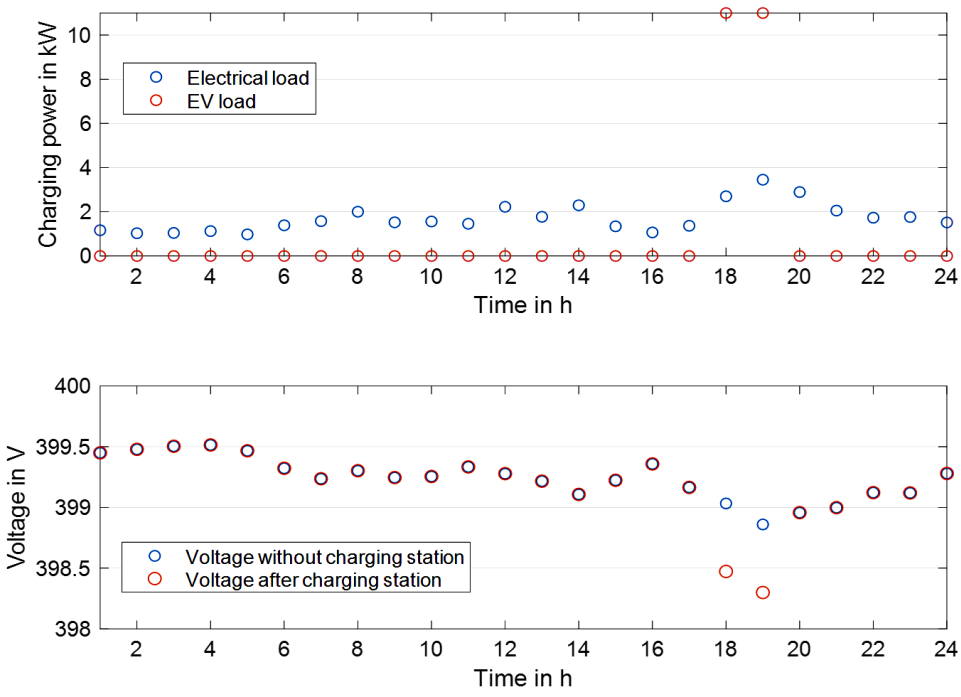

Figure 5.8 Impact of EV charging on load and voltage

The EV is charging from 6 PM to 8 PM. For that reason, the voltage drops a little due to the EV load. However, as the grid is stable in this case study, the voltage drop will not be massive. The voltage drop can be critical at a large string, especially on the last load connected. The microgrid has two strings connected to the PCC in the present study. The shorter string shown in Figure 5.1 is 500 meters, while the more extensive string is 900 meters long. A private charging station is placed at K8 in the trend scenario, and thus its influence on the string voltage is shown in Annex E.3. The expected voltage profiles for the settlement area in the trend scenario for 2031 are shown in Figure 5.9. Without a charging station, the settlement area's minimum voltage is around 397 V. In the trend scenario for 2022, the minimum voltage drops to 391.4 V once the charging station is installed. After the deployment of private charging stations, the high voltage bins observed in voltage bins without charging stations around nominal voltage are pushed toward 398 V.

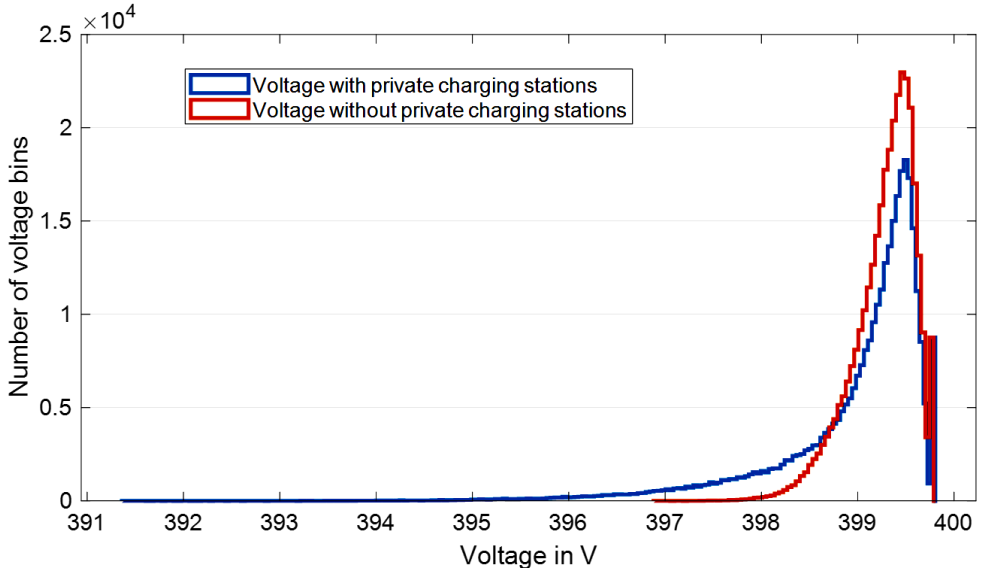

Figure 5.9 Comparison of voltage profile with and without private charging stations in trend scenario

5.2.3 Development of public charging stations

As indicated in section 3.3, EVs will charge from public charging stations 15 percent of the time [130]. Furthermore, an EVCS often consists of two columns so that two EVs can be charged simultaneously with the rated power of the EVCS. The following statements have been planned for the public charging station in the settlement area:

- The number of EVCS based on occupancy time
- The placement for EVCS

5.2.3.1 Number of EVCS based on occupancy time

The optimal number of charging stations is determined based on the acceptable occupancy time of the EVCS, as described in section (3.3). When EV users arrive at a specific time, they must wait while the EVCS is used. It is clear from Figure 5.6 that the likelihood of simultaneous charging is high at a particular peak for the two EVs in public EVCS. The total number of EVs in the worst-case (positive scenario) rises from 1 to 43, and the occupancy time EV is displayed in Figure 5.10.

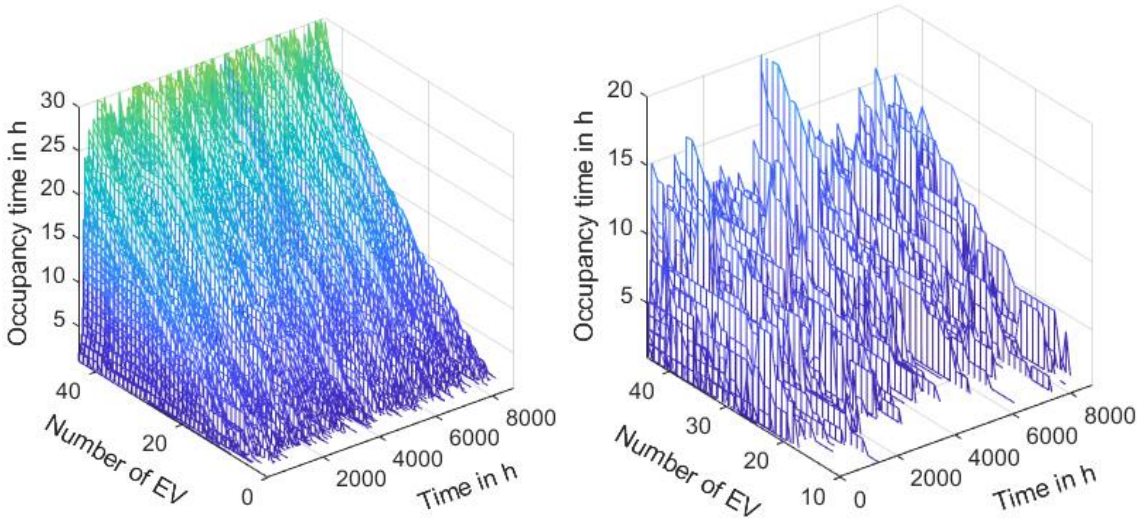

Figure 5.10 Occupancy time for EVCS=1 (left side) and EVCS=2 (right side)

From Figure 5.10, the occupancy time is calculated as the sum of all EVs waiting for a charging slot. The installation of another EVCS reduces occupancy time by roughly 50 percent for most of the year. Table 5.5 shows the occupancy time per day for increasing EVCS installation.

Table 5.5 Average EVCS occupancy time per day in hours

Number of EV	EVCS = 1	EVCS = 2	EVCS = 3	EVCS ≥ 4
1-10	0	0	0	0
10-20	0-0.35	0-0.02	0	0
20-30	0.41-1.54	0.02-0.13	0	0
30-40	1.61-3.55	0.15-0.54	0-0.06	0
Over 40	3.81-6.76	0.67-1.45	0.15-0.42	0-0.039

If EVs are greater than 20, the occupancy time for the situation EVCS=1 reported in Table 5.5 is much longer. The number of installed EVCS is represented as a heatmap when the total waiting time in hours for an EV is compared to the rise in the number, where high user comfort may be obtained at the cost of additional installation. If two EVCS are installed for a limited

number of EVs, the occupancy time for the EV is zero. The anticipated EVCS for the planning Horizon is indicated in Table 5.6 using an EVCS occupancy duration of fewer than 30 minutes as an acceptable value.

Table 5.6 Number of EVCS for acceptance occupancy time of 30 minutes

Scenario	2022	2023	2024	2025	2026	2027	2028	2029	2030	2031
Negative	1	1	1	1	1	1	1	1	1	1
Trend	1	1	1	1	1	1	1	2	2	3
Positive	1	1	1	1	1	1	2	2	3	4

The arrival of EVs for charging is primarily influencing the occupancy time. The arrival of EVs is mainly noticed in the evening, as shown in Figure 3.5. The utilization of an EVCS by the number of EVs is an interesting parameter to be evaluated for a certain occupancy time. For an EVCS without any occupancy time, the EVs charged 15 percent of the time, as described in section 3.2. However, the utilization will change by introducing the occupancy time. The occupancy of fewer than 30 minutes and the utilization of the number of EVCS for the trend scenario in 2031 are shown in Figure 5.11. The utilization of the EVCS will increase with the number of EVs. Similarly, The increase in the EVs increases the occupancy time. Due to this, the increase in the occupancy time increases the utilization of the EVCS.

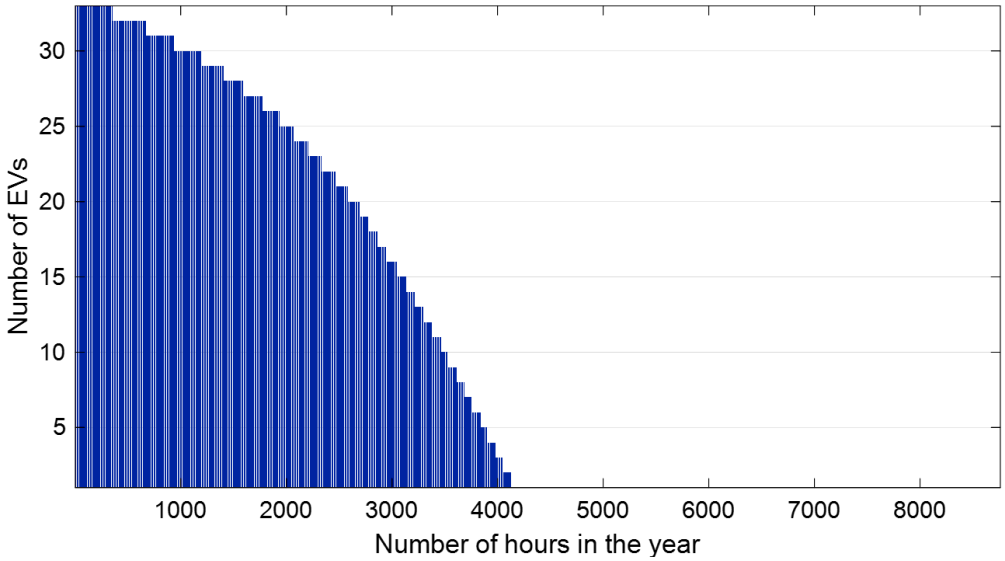

Figure 5.11 Utilization of EVCS for less than 30-minute occupancy time

From Figure 5.11, the utilization of the EVCS in terms of the number of hours in the year is 39.2 percent. Compared to the assumed value of 15 percent, it is concluded that the occupancy time of 30 minutes will increase the utilization by 24 percent more. Critically, the acceptability of this waiting time by the EVCS users is a barrier. However, the decision-making is based on an economic point of view as a trade-off between the lowest possible occupancy

time and user acceptancy. Due to this, less occupancy time leads to less utilization which can not be economical, and higher occupancy time leads to less acceptancy. From Table 5.5 and Figure 5.11, an occupancy time of fewer than 30 minutes seems to be ideal due to the economical utilization and comparable number of EVs per EVCS.

5.2.3.2 Placement of public EVCS

Typically, the best place to install a high load is near the transformers. However, this is true for a transformer with a single string. This microgrid electrical network consists of multiple strings. This leads to different influences if a new component is placed. In addition to the connection point, EVCS placement is subject to several criteria, including the available places to charge the EVs, such as park places, and suitable areas, such as proximity to markets and public transport. If the location of the EVCS place is known, the suitability of different connection nodes in other strings is investigated using the NVSI according to section 3.4. When the EVCS is put on node 1, its effect on voltage is not confined to that node but may be seen across the microgrid. As seen in equation (3.4), the NVSI examined the impact of an EVCS on all nodes belonging to the settlement. The results for the NVSI of the various nodes are summarized in Figure 5.12.

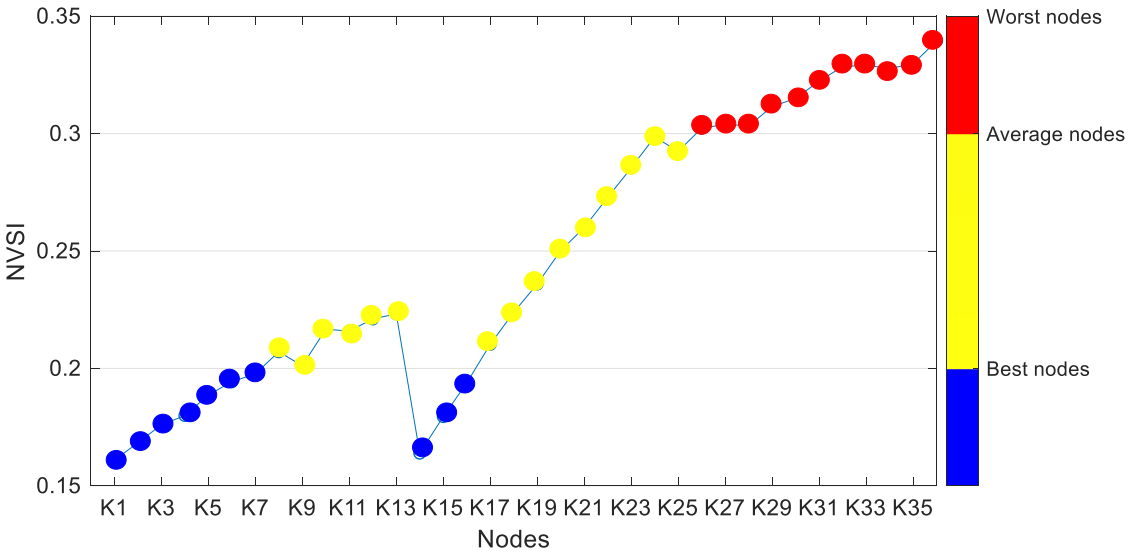

Figure 5.12 NVSI for the settlement area

The best connection point for an EVCS is the nodes with the lowest NVSI. In general, the nodes of a shorter string with fewer houses are preferable to a longer string with a more significant number of houses.

However, not all nodes in the former string are insensitive to all nodes in the later string. From Figure 5.12, the 2nd node of the first string shows higher NVSI than the 1st node of the second string. This concludes that the 2nd best location for an EVCS is the first node of string 2. Ten

nodes are qualified as best prospects nodes if their NVSI is less than 0.2, as illustrated in Figure 5.12. Once the optimum nodes for one EVCS have been identified, the ideal configurations for several EVCS are investigated. Table 5.7 shows the ideal configuration for the trend scenario mentioned in section 3.4 based on the Monte-Carlo simulation.

Table 5.7 Configuration suggestion for trend scenario in 2031

Knoten	**1**	**2**	**3**	**4**	**5**	**6**	**7**	**8**	**9**	**10**
K1	1	1	1	1	1	1	1	0	0	0
K14	1	1	0	1	0	0	0	1	1	0
K2	1	0	1	0	1	0	0	1	0	0
K3	0	0	0	1	0	1	0	0	0	1
K15	0	1	0	0	1	1	1	0	0	0
K4	0	0	1	0	0	0	0	0	0	1
K5	0	0	0	0	0	0	1	0	1	0
K16	0	0	0	0	0	0	0	1	0	0
K6	0	0	0	0	0	0	0	0	1	0
K7	0	0	0	0	0	0	0	0	0	1

Each column in Table 5.7 represents one configuration of EVCS placement. Finally, the first configuration is chosen to place EVCS for the investigated settlement area in 2031, based on the optimum configuration from Table 5.7. Commercial real estate and parking spaces with many users will be close by, making EVCS installation a viable option to be placed in this area, as shown in Figure 5.13.

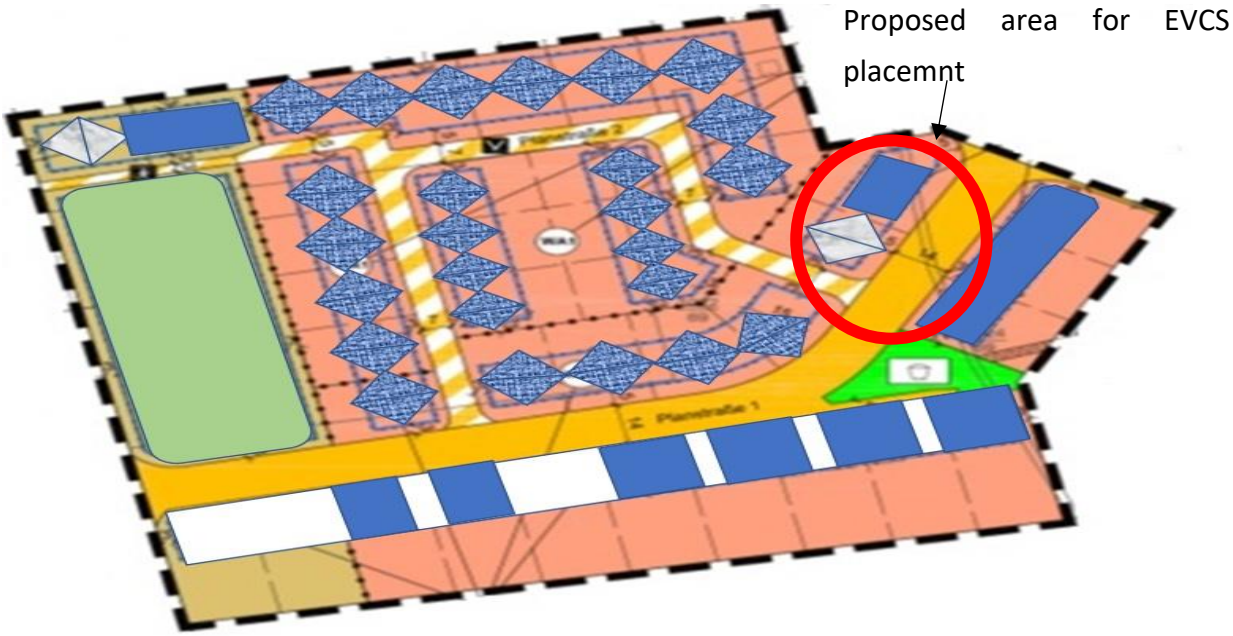

Figure 5.13 Proposed area for EVCS placement for trend scenario in 2031

5.3 Deterministic microgrid planning and operation for e-mobility

As the heat and electrical demand are defined, the microgrid consisting of DERs is optimally sized using the Mixed-integer nonlinear problem described in section 4.1. The optimization is solved with a gurobi solver, and the Yalmip tools box is used to formulate the optimization problem [189]. In light of the trend scenario, the analysis of microgrid planning and operation is divided into the following sub-categories:

- Optimal DERs capacities
- Settlement area energy balance and operational hours of DERs in the electrical grid
- Electrical grid analysis in terms of voltage
- Settlement area energy balance and operational hours of DERs in the heating grid
- Heat grid analysis in terms of losses
- Cost analysis of settlement area
- Sensitive analysis

The optimal operation of the electrical grid and the heat grid is evaluated to analyze the effectiveness of DERs in the microgrid. Other parameters, apart from EV load, emission cost, and grid emission intensity, are assumed to behave in the same way throughout the planning horizon. As a result, examining the operation horizon for 2031 will be enough to conclude the previous year's operation.

5.3.1 Optimal DERs capacities

The planning is considered to be a multi-period where the capacities are decided every year. The last year of the planning horizon can be seen as the final capacity for future planning. Any capacities for any year in this planning horizon are ideal. For instance, in a 5-year planning horizon, any capacities are optimal at the end of 5 years. Figure 5.14 shows the capabilities of DERs for the trend scenario based on the input prices indicated in section 4. Annex E.4 shows the capacities that resulted from the negative and positive scenarios. The EESS and TESS capacities are measured in kWh, whereas the generating units, heat pump, and electrolyzer are measured in kW, and the HESS is measured in m^3. As seen in Figure 5.14, generation sizes expand exponentially as the number of EVs increases. PV, wind, and EESS will reach their maximum capacity in 2026, and as EVs grow more prevalent, the fuel cell will rise to handle the larger load.

Due to the fact that the fuel cell creates both heat and electricity, it has a larger capacity than the EESS. However, if the electric load grows due to the increase in the number of EVs, the EESS gains more capacity. This is because the fuel cell is more costly, and the heat load is not

changing on the planning horizon. Consequently, an increase in the electric vehicle sparked a slight increase in the fuel cell, resulting in a minor drop in the heat pump. With the rise in the fuel cell, the hydrogen storage and electrolyzer will also increase.

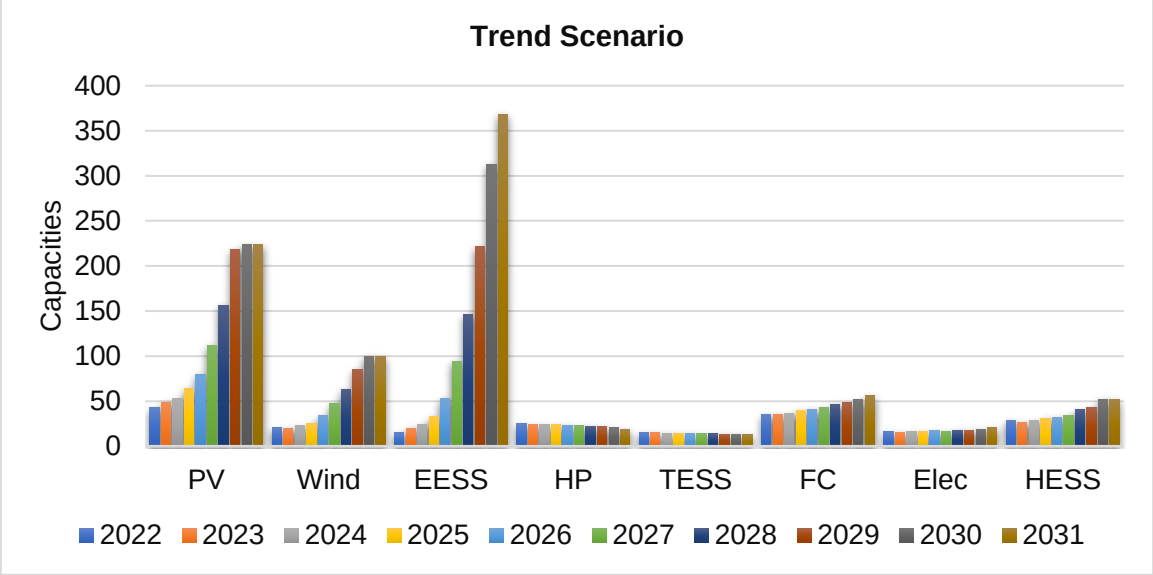

Figure 5.14 Microgrid capacity

The community is situated in a residential part of the city. As a result, traditional large wind turbines are not viable to construct. On the other hand, small wind turbines must be put in communities to meet GHG reduction requirements. Small private wind turbines will not be able to be built in the examined settlement area since the houses are equipped with PV systems. As a result, medium-sized wind turbines with low noise and fewer areas are advised. A medium-sized wind turbine with a hub height of 20 m and rated power of 15 kW is commercially available [190]. For district heating, the larger systems for heat pumps, fuel cells, and TESS are available on a kW scale [191,192].

5.3.2 Electrical grid energy balance and operational hours of DERs

The energy balance in the electrical grid is analyzed in this part to indicate the importance of optimal operation. The daily load and generation profiles related to operation for a winter day in 2031 are shown in Figure 5.15. The operation for a summer day can be seen in Annex E.5. There are three EVCS, and only one is operational at 5 PM on this day. The private charging stations are also included in the microgrid grid load. Figure 5.15 shows how wind and solar energy contribute to charging the EESS at times when there is less load. There is no need for grid import because wind generation is high on this day, and the optimization attempts to restrict grid import as much as possible.

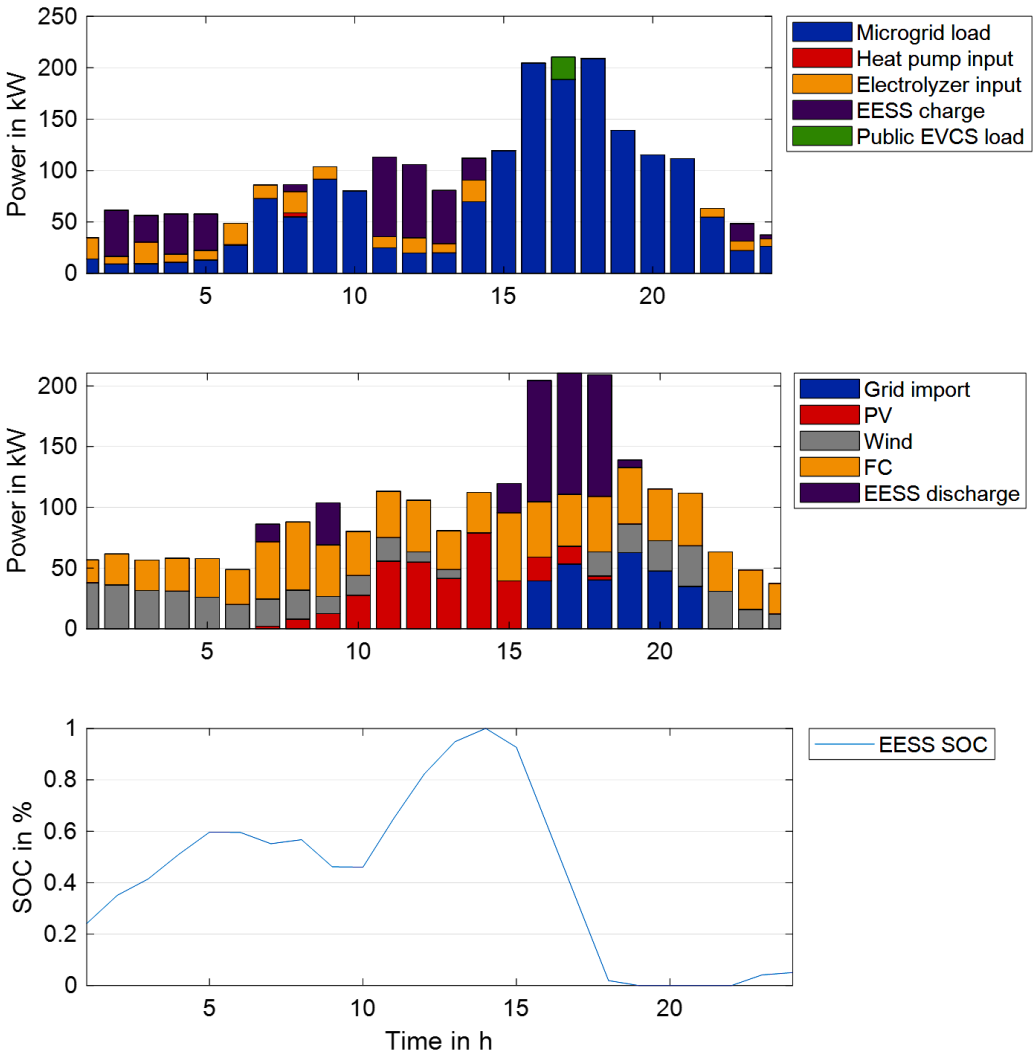

Figure 5.15 Energy balance of microgrid electricity grid (20th January)

Around midday, the EESS requires additional energy from PV and wind to be released at a high load time in the evening. The fuel cell needs a constrained supply of hydrogen, which is provided by the electrolyzer and HESS, due to which the electrolyzer also operates simultaneously. The fuel cell is running more than other DERs due to the heating demand. The sum of microgrid demand on this day is 2.3 MWh, which includes demand from heat pumps, electrolyzers, EESS charging, and private and public charging stations. As the day is winter and the fuel cell also provides heating, the fuel cell delivers the most energy, accounting for 37.8 percent of total demand. The wind contributes approximately 19.2 percent, and battery discharge accounts for 16 percent. PV provides about 15.2 percent, and the rest of the energy is imported from the grid. The shift of renewables to high-demand times can be seen in Figure 5.15. The operation of the DERs will be different from day to day based on the variation of

input parameters such as irradiance, wind speed, heating, and electrical load. The DER's operational hours are shown in Figure 5.16.

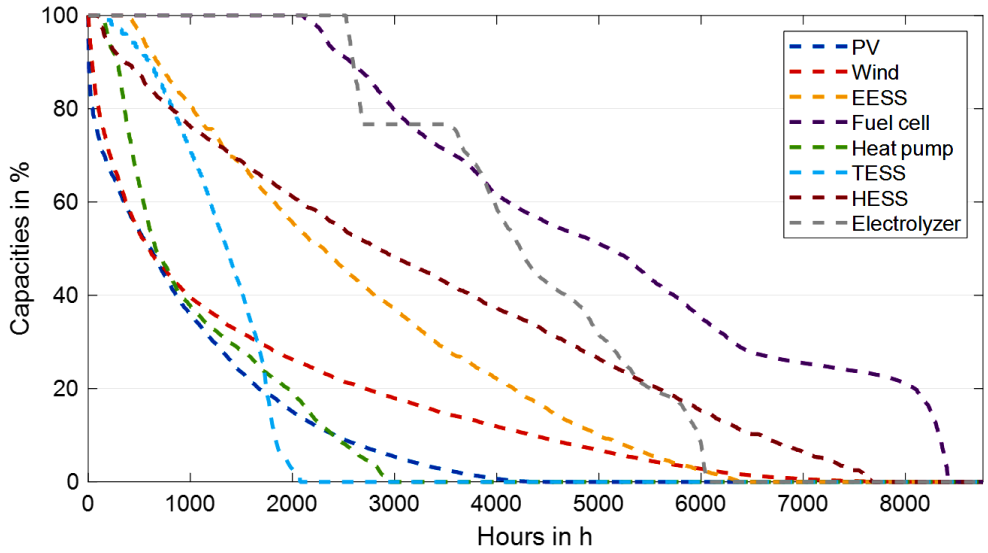

Figure 5.16 Operational hours of DERs

The operational hours of wind power are higher than those of PV power, as illustrated in Figure 5.16. Due to the fact that the analyzed settlement area is in Germany, which has a greater wind potential than PV. The TESS and HP have fewer operational hours because the fuel cell will run most of the time, as it will be better due to combined heat and power. The operational hours of the fuel cell should be equal to the electrolyzer and HESS's operational hours to ensure a constant supply of hydrogen. The electrolyzer is the only source of hydrogen, due to which it is operated higher time with full capacity to supply the hydrogen for HESS. The sum of all hydrogen produced and consumed in the year is 26,883 m^3. Although, the fuel cell is believed to be operated more due to its combined heat and power attribute. From the standpoint of the electrical grid, EESS has higher operational hours than other DERs. This is because EESS will decrease the grid import by storing the excess energy from renewable energy sources.

5.3.3 Electrical grid analysis in terms of voltage

The operation is optimal with the least possible operational cost and a stable voltage. The voltage profile for the microgrid for trend 2031 is shown in Figure 5.17. The voltage closest to the nominal voltage is shown as yellow color in Figure 5.17. The blue color indicates the lower voltage values of the string. The minimum voltage noticed is 397.5 V. The time in Figure 5.17 starts from January to December. The middle section of the hours represents the summer. It can be seen that the voltage is more stable in summer as compared to winter due to the electricity needed for the heating requirement. The heating requirement is fulfilled by the heat pump and fuel cell, which require hydrogen from the electrolyzer.

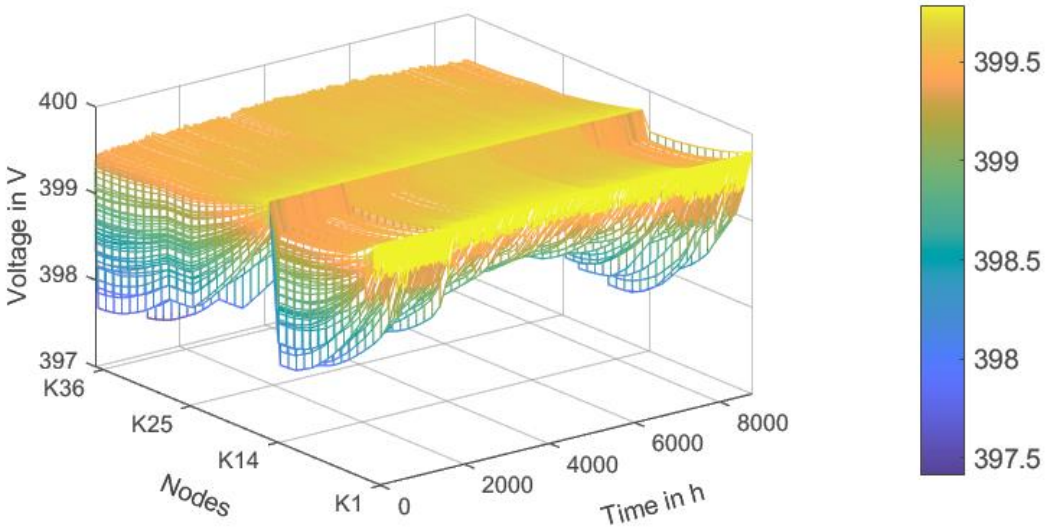

Figure 5.17 Voltage profile

Furthermore, from Figure 5.17, even a modest microgrid can manage the amount of EVs predicted in a trend scenario without experiencing any voltage issues. The microgrid's voltage profile must be considered to maintain the settlement area's stable and secure functioning. Two cases have been presented to illustrate the relevance of DERs planning, taking voltage into account.

- *Case 1:* The microgrid is designed and optimized without any DERs. In this case, the grid provides demand for the microgrid
- *Case 2:* The microgrid is optimally planned and operated with all DERs

The private charging station placement for the settlement area can be seen in Annex E.3. All the nodes of string 1 have one private charging station in trend 2031. Furthermore, in trend 2031, the nodes K1 are K2 are connected to two public EVCS. Figure 5.17 shows the voltage of string one at the observed time step with the lowest voltage. Note that the voltage drops can be handled with other methods, but with the introduction of DERs, the voltage is adjusted here with green energy and minimum cost. The distribution of voltage bins for the whole settlement area for both cases can be seen in Annex E.6. Note that these voltages are only problematic due to the integration of the EV and EVCS. But the solution is global and can be implemented for general voltage problems in weak grids. The minimum voltage has been restored from 394 V to 399 V in Figure 5.18, primarily due to DERs usage. This recovery is achievable because most of the DERs are placed at the K0 node, where the voltage is treated, and the voltage drops of the strings connected to K0 become less. The string length, house types, cable type, and EV distribution over the string are critical parameters. The optimization will adjust the sizes and optimal operation to make the voltage in the particular region.

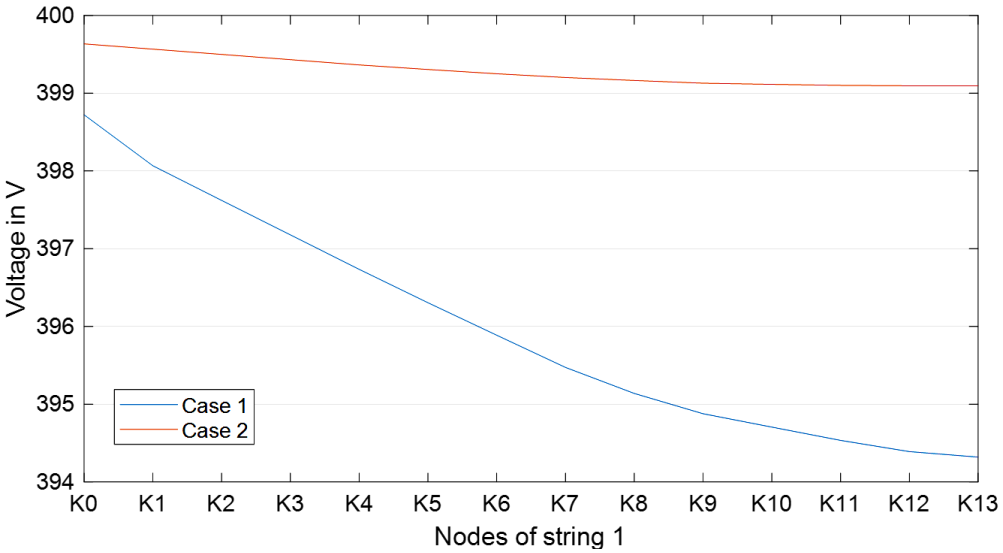

Figure 5.18 Comparison of cases 1 and 2 on string 1 of the settlement area

Although, the aim of the proposed microgrid is not to deal with the voltage problems as the grids in the location of the settlement area are very stable. The technical question regarding the grid perturbation in terms of voltage by introducing DERs due to the e-mobility seems to be effective. Considering the portability of the proposed methodologies, the voltage problems that occur in the microgrids due to the e-mobilities can be solved in the case studies with weak grids.

5.3.4 Heat grid energy balance and operational hours of DERs

The heat energy balance in the electrical grid is analyzed in this part to indicate the importance of optimal operation in the heat grid. The daily heat load and generation profiles related to operation for a winter day are shown in Figure 5.19. The heating load is covered most of the time with the fuel cell because it combines heat and power and less time with the heat pump. The sum of heating demand for the settlement area is 1.74 MWh, with a TESS charge of 0.035 MWh.

The overall generation for the day is 1.86 MWh, with 1.49 MWh from the fuel cell, 0.35 MWh from the heat pump, and 0.013 MWh from TESS. There is a surplus of 0.12 MWh, which are the losses in the heat grid. The heating losses are 6.4 percent of the total generation on this day. The TESS needs to be discharged at times when the electrical load is low because the fuel cell will not be economical to be operated. To be discharged at these particular times, the optimization aims to charge the TESS at the time when the fuel cell is already operated due to electrical demand. If the fuel cell is not enough, the heat pump contributes to the heating demand and charging TESS.

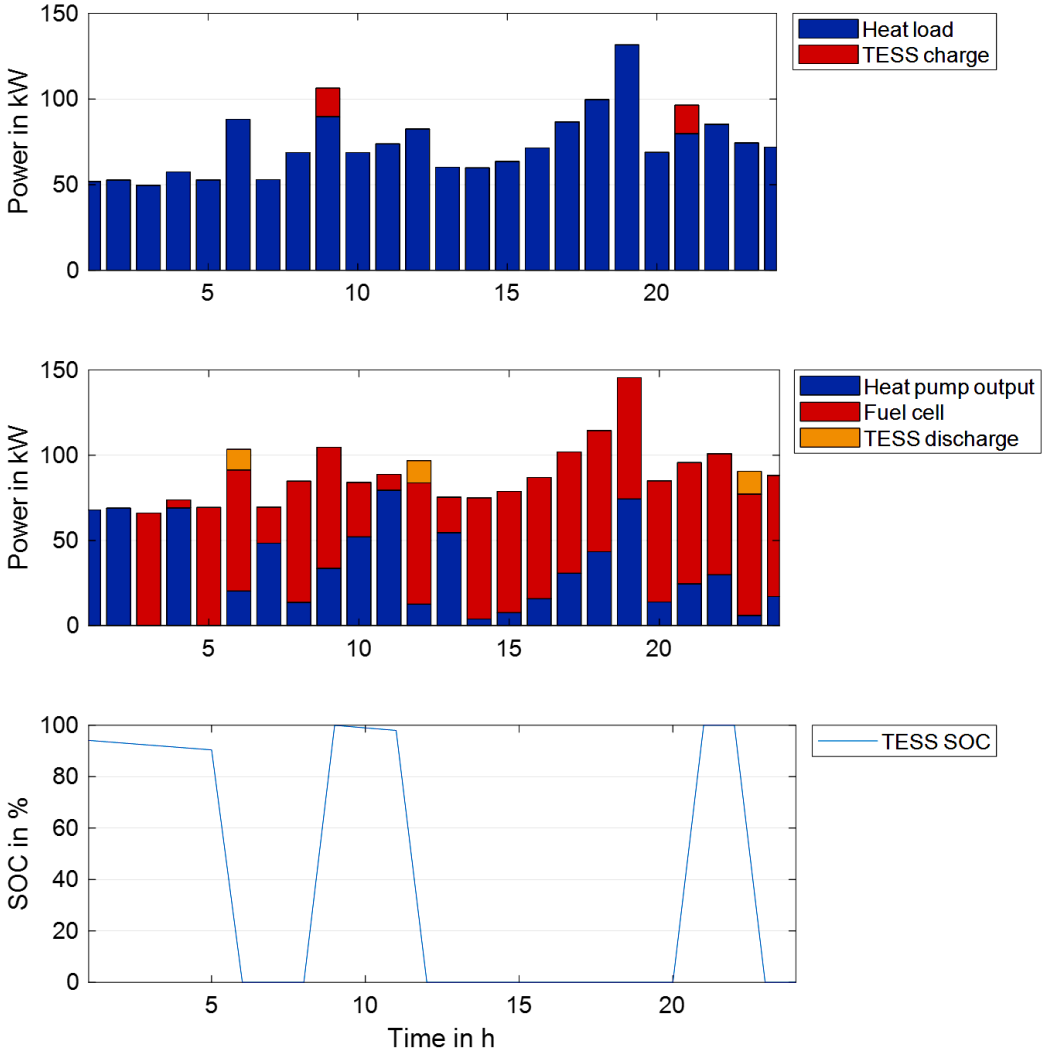

Figure 5.19 Heat balance of settlement area (20th January)

5.3.5 Heat grid analysis

The heat grid described in section 2.5 is assumed to be a low-temperature grid due to the heat pump and fuel cell limitation in temperature provision. However, the low-temperature heating grid with a supply temperature of 50 °C is enough to tackle DHW demand. Furthermore, the temperature for DHW must be above 50 °C to eliminate the bacteria such as legionella. Legislatively in Germany, a minimum of 50 °C needs to maintain to eliminate legionella [109].

Similar to the voltage profile, the heat grid has supply and return temperatures described in section 2.5. String 1 of the heat grid from Figure 5.2 is studied in this part to evaluate the supply and return temperature while supplying heating demand. The string comprises six heating nodes, all of which are powered by heating node 2.

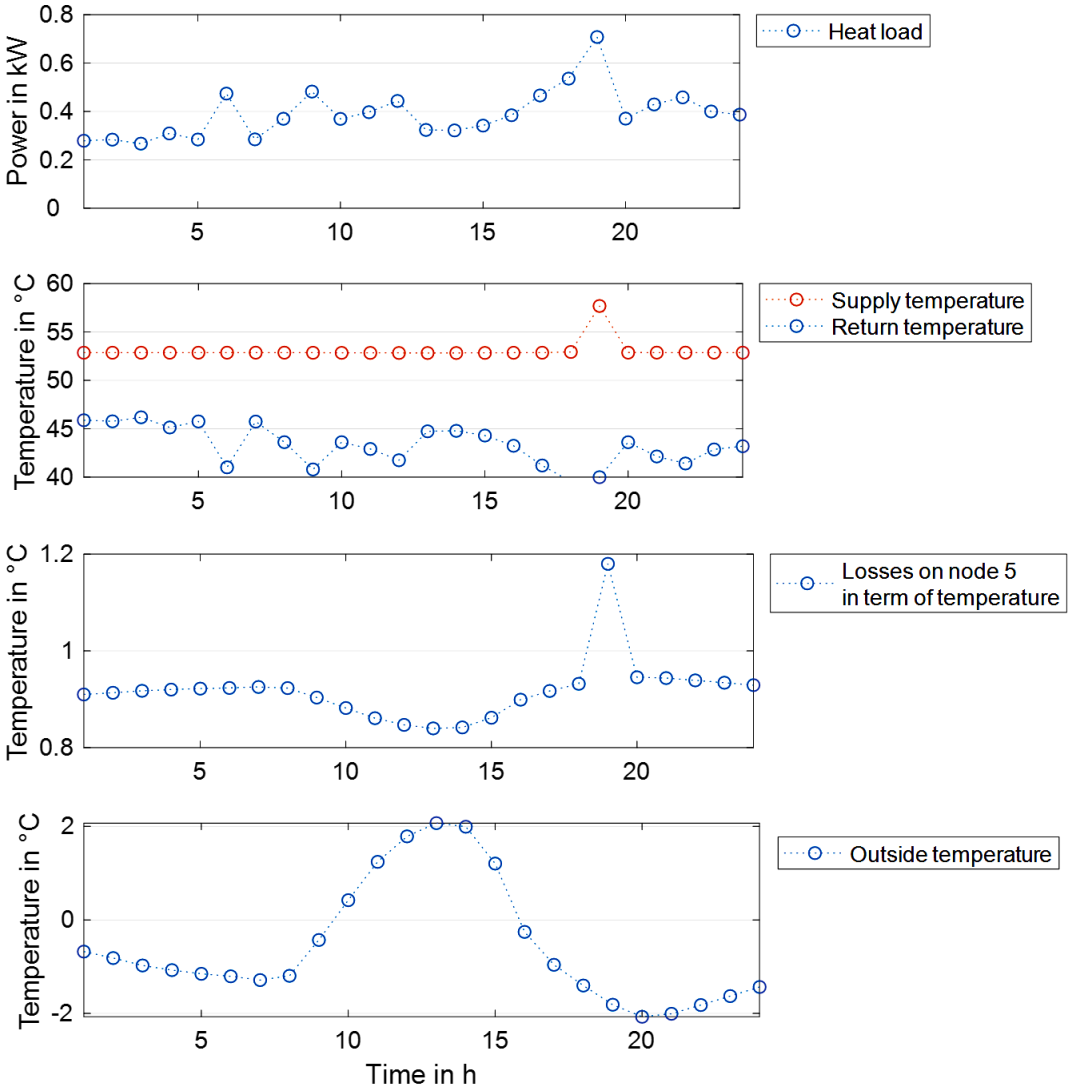

Figure 5.20 Heat grid at node 5 in the heat grid string 1 of the settlement area

More considerable temperature differences, in general, result in higher losses; for example, if the outside temperature is cold, the supply temperature will be cooler during the provision of heating demand. If the outside is warm and the heating material is warm (in supply), the temperature difference between the two is slight. Unless a more significant temperature difference is required at 7 PM, the supply temperature remains constant when the load increases. In section 2.5, the return temperature is a limitation, with a minimum of 10 °C. The losses are higher at this time of day than at other times because the outside temperature is lower and the supply temperature is higher, resulting in a more significant temperature differential. The outside temperature is higher between 10 AM and 3 PM, resulting in less temperature loss. The heating losses in heating string 1 of the heat grid are shown in Annex E.7. The supply and return temperature of node 1 of the settlement heat grid is shown in Figure 5.21.

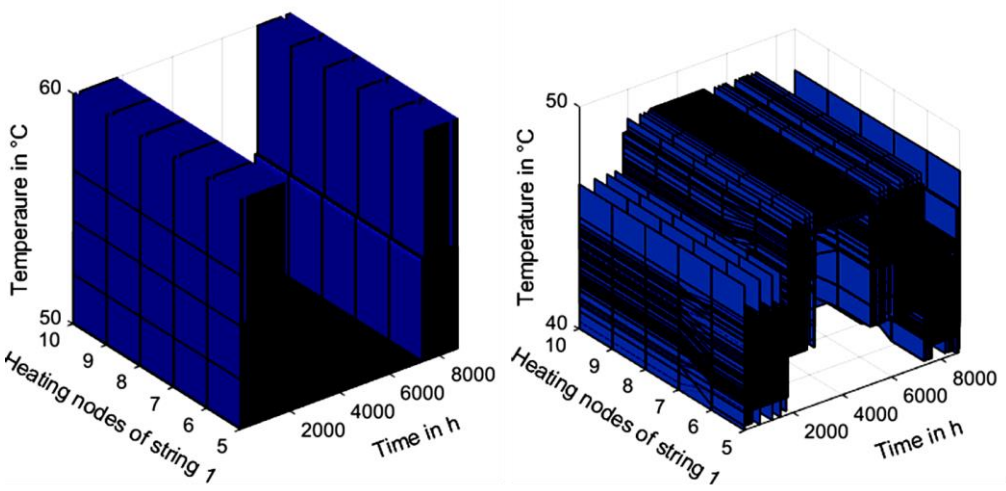

Figure 5.21 Supply temperature (left) and return temperature(right)

Higher heating demand needs a higher temperature difference between supply and return. From Figure 5.21, the supply temperature mimics the heating load on the operation horizon. In winter, the supply temperature is high, the return temperature is low, and vice versa in summer. Higher temperature is needed to supply when the heating demand increase. The supply temperature is from 50 °C to 60 °C in winter and around 50 °C in summer. The return temperature will look opposite to the supply temperature as the heating is extracted from the nodes in winter. The return temperature is higher in the summertime as the heating demand consists of DHW. In the heating grid, the losses through the lines have been considered, due to which a more significant size of the heat pump is needed to cover this extra load. The outside temperature plays an essential role in the losses of the heating grid. The heating losses are shown in Figure 5.22.

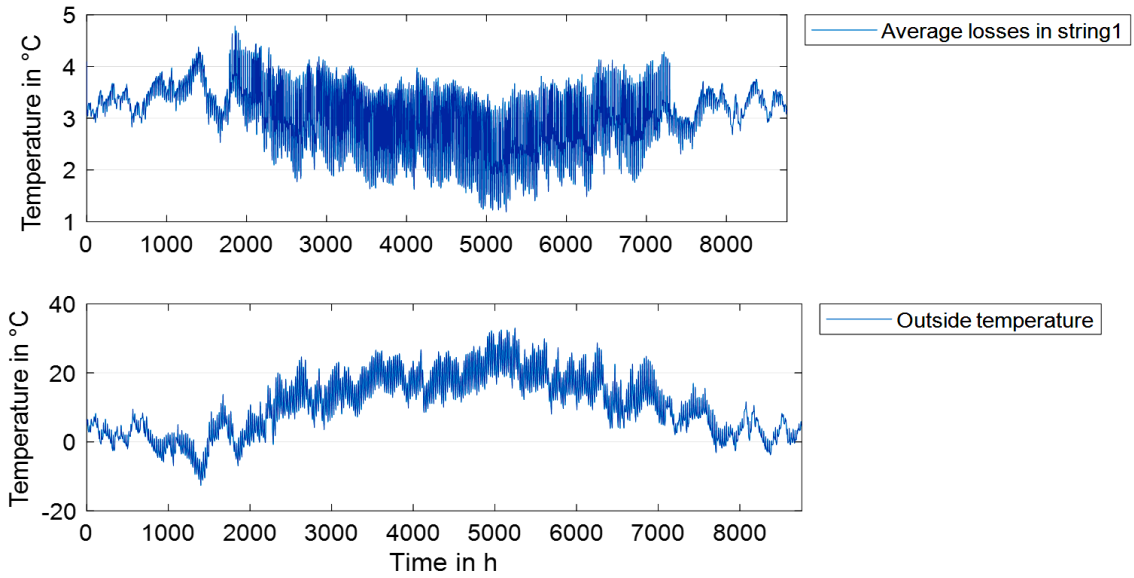

Figure 5.22 Losses in string 1 of the settlement heat grid

It can be seen that the heating losses are minimum, where the heating demand is the lowest, as shown in Figure 5.22. The heating sources are running with low output power at low heating demand. Even with this low output power, a higher supply temperature can be achieved as the temperature extracted at this point is low. Due to this, the temperature difference between supply and return temperatures is relatively low.

5.3.6 Microgrid cost analysis

The optimization objective of the deterministic approach defined in section 4.1 is to plan and operate with minimum cost. The settlement area's total cost includes investment, operational, and emissions penalty costs. The total cost of the microgrid for the planning horizon for negative, trend and positive scenarios is given in Figure 5.23.

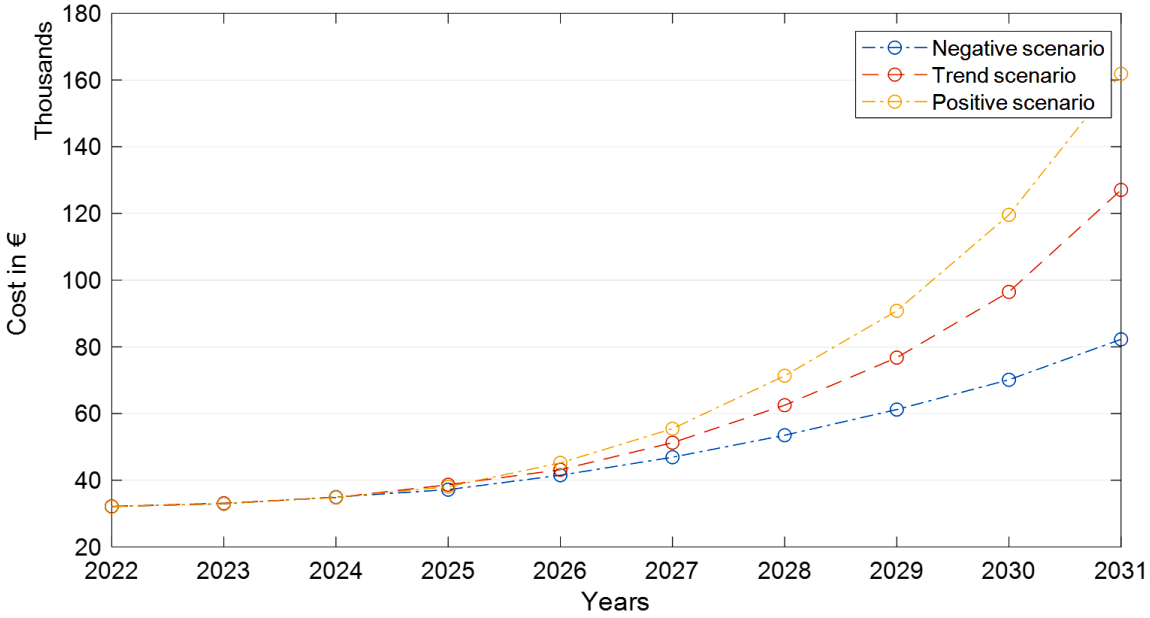

Figure 5.23 Overall cost of the settlement area for different scenarios

Due to the same number of EVs, the cost of the microgrid at the start of the planning horizon is nearly the same. As the number of electric vehicles increases toward the end of the planning horizon, the cost difference between scenarios will widen. In 2031, taking the trend scenario as a reference, this cost will be 12.6 percent lower in a negative scenario. The percentage of cost rise in 2031 for the positive scenario compared to the trend scenario is 32 percent in 2031. The increase in the settlement's overall cost per increase in the number of EVs is evaluated. It is observed that per EV will increase by 2.3 to 2.9 percent in the cost of the settlement. This comparison of the overall cost in terms of investment, operation, and penalty cost related to CO_2 is shown in Figure 5.24. In the trend scenario, Investment costs generated 58.4 percent of the total cost, operating costs contributed 38.4 percent, and CO2 costs contributed just 3.1 percent. The trend in Figure 5.24, the costs will follow the capacities. Due

to this, it can be observed that the investment cost has a significant influence on the capacities.

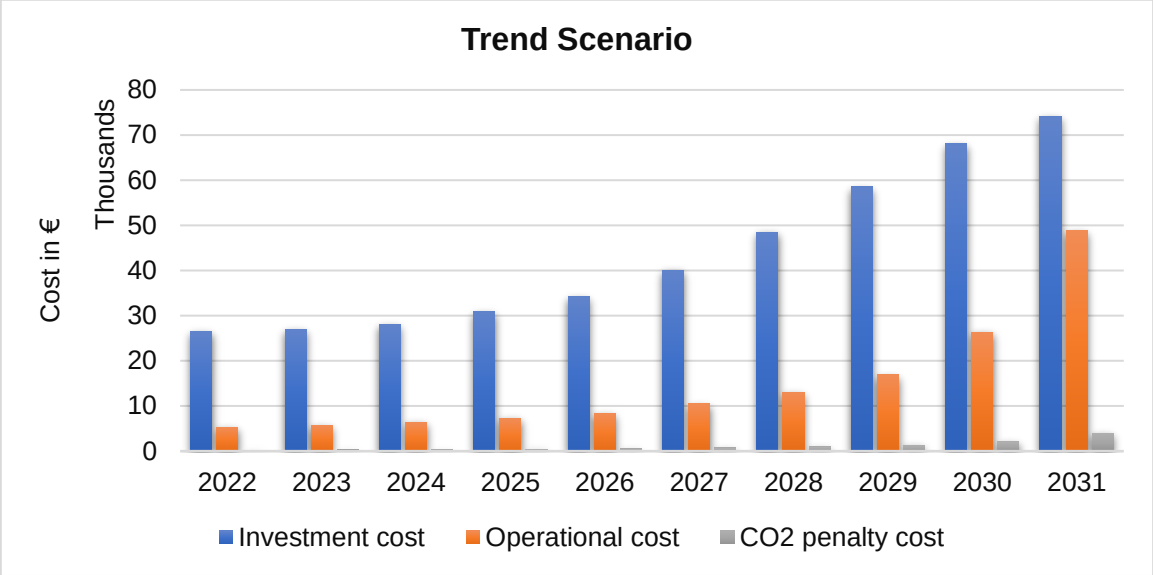

Figure 5.24 Cost analysis of microgrid

The operation cost comprises the electricity imported from the connected grid and the maintenance cost of DERs, which is assumed to be 1 percent of the capital cost of DERs. The investment cost will increase at a low rate till 2026, but after that, the number of EVs will increase more rapidly, resulting in a steep increase in capacities. The EV is still rising till 2031, which needs to be fulfilled by the grid import. The penalty cost for CO_2 emission is not increasing at a high rate because the emission cost certificate for CO_2 is rising every year. The optimization tries to minimize it as much as possible. Compared to operation cost, the CO_2 penalty cost is too low because the CO_2 emission certificate cost per tonne is still too low in Germany. For that reason, CO_2 cost is maybe not the best instrument to support local decentral DERs. The high number of EVs will increase the load, due to which the operational cost compared to CO_2 emission cost will grow at a higher rate. This may become a barrier for a microgrid investment with the motivation of less CO_2 emissions. Due to this, the emission certificate cost needed to be increased to support higher renewables integration in the communities.

5.3.7 Flexible tariff system

A flexible tariff system would here the better choice to increase the local use of renewable energy sources by using the storage system more efficiently. Due to this, the operational cost can be decreased, resulting in a more sustainable and emission-effective microgrid. The proposed tariff is calculated based on the white tariff system introduced in section 4.3 to increase the local usage of renewable energy sources. In this tariff, the microgrid has to pay

five times more in the peak time, three times more in the intermediate time, and an equal amount at the off-peak time than the flat tariff described in section 4.3. However, the white tariff is a variable peak pricing type, and the proposed tariff is real-time pricing. Real-time pricing is used because the EV arrival is random and can shift the peaks in the evening and forth.

5.3.7.1 Microgrid planning with flexible tariff

The white tariff system is compared with the flat tariff system to evaluate the effectiveness of the proposed tariff system for the settlement area. The dimension of the microgrid capacities for a flexible and flat tariff is given in Figure 5.25 for the trend scenario in 2031.

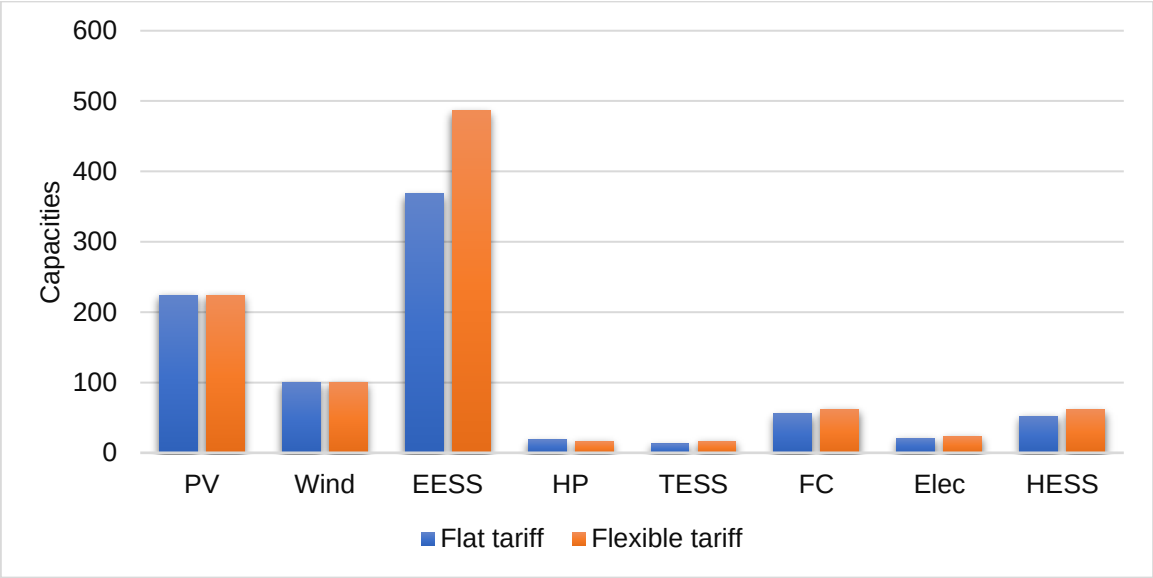

Figure 5.25 microgrid dimensions in flat and Flexible tariff

The capacity of the energy storage system is significantly increased. The cost of electricity is higher in the white tariff during peak times. Therefore, the energy storage system charges cheaply and discharges at high-cost times. The HESS has decreased because the electrolyzer and fuel cell capabilities have decreased.

5.3.7.2 Optimal operation with flexible tariff

By shifting energy, the EESS and TESS contribute to the lowest feasible cost of power, as demonstrated in Figure 5.26. The EESS is charged in the morning and released in the evening at approximately 7 PM, as shown in Figure 5.26. Similarly, the TESS charges at a low price time since heat-producing systems like heat pumps must operate at a low price time. The sum of electrical demand is 1.85 MWh on this day. The heat pump and electrolyzer demands are 50 kWh and 445.8 kWh, respectively. The grid import is required for a small amount of time at 6 PM and 7 PM. The energy generated by PV and wind is 291 kWh and 1 MWh, respectively. EESS is responsible for 400 kWh, which is around 21 percent of the total load. This indicates

that approximately 21 percent of the load has been transferred to off-peak hours by the EESS. The fuel cell fulfills the remaining need.

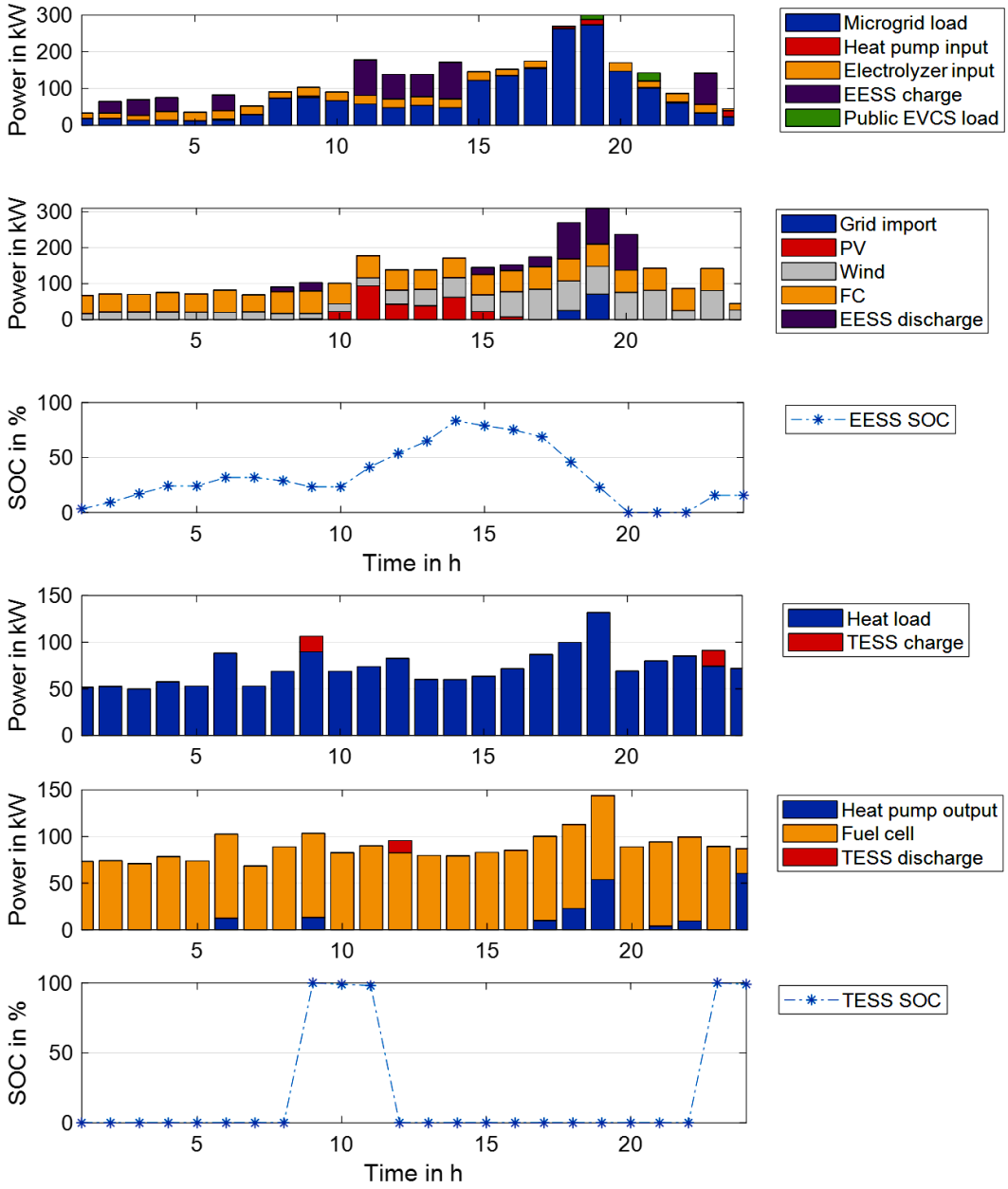

Figure 5.26 electrical and heat energy balance of the settlement area (21st February)

5.3.7.3 Comparison between flexible and flat tariff system

The cost of the investigated settlement area under flexible and flat tariffs for the trend scenario in 2031 is shown in Figure 5.27. The investment cost is higher in the flexible tariff than flat tariff because the energy storage systems are larger in capacity. In a flexible tariff system, energy storage systems must be more significant and run more often to transfer the energy from a low price to a higher price time. It will be more cost-effective to acquire at a low price and discharge at peak periods if grid import is necessary.

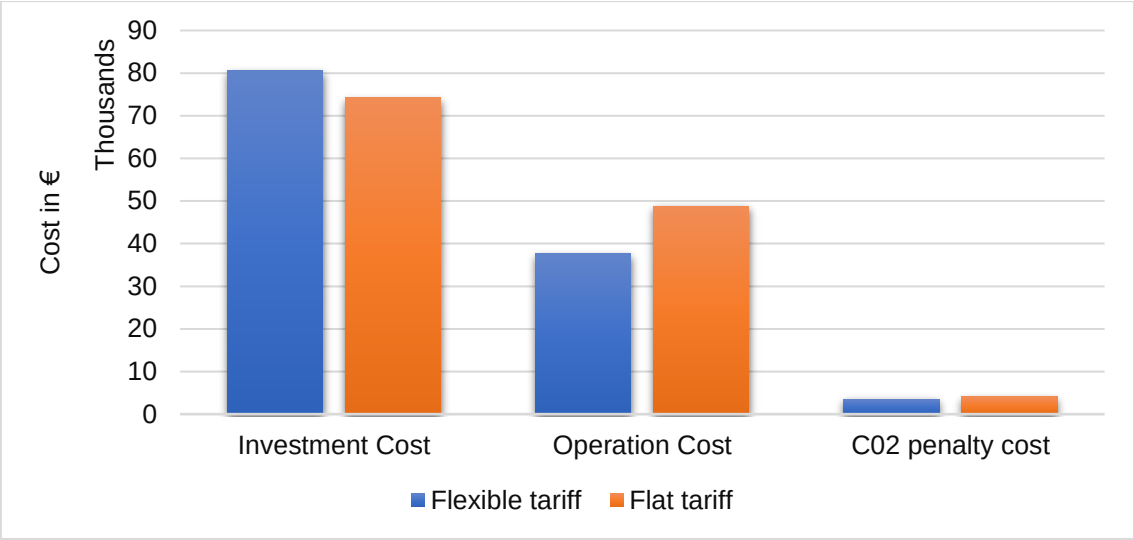

Figure 5.27 Flexible versus flat tariff

The overall cost of a flexible tariff is 4.2 percent lower than the flat tariff because the decrease in grid import cuts operational expenses significantly. The CO_2 penalty cost is higher in the flexible tariff system as a higher amount of grid import is needed. The high peak time resulted from the integration of e-mobility mostly occurs at a high price time. In the flexible tariff system, it will be more cost-effective to use energy storage systems to provide these high peaks at high price times by charging them during low price times. In the flat tariff system, as the electricity price is the same, the energy storage will be charged mostly from renewables. Due to this, the grid is imported more in the flexible tariff as compared to the flat tariff but at a cheaper price. The operational and CO_2 cost comparison is flat and flexible tariffs can be seen in Annex E.8. The decision-makers can save up to 12 percent on the operational cost and 4.2 percent on the overall cost of the microgrid. Due to this, it is observed that the flexible tariff based on the white tariff outperforms the flat tariff in microgrid planning and operation. The flexible tariff will be more effective if the demand response programs are considered. However, Without any demand response programs, considering the aim of powering the e-mobility infrastructure with the least possible CO_2 emissions, the flat tarri is better to be implemented.

5.3.8 Sensitive analysis

This structure is compared with the settlement area structure shown in Figure 5.2 based on the cost analysis of the settlement area. The sensitivity analysis is evaluated using the trend scenario. Furthermore, it is believed that the impact of sensitivity analysis on microgrid structure would be the same regardless of the year in the planning horizon, hence, 2022 will be used in this part. A sensitive analysis is performed for the trend scenario in 2031. It is assumed that changing the following aspect impacts microgrid planning and operation.

- ❖ *DERs replacement:* The hydrogen system (Fuel cell, electrolyzer, and hydrogen storage) is unnecessary.
- ❖ *DERs capacity limit:* The microgrid connected to a low voltage grid is legislated and a higher amount of DERs are allowed to be installed

5.3.8.1 DERs replacement

The hydrogen system is removed, and the heat pump alongside TESS provides a heating grid. The cost comparison of both microgrid structures is shown in Table 5.8.

Table 5.8 Comparison of the settlement cost with and without hydrogen system

Microgrid structure	Investment cost in €	Operational cost in €	CO_2 penalty cost in €
Without hydrogen system	21097.04	29850.94	1264.269
With hydrogen system	26575.19	5349.26	219.64

The investment cost has dropped, but the operating costs have increased due to direct renewable energy consumption reduction. The amount of electricity drawn from the grid was raised by 23 percent. Since the grid import is the principal source of CO_2, this rise also increases CO_2 emissions. In terms of cost, it is more economical and emission-effective to use the hydrogen system in the microgrid.

5.3.8.2 DERs capacity limit

The maximum capacity of DERs is limited since the microgrid is connected to a low-voltage grid. The electricity capacity limit for each DER is increased to 600 kW in this section. Figure 5.28 depicts the dimensions of DERs in the microgrid.

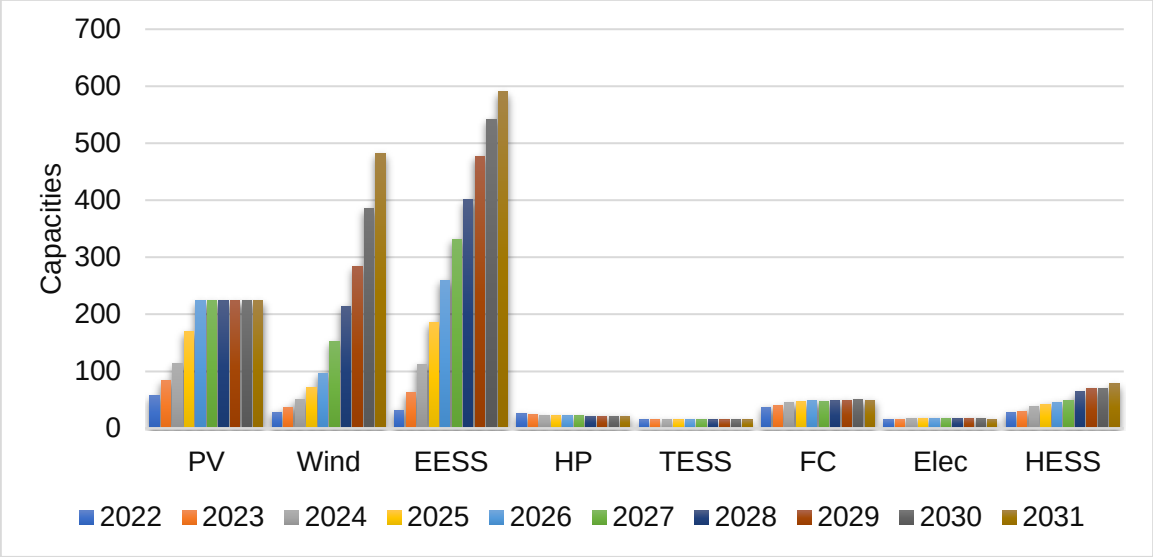

Figure 5.28 Dimensions of DERs in the investigated settlement area

The EESS and TESS capacities are measured in kWh, whereas the generating units, heat pump, and electrolyzer are measured in kW, and the HESS is measured in m^3. Allowing higher capacity limits will increase EESS and wind capacities by a high amount. The PV system will not increase after 224 kW as the limit is calculated as per available space for the PV installation, as described in section 2.11. Comparing Figure 5.28 and Figure 5.14 in section 5.3.1, the increase in the wind and EESS reduces the rise in fuel cell capacity because the fuel cell, electrolyzer, and HESS systems are more expensive than the wind and EESS.

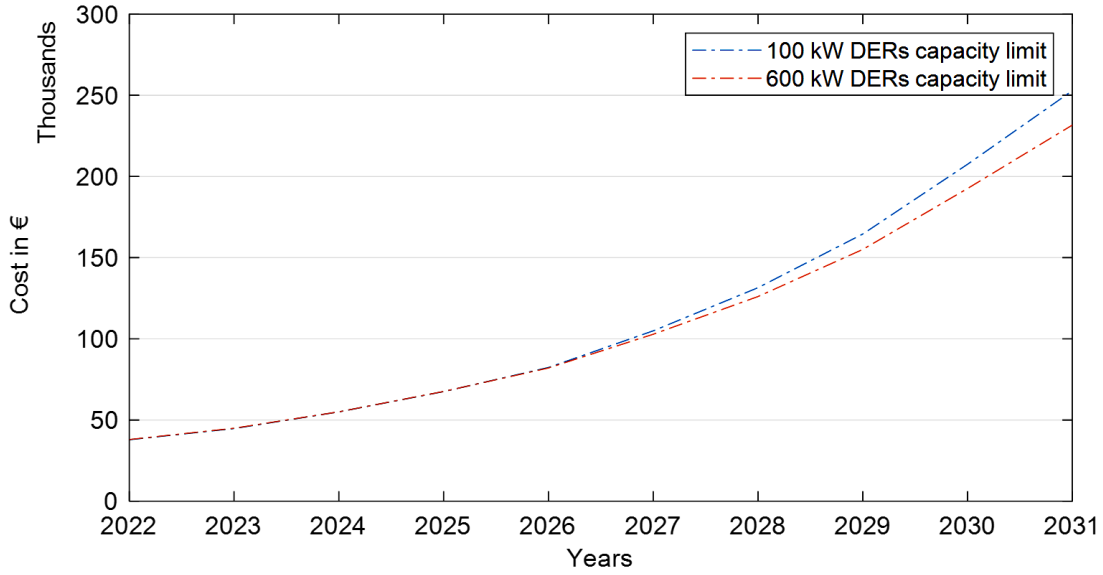

Figure 5.29 Comparision of 100 kW and 600 kW capacity limit

The cost stays the same until 2026 since the capacities rise at the same pace in both situations until the EESS reaches its power capacity. After 2026, the higher DERs limits did not result in a huge cost increase because the operating cost is increasing with the rise in the number of EVs. The CO_2 emission penalty cost is also reduced by reducing the operation cost. In conclusion, microgrids need to be allowed higher limits to accommodate more and more renewables. The negative impact of high limits of DERs can then be dealt with locally in the microgrid by different methodologies such as demand response and control policies. A solution is to integrate the microgrid with a middle voltage grid. However, from Figure 5.28, such a high wind installation capacity is not possible as it depends on people and space's local conditions and acceptance. By increasing these hosting capacities of DERs, the overall cost will be reduced compared to capacities limitation, as shown in Figure 5.29.

5.4 Microgrid planning and operation with stochastic optimization

The increase in the EV and EVCS is inevitable, as described in section 5.2. The forecast is just based on the factors described in section 3.1. However, it is challenging to forecast these rises in the EVCS accurately because any of these factors may change. Based on the recent crises

such as pandemics and shortages of semiconductor materials, EV production has been affected immensely, affecting the installation of EVCS. It is clear that the actual number of EV and EVCS installations has not been following the trends due to several reasons. This is predicted to have a significant impact on microgrid planning and operation.

Furthermore, the EV arrivals on a day, charging from a public EVCS and privately, have a high associated load. Any uncertainty related to EV arrival can influence microgrid planning and operation. The following aspects are analyzed to evaluate the impact of multi-type uncertainty on the investigated settlement area. For the evaluation of the results, the trend scenario is considered.

- ❖ Consideration of Long-term uncertainty
- ❖ Consideration of Short-term and Long-term uncertainty

For the evaluation of the results, the trend scenario is considered. Furthermore, Due to the fact that the flat tariff is already in place in Germany, the flat tariff is used in the stochastic optimization approach. Note that the microgrid is considered in a risk-averse manner (risk-avoiding). If the ability of the DERs of the microgrid to amount of uncertainties occurs will define the robustness of the microgrid. A best-case in terms of a risk-averse microgrid is when fewer uncertainties occur and vice versa. However, the uncertainties are uncontrollable, due to which the robustness of the microgrid should be planned.

5.4.1 Consideration of Long-term uncertainty

The long-term uncertainties related to EVCS are modeled using IGDM, as described in section 4.2.1. The envelope bound for the number of EVCS shows the boundary of the uncertainty region. For α_{EVCS}=1, the envelope bound for the number of EVCS for the last five years of the planning horizon is shown in Figure 5.30.

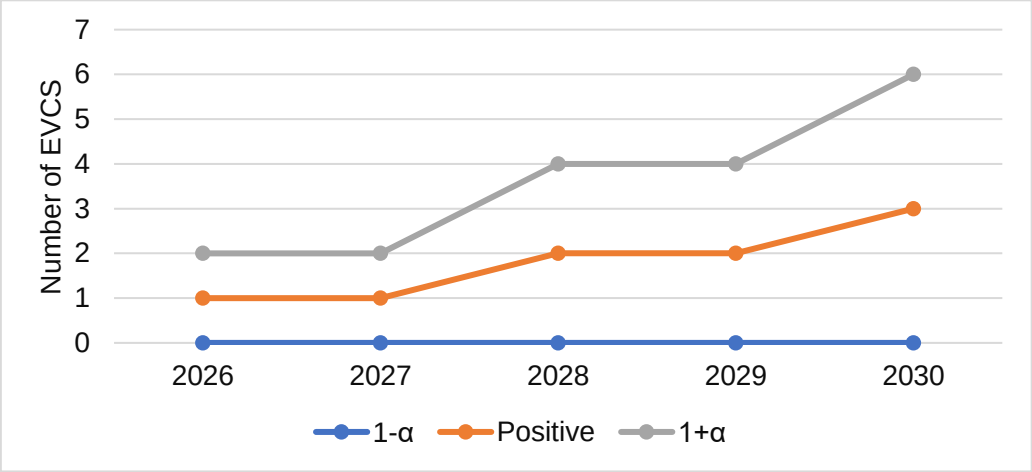

Figure 5.30 Number of EVCS

It can be concluded that the outer boundary of the envelope will be the worst-case (Highest uncertainty), and the inner boundary (Lowest uncertainty) represents the best-case for the microgrid.

The optimization aims to increase the robust region α_{EVCS} concerning the allowed budget f_{b}. The allowed budget is defined as the percentage increase in the cost of the microgrid achieved from the deterministic optimization. f_{b} will be equal to the cost of the deterministic microgrid if the allowed budget is 1. The decision-maker can adjust this factor at the planning stage based on the amount of acceptance to pay more for the microgrid's robustness against uncertainty. The α_{EVCS} will change depending on the specified f_{b} and the highest attainable α_{EVCS} will be the ultimate microgrid robustness against EVCS uncertainty. The robustness of the microgrid with the change in the allowable budget is shown in Figure 5.31. It can be seen from Figure 5.31 that the uncertainty region increases linearly with an increase in the allowable cost budget. A 100 percent robust region can be achieved with an allowable budget of 1.8. This means that 1.8 times (80 Percent) more cost is needed for the microgrid to handle all uncertainties in the envelope. For an allowable budget equal to the deterministic cost, the microgrid has similar DERs capacities as computed in the deterministic optimization model.

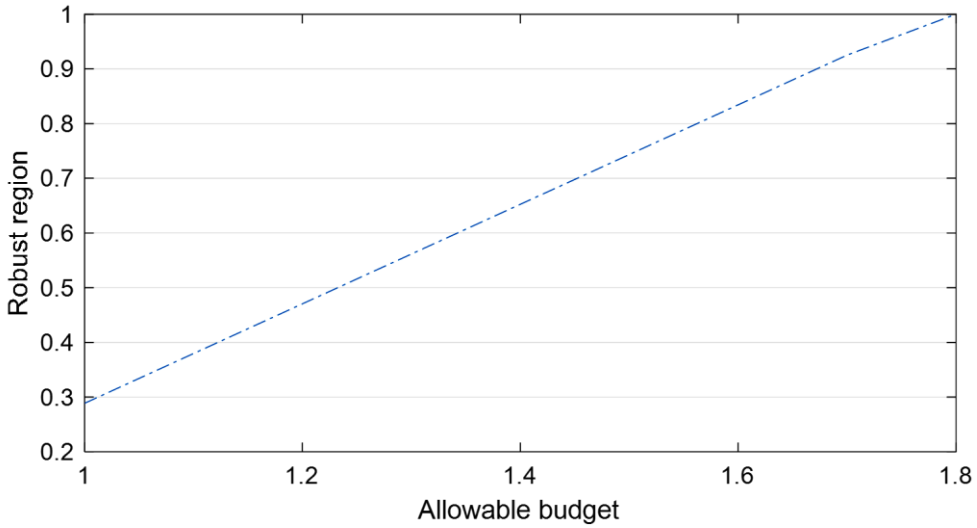

Figure 5.31 Robust region versus allowable budget

The comparison of capacities of DERs for an allowable budget equal to the deterministic approach is shown in Annex E.9. However, considering the allowable budget equal to deterministic cost, the microgrid has only 28.8 percent of robustness under long-term uncertainty, as shown in Figure 5.31. A higher budget increased the capacities of the DERs to power the extra amount of EVCS, which will increase the robustness of the microgrid. The capacities of DERs for trend scenarios for a 100 percent robust (allowable budget of 1.8) are shown in Figure 5.32. Uncertainties are unavoidable, but the number of uncertainties is

difficult to estimate. As a result, a fully robust microgrid is proposed at a higher cost during the planning stage.

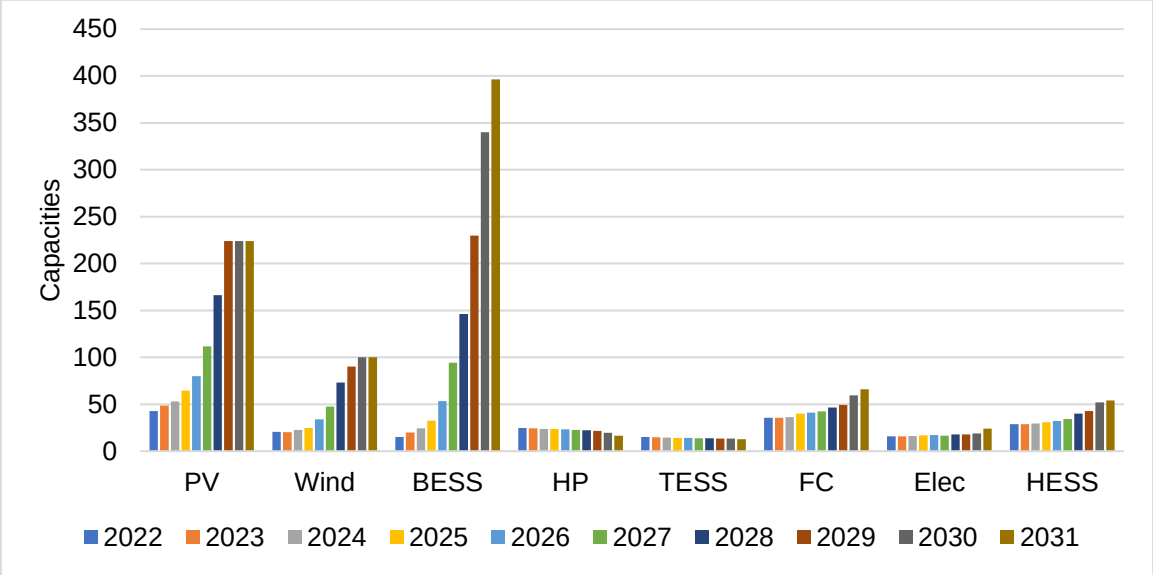

Figure 5.32 Microgrid capacities of trend scenario

It may be more expensive to tackle these uncertainties economically and technically if the microgrid is designed for less resilience and more uncertainty occurs. However, the results of the microgrid dimension for different robustness are shown in Annex E.9. The 80 percent increase in the microgrid's cost budget to meet the additional number of EVCS enhances the capacity of the PV and EESS. This increase in PV, wind, and EESS will ensure that the EVCS is powered more by renewable energy. The comparison in the rise in the capacities of DERs of microgrids for the planning horizon can be seen in Annex E.9. Most of the long-term uncertainties occur at the end of the planning horizon. In these years, the PV and wind systems can not be increased further due to the limit announced in section 5.1. Due to this, the capacity of the EESS and fuel cell increases more as compared to the deterministic approach. As the number of EVCS rises, the number of uncertainties increases. As illustrated in Figure 5.32, the capacities increase in the same fashion. The heating equipment is not frequently changed because the heating grid and heating demand are consistent. The slight drop in the heat pump is caused by an increase in the fuel cell required to generate electric power due to uncertainties in conjunction with other generation units. The proposed method based on IGDM is highly recommended over the deterministic approach when there is a chance of the occurrence of long-term uncertainty, which can not be realized through the deterministic optimization approach.

5.4.2 Consideration of short-term and long-term uncertainty

The short-term uncertainties are handled by chance constraint described in 4.2.2. If there is no uncertainty in the energy balance, it is always viable. If the uncertainty is not a distribution function, including uncertainty in the energy balance will be simple. The confidence level $(1 - \epsilon)$ shows the portion of the probability distribution function from the ambiguity set in which the energy balance, including uncertainty, is not violated. The higher confidence level indicates that more area is covered in the distribution function. The ϵ shows the tolerance level of the microgrid against short-term uncertainty. The robust region will increase with the confidence level decrease as fewer EV arrives as the distribution. The allowable budget level and confidence level decide the robustness. The increase in the confidence level will also affect the robust region. The decrease in the confidence level and the robust region is presented in Figure 5.33. The short-term uncertainty will be severe and behave the same way through the planning horizon. The short-term uncertainty is assumed to be unknown at the planning stage. The chance-constraint DRO handles the short-term uncertainty ambiguity set in the planning horizon. Due to this, it is ensured through chance-constraint DRO that if severe uncertainty occurs in the microgrid in the future, the microgrid is robust enough to hedge against it with a generated confidence level. As shown in Figure 5.33, the investigated settlement area is 35 percent robust with the ambiguity set defined in section 4.2.2.

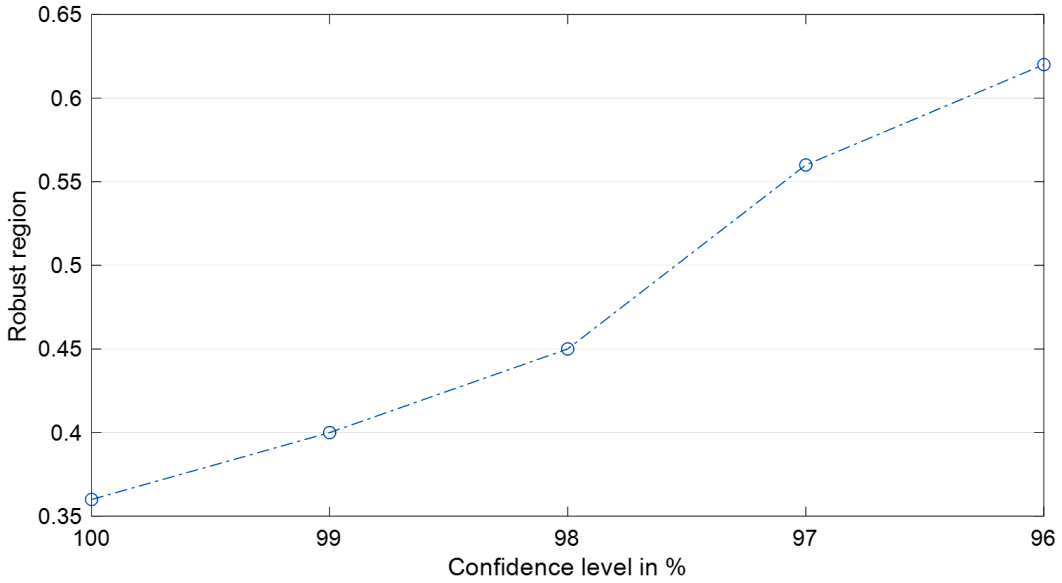

Figure 5.33 Impact of short-term uncertainty over the robust region

This means that the microgrid is able to hedge 35 percent of the uncertainties even with a zero-tolerance level (100 percent confidence level). If the microgrid is planned and operated without considering any short-term uncertainty, the confidence level is 100 percent. However, the confidence level can be decreased to induct more uncertainties, due to which the robust

region is increased. The decision-makers can then decide on less robustness (lower cost) or high robustness (higher cost) microgrids, depending on the requirements. The lower confidence increases the robust region, and similarly, the allowable budget also increases the robust region. Due to this, allowing more short-term uncertainty (lower confidence level) and more long-term (higher allowable budget) increases the cost but reduces the risk (risk-averse). The risk-averse microgrid with an allowable budget of 1.8 and 96 percent is proposed for the investigated settlement area. The microgrid cost for the different confidence levels is presented in Table 5.9.

Table 5.9 Microgrid cost with long and short-term uncertainty in trend 2031 (fb=1.8)

Confidence level in %	**Investment cost**	**Operational cost**	**CO_2 penalty cost**
100	133564.80	42498.14	4028.32
99	135359.57	43396.29	4134.56
98	137154.79	43998.55	4216.66
97	138949.37	44595.43	4358.33
96	140744.09	45404.23	4414.53

A confidence level from 96 to 100 percent is allowed. In a deterministic approach, the investment cost is roughly 74,000 euros, and the operational costs are around 48,000 euros. The long-term uncertainty with fb=1.8 increases the investment cost to approximately 133,000 euros. With a 100 percent confidence level, the cost of the microgrid considering long-term uncertainty will be equal to a microgrid with long and short-term uncertainty. The load margin that cannot be fulfilled due to short-term uncertainty is allowed when the confidence level falls. The capacities in trend 2031 with a confidence level of 96 percent and an allowable budget of 1.8 are shown in Figure 5.34.

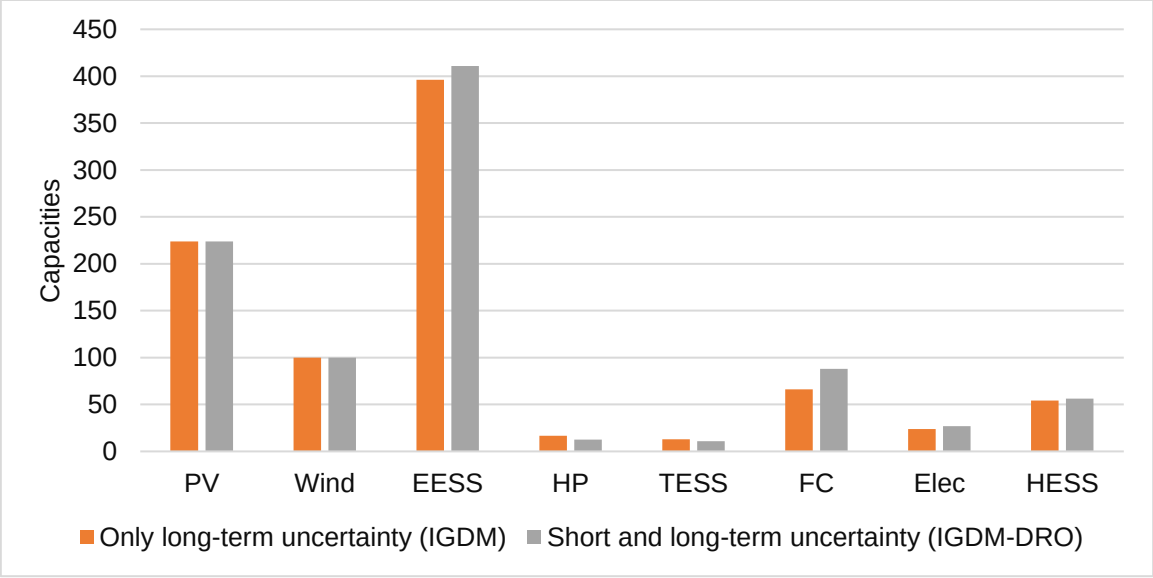

Figure 5.34 Comparision of IGDM and IGDM-DRO

As the confidence level decreases, the cost of the investigated settlement increases. Because the arrival of electric vehicles is very unpredictable, it can be more cost-effective at the planning stage to allow less significant confidence level (more tolerance level) margins. From Table 5.9, it is concluded that the decrease of 1 percent confidence level will increase roughly 3 to 4.5 percent in the cost of the microgrid. The increase in the cost of the microgrid results from the increase in capacities. The capacities of renewable energy sources in trend 2031 for IDGM and IGDM-DRO are likely to be similar because of the limit. However, the extra energy needed to fulfill the short-term uncertainties increases the EESS and fuel cell. The slight decrease in the heat pump and TESS is caused by the increase in the fuel cell.

5.4.3 Comparison between deterministic and IGDM-DRO

The comparison of the proposed holistic approach with the deterministic microgrid planning and operation for the investigated settlement for trend 2031 is shown in Table 5.10. The long-term uncertainty only comes into play at the end of the planning horizon. Typically, however, DER is operated for a planning horizon of 10 years, so planning with uncertainties makes sense. As the short-term uncertainties have a relatively small impact on the cost of the microgrid, as shown in Table 5.9 and Figure 5.34, the confidence level of 96 percent is considered for the comparison.

Table 5.10 Comparison of deterministic and IGDM-DRO approaches

Method	**Deterministic approach**	**IGDM-DRO**		
Robust region in %	-	0	50	100
Overall cost in €	127029.39	128576.97	184192.6	215563.6

Note that the robust region of 100 percent was achieved at an allowable budget of 1.8. Similarly, 50 percent was achieved with an allowable budget of 1.45. From Table 5.10, the IGDM-DRO acquired more cost as compared to the deterministic approach. However, the developed approach is better than the deterministic approach due to the following reasons:

- Consideration of uncertainties in the microgrid planning and operation, due to which the decision-makers can plan the microgrid under multi-type uncertainty
- Enables the decision-makers to plan the decision on the basis of cost versus robustness

Given that the deterministic version is better in terms of cost and the IGDM-DRO is better in terms of robustness, a combination of the two methods will be effective in terms of trade-off.

5.4.4 Scalability solution

As the planning problem is for a future scenario in term years, this computational time is acceptable. However, the IGDM-DRO optimization becomes intractable with the case study of the presented new settlement area due to many equations, variables, and types of problems. Due to this, the tractable solution is proposed. The input data is scaled with 10-day type categories, as described in section 2.3. It has been assumed that the load and generation behave the same as defined with the day type categories. The bender decomposes the problem with day-type categories. The result of the multi-cut bender decomposition for trend scenarios in the planning horizon is shown in Table 5.11.

Table 5.11 Tractability using multi-cut bender decomposition

	Original Problem	**Decomposed**
Equations	1,051,727	29,3205
variables	39,595,272	1,084,879
Binary variable	52,560	4,780
Solution time	Intractable	5 h, 27 min

The proposed methodology is efficient as computation time and effort is saved. The bender decomposition must converge, and due to its iterative nature, the less time it takes to converge, the more solution time can be saved. The convergence for the multi-cut bender decomposition for a year (trend 2022) is shown in Figure 5.35.

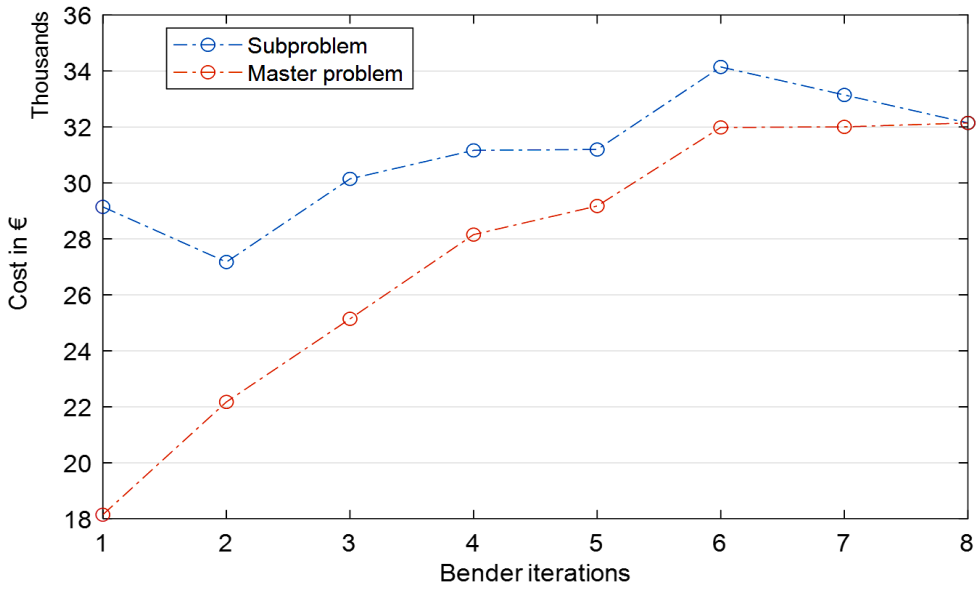

Figure 5.35 Convergence for multi-cut bender decomposition

Figure 3.5 shows the convergence for the bender decomposition for IGDM-DRO with an allowable budget of 1 (equal to the deterministic approach) and a confidence level of 100 percent. Due to this, the cost of the microgrid in trend 2022 is approximately equal in

deterministic and stochastic approaches as the uncertainties are minimal, as given in Figure 5.23. However, although uncertainties are minimal, there is a slight change in the cost due to different methods in deterministic (32,144 €) and IGDM-DRO (32,768 €). IGDM-DRO's objective in the master problem is to increase the robust region. As a result, the investment cost is handled as a constraint, as mentioned in section 4.2.3. As a matter of fact, the convergence might vary for each year of the planning horizon. The solution is found in the eighth iteration this year. The solution time will fluctuate as the number of bender iterations increases. However, it was discovered that the number of iterations has never exceeded 13. As a result, the IGDM-DRO is always tractable with multi-cut bender decomposition.

6 Conclusion and outlook

In the scope of this dissertation, a new holistic approach for microgrid planning and operation for e-mobility under the consideration of multi-type uncertainties was proposed and discussed. The scope of this study was to develop a cost-efficient, emission-effective, and technically sound microgrid from scratch for the development of e-mobility infrastructure, as well as to analyze the consequences of e-mobility-related uncertainties on the microgrid.

Due to the motivation to address climate change, the development of renewable energy sources, energy storage systems, and sector coupling technologies, also known as distributed energy resources, is inevitable in sectors such as electricity, heat, and industry. Similarly, the e-mobility infrastructure is developing rapidly as a result of this motivation. Renewable energy sources must power the e-mobility infrastructure to achieve environmental effectiveness over combustion engine vehicles. However, the existing power systems are not always capable of handling the additional power and adverse effects of large-scale deployment of e-mobility infrastructure.

Nonetheless, the microgrid components with the e-mobility infrastructure must be optimally planned and operated to prevent high costs, technical issues, and emissions. The existing methods in the literature for optimal planning and operation lack the method for e-mobility infrastructure. As a result, a compact methodology for e-mobility infrastructure planning is proposed. The proposed method includes a retropolation method for planning the increase in the number of electric vehicles, Monte-Carlo simulation for EV behaviors, EVCS number based on occupancy time, and public EVCS placement based on Monte-Carlo simulation.

In the microgrid planning and operation, the DERs and the e-mobility infrastructure may cause technical problems in the grid, such as voltage issues. Due to this, technical issues must be included in the microgrid planning and operations so that these problems can be avoided. The current dissertation uses linearized optimal power flow equations to model voltage perturbation in the electrical grid. In addition, the heat losses for the low-temperature heating grid are included. Finally, a deterministic approach for microgrid planning and operation is developed for e-mobility infrastructure to minimize investment, operational, and CO_2 penalty costs considering the above-stated technical parameters. The deterministic microgrid planning and approach are tested with flat and flexible tariffs. The flexible tariff system is modeled based on the white tariff system implemented in Brazil.

The e-mobility infrastructure development has been associated with multi-type (short-term and long-term) uncertainties. Direct and indirect variables such as the rise in the number of

EVs, battery technology, and government incentives significantly influence the planning of the number of EVCS. As a result, forecasting the number of EVCS is challenging, and thus the number of EVCS is regarded as a long-term uncertainty. The daily arrivals of EVs are also highly unpredictable due to the user's random behavior for traveling and charging. These uncertainties might result in a high risk for microgrid planning and operation in microgrid planning and operation. Due to this, in this dissertation, a new stochastic method was developed, which gives a risk-averse strategy for microgrid planning and operation by including long-term and short-long uncertainties. The number of public electric vehicle charging stations as a long-term uncertainty is modeled with the information gap decision method (IGDM). Additionally, the short-term uncertainties are handled with distributional robust optimization (DRO). The proposed method is referred to as IGDM-DRO to tackle the microgrid planning and operation under multi-type uncertainty related to e-mobility. Finally, to avoid the intractability of the proposed method, the multi-cut bender decomposition is implemented for IGDM-DRO.

The deterministic and stochastic approaches are merged into a new holistic approach to consider the optimal microgrid planning and operation in terms of cost and robustness at the same time. The microgrid is optimally planned and operated with the objective of robustness and cost. The cost of the microgrid included investment, operation, and CO_2 penalty costs. In the CO_2 penalty cost, the declining emission intensity in the electrical grid due to the increasing renewables and the increase in the emission certificate cost is considered.

The methods were implemented in a case study of a new settlement area Alte Ziegelei Magdeburg, Germany. The settlement area is planned from scratch, where the statistics and available areas for PV systems, electrical, and heat grid with settlement demand are modeled. A microgrid based on the above-stated method is planned for a planning horizon of 10 years for the investigated settlement area.

Based on people's acceptance, three scenarios (negative, trend, and positive) for the development of the number of electric vehicles are generated. Based on investment costs, operational costs, driving benefits, and other benefits, a projection for the percentage of EVs over conventional cars in 2026 is made. The rising rate of EVs is then retropolated till 2026 and extrapolated till the end of the planning horizon. It was concluded that the number of EVs will be one in 2022, which will be raised to 17, 33, and 43 in negative, trend, and positive scenarios, respectively. At the end of the planned horizon, electric vehicles might constitute up to 31 percent of all vehicles. In the investigated settlement area, these EVs will be charged at home using private charging stations with a rated power of 11 kW and at public electric vehicle charging stations (EVCS) with a rated power of 22 kW. Based on the results for EVs

behaviors from the Monte-Carlo simulation, the EVs will increase the electrical load up to 48 percent n a particular day. Furthermore, because consumers arrive at their homes mostly at the same time in the evening, roughly 3 to 34 percent of all EVs might be charging simultaneously, resulting in a significant peak in the settlement load. In the trend scenario, the EV in the settlement area will require at least three EVCS by 2031, based on EVCS occupancy times of less than 30 minutes. The planned three EVCS must be installed at the nodes with a node voltage-sensitive index (NVSI) of less than 0.2. Due to this, the optimal location for the public EVCS was concluded to be K1, K14, and K2.

The investigated settlement area is optimally planned and operated using a deterministic optimization approach based on the rise in the EV. When comparing the negative, trend, and positive scenarios, the overall cost of the investigated settlement area decreased by 12.6 percent in the negative scenario and increased by 32 percent in the positive scenario. A rise per EV in the settlement area indicates a 2.3 to 2.9 percent increase in overall cost. The dimension of the DERs in the investigated settlement area for the trend scenario for 2031 is shown in Table 6.1.

Table 6.1 DERs dimension in 2031 for investigated settlement area

DERs	**PV**	**Wind**	**EESS**	**HP**	**TESS**	**FC**	**Elec**	**HESS**
Capacities	224. kW	100 kW	368.3 kWh	18.6 kW	12.8 kWh	56.0 kW	20.8 kW	52.3 m^3

It was concluded that implementing these DERs in the settlement area needed an overall cost of 127029 € in the trend scenario. From the overall cost, 58.4 percent of the cost is contributed by investment cost, 38.4 percent is contributed by operation cost, and only 3.1 percent is contributed by the CO_2 Penalty cost. The CO_2 Penalty cost is less due to the low emission certificate cost set by the government. Due to this, the CO2 penalty cost might not be a good instrument to support the local use of renewable energy sources at this moment. The operational cost can still be minimized by 12 percent, which decreases the overall cost by 4 percent if the proposed flexible tariff is used in the settlement area in the trend scenario. However, due to the higher CO_2 emissions and the demand response programs being out of this dissertation's context, the flat tariff system has been used for further demonstrations of the results. Because of its combined heat and electricity feature, the hydrogen system (fuel cell, electrolyzer, and hydrogen storage system) fuel was shown to be the most effective among the DERs in terms of utilization. By adding a hydrogen system, the overall cost has been decreased up to 38 percent.

Considering the multi-type uncertainties, it was concluded that the microgrid resulting from the deterministic approach is just 28 percent robust against the long-term uncertainty. Such

low robustness will be risky in long-term planning. To achieve full robustness, the cost of the microgrid needs to be increased by 80 percent. If the confidence level is reduced to 96 percent by including short-term uncertainty, robustness of around 60 percent will be obtained. With the robustness of the allowable budget of 80 percent and confidence level of 96 percent, 66.7 percent of the cost has been increased as compared deterministic approach in the trend scenario in 2031. The increase in the cost resulted from the higher capacities needed to hedge the uncertainties. Due to this, the deterministic approach is considered to be better in terms of cost, and IGDM-DRO is recommended if the robustness against uncertainties needs to be planned.

By the proposition of scalability for the IGDM-DRO by using multi-cut bender decomposition in the current dissertation, the methodology is well suited for planning and operation under multi-type uncertainties for larger settlement areas such as cities. However, high computational time with a duration of days depending on the grid sizes is expected. As e-mobility infrastructure planning under uncertainties is more effective in larger cities, a further decrease in computational time can be a future research area. A study on the propagation of these uncertainties to other sectors, such as gas and heat, is also worthy. In general, the microgrid has other associated short and long-term uncertainty such as daily renewables generation, declining or inclining cost of the DERs, and technological development. Considering a higher number of uncertainties will give a better perspective on microgrid planning and operation. The replacement of DERs, such as PV systems and energy storage systems, will increase the material waste trash, which is not environmentally friendly. Considering a study to minimize the DERs trash as much as possible might be an interesting field of further research. The introduction of microgrids can well handle the development of the e-mobility infrastructure in the cities. However, there is still a limitation in terms of capacities for DERs installations due to the negative impacts of DERs. It is recommended that the microgrids need to be allowed to install higher capacity DERs to accommodate more renewable energy sources. The negative impact of the DERs can be dealt with locally in the microgrid by a different method, such as demand response and control policies. A solution is to integrate the microgrid with a middle voltage grid. However, higher wind installation capacity is not always possible, depending on people and space's local conditions and acceptance.

Bibliography

[1] Clean Energy Wire. *Germany's greenhouse gas emissions and energy transition targets*. Available at: https://www.cleanenergywire.org/factsheets/germanys-greenhouse-gas-emissions-and-climate-targets; 2014 [accessed 30.08.2021].

[2] IEA. *Greenhouse Gas Emissions from Energy Data Explorer – Data Tools - IEA*. Available at: https://www.iea.org/data-and-statistics/data-tools/greenhouse-gas-emissions-from-energy-data-explorer [accessed 30.08.2021].

[3] Energy.gov. *"GRID 2030" A NATIONAL VISION FOR ELECTRICITY'S SECOND 100 YEARS | Department of Energy*. Available at: https://www.energy.gov/oe/downloads/grid-2030-national-vision-electricity-s-second-100-years [accessed 21.09.2021].

[4] IEA. *Technology Roadmap - Smart Grids – Analysis - IEA*. Available at: https://www.iea.org/reports/technology-roadmap-smart-grids [accessed 28.09.2021].

[5] www.districtenergy.org. *Features and Benefits - Microgrids*. Available at: https://www.districtenergy.org/microgrids/about-microgrids97/features [accessed 09.02.2021].

[6] Hirsch A, Parag Y, Guerrero J. Microgrids: A review of technologies, key drivers, and outstanding issues. *Renewable and Sustainable Energy Reviews* 2018;90:402–11, doi:10.1016/j.rser.2018.03.040.

[7] Li Z, Xu Y. Optimal coordinated energy dispatch of a multi-energy microgrid in grid-connected and islanded modes. *Applied Energy* 2018;210:974–86, doi:10.1016/j.apenergy.2017.08.197.

[8] Styczynski ZA, Komarnicki P. E-Energy- Projekt RegModHarz und IKTEM-ProjektHarz.EE-Mobility: Integration von Elektromobilität in den Netzbetrieb. Darmstadt: Innovative Informations- und Kommunikationstechnologien als Rückgrat von Smart Distribution 2011; April.

[9] Franz P, Talavera I, Hanson J, Sgoff I. Optimized regulation of dispersed generation units for minimization of reactive power consumption. In: *2015 IEEE Power & Energy Society Innovative Smart Grid Technologies Conference (ISGT)*; 2015, p. 1–5.

[10] Capgemini. *Electric vehicle development: Will there be enough charging points in the next decades?* Available at: https://www.capgemini.com/insights/research-library/electric-vehicle-charging-infrastructure-development/; 2022 [accessed 28.09.2022].

[11] Hussain A, Arif SM, Aslam M. Emerging renewable and sustainable energy technologies: State of the art. *Renewable and Sustainable Energy Reviews* 2017;71:12–28, doi:10.1016/j.rser.2016.12.033.

[12] Li C, Jia X, Zhou Y, Li X. A microgrids energy management model based on multi-agent system using adaptive weight and chaotic search particle swarm optimization considering

demand response. *Journal of Cleaner Production* 2020;262:121247, doi:10.1016/j.jclepro.2020.121247.

[13] Alberizzi JC, Rossi M, Renzi M. A MILP algorithm for the optimal sizing of an off-grid hybrid renewable energy system in South Tyrol. *Energy Reports* 2020;6:21–6, doi:10.1016/j.egyr.2019.08.012.

[14] Huang W, Zhang N, Yang J, Wang Y, Kang C. Optimal Configuration Planning of Multi-Energy Systems Considering Distributed Renewable Energy. *IEEE Transactions on Smart Grid* 2019;10:1452–64, doi:10.1109/TSG.2017.2767860.

[15] Ehsan A, Yang Q. Scenario-based investment planning of isolated multi-energy microgrids considering electricity, heating and cooling demand. *Applied Energy* 2019;235:1277–88, doi:10.1016/j.apenergy.2018.11.058.

[16] Control Engineering Russia. *MicroGrid — ответ на новые вызовы электроэнергетики - Control Engineering Russia*. Available at: https://controlengrussia.com/otraslevye-resheniya/microgrid/; 2017 [accessed 28.09.2022].

[17] Irina Volkova, Viktor Kolesnik. Developing Microgrid in Local Energy Systems in Russia: Barriers and Opportunities: A Structural-innovative Model for the Development of Energy Sector in Russia The; 2012. Available at: https://publications.hse.ru/chapters/71899653.

[18] Khokhlov A, Melnikov Y, Veselov F, Kholkin D, Datsko K. *Distributed energy resources in Russia: Development Potential*. SKOLKOVO Energy Centre; 2018.

[19] Rehman OA, Palomba V, Frazzica A, Cabeza LF. Enabling Technologies for Sector Coupling: A Review on the Role of Heat Pumps and Thermal Energy Storage. *Energies* 2021;14:1–30.

[20] Sandvall AF, Ahlgren EO, Ekvall T. Cost-efficiency of urban heating strategies – Modelling scale effects of low-energy building heat supply. *Energy Strategy Reviews* 2017;18:212–23, doi:10.1016/j.esr.2017.10.003.

[21] Ernström TC. *Thermal Energy Storage - Overview and basic principles*. Available at: https://celsiuscity.eu/thermal-energy-storage/; 2020 [accessed 02.12.2021].

[22] Settino J, Sant T, Micallef C, Farrugia M, Spiteri Staines C, Licari J, Micallef A. Overview of solar technologies for electricity, heating and cooling production. *Renewable and Sustainable Energy Reviews* 2018;90:892–909, doi:10.1016/j.rser.2018.03.112.

[23] Zidan A, Gabbar HA, Eldessouky A. Optimal planning of combined heat and power systems within microgrids. *Energy* 2015;93:235–44, doi:10.1016/j.energy.2015.09.039.

[24] Iria J, Heleno M, Cardoso G. Optimal sizing and placement of energy storage systems and on-load tap changer transformers in distribution networks. *Applied Energy* 2019;250:1147–57, doi:10.1016/j.apenergy.2019.04.120.

[25] Cao X, Wang J, Zeng B. Networked Microgrids Planning Through Chance Constrained Stochastic Conic Programming. *IEEE Transactions on Smart Grid* 2019;10:6619–28, doi:10.1109/TSG.2019.2908848.

[26] Tan B, Chen H, Zheng X, Huang J. Two-stage robust optimization dispatch for multiple microgrids with electric vehicle loads based on a novel data-driven uncertainty set. *International Journal of Electrical Power & Energy Systems* 2022;134:107359, doi:10.1016/j.ijepes.2021.107359.

[27] Wu C, Gao S, Liu Y, Song TE, Han H. A model predictive control approach in microgrid considering multi-uncertainty of electric vehicles. *Renewable Energy* 2021;163:1385–96, doi:10.1016/j.renene.2020.08.137.

[28] Amamra SA, Marco J. Vehicle-to-Grid Aggregator to Support Power Grid and Reduce Electric Vehicle Charging Cost. *IEEE Access* 2019;7:178528–38, doi:10.1109/ACCESS.2019.2958664.

[29] Jia L, Hu Z, Song Y, Luo Z. Optimal siting and sizing of electric vehicle charging stations. In: *2012 IEEE International Electric Vehicle Conference*; 2012, p. 1–6.

[30] Sadeghi-Barzani P, Rajabi-Ghahnavieh A, Kazemi-Karegar H. Optimal fast charging station placing and sizing. *Applied Energy* 2014;125:289–99, doi:10.1016/j.apenergy.2014.03.077.

[31] Shao-yun GE, Liang FENG, Hong LIU, Long WANG. The Planning of Electric Vehicle Charging Stations in the Urban Area. In: *Proceedings of the 2nd International Conference on Electronic & Mechanical Engineering and Information Technology (EMEIT 2012):* Atlantis Press; 2012, p. 1598–604.

[32] Dong X, Mu Y, Jia H, Yu X, Zeng P. Heuristic Planning Method of EV Fast Charging Station on a Freeway Considering the Power Flow Constraints of the Distribution Network. *Energy Procedia* 2017;105:2422–8, doi:10.1016/j.egypro.2017.03.696.

[33] Pan L, Yao E, Yang Y, Zhang R. A location model for electric vehicle (EV) public charging stations based on drivers' existing activities. *Sustainable Cities and Society* 2020;59:102192, doi:10.1016/j.scs.2020.102192.

[34] Phonrattanasak P, Leeprechanon N. Optimal placement of EV fast charging stations considering the impact on electrical distribution and traffic condition. In: *2014 International Conference and Utility Exhibition on Green Energy for Sustainable Development (ICUE)*; 2014, p. 1–6.

[35] Dharmakeerthi CH, Mithulananthan N, Saha TK. Modeling and planning of EV fast charging station in power grid. In: *2012 IEEE Power and Energy Society General Meeting*; 2012, p. 1–8.

[36] Liu Zf, Zhang W, Ji X, Li K. Optimal Planning of charging station for electric vehicle based on particle swarm optimization. In: *IEEE PES Innovative Smart Grid Technologies*; 2012, p. 1–5.

[37] Rini dP, Shamsuddin SM, Yuhaniz S. Particle Swarm Optimization: Technique, System and Challenges. *International Journal of Computer Applications* 2011;1, doi:10.5120/ijais-3651.

[38] Prasomthong J, Ongsakul W, Meyer J. Optimal placement of vehicle-to-grid charging station in distribution system using Particle Swarm Optimization with time varying acceleration coefficient. In: *2014 International Conference and Utility Exhibition on Green Energy for Sustainable Development (ICUE)*; 2014, p. 1–8.

[39] Yan L. Optimal layout and scale of charging stations for electric vehicles. In: *2016 China International Conference on Electricity Distribution (CICED)*; 2016, p. 1–5.

[40] Li Y, Li L, Yong J, Yao Y, Li Z. Layout Planning of Electrical Vehicle Charging Stations Based on Genetic Algorithm. In: Wan X, editor. *Electrical Power Systems and Computers*. Berlin, Heidelberg: Springer Berlin Heidelberg; 2011, p. 661–8.

[41] Mardle S, Pascoe S. An overview of genetic algorithms for the solution of optimisation problems. *Computers in Higher Education Economics Review* 1999;13:16–20.

[42] Ge S, Feng L, Liu H. The planning of electric vehicle charging station based on Grid partition method. In: *2011 International Conference on Electrical and Control Engineering*; 2011, p. 2726–30.

[43] Pazouki S, Mohsenzadeh A, Haghifam MR. Optimal planning of PEVs Charging Stations and Demand Response programs considering distribution and traffic networks. In: *2013 Smart Grid Conference (SGC)*; 2013, p. 90–5.

[44] Wan X (ed). *Electrical Power Systems and Computers*. Berlin, Heidelberg: Springer Berlin Heidelberg; 2011.

[45] Xiangwu Yan, Cong Duan, Xiao Chen, Zhengyang Duan. Planning of Electric Vehicle charging station based on hierarchic genetic algorithm. In: *2014 IEEE Conference and Expo Transportation Electrification Asia-Pacific (ITEC Asia-Pacific)*; 2014, p. 1–5.

[46] You PS, Hsieh YC. A hybrid heuristic approach to the problem of the location of vehicle charging stations. *Computers & Industrial Engineering* 2014;70:195–204, doi:10.1016/j.cie.2014.02.001.

[47] Liu Z, Wen F, Ledwich G. Optimal Planning of Electric-Vehicle Charging Stations in Distribution Systems. *IEEE Transactions on Power Delivery* 2013;28:102–10, doi:10.1109/TPWRD.2012.2223489.

[48] Ip A, Fong S, Liu E. Optimization for allocating BEV recharging stations in urban areas by using hierarchical clustering. In: *2010 6th International Conference on Advanced Information Management and Service (IMS)*; 2010, p. 460–5.

[49] Lam AY, Leung YW, Chu X. Electric vehicle charging station placement. In: *2013 IEEE International Conference on Smart Grid Communications (SmartGridComm)*; 2013, p. 510–5.

[50] Aien M, Hajebrahimi A, Fotuhi-Firuzabad M. A comprehensive review on uncertainty modeling techniques in power system studies. *Renewable and Sustainable Energy Reviews* 2016;57:1077–89, doi:10.1016/j.rser.2015.12.070.

[51] Wei F, Wu QH, Jing ZX, Chen JJ, Zhou XX. Optimal unit sizing for small-scale integrated energy systems using multi-objective interval optimization and evidential reasoning approach. *Energy* 2016;111:933–46, doi:10.1016/j.energy.2016.05.046.

[52] Bao Z, Zhou Q, Wu L, Yang Z, Zhang J. Optimal capacity planning of MG with multi-energy coordinated scheduling under uncertainties considered. *IET Gener. Transm. Distrib.* 2017;11:4146–57, doi:10.1049/iet-gtd.2016.1622.

[53] Yu J, Ren J, Zhou M. A chance-constrained programming based dynamic economic dispatch of wind farm and pumped-storage power station. *Dianwang Jishu/Power System Technology* 2013;37:2116–22.

[54] Chen C, Xing J, Li Q, Liu S, Ma J, Chen J, Han L, Qiu W, Lin Z, Yang L. Wasserstein distance-based distributionally robust optimal scheduling in rural microgrid considering the coordinated interaction among source-grid-load-storage. *Energy Reports* 2021;7:60–6, doi:10.1016/j.egyr.2021.05.073.

[55] Liu S, Lin Z, Zhao Y, Liu Y, Ding Y, Zhang B, Yang L, Wang Q, White SE. Robust System Separation Strategy Considering Online Wide-Area Coherency Identification and Uncertainties of Renewable Energy Sources. *IEEE Transactions on Power Systems* 2020;35:3574–87, doi:10.1109/TPWRS.2020.2971966.

[56] Wei W, Liu F, Mei S. Distributionally Robust Co-Optimization of Energy and Reserve Dispatch. *IEEE Transactions on Sustainable Energy* 2016;7:289–300, doi:10.1109/TSTE.2015.2494010.

[57] Xie R, Wei W, Khodayar ME, Wang J, Mei S. Planning Fully Renewable Powered Charging Stations on Highways: A Data-Driven Robust Optimization Approach. *IEEE Transactions on Transportation Electrification* 2018;4:817–30, doi:10.1109/TTE.2018.2849222.

[58] Wei J, Zhang Y, Wang J, Cao X, Khan MA. Multi-period planning of multi-energy microgrid with multi-type uncertainties using chance constrained information gap decision method. *Applied Energy* 2020;260:114188, doi:10.1016/j.apenergy.2019.114188.

[59] Subramani G, Ramachandaramurthy VK, Padmanaban S, Mihet-Popa L, Blaabjerg F, Guerrero JM. Grid-Tied Photovoltaic and Battery Storage Systems with Malaysian Electricity Tariff—A Review on Maximum Demand Shaving. *Energies* 2017;10, doi:10.3390/en10111884.

[60] de Campos D, Aranha Neto EA, Fernandes RC, Hauer I, Richter A. Optimal tariff system for integration of distributed resources based on a comparison of Brazil's and Germany's system. In: *2016 IEEE Symposium Series on Computational Intelligence (SSCI)*; 2016, p. 1–8.

[61] Faisal M, Hannan MA, Ker PJ, Hussain A, Mansor MB, Blaabjerg F. Review of Energy Storage System Technologies in Microgrid Applications: Issues and Challenges. *IEEE Access* 2018;6:35143–64, doi:10.1109/ACCESS.2018.2841407.

[62] Tant J, Geth F, Six D, Tant P, Driesen J. Multiobjective Battery Storage to Improve PV Integration in Residential Distribution Grids. *IEEE Transactions on Sustainable Energy* 2013;4:182–91, doi:10.1109/TSTE.2012.2211387.

[63] Inthamoussou FA, Pegueroles-Queralt J, Bianchi FD. Control of a Supercapacitor Energy Storage System for Microgrid Applications. *IEEE Transactions on Energy Conversion* 2013;28:690–7, doi:10.1109/TEC.2013.2260752.

[64] Teng F, Miles J, Thomson A, Strbac G, Brandon N, Pudjianto D. Potential value of energy storage in the UK electricity system. *Proceedings of the ICE - Energy* 2015;168:1–11, doi:10.1680/ener.14.00033.

[65] Weniger J, Tjaden T, Quaschning V. Sizing of Residential PV Battery Systems. *Energy Procedia* 2014;46:78–87, doi:10.1016/j.egypro.2014.01.160.

[66] Ratnam EL, Weller SR, Kellett CM. Scheduling residential battery storage with solar PV: Assessing the benefits of net metering. *Applied Energy* 2015;155:881–91, doi:10.1016/j.apenergy.2015.06.061.

[67] Linssen J, Stenzel P, Fleer J. Techno-economic analysis of photovoltaic battery systems and the influence of different consumer load profiles. *Applied Energy* 2017;185:2019–25, doi:10.1016/j.apenergy.2015.11.088.

[68] Castillo-Cagigal M, Caamaño-Martín E, Matallanas E, Masa-Bote D, Gutiérrez A, Monasterio-Huelin F, Jiménez-Leube J. PV self-consumption optimization with storage and Active DSM for the residential sector. *Solar Energy* 2011;85:2338–48, doi:10.1016/j.solener.2011.06.028.

[69] Brusco G, Burgio A, Menniti D, Pinnarelli A, Sorrentino N. The economic viability of a feed-in tariff scheme that solely rewards self-consumption to promote the use of integrated photovoltaic battery systems. *Applied Energy* 2016;183:1075–85, doi:10.1016/j.apenergy.2016.09.004.

[70] Bertsch V, Geldermann J, Lühn T. What drives the profitability of household PV investments, self-consumption and self-sufficiency? *Applied Energy* 2017;204:1–15, doi:10.1016/j.apenergy.2017.06.055.

[71] Pyrgou A, Kylili A, Fokaides PA. The future of the Feed-in Tariff (FiT) scheme in Europe: The case of photovoltaics. *Energy Policy* 2016;95:94–102, doi:10.1016/j.enpol.2016.04.048.

[72] Quoilin S, Kavvadias K, Mercier A, Pappone I, Zucker A. Quantifying self-consumption linked to solar home battery systems: Statistical analysis and economic assessment. *Applied Energy* 2016;182:58–67, doi:10.1016/j.apenergy.2016.08.077.

[73] Ruth M, Pratt A, Lunacek M, Mittal S, Wu H, Jones W. *Effects of Home Energy Management Systems on Distribution Utilities and Feeders under various Market structures*; 2015.

[74] Jayawardana HA, Agalgaonkar AP, Robinson DA. Novel control strategy for operation of energy storage in a renewable energy-based microgrid. In: *2015 Australasian Universities Power Engineering Conference (AUPEC)*; 2015, p. 1–6.

[75] Ratnam EL, Weller SR, Kellett CM. An optimization-based approach for assessing the benefits of residential battery storage in conjunction with solar PV. In: *2013 IREP Symposium Bulk Power System Dynamics and Control - IX Optimization, Security and Control of the Emerging Power Grid*; 2013, p. 1–8.

[76] Wu Z, Tazvinga H, Xia X. Demand side management of photovoltaic-battery hybrid system. *Applied Energy* 2015;148:294–304, doi:10.1016/j.apenergy.2015.03.109.

[77] Tazvinga H, Zhu B, Xia X. Optimal power flow management for distributed energy resources with batteries. *Energy Conversion and Management* 2015;102:104–10, doi:10.1016/j.enconman.2015.01.015.

[78] Tazvinga H, Xia X, Zhu B. Optimal Energy Management Strategy for Distributed Energy Resources. *Energy Procedia* 2014;61:1331–4, doi:10.1016/j.egypro.2014.11.1093.

[79] Tazvinga H, Xia X, Zhang J. Minimum cost solution of photovoltaic–diesel–battery hybrid power systems for remote consumers. *Solar Energy* 2013;96:292–9, doi:10.1016/j.solener.2013.07.030.

[80] Hove T, Tazvinga H. A techno-economic model for optimising component sizing and energy dispatch strategy for PV-diesel-battery hybrid power systems. *Journal of Energy in Southern Africa* 2012;23:18–28, doi:10.17159/2413-3051/2012/v23i4a3175.

[81] Zangheri P, Armani R, Pietrobon M, Pagliano L, Boneta M, Müller A, Kockat J, Rohde C, Fraunhofer IS. *Heating and cooling energy demand and loads for building types in different countries of the EU*. Available at: https://www.entranze.eu/files/downloads/D2_3/Heating_and_cooling_energy_demand_and_loads_for_building_types_in_different_countries_of_the_EU.pdf; 2014 [accessed 03.03.2017].

[82] Pillai GG, Putrus GA, Pearsall NM. Generation of synthetic benchmark electrical load profiles using publicly available load and weather data. *International Journal of Electrical Power & Energy Systems* 2014;61:1–10, doi:10.1016/j.ijepes.2014.03.005.

[83] Richter A, Garcia VV, Haue I (eds). *Electricity consumers profiling- German Load Profiles*: Consumer control in Smart Grids Second ELECON Workshop; 2014.

[84] Bauer A, Möller S, Gill B, Schröder F. When energy efficiency goes out the window: How highly insulated buildings contribute to energy-intensive ventilation practices in Germany. *Energy Research & Social Science* 2021;72:101888, doi:10.1016/j.erss.2020.101888.

[85] Tjaden T, Bergner J, Weniger J, Quaschning V. *Representative electrical load profiles of residential buildings in Germany with a temporal resolution of one second*; 2015.

[86] Bost M, Hirschl B, Aretz A. *Effekte von Eigenverbrauch und Netzparität bei der Photovoltaik: Effekte von Eigenverbrauch und Netzparität bei der Photovoltaik*: Greenpeace Energy eG, Hamburg.

[87] Bundesministerium für Umwelt, Naturschutz, Bau und Reaktorsicherheit. *Stromspiegel für Deutschland 2014:Vergleichswerte für den Stromverbrauch*; 2014.

[88] Openei.org. *Commercial and Residential Hourly Load Profiles for all TMY3 Locations in the United States*. Available at: https://openei.org/datasets/files/961/pub/; 2013 [accessed 10.10.2021].

[89] VDI, Association of German Engineers. *VDI 4655:2008-05: Reference load profiles of single-family and multi-family houses for the use of CHP systems*; 2008.

[90] *Passipedia - The Passive House Resource [Passipedia EN]*. Available at: https://passipedia.org/start; 2017 [accessed 17.12.2017].

[91] Telle J-S. *Potentialanalyse verschiedener Betriebsstrategien und Geschäftsmodelle eines Quartierspeichers innerhalb einer PV-Klimaschutzsiedlung unter Berücksichtigung einer Sektorkopplung*. Master thesis, OvGU bibliothek. Magdeburg; 2017.

[92] Islam FR, Prakash K, Mamun KA, Lallu, Pota HR. Aromatic Network: A Novel Structure for Power Distribution System. *IEEE Access* 2017;5:25236–57, doi:10.1109/ACCESS.2017.2767037.

[93] Strunz K, Abbasi E, Fletcher R, Hatziargyriou N, Iravani R, Joos G. *TF C6.04.02 TB 575 -- Benchmark Systems for Network Integration of Renewable and Distributed Energy Resources*; 2014.

[94] KEI IND | KEI IND. *Electrical Wires & Cables Manufacturer Supplier in India - KEI IND*. Available at: http://www.kei-ind.com/images/pdf/lt-cables/4core-aluminium-pvc-armoured.pdf; 2018 [accessed 23.06.2020].

[95] gridcables.com. *4 Core Aluminium PVC Armoured power cables*. Available at: https://www.gridcables.com/pdfs/4-core-al-armd.pdf [accessed 23.06.2020].

[96] Federal Ministry for Economics Affairs and Climate. *Grids and infrastructure*. Available at: https://www.bmwk.de/Redaktion/EN/Artikel/Energy/electricity-grids-of-the-future-01.html [accessed 20.12.2021].

[97] Beuth publishing DIN. *DIN EN 50160:2011-02*. Available at: https://www.beuth.de/en/standard/din-en-50160/136886057; 2010 [accessed 11.12.2021].

[98] faraday.emu.edu.tr. *Newton-Raphson power flow*. Available at: https://faraday.emu.edu.tr/EENG457/.

[99] Testbook. *Compared to Gauss-Seidel method, Newton-Raphson method*. Available at: https://testbook.com/question-answer/compared-to-gauss-seidel-method-newton-raphson-me--5811c4df0328213fe95811be; 2021 [accessed 21.09.2021].

[100] Farivar M, Low SH. Branch Flow Model: Relaxations and Convexification—Part I. *IEEE Transactions on Power Systems* 2013;28:2554–64, doi:10.1109/TPWRS.2013.2255317.

[101] Rigo-Mariani R, Debusschere V, Alvarez-Herault MC. A Modified DistFlow for Distributed Generation Planning Problems in Radial Grids. In: *IECON 2020 The 46th Annual Conference of the IEEE Industrial Electronics Society*; 2020, p. 1626–32.

[102] Fawzi H. On representing the positive semidefinite cone using the second-order cone. *Mathematical Programming* 2016;175, doi:10.1007/s10107-018-1233-0.

[103] Baran ME, Wu FF. Optimal capacitor placement on radial distribution systems. *IEEE Transactions on Power Delivery* 1989;4:725–34, doi:10.1109/61.19265.

[104] Baran ME, Wu FF. Network reconfiguration in distribution systems for loss reduction and load balancing. *IEEE Transactions on Power Delivery* 1989;4:1401–7, doi:10.1109/61.25627.

[105] Lobo MS, Vandenberghe L, Boyd S, Lebret H. Applications of second-order cone programming. *Linear Algebra and its Applications* 1998;284:193–228, doi:10.1016/S0024-3795(98)10032-0.

[106] Alizadeh F, Goldfarb D. Second-Order Cone Programming. *Mathematical Programming* 2001;95, doi:10.1007/s10107-002-0339-5.

[107] Kauko H, Kvalsvik KH, Rohde D, Hafner A, Nord N. Dynamic modelling of local low-temperature heating grids: A case study for Norway. *Energy* 2017;139:289–97, doi:10.1016/j.energy.2017.07.086.

[108] Ernström TC. *Case studies of Low Temperature District Heating systems*. Available at: https://celsiuscity.eu/case-studies-low-temperature-district-heating-systems/; 2020 [accessed 12.11.2021].

[109] Liu X, Wu J, Jenkins N, Bagdanavicius A. Combined analysis of electricity and heat networks. *Applied Energy* 2016;162:1238–50, doi:10.1016/j.apenergy.2015.01.102.

[110] Chen D, Bai X. Multi-Energy Flow Calculation Considering the Convexification Network Constraints for the Integrated Energy System. *Frontiers in Energy Research* 2021;9:718151, doi:10.3389/fenrg.2021.718151.

[111] Association of German Engineers. *VDI_4650: calculation of seasonal performance factor of heat pumps Electric heat pumps for space heating and domestic hotwater*; 2016.

[112] Bundesministerium für Wirtschaft und Ausfuhrkontrolle. *Liste der förderfähigen Wärmepumpen mit Prüf-/Effizienznachweis: Bundesförderung für effiziente Gebäude – Einzelmaßnahmen (BEG EM) Zuschuss*. Available at: https://www.bafa.de/SharedDocs/Downloads/DE/Energie/beg_waermepumpen_anlagenliste.pdf?__blob=publicationFile&v=136; 2021 [accessed 25.12.2021].

[113] Abo-Elyousr FK, Guerrero JM, Ramadan HS. Prospective hydrogen-based microgrid systems for optimal leverage via metaheuristic approaches. *Applied Energy* 2021;300:117384, doi:10.1016/j.apenergy.2021.117384.

[114] Enapter. *What is the energy content of hydrogen?* Available at: https://www.enapter.com/newsroom/kb_post/what-is-the-energy-content-of-hydrogen [accessed 02.09.2021].

[115] *Fuels - Higher and Lower Calorific Values*. Available at: https://www.engineeringtoolbox.com/fuels-higher-calorific-values-d_169.html; 2021 [accessed 02.07.2022].

[116] Energy.gov. *Types of Fuel Cells*. Available at: https://www.energy.gov/eere/fuelcells/types-fuel-cells; 2021 [accessed 01.09.2021].

[117] Scribner Associates. *How To Estimate Required Fuel Flow For PEM Cells - Scribner Associates*. Available at: https://www.scribner.com/faq/3-how-to-estimate-required-fuel-flow-for-pem-cells/; 2017 [accessed 23.09.2021].

[118] Freie University Berlin Germany. *Open Data (DWD)*. Available at: https://www.geo.fu-berlin.de/met/bibliothek/Open-Data-DWD/index.html [accessed 02.10.2021].

[119] Abdelrahem M, Hackl CM, Kennel R. Simplified model predictive current control without mechanical sensors for variable-speed wind energy conversion systems. *Electrical Engineering* 2017;99:367–77, doi:10.1007/s00202-016-0433-y.

[120] *Wind Turbine Power Calculations*. Available at: https://www.academia.edu/28341943/Wind_Turbine_Power_Calculations [accessed 04.01.2017].

[121] Culligan MJ, Botkin J. Impact of Tilt Angle on System Economics for Area Constrained Rooftops: Economics; 2011.

[122] Lang T, Ammann D, Girod B. Profitability in absence of subsidies: A techno-economic analysis of rooftop photovoltaic self-consumption in residential and commercial buildings. *Renewable Energy* 2016;87:77–87, doi:10.1016/j.renene.2015.09.059.

[123] EnergySage Blog. *Most Efficient Solar Panels: Solar Panel Efficiency Explained | EnergySage*. Available at: https://news.energysage.com/what-are-the-most-efficient-solar-panels-on-the-market/; 2022 [accessed 21.07.2021].

[124] Brinken J, Hauer I, Helm S, Schulz T, Schmidtke N. *Integrated Charge Site Allocation for Electric Vehicles*; 2020.

[125] Otto C. *Mit Retropolation methodisch in die Zukunft navigieren*. Available at: https://www.maschinenmarkt.vogel.de/mit-retropolation-methodisch-in-die-zukunft-navigieren-a-408221/ [accessed 21.09.2021].

[126] *Neuzulassungen*. Available at: https://www.kba.de/DE/Statistik/Fahrzeuge/Neuzulassungen/neuzulassungen_node.html [accessed 04.09.2021].

[127] Tayyab M, Helm S, Hauer I, Brinken J, Schmidtke N. Infrastructure linking for placement of Charging stations using Monte Carlo simulation. In: *2020 6th IEEE Congress on Information Science and Technology (CiSt)*; 2020, p. 436–41.

[128] Zhou Y, Li Z, Wu X. The Multiobjective Based Large-Scale Electric Vehicle Charging Behaviours Analysis. *Complexity* 2018;2018:1–16, doi:10.1155/2018/1968435.

[129] BDEW Bundesverband der Energie- und Wasserwirtschaft e.V. *Meinungsbild E-Mobilität: Meinungsbild der Bevölkerung zur Elektromobilität*. Available at:

https://www.bdew.de/service/anwendungshilfen/meinungsbild-e-mobilitaet/; 2019 [accessed 09.02.2021].

[130] Naik S, Khatod D, Sharma M. Optimal allocation of distributed generation in distribution system for loss reduction. *IACSIT Coimbatore Conferences* 2012:42–6.

[131] Nghia LT, Giang TT, Anh QH, Binh PT, An N, Hau PH. A voltage sensitivity index application for power system load shedding considering the generator controls. *International Journal of Advanced Engineering, Management and Science* 2019.

[132] Ziegler C, Richter A, Hauer I, Wolter M. Technical Integration of Virtual Power Plants enhanced by Energy Storages into German System Operation with regard to Following the Schedule in Intra-Day. In: *2018 53rd International Universities Power Engineering Conference (UPEC)*; 2018, p. 1–6.

[133] *What will happen to solar panels after their useful lives are over? | Greenbiz*. Available at: https://www.greenbiz.com/article/what-will-happen-solar-panels-after-their-useful-lives-are-over; 2018 [accessed 03.06.2022].

[134] *How Long do Wind Turbines Last? Can their Lifetime be Extended?* Available at: https://www.twi-global.com/technical-knowledge/faqs/how-long-do-wind-turbines-last#:~:text=A%20good%20quality%2C%20modern%20wind,correct%20maintenance%20procedures%20being%20followed. [accessed 05.06.2021].

[135] Dancker J, Wolter M, Roßberg J, Tsotsas E. Increasing self-sufficiency in a micro grid: integrated vs. non-integrated energy system approach. In: *2018 53rd International Universities Power Engineering Conference (UPEC)*; 2018, p. 1–6.

[136] Alberto Rossi Espagnet. Techno-Economic Assessment of Thermal Energy Storage integration into Low Temperature District Heating Networks. In: ; 2016.

[137] Glatzmaier G. *Developing a Cost Model and Methodology to Estimate Capital Costs for Thermal Energy Storage*. United States; 2011.

[138] Environmental and Energy Study Institute (EESI). *Fact Sheet | Energy Storage (2019) | White Papers | EESI*. Available at: https://www.eesi.org/papers/view/energy-storage-2019; 2010 [accessed 04.04.2021].

[139] Li B, Roche R, Miraoui A. Microgrid sizing with combined evolutionary algorithm and MILP unit commitment. *Applied Energy* 2017;188:547–62, doi:10.1016/j.apenergy.2016.12.038.

[140] Popovski E, Fleiter T, Santos H, Leal V, Fernandes EO. Technical and economic feasibility of sustainable heating and cooling supply options in southern European municipalities-A case study for Matosinhos, Portugal. *Energy* 2018;153:311–23, doi:10.1016/j.energy.2018.04.036.

[141] Bluecorona_seo. *How Long Will My HVAC System Last? | Life Expectancy of HVAC*. Available at: https://www.conditionedairinc.com/blog/how-long-will-hvac-system-last; 2022 [accessed 08.12.2021].

[142] *Combined Heat and Power (CHP) | WBDG - Whole Building Design Guide*. Available at: https://www.wbdg.org/resources/combined-heat-and-power-chp; 2016 [accessed 14.09.2021].

[143] National Renewable Energy Laboratory (NREL). 1–10 kW Stationary Combined Heat and Power Systems Status and Technical Potential. Colorado: U.S. Department of Energy Hydrogen and Fuel Cells Program; 2010.

[144] IRENA. *Green hydrogen cost reduction: Scaling up electrolysers*. Available at: https://irena.org/-/media/Files/IRENA/Agency/Publication/2020/Dec/IRENA_Green_hydrogen_cost_2020.pdf; 2020 [accessed 12.09.2021].

[145] International Council on Clean Transportation. *Estimating electric vehicle charging infrastructure costs across major U.S. metropolitan areas - International Council on Clean Transportation*. Available at: https://theicct.org/publication/estimating-electric-vehicle-charging-infrastructure-costs-across-major-u-s-metropolitan-areas/; 2021 [accessed 29.09.2021].

[146] *Electric Vehicle Charging Stations | GNY Insurance*. Available at: https://www.gny.com/products/electric-vehicle-charging-stations; 2019 [accessed 23.07.2021].

[147] Fleer J, Zurmühlen S, Badeda J, Stenzel P, Hake J-F, Sauer DU. Model-based Economic Assessment of Stationary Battery Systems Providing Primary Control Reserve. *Energy Procedia* 2016;99:11–24, doi:10.1016/j.egypro.2016.10.093.

[148] *National emissions trading*. Available at: https://www.dehst.de/EN/national-emissions-trading/national-emissions-trading_node.html [accessed 29.09.2021].

[149] *Greenhouse gas emission intensity of electricity generation in Europe*. Available at: https://www.eea.europa.eu/ims/greenhouse-gas-emission-intensity-of-1 [accessed 16.01.2021].

[150] Ben-Haim Y (ed). *Info-Gap Decision Theory (Second Edition)*. Oxford: Academic Press; 2006.

[151] Kazemi M, Ivatloo BM, Ehsan M. Risk-Constrained Strategic Bidding of GenCos Considering Demand Response. *IEEE Transactions on Power Systems* 2015;30:376–84, doi:10.1109/TPWRS.2014.2328953.

[152] McCormick GP. Computability of global solutions to factorable nonconvex programs: Part I — Convex underestimating problems. *Mathematical Programming* 1976;10:147–75, doi:10.1007/BF01580665.

[153] Birge JR, Louveaux F. *Introduction to Stochastic Programming*: Springer New York; 2006.

[154] EL GHAOUI L, Lebret H. Robust Solutions To Least-Squares Problems With Uncertain Data. *SIAM Journal on Matrix Analysis and Applications* 2000;18, doi:10.1137/S0895479896298130.

[155] *Robust Optimization | vanparys*. Available at: https://web.mit.edu/vanparys/www/topics/dro/; 2019 [accessed 05.09.2021].

[156] Luo F, Mehrotra S. Distributionally robust optimization with decision dependent ambiguity sets. *Optimization Letters* 2020;14:2565–94, doi:10.1007/s11590-020-01574-3.

[157] Hanasusanto GA, Roitch V, Kuhn D, Wiesemann W. A distributionally robust perspective on uncertainty quantification and chance constrained programming. *Mathematical Programming* 2015;151:35–62, doi:10.1007/s10107-015-0896-z.

[158] Ding K, Wang M, Huang N. Distributionally robust chance constrained problem under interval distribution information. *Optimization Letters* 2018;12:1315–28, doi:10.1007/s11590-017-1160-7.

[159] Blackmore L, Ono M. Convex Chance Constrained Predictive Control Without Sampling. *AIAA Guidance, Navigation, and Control Conference and Exhibit* 2009, doi:10.2514/6.2009-5876.

[160] Geletu A, Klöppel M, Hoffmann A, Li P. A tractable approximation of non-convex chance constrained optimization with non-Gaussian uncertainties. *Engineering Optimization* 2015;47:495–520, doi:10.1080/0305215X.2014.905550.

[161] Shi Z, Liang H, Huang S, Dinavahi V. Distributionally Robust Chance-Constrained Energy Management for Islanded Microgrids. *IEEE Transactions on Smart Grid* 2019;10:2234–44, doi:10.1109/TSG.2018.2792322.

[162] Schütz T, Hu X, Fuchs M, Müller D. Optimal design of decentralized energy conversion systems for smart microgrids using decomposition methods. *Energy* 2018;156:250–63, doi:10.1016/j.energy.2018.05.050.

[163] Conejo A, Castillo E, Mínguez R, García R. Decomposition Techniques in Mathematical Programming Engineering and Science Applications. *Decomposition Techniques in Mathematical Programming: Engineering and Science Applications* 2006, doi:10.1007/3-540-27686-6.

[164] Kazempour J. *Optimization problems with Decomposable structure*. Available at: http://www.energy-markets-school.dk/documents/2016/Jalal.pdf; 2016.

[165] Rahmaniani R, Crainic TG, Gendreau M, Rei W. The Benders Decomposition Algorithm: A Literature Review. *European Journal of Operational Research* 2017;259:801–17, doi:10.1016/j.ejor.2016.12.005.

[166] Benders JF. Partitioning procedures for solving mixed-variables programming problems. *Numerische Mathematik* 1962;4:238–52, doi:10.1007/BF01386316.

[167] Rei W, Gendreau M, Soriano P. Local branching cuts for the 0-1 integer L-Shaped algorithm 2007.

[168] Saharidis GKD, Minoux M, Ierapetritou MG. Accelerating Benders method using covering cut bundle generation. *International Transactions in Operational Research* 2010;17:221–37, doi:10.1111/j.1475-3995.2009.00706.x.

[169] Côté G, Laughton MA. Large-scale mixed integer programming: Benders-type heuristics. *European Journal of Operational Research* 1984;16:327–33, doi:10.1016/0377-2217(84)90287-X.

[170] Fischetti M, Salvagnin D, Zanette A. A note on the selection of Benders' cuts. *Math. Program.* 2010;124:175–82, doi:10.1007/s10107-010-0365-7.

[171] McDaniel D, Devine M. A Modified Benders' Partitioning Algorithm for Mixed Integer Programming. *Management Science* 1977;24:312–9.

[172] Magnanti TL, Wong RT. Accelerating Benders Decomposition: Algorithmic Enhancement and Model Selection Criteria. *Operations Research* 1981;29:464–84.

[173] Papadakos N. Practical enhancements to the Magnanti–Wong method. *Operations Research Letters* 2008;36:444–9, doi:10.1016/j.orl.2008.01.005.

[174] Saharidis GK, Ierapetritou MG. Improving benders decomposition using maximum feasible subsystem (MFS) cut generation strategy. *Computers & Chemical Engineering* 2010;34:1237–45, doi:10.1016/j.compchemeng.2009.10.002.

[175] Birge JR, Louveaux FV. A multicut algorithm for two-stage stochastic linear programs. *European Journal of Operational Research* 1988;34:384–92, doi:10.1016/0377-2217(88)90159-2.

[176] Oliveira F, Grossmann IE, Hamacher S. Accelerating Benders stochastic decomposition for the optimization under uncertainty of the petroleum product supply chain. *Computers & Operations Research* 2014;49:47–58, doi:10.1016/j.cor.2014.03.021.

[177] Schwele A, Kazempour J, Pinson P. Do unit commitment constraints affect generation expansion planning? A scalable stochastic model. *Energy Systems* 2020;11:247–82, doi:10.1007/s12667-018-00321-z.

[178] *gridX – The increasing importance of flexible tariffs*. Available at: https://www.gridx.ai/blog/time-of-use-flexible-tariffs [accessed 26.06.2021].

[179] Tayyab M, Hauer I, Klabunde C, Wolter M. Optimal hybrid storage planning under different tariffs in a microgrid. In: *2020 IEEE PES Innovative Smart Grid Technologies Europe (ISGT-Europe)*; 2020, p. 61–5.

[180] *Flächennutzungsplan der Gemeinde Barleben mit den Ortschaften Barleben, Ebendorf und Meitzendorf. Seite - PDF Free Download*. Available at: https://docplayer.org/190268900-Flaechennutzungsplan-der-gemeinde-barleben-mit-den-ortschaften-barleben-ebendorf-und-meitzendorf-seite.html [accessed 29.09.2021].

[181] Center for Climate and Energy Solutions. *Microgrids - Center for Climate and Energy Solutions*. Available at: https://www.c2es.org/content/microgrids/; 2017 [accessed 02.11.2021].

[182] Tayyab M, Hauer I, Klabunde C, Wolter M. Optimal storage design and operation in a new settlement area under consideration of sector coupling and renewable energy generation. In: *2018 53rd International Universities Power Engineering Conference (UPEC)*; 2018, p. 1–6.

[183] Vizzuality. *Renewable Energy Sources Act (EEG, latest version EEG 2021) - Germany - Climate Change Laws of the World*. Available at: https://climate-laws.org/geographies/germany/laws/renewable-energy-sources-act-eeg-latest-version-eeg-2021 [accessed 29.09.2021].

[184] Res-legal. *Legal sources on renewable energy: Feed-in tariff (EEG feed-in tariff)*. Available at: http://www.res-legal.eu/search-by-country/germany/single/s/res-e/t/promotion/aid/feed-in-tariff-eeg-feed-in-tariff/lastp/135/; 2019 [accessed 12.12.2021].

[185] bundesministerium für verkehr bau und stadtentwicklung. *MiD 2008: Mobilität in Deutschland 2008*. Available at: http://www.mobilitaet-in-deutschland.de/pdf/infas_MiD2008_Abschlussbericht_I.pdf; 2008 [accessed 04.07.2019].

[186] Statista. *Number of new car registrations in Germany 1955-2021 | Statista*. Available at: https://www.statista.com/statistics/587730/new-car-registrations-germany/ [accessed 05.01.2022].

[187] Statista. *Number of cars registered in Germany 1960-2022 | Statista*. Available at: https://www.statista.com/statistics/587764/number-of-registered-cars-germany/ [accessed 05.01.2022].

[188] Lofberg J. YALMIP a toolbox for modeling and optimization in MATLAB. In: *2004 IEEE International Conference on Robotics and Automation (IEEE Cat. No.04CH37508)*; 2004, p. 284–9.

[189] Bauer L. *enbreeze 15 kW - 15,00 kW - Windkraftanlage*. Available at: https://www.wind-turbine-models.com/turbines/1701-enbreeze-15-kw [accessed 09.01.2022].

[190] US Fuel Cell Council. *Commercially available fuel cell products*; https://www.hydrogen.energy.gov/pdfs/htac_fc_products.pdf [accessed 15.01.2022].

[191] Thomas Nowak. *Large scale heat pumps in europe*. Available at: https://www.ehpa.org/fileadmin/documents/Large_heat_pumps_in_Europe_final.pdf [accessed 12.01.2022].

[192] Oswald B. *Berechnung von Drehstromnetzen*. Hannover: Springer Vieweg; 2017.

[193] Wolter M. *Skript zur Vorlesung „Elektrische Netze 1“: Stationäre und quasistationäre Netzberechnung*; 2020 [accessed 09.02.2021].

[194] Siemens AG. *Technical Series, Edition 16: Transformer Selection according to Utilisation Profiles*. Available at: https://assets.new.siemens.com/siemens/assets/api/uuid:5ccfddb0ac6ab1bffa76fb7dd4c6e7e3e97b5d6c/16-transformer-selection-according-to-utilisation-profiles.pdf; 2016 [accessed 04.11.2021].

[195] Kekatos V. *DistFlow and LinDistFlow*. Available at: https://www.faculty.ece.vt.edu/kekatos/pdsa/Lecture11.pdf; 2021.

[196] Ashuri T, Zaaijer MB, Martins JR, Zhang J. Multidisciplinary design optimization of large wind turbines—Technical, economic, and design challenges. *Energy Conversion and Management* 2016;123:56–70, doi:10.1016/j.enconman.2016.06.004.

[197] Frate GF, Cherubini P, Tacconelli C, Micangeli A, Ferrari L, Desideri U. Ramp rate abatement for wind energy integration in microgrids. *Energy Procedia* 2019;159:292–7, doi:10.1016/j.egypro.2019.01.013.

[198] Hernandez AL, Diaz N, Savaghebi M, Feng W, Sun K, Vasquez JC, Guerrero J. *Generation and demand scheduling for a grid-connected hybrid microgrid considering price-based incentives*; 2017.

[199] El-Hendawi M, A.Gabbar H, El-Saady G, A. Ibrahim E-N. Optimal operation and battery management in a grid-connected microgrid. *Journal of International Council on Electrical Engineering* 2018;8:195–206, doi:10.1080/22348972.2018.1528662.

[200] Maleki A, Rosen M, Pourfayaz F. Optimal Operation of a Grid-Connected Hybrid Renewable Energy System for Residential Applications. *Sustainability* 2017;9:1314, doi:10.3390/su9081314.

[201] Wikipedia contributors. *Comparison of commercial battery types - Wikipedia*. Available at: https://en.wikipedia.org/wiki/Comparison_of_commercial_battery_types; 2019 [accessed 21.03.2019].

[202] Yang Y, Bremner S, Menictas C, Kay M. Battery energy storage system size determination in renewable energy systems: A review. *Renewable and Sustainable Energy Reviews* 2018;91:109–25, doi:10.1016/j.rser.2018.03.047.

[203] Bauer T, Steinmann W-D, Laing D, Rainer T. Thermal energy storage materials and systems;15:131–77.

[204] EASE Storage. *Thermal Hot Water Storage*. Available at: https://ease-storage.eu/wp-content/uploads/2016/03/EASE_TD_HotWater.pdf [accessed 24.04.2017].

[205] Luo L, Abdulkareem SS, Rezvani A, Miveh MR, Samad S, Aljojo N, Pazhoohesh M. Optimal scheduling of a renewable based microgrid considering photovoltaic system and battery energy storage under uncertainty. *Journal of Energy Storage* 2020;28:101306, doi:10.1016/j.est.2020.101306.

[206] J. Zhou, W. Liu, X. Chen, M. Sun, C. Mei, S. He, H. Gao, J. Liu. A Distributionally Robust Chance Constrained Planning Method for Integrated Energy Systems. In: *2019 IEEE PES Asia-Pacific Power and Energy Engineering Conference (APPEEC)*; 2019, p. 1–5.

[207] Zymler S, Kuhn D, Rustem B. Distributionally robust joint chance constraints with second-order moment information. *Mathematical Programming* 2013;137:167–98, doi:10.1007/s10107-011-0494-7.

List of symbols/abbreviations

Symbols

m	Meter
a	Annual
W	Watt
°K	Kelvin
°C	Celsius
T_{m}	Average temperature for the day type
F_{DT}	Heating energy factor
T_{o}	Threshold temperature
$\phi_{\mathrm{h,DT}}$	Deviation factor for each day type category
N_{DT}	Number of days in the day type
$Q_{\mathrm{h.a}}$	Annual heating energy demand
$Q_{\mathrm{h,DT}}$	Daily space heating energy demand for a particular day type
$\mathrm{A_h}$	Area of the specific building
$Q_{\mathrm{Sh.a}}$	Specific annual space heating demand
$Q_{\mathrm{h,DT,Min}}$	Heating energy demand per minute
$Q_{\mathrm{D,a}}$	Annual DHW demand
$Q_{\mathrm{SD,a}}$	Specific DHW heating energy demand
N_{h}	Number of persons or number of dwellings
mm	Milli-meter
kA	Kilo-ampere
P_{in}	Active power injected
Q_{in}	Reactive power injected
$\boldsymbol{A}$	Connecting matrix away from nodes
P_{S}	Branch active power
I_{ij}	Branch current from node *i* to node j
Q_{S}	Branch reactive power
$\boldsymbol{B}$	Connecting matrix into nodes
R_{ij}	Resistance of the branch from node i to node j
X_{ij}	Reactance of the branch from node i to node j
U	Voltage
I_{max}	Thermal limit of cable
U_{k}	Nominal voltage
U_{min}	Minimum allowed voltage

$U_{\max}$	Maximum allowed voltage
$P_{\mathrm{S,\,min}}$	Minimum allowed active branch power
$P_{\mathrm{S,\,max}}$	Maximum allowed active branch power
$Q_{\mathrm{S,\,min}}$	Minimum allowed reactive branch power
$Q_{\mathrm{S,\,max}}$	Maximum allowed reactive branch power
$\dot{m}$	Mass flow rate
TN_{pos}	Heating node temperature in the positive direction
TN_{neg}	Heating node temperature in the positive direction
$TB_{\mathrm{in,neg}}$	Temperature into the heating branch in the negative direction
$TB_{\mathrm{in,\,pos}}$	Temperature into the heating branch in the positive direction
$TB_{\mathrm{out,\,pos}}$	Temperature out of the heating branch in the positive direction
$TB_{\mathrm{out,neg}}$	Temperature out of the heating branch in the negative direction
L_{p}	Length of the pipe
λ_{p}	Conductivity of pipe
Q_{p}	Specific heating capacity
T_{outside}	Outside temperature
$P_{\mathrm{HP,in}}$	Electricity requirement for heat pumps
F_{ϑ}	Correction factor
$F_{\Delta\vartheta}$	Correction factor for the deviating temperature difference in condenser during operation
η	Electrical efficiency
T°	Temperature at standard conditions
p°	Pressure at standard conditions
Θ	Heating efficiency
γ	Binary variables
t	Time
E	Energy capacity
ρ	Density
C_{p}	Betz value
P_{R}	Performance ratio
G	Horizontal irradiance
y	Years
N_{EV}	Number of EVs

X_{o}	Number of EVs in the initial year
τ	Difference between the current year and initial year
$\mathcal{M}$	Rise rate for EVs
tr	Travel time
t_{ch}	Charging time
Y	Planning horizon
C_{inv}	investment cost
C_{op}	operational cost
$C_{\mathrm{penalty,\ CO_2}}$	Penalty cost
P_{grid}	Energy import from the electrical grid
C_{grid}	Energy import cost from the electrical grid
EM_{Grid}	Emission intensity parameter for the electricity grid
α_{EVCS}	Uncertainty region
Γ	Uncertainty set
$\widehat{N}_{\mathrm{EVCS}}$	Uncertain number of EVCS
$\hat{C}_{\mathrm{inv}}$	Investment cost after the consideration of uncertainty
W_{T}	White tariff
D_{p}	Peak demand
D_{in}	Intermediary
D_{op}	Off-peak
WT_{wd}	Weekdays
$k\mathrm{z}$	Relation between the price of conventional and white tariffs
p	Number of weekdays
q	Number of Saturdays
r	Number of Sundays
D_{s}	Demand on Saturday
D_{d}	Demand on Sunday
Ω	Family of distribution for the EV arrivals
μ	Mean
σ	Standard deviation
χ	Probability distribution of the EV arrivals survey
ϵ	Tolerance level
$\mathrm{P_r}$	Probability
ζ	Dual variables
λ_{c}	Auxiliary variable for operational cost

Abbreviations

GHG	Greenhouse gases
RES	Renewable energy sources
DERs	Distributed energy resources
PV	Photovoltaic
EESS	Electrical energy storage system
TESS	Thermal energy storage
HESS	Hydrogen energy storage systems
ICE	Internal combustion engines
EV	Electric vehicles
EVCS	Electric vehicle charging station
CHP	Combined heat and power
P2H	Power to heat
GA	Genetic algorithm
PSO	Particle swarm optimization
DHW	District hot water
SCOP	Seasonal Coefficient of performance
MINP	Mixed-integer nonlinear programming
DRO	Distribution robust optimization
IGDM	Information gap decision method
BESS	Battery energy storage system
MILP	Mixed-integer linear programming
ESS	Energy storage system
SFH	Single-family houses
MFH	Multi-family houses
CRE	Commercial real estate
EnEV	energy saving ordinance
IZES	Institut für ZunkunftsEnergieSysteme
HTW	University of Applied Sciences
DIN	German Institute for Standardization
VDI	Verein Deutscher Ingenieure
UWH	Transition Workday Fine
UWB	Transition Workday cloudy
USH	Transition Holiday Fine
USB	Transition Holiday cloudy
SWX	Summer Workday Fine/cloudy

SSX	Summer Holiday Fine/cloudy
WWH	Winter Workday Fine
WWB	Winter Workday cloudy
WSH	Winter Holiday Fine
WSB	Winter Holiday cloudy
DWD	Deutscher Wetterdienst
NR	Newton-raphson
SDP	Semi definite programming
SOCP	Second-order cone programming
min	Minimum
max	Maximum
HN	Heating nodes
HB	Heating branches
SOC	State of charge
GCR	Ground coverage ratio
SOFC	Solid oxide fuel cells
PEM	polymer electrolyte membrane fuel cells
SOC	State of charge
NVSI	Node voltage-sensitive index
DG	Distributed generation
SP	Stochastic programming
RO	Robust optimization
VAR	Value at risk
CVAR	Conditional value at risk
KBA	Germany's federal motor vehicle authority

List of Figures

List of Table

A. Appendix: Introduction

The power to heat classification in a multi-energy microgrid is shown in Figure A.1.

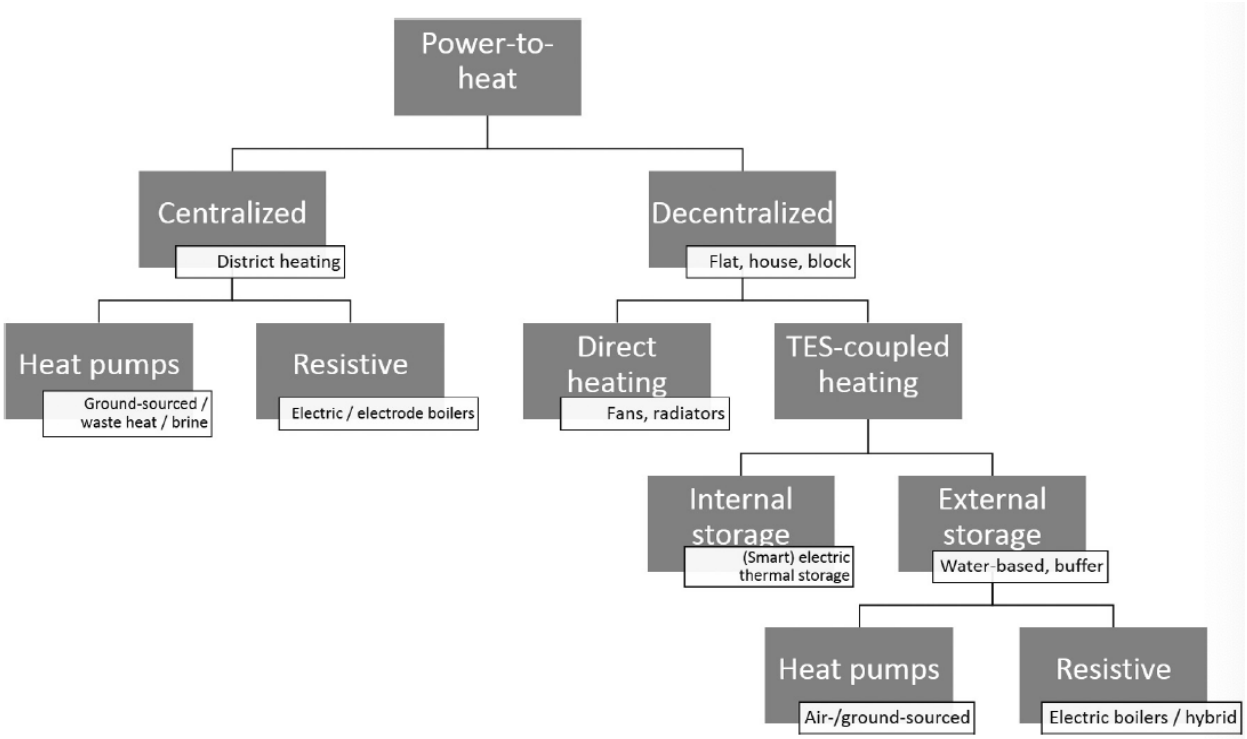

Figure A.1 P2H structure [19]

B. Appendix: Component modeling

B.1 Electrical load profile

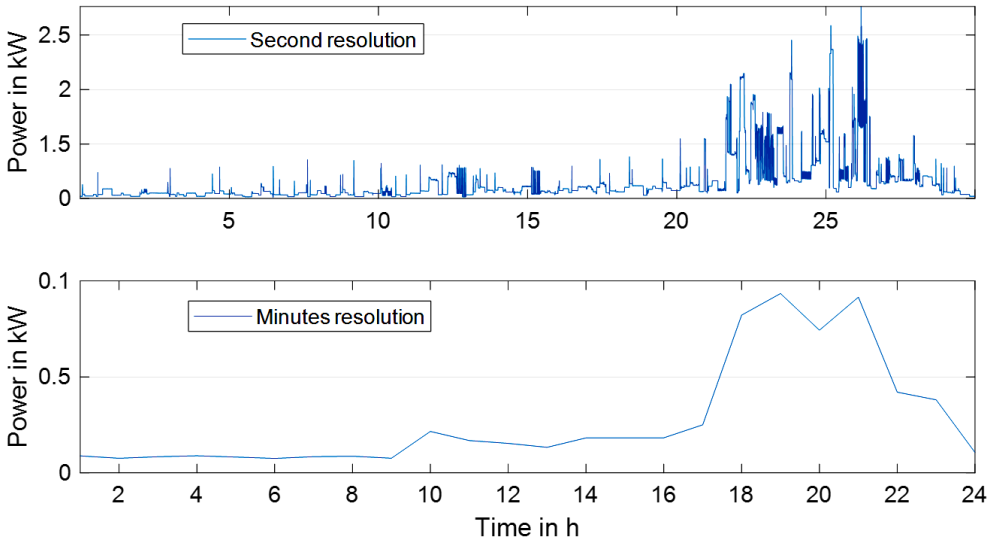

Figure B.1 Comparison between Second and hour resolution

B.2 Electrical grid modeling

B.2.1 NR power flow used for the EVCS placement algorithm

Electrical lines can be calculated according to the Pi equivalent circuit diagram shown in Figure B.2 [193,194]. The calculations in this section are primarily taken from references [193,194]. The capacitive and inductive coupling results in a fully occupied impedance matrix for the three conductors.

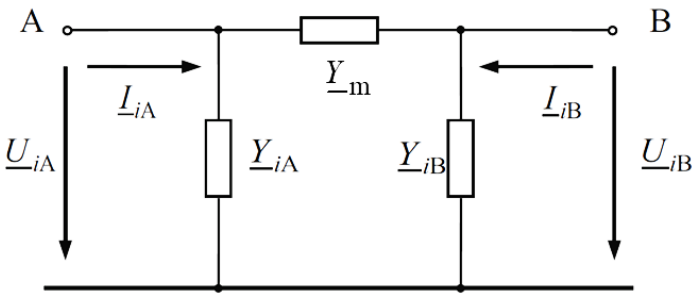

Figure B.2 Pi equivalent circuit diagram [194]

It makes sense to work with the reciprocal of the impedances, and the admittances for further consideration. The complex admittance resistance of the line is determined by an ohmic resistance (R) and an inductance (L) as well as two capacitances (C) as given in (B.1) and (B.2).

$$\underline{Y}_{\mathrm{A}} = \underline{Y}_{\mathrm{B}} = \frac{1}{2}(G + j\omega C) \tag{B.1}$$

$$\underline{Y}_{\mathrm{m}} = R + j\omega L \tag{B.2}$$

The current equation for modeling the line is set up from the equivalent circuit diagram. Here the admittance for the current flow directions from point A in idle, A to B, B to A, and B in idle is determined by (B.3), (B.4), and (B.5).

$$\underline{Y}_{\mathrm{AA}} = \underline{Y}_{\mathrm{A}} + \underline{Y}_{\mathrm{m}} \tag{B.3}$$

$$\underline{Y}_{\mathrm{AB}} = \underline{Y}_{\mathrm{BA}} = -\underline{Y}_{\mathrm{m}} \tag{B.4}$$

$$\underline{Y}_{\mathrm{BB}} = \underline{Y}_{\mathrm{B}} + \underline{Y}_{\mathrm{m}} \tag{B.5}$$

Since the asymmetrical structure of the equipment and symmetrical consumption of the consumers is assumed, a single-phase analysis is sufficient. The calculated admittances result from the line occupancy and the couplings between the conductors and are represented as a current equation for the connection with other equipment according to the junction method as given in (B.6).

$$\begin{bmatrix} \underline{\boldsymbol{i}}_{\mathrm{A}} \\ \underline{\boldsymbol{i}}_{\mathrm{B}} \end{bmatrix} = \begin{bmatrix} \underline{\boldsymbol{Y}}_{\mathrm{AA}} & \underline{\boldsymbol{Y}}_{\mathrm{AB}} \\ \underline{\boldsymbol{Y}}_{\mathrm{BA}} & \underline{\boldsymbol{Y}}_{\mathrm{BB}} \end{bmatrix} \begin{bmatrix} \underline{\boldsymbol{u}}_{\mathrm{A}} \\ \underline{\boldsymbol{u}}_{\mathrm{B}} \end{bmatrix} \tag{B.6}$$

The transformer is then modeled with Delta-Wye (Dy5) type [193].

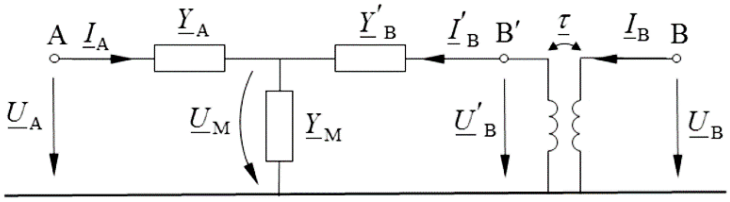

Figure B.3 Dy5 transformer model [194]

In the Dy5, the middle voltage side is connected in a delta fashion, and the low voltage side is connected in a star [193]. A phase shift of 150 ° is taken into account between the primary and secondary sides. To set up the current equation, the admittances of the individual equivalent circuits are required in parallel to the modeling of the line. The ohmic and reactive resistances, as well as the transformation ratio (τ) from the primary to the secondary side, are determined from the transformer parameters as given in (B.7) and (B.8) [193].

$$R_{\mathrm{A}} = R'_{\mathrm{B}} = \frac{1}{2}\frac{P_{\mathrm{k}}}{3I_{\mathrm{r}}^2} \tag{B.7}$$

$$X_{\mathrm{A}} = X'_{\mathrm{B}} = \frac{1}{2}u_s\frac{U_{\mathrm{T}}^2}{\sqrt{3}S_{\mathrm{T}}} \tag{B.8}$$

Where P_{k} is the short circuit losses of the transformer. I_{r} is the rated current and is equal to the rated power of the transformer (S_{T}) divide by voltage at the primary side (U_{T}). The value of P_{k} is assumed to be 7.6 kW [195]. u_{s} is the relatively short circuit voltage. The value of u_{s} is assumed to be 5.9 percent [195]. The admittances can then be derived from the circuit diagram so that equivalent circuits can be determined for the primary and secondary sides as well as the center point described from (B.9) till (B.12).

$$\underline{Y}_{\mathrm{A}} = \frac{1}{R_{\mathrm{A}} + jX_{\mathrm{A}}} \tag{B.9}$$

$$\underline{Y}'_{\mathrm{B}} = \frac{1}{R'_{\mathrm{B}} + jX'_{\mathrm{B}}} \tag{B.10}$$

$$\underline{Y}_{\mathrm{m}} = \frac{1}{R_{\mathrm{Fe}}} + \frac{1}{jX_{\mathrm{h}}} \tag{B.11}$$

$$R_{\mathrm{Fe}} = \frac{U_{\mathrm{T}}^2}{P_{\mathrm{o}}} \tag{B.12}$$

Where P_{o} is the no-load loss of the transformer and is assumed to be 1.1 kW [195]. The winding sizes are represented using the node point method as an admittance matrix, based on the primary side as given in (B.13).

$$\begin{bmatrix} \underline{\boldsymbol{i}}_{\mathrm{A}} \\ \underline{\boldsymbol{i}}_{\mathrm{B}} \end{bmatrix} = \frac{\mathbf{1}}{\underline{\boldsymbol{Y}}_{\mathrm{A}} + \underline{\boldsymbol{Y}}'_{\mathrm{B}} + \underline{\boldsymbol{Y}}_{\mathrm{m}}} \begin{bmatrix} \underline{\boldsymbol{Y}}_{\mathrm{A}}(\underline{\boldsymbol{Y}}'_{\mathrm{B}} + \underline{\boldsymbol{Y}}_{\mathrm{m}}) & -\tau\underline{\boldsymbol{Y}}_{\mathrm{A}}\underline{\boldsymbol{Y}}'_{\mathrm{B}} \\ -\tau\underline{\boldsymbol{Y}}_{\mathrm{A}}\underline{\boldsymbol{Y}}'_{\mathrm{B}} & |\tau|^2\underline{\boldsymbol{Y}}'_{\mathrm{B}}(\underline{\boldsymbol{Y}}_{\mathrm{A}} + \underline{\boldsymbol{Y}}_{\mathrm{m}}) \end{bmatrix} \begin{bmatrix} \underline{\boldsymbol{u}}_{\mathrm{A}} \\ \underline{\boldsymbol{u}}_{\mathrm{B}} \end{bmatrix} \tag{B.13}$$

A diagonal matrix with all resources $\underline{Y}_{\mathrm{T}}$ can then be created, and the node admittance matrix $\underline{Y}_{\mathrm{KK}}$ can be set up using the node-terminal incidence matrix K_{KT}

$$\underline{\boldsymbol{Y}}_{\mathrm{T}} = \begin{bmatrix} \underline{\boldsymbol{Y}}_{\mathrm{T,AA}} & \underline{\boldsymbol{Y}}_{\mathrm{T,AB}} & & \\ \underline{\boldsymbol{Y}}_{\mathrm{T,BA}} & \underline{\boldsymbol{Y}}_{\mathrm{T,BB}} & & \\ & & & \\ & & \underline{\boldsymbol{Y}}_{\mathrm{L,AA}} & \underline{\boldsymbol{Y}}_{\mathrm{L,AB}} \\ & & \underline{\boldsymbol{Y}}_{\mathrm{L,BA}} & \underline{\boldsymbol{Y}}_{\mathrm{L,BB}} \end{bmatrix} \tag{B.14}$$

$$\underline{Y}_{\mathrm{KK}} = -K_{\mathrm{KT}}\underline{Y}_{\mathrm{T}}K_{\mathrm{KT}}^{\mathrm{T}} \tag{B.15}$$

In addition to the $\underline{Y}_{\mathrm{KK}}$, the loads and the generators, and the nominal voltage serve as input data for the load flow calculation. The definition of the slack node (reference node) ensures a balanced power balance and means that a constant voltage U, with an associated angle δ, is specified. The slack node is assumed to be at the medium-voltage level. All other nodes are defined as load nodes, i.e., active and reactive power is specified as load or generation. The calculation of the power balance of the network nodes is based on the Newton-Raphson method. The network power can be calculated with the help of the established nodal admittance matrix and the network voltage and divided into active and reactive power.

$$\underline{s}_{\mathrm{N}} = 3\underline{U}_{\mathrm{K}}(\underline{Y}_{\mathrm{KK}}\underline{u}_{\mathrm{K}})^{*} \tag{B.16}$$

The difference between network and node power and network and node reactive power can be set to zero to create a balanced balance. The first step in this strategy is to make initial guesses about all unknown variables (voltage magnitude and angles at Load Buses and voltage angles at Generator Buses). After that, a Taylor Series is written for each of the power balance equations in the system of equations, with the higher-order terms omitted. Approximate values or improvement vectors of ΔU and Δδ are computed using a Taylor series expansion. As a result, a linear system of equations looks like in (B.17).

$$\begin{bmatrix} \frac{\partial \Delta p}{\partial \delta} & \frac{\partial \Delta p}{\partial u} \\ \frac{\partial \Delta q}{\partial \delta} & \frac{\partial \Delta q}{\partial u} \end{bmatrix}_{\mathrm{v}} \begin{bmatrix} \partial \delta \\ \partial u \end{bmatrix}_{\mathrm{v+1}} = \begin{bmatrix} \partial p \\ \partial q \end{bmatrix}_{\mathrm{v}} \tag{B.17}$$

$$J_{\mathrm{v}}\Delta x_{\mathrm{v+1}} = \Delta y_{\mathrm{v}} \tag{B.18}$$

B.2.2 SOCP Distflow used for the optimal power flow

The structure of the two-node system is shown in Figure B.4. The bus injection model is the standard approach for calculating the power flow [105]. The voltages, currents, and power injection on the nodes are all considered. The bus injection concepts do not directly address the power flow on individual branches. On the other hand, the Branch Flow Approach concentrates on currents and powers on the branches.

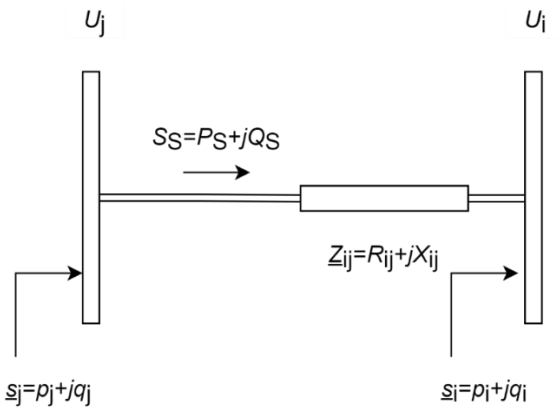

Figure B.4 Two-node branch flow [105]

The branch flow equation is given as,

$$\underline{U}_j - \underline{U}_i = \underline{Z}_{ij}\underline{I}_{ij} \tag{B.19}$$

$$\underline{U}_i = \underline{U}_j - \underline{Z}_{ij}\underline{I}_{ij} \tag{B.20}$$

$$\underline{S}_S = \underline{U}_j\underline{I}_{ij}^* \tag{B.21}$$

$$\underline{S}_S - \underline{Z}_{ij}\left|\underline{I}_{ij}\right|^2 + \underline{s}_i = \sum \underline{S}_{in} \tag{B.22}$$

Relaxing the branch flow equation by introducing the square of the voltage and current magnitude [105]

$$U = \left|\underline{U}\right|^2 \tag{B.23}$$

$$I_{ij} = \left|\underline{I}_{ij}\right|^2 \tag{B.24}$$

Then the equation (B.22) becomes

$$P_S - R_{ij}I_{ij} + p_S = \sum P_{in} \tag{B.25}$$

$$Q_S - X_{ij} I_{ij} + q_S = \sum Q_{in} \tag{B.26}$$

The equation (B.25) and (B.26) can be transformed into the equation using matrices A and B. By the ohms law square, both sides of the equation are multiplied with the complex conjugate. Considering the following basic rule of a complex number in mathematics given as

$$\underline{Z} = R + jX \qquad\qquad \underline{Z}^* = R - jX \tag{B.27}$$

The magnitude of the complex number square is given in (B.26) and replacing values given as,

$$|Z|^2 = (R + jX)(R - jX) = R^2 + X^2 \tag{B.28}$$

$$Q_S - X_{ij} I_{ij} + q_S = \sum Q_{in} \tag{B.29}$$

$$\underline{U_i} \underline{U_j}^* = (\underline{U_j} - \underline{Z_{ij}} I_{ij})(\underline{U_j} - \underline{Z_{ij}} I_{ij})^* \tag{B.30}$$

$$\underline{U_i} \underline{U_i}^* = (\underline{U_j} \underline{U_j}^* - U_j^* \underline{Z_{ij}} I_{ij} - U_j \underline{Z_{ij}^*} I_{ij}^* + \underline{Z_{ij}} I_{ij} \underline{Z_{ij}^*} I_{ij}^* \tag{B.31}$$

The product of a complex number with its conjugate is equal to the square of the number's modulus

$$|U_i|^2 = \left|U_j\right|^2 - U_j^* \underline{Z_{ij}} I_{ij} - U_j \underline{Z_{ij}^*} I_{ij}^* + \left|Z_{ij}\right|^2 \left|I_{ij}\right|^2 \tag{B.32}$$

From equation (B.28), equation (B.32) becomes

$$U_i = U_j - 2\left(U_j \underline{Z_{ij}^*} I_{ij}^*\right) + \left|Z_{ij}\right|^2 \left|I_{ij}\right|^2 \tag{B.33}$$

From (B.23) and (B.24) replacing the quadratic term, the final term is drawn as given,

$$U_i = U_j - 2\left(\underline{S_S} \underline{Z_{ij}^*}\right) + \left|\underline{Z_{ij}}\right|^2 I_{ij} \tag{B.34}$$

$$U_i = U_j - 2\left(P_S + jQ_S)(R_{ij} - jX_{ij}\right)\right) + \left|\underline{Z_{ij}}\right|^2 I_{ij} \tag{B.35}$$

$$U_i = U_j - 2\left(R_{ij} P_S + R_{ij} jQ_S - P_S\, jX_{ij} - (jQ_S)(jX_{ij})\right) + \left|\underline{Z_{ij}}\right|^2 I_{ij} \tag{B.36}$$

$$U_i = U_j - 2\left(R_{ij} P_S + R_{ij} jQ_S - P_S\, jX_{ij} + Q_S X_{ij}\right) + \left|\underline{Z_{ij}}\right|^2 I_{ij} \tag{B.37}$$

$$U_i = U_j - 2(Real\left(R_{ij} P_S + R_{ij} jQ_S - P_S\, jX_{ij} + Q_S X_{ij}\right)) + \left|\underline{Z_{ij}}\right|^2 I_{ij} \tag{B.38}$$

$$U_i = U_j - 2\left(R_{ij} P_S + X_{ij} Q_S\right) + \left(R_{ij}^2 + X_{ij}^2\right) I_{ij} \tag{B.39}$$

B.3 District heating grid model

Some of the low-temperature heating grid case studies are given in Table B.1.

Table B.1 case studies of low-temperature heating grid [109]

Case study	Country	Supply temperature (°C)	Return temperature (°C)
Aarhus	Denmark	55	30
Albertslund	Denmark	35-40	10-15
Birmingham	United Kingdom	55	35
Kassel	Germany	40	-
Kortrijk	Belgium	50	25
Okotoks	Canada	37-55	-
Slough	United Kingdom	55	25

B.4 Battery energy storage system (BESS) as electric energy storage system (EESS)

EESS can be classified as non - rechargeable (primary battery) and rechargeable (secondary) batteries. Vanadium redox flow batteries (VRFB), zinc-bromine (ZnBr), sodium-sulfate (NaS), zero-emission batteries research activity (ZEBRA), lead-acid (LA), lithium-ion (Li-ion), Nickel-cadmium battery (NiCd), and nickel-metal hydride (NiMH) belongs to the rechargeable batteries, which have basic parameters like efficiency, power density, energy density and environmental [196].

The mature technology as LA BESS is a 150-year-old device with a short lifespan. These batteries are needed to be replaced every 4-5 years, which raises the system's lifetime cost [197]. Undoubtedly, the appearing energy battery technologies such as Li-ion, NaS, and flow batteries (for example, VRFB) have more beneficial features. Li-ion batteries are often used in power systems due to lower maintenance, superior safety, and volumetric and gravimetric energy densities. Less weight and size also improve their advantages [198]. Based on the above literature, the conclusion for BESS is shown in Table B.2.

Table B.2 BESS types and characteristics

Parameters	LA	NiCd	NaS	Li-ion	VRFB
Power rating	0-20 MW	0-40MW	50kW-8MW	0-100kW	30kW-3MW
Energy density (Wh/kg)	30-50,	50-75,	150-250,	75-200,	15-50,
Power density (W/kg)	75–300,	150–300	150–230	150–315	-
Discharge time	Hours	Hours	Hours	Hours	Hours
Lifetime	5–20	10–20	10–15	5–20	5–20
Storage duration	Mins– days	Mins–days	Sec-hours	Mins–days	Hrs–months

Parameters	LA	NiCd	NaS	Li-ion	VRFB
Self-discharge per day	0,1%-0,3%	0,2%-0,6%	20%	0,1%-0,3%	Small
Cycles	500–1000	2000–2500	2500	1000–10000+	12000+
Efficiency (%)	70–90%	60–73%	75–90%	85–95%	65–85%
Response time	Seconds	Seconds	Seconds	Seconds	Seconds
Class	Long term	Long term	Short term	Long term	Real long term
Capital cost ($/KW)	200–300	500–1500	1000– 3000	1200–4000	600–1500
Capital cost ($/KWh)	120–150	800–1500	300–500	300–1300	150–1000
Impact on environment	Very poisonous, contaminating the soil and water	Toxic, dangerous for health and environment	The liquid sodium reacts easily with the water in the atmosphere	Rather a low impact, mostly through emissions in the manufacturing of the cells.	Toxic remains.

Li-ion batteries are characterized by energy density, cell voltage, cycle life, cost, and rate capability. The existing seven renowned Li-ion battery chemistries are presented as lithium manganese oxide, lithium nickel-cobalt aluminum oxide, lithium nickel-manganese-cobalt oxide, lithium iron phosphate, lithium manganese-oxide cathode, lithium nickel-manganese-cobalt oxide cathode, and lithium-iron-phosphate cathode. The flow batteries are uncompetitive in the cost market with Li-ion and LA batteries, analyzed in the study [199]. The reference [200] has paid attention to the high efficiency (95 percent) of the Li-ion technology, long calendar, and cycle life (20 years at 60 percent Depth of Discharge (DOD) per day). However, some batteries have many advantages and disadvantages in connection with lifetime, cycle time, and costs. The comparison of parameters of 5 types of batteries is considered in Table B2 [201,202].

B.5 Thermal electric energy storage (TESS)

In the physical sense, heat or cold is a type of energy that may be stored in a variety of ways and used for a variety of purposes. Thermal energy storage can be classified in several ways as shown in Figure B.5.

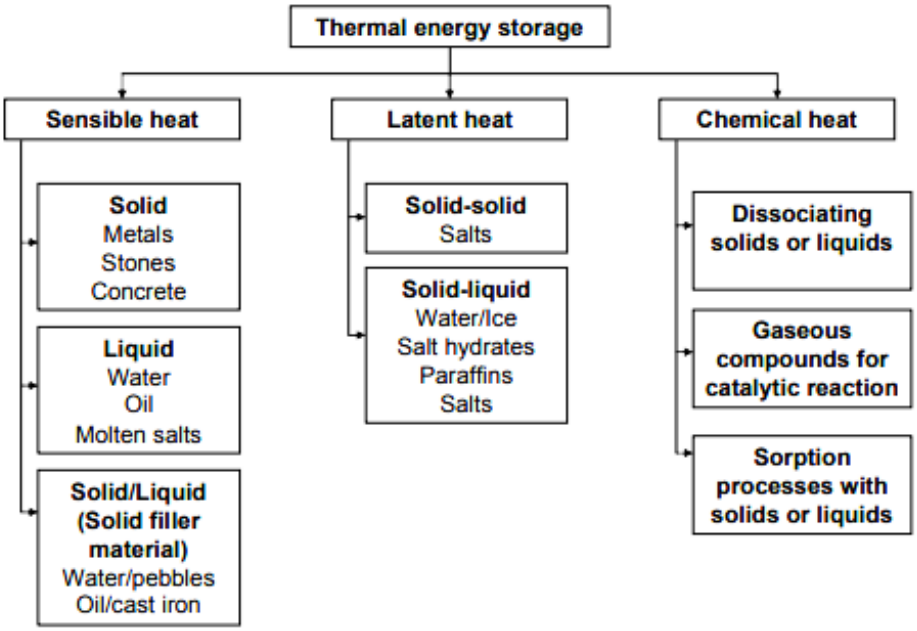

Figure B.5 TESS types [203]

There are three types of TES systems that are routinely used:

- Sensible heat storage causes an increase or decrease in the temperature of the storage material; the amount of energy stored is proportional to the temperature difference between the employed materials.
- Latent heat storage is associated with a phase transformation of the storage materials (phase change materials - PCM). The physical phase of the storage materials changes from solid to liquid and vice versa. At a steady temperature, the phase transition is always accompanied by heat absorption or release. As a result, the added or released heat is undetectable and appears to be latent. The heat (enthalpy) required for melting and freezing is equal to stored energy.
- Thermochemical heat storage uses reversible thermochemical reactions to store heat. An endothermic process stores energy in chemical compounds, which can then be recovered by recombining the compounds in an exothermic reaction. The heat stored and released is the same as the heat of the reaction (enthalpy).

The fact that TES systems are diverse in terms of temperature, power level, and heat transfer fluids and that each application has its own set of operating parameters is one of its distinguishing features. This necessitates a thorough understanding of a wide range of storage designs, media, and processes. The temperatures range from below 0°C (e.g., ice slurries and latent heat ice storage) to about 1000°C (e.g., regenerator in the high-temperature industry). Water is the most common liquid storage medium in the intermediate temperature range (0 to 120 °C) (e.g., space heating). Heating, ventilation, air conditioning (HVAC), and residential

hot water supply use this low-temperature heat. The temperature range above 120 °C for applications in concentrated solar power (CSP) generation is the main topic of this chapter. Similar high-temperature TES devices can be used for industrial waste heat recovery.

The hot water tank is an essential part of the thermal storage system. On the market, there is a wide range of designs and capacities, most of which are geared toward residential applications (houses and multi-dwelling structures) and industrial and commercial systems. The water heater, which can be built into the tank or installed outside, is the second component. The water heater might be dedicated to hot water production, or it can be used for many purposes (space heating, cogeneration, etc.). When considering the storage system's efficiency, it's essential to evaluate the efficiency of both primary components: the tank and the water heater. This is one of the key reasons why an HP is being used in more and more home applications to provide domestic hot water. The parameters for TESS are given in Table B.3.

Table B.3 TESS parameters [204]

Parameters	**Small residential**	**Multi-dwelling building**
Power range	Max 40 kW	Max 400 kW
Energy range	6 kWh - 25 kWh	25 kW – 320 kWh
Discharge time	≤1 h	≤1 h
Cycle life	No limit	No limit
Life duration	15- 30 years	20 – 40 years
Reaction time	Sec	Sec
Efficiency	50-85 %	70 – 95 %
Energy(power) density	0.06 kWh/kg	0.08 kWh/kg
CAPEX: Energy	40 €/kWh	15 €/kWh

C. Appendix: E-mobility infrastructure

C.1 Monte-Carlo simulation

Monte-Carlo simulation is a computer-assisted mathematical technique for incorporating risk into quantitative analysis and decision-making. Professionals in various sectors, including economics, project planning, energy, industry, education, research and technology, health, oil and natural gas, mobility, and the environment, employ the approach. For each given course of action, the Monte-Carlo simulation provides the judgment with a range of probable outcomes as well as the probabilities that they will occur. It depicts the ability to impact outcomes of going all-in and the most prudent course of action and all probable outcomes for an intermediate decision. The Monte-Carlo simulation can be formed with the following steps:

- Determine the variables and create a model
- An initial sensitive analysis to identify the parameters (variables) for which the probability distribution should be evaluated
- Determine the form of each random variable's probability distribution
- Random variable sampling (Creation of random variable sample)
- Statistical analysis of the generated results by the iteration of the simulation

For a Monte-Carlo simulation, the random samples need to be drawn from a distribution function. There are two ways to classify distributions: discrete or continuous. The distribution exists in a probability density function (PDF) or a cumulative distribution function (CDF). The fitted curved in section 5.3 is analyzed by PDF in the present study. The standard PDFs for a function for the variable (*x*) in the Monte-Carlo simulation is as follows:

Normal

$$f(x:\mu,\sigma) = \frac{1}{\sigma\sqrt{2\Pi}} e^{\frac{-(x-\mu)^2}{2\sigma^2}} \quad -\infty < x < \infty \tag{C.1}$$

μ: mean

σ: standard deviation

For the morning arrival:

μ=8.4

σ=1.50

For the morning arrival:

μ=16.588

σ=1.953

T-location-distribution

$$f(x:\mu,\sigma,\partial)=\frac{\Gamma(\frac{\partial+1}{2})}{\sigma\sqrt{\partial\pi}\,\Gamma(\frac{\partial}{2})}\left[\frac{\partial+(\frac{x-\mu}{\sigma})^2}{\partial}\right]^{-\frac{\partial+1}{2}} \quad \text{(C.2)}$$

Γ is the gamma function

∂: shape parameter

For kilometer traveled:

μ=2.67

σ=1.50

∂=1.24

For the duration of travel:

μ=5.64

σ=2.48

∂=1.62

Gamma

$$f(x:k1,k2)=\frac{1}{k2^{k1}\Gamma(k1)}x^{k1-1}e^{\frac{x}{k2}} \quad \text{(C.3)}$$

$$\Gamma(k1)=\int_0^{\infty}t^{k1}e^{-t}dt \quad \text{(C.4)}$$

$\Gamma(k1)$: Gamma function

K1: Parameters shape

K2: Parameter scale

Apart from the distributions utilized in this study, there are several alternative distribution functions available such as Lognormal, Beta, Weibull, Logistic, Log-Logistic, Birnbaum Saunders, Exponential, and Rayleigh

C.2 EV arrival time distributions

The distribution of EV arrival in different districts from project INKOLA [125].

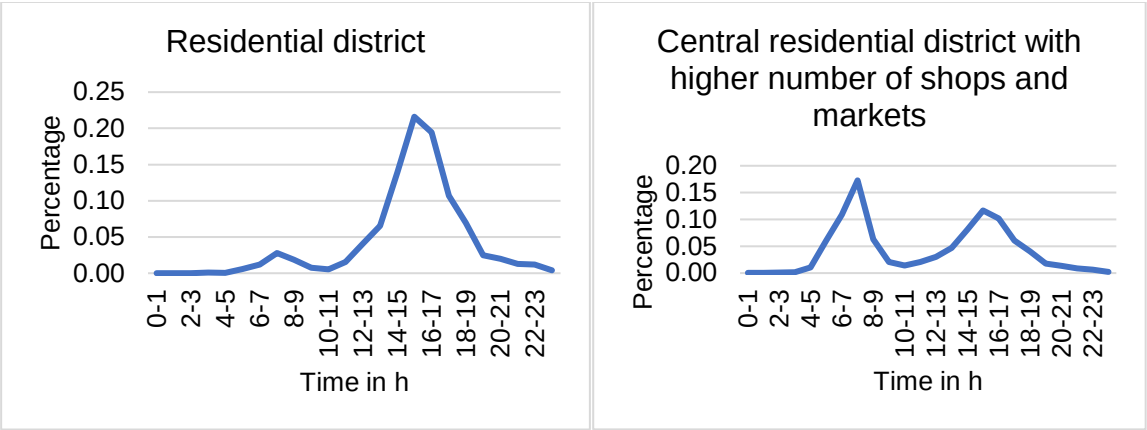

Figure C.1 EV arrivals

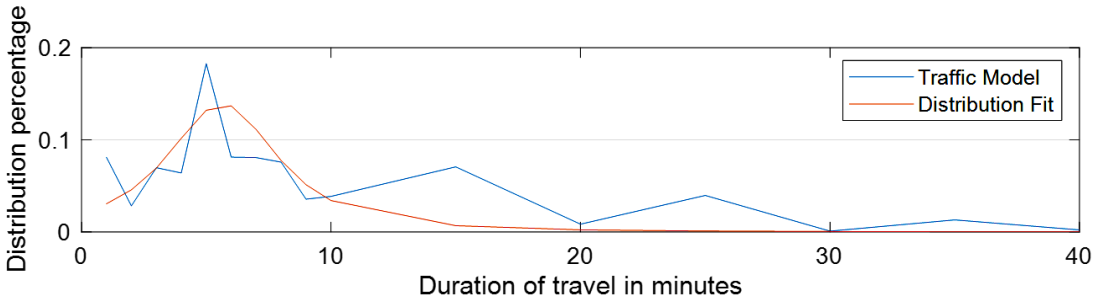

Figure C.2 distribution fit for the duration of travel

C.3 Methodology for EVCS occupancy time

The EV has three states charged, waiting, or queuing for charging. Three variables represent the three states. EV_charge variable holds the ID of EVs that require charging, $EV\_charging$ variable holds the ID of EVs already charging at the charging station, and the $EV\_waiting$ variable has the ID of EVs in the waiting queue from the previous time step. After setting those variables at the start of the iteration, the $EV\_charging$ state is checked first, as shown in Figure C.3 (left). If two EVs are charging, then the EVs arriving at that time are added to the waiting queue. If there is one EV charging, one slot is empty and is assigned from the waiting queue, if any, or from the EVs arriving at that time. After setting the EVs to an empty slot, updating variables for the next step is done, as shown in Figure C.3 (right). If there are no EVs charging, then two slots are empty, and already waiting EVs are given priority, and if there are any left, then EVs arriving at that time step are assigned.

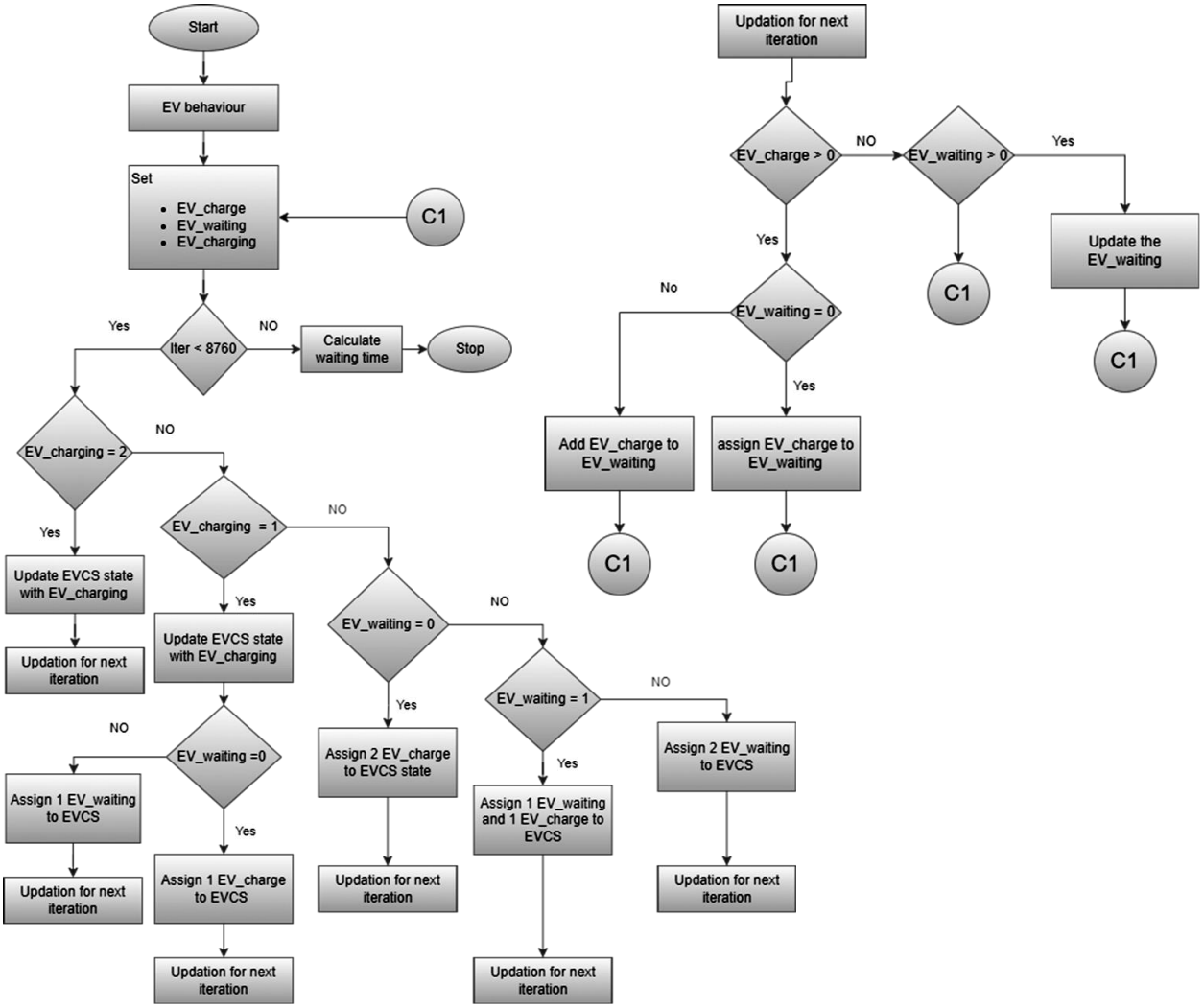

Figure C.3 Method for calculation of occupancy time

D. Appendix: Optimization

D.1 Information gap decision method (IGDM)

The IGDM was first proposed in [151]. IGDM comes under the class of non-probabilistic, likelihood-free uncertainty modeling methods that can make decisions that make the system robust against severe uncertainty. IGDT deals mainly with the type of problems where a particular critical performance requirement must be met while taking uncertainty into account [151].

$$r(d, \mathrm{w}) \geq r^* \tag{D.1}$$

Where r is the performance function that relates the decision variables and the uncertainty. r^* is the critical performance level. d is the decision space, while w is the uncertainty space. The optimizer controls decision variables but not the uncertainty variable, which depends on some unknown parameter or behavior. The concept of IGDT can be reduced to a problem statement of selecting the best decision in d, satisfying the critical performance requirement of (D1), given that the actual value of W is uncertain. However, the problem is still not complete as the uncertainty associated with the variable is not clearly defined except that it lies in uncertainty space. The definition does not assign a probability or likelihood of the true value taking a value in a certain interval that lies in the uncertainty space. Instead, it is assumed that a point estimate of the true value is termed a predicted value. As the main purpose of introducing IGDM is to tackle problems with severe uncertainty, there is a need for a clear definition of severe uncertainty.

Severe uncertainty is a condition in which it is difficult to forecast what will happen in the future due to a lack of sufficient data. As a result, while dealing with severe uncertainty situations, it's important to recall the nature of decision-making based on estimating quality and the uncertainty space.

D.1.1 IGDM robustness

Since the traditional IGDM is not well-defined, it is formulated as a robust model defined as IGDM robustness given as,

$$\hat{\alpha}(d, \widetilde{w}) = max\{\alpha \geq 0 : r^* \leq r(d, \mathrm{w})\} \qquad \forall w \in W(\alpha, \widetilde{w}) \quad \text{(D.2)}$$

Unlike the previous formulation, the uncertainty space is clearly defined by size α centered around the predicted value $\widetilde{w}$. Hence, it is safe to say that the uncertainty set W is the smallest subset of the uncertainty space (ϖ) such that the $W(\alpha, \widetilde{w}) \subseteq \varpi \quad \forall\, \alpha \geq 0$.

The decision problem is reformulated based on the robustness of the decision equal to the largest possible value of α such that the decision satisfies the critical performance requirement ($r^* \leq r(d, \mathrm{w})$). The idea of robustness is defined as the largest safe deviation from the estimate$\widetilde{w}$, where the worst-case w in $W(\alpha, \widetilde{w})$ determines whether the deviation of α from w is safe concerning decision d. A higher value of α implies the model is more robust towards severe uncertainty. The regions of uncertainty are nested, which gives a set that has varied intervals based on the value of α. The ideal case is when the $\alpha = 0$, and the second case is when uncertainty space is increased with a range of a factor ($\varepsilon 1$) given as

$$\Gamma(0, \widetilde{w}) = \widetilde{w} \tag{D.3}$$

$$\Gamma(\alpha, \widetilde{w}) \subseteq \ \Gamma(\alpha + \varepsilon 1, \widetilde{w}), \qquad \forall \alpha, \varepsilon 1 \geq 0 \tag{D.4}$$

D.1.2 IGDM for Microgrid planning and operation

The general formulation is shown when applying IGDM for microgrid planning and operation.

$$\min_{\mathrm{X}} f(X, \gamma) \qquad \forall\, \gamma \in \Gamma \tag{D.5}$$

$$H_{\mathrm{i}}(X, \gamma) \leq 0 \qquad \forall\, i \in \Psi_{\mathrm{ineq}} \tag{D.6}$$

$$G_{\mathrm{j}}(X, \gamma) = 0 \qquad \forall\, j \in \Psi_{\mathrm{eq}} \tag{D.7}$$

$$\forall\ \gamma \in \Gamma(\overline{\gamma}, \alpha) = \{\gamma : |\frac{\gamma - \overline{\gamma}}{\overline{\gamma}}| \leq \alpha\} \tag{D.8}$$

Where there is a set of decision variables (X), vectors of uncertain input parameters (γ), and uncertainty sets ($\Gamma(\overline{\gamma}, \alpha)$). These sets and variables are associated with the input parameters, equality constraints (Ψ_{eq}), equality constraints (Ψ_{ineq}) and the objective function. The uncertainty set defined in (D8) is the defining factor of the model. Where uncertain input is a function of two parameter's forecasted values ($\overline{\gamma}$) and the deviated value (γ). The deviation, also known as the radius of the uncertainty region, controls the uncertainty range. The IGDM-based microgrid planning and operation can be done in the following approaches.

- Risk-averse
- Risk seeker

D.1.2.1 Risk Averse

Decision-maker has two options when the realized uncertainty is different from the estimated base value. Robust decision-making in such a way that they are made in the face of the risk of possible errors from the predicted unknown input parameter [50]. It is mostly selected by

conservative decision-makers to make a robust decision. The model must be optimized while maximizing the radius of uncertainty given by (D9).

$$\max_{X} \hat{\alpha} \tag{D.9}$$

$$H_{\mathrm{i}}(X,\gamma) \leq 0, \qquad \forall\, i \in \Psi_{\mathrm{ineq}} \tag{D.10}$$

$$G_{\mathrm{j}}(X,\gamma) = 0 \qquad \forall\, j \in \Psi_{\mathrm{eq}} \tag{D.11}$$

$$f(X,\gamma) \leq \Lambda_c \tag{D.12}$$

$$\Lambda_c = f_b(X,\gamma) + \delta_c |f_b(X,\gamma)| \qquad \gamma \in \Gamma \tag{D.13}$$

δ_c is the possible deviation allowed from the base value and is set by the decision-maker. It can be viewed as the degree of acceptable tolerance in the presence of uncertainties. Λ_c is the critical value of the objective function that should not be violated.

D.1.2.2 Risk seeker

Risk seeker strategy, selected by optimistic decision-makers looking at the uncertain events that may positively affect the objective function. It indicates the greediness of the decision-maker as its main idea is profit-seeking. Unlike in the risk-averse strategy, the decision here is made to take advantage of the existing uncertainty using the lack of information and is made by minimizing the radius of uncertainty given as,

$$\min_{X} \hat{\alpha} \tag{D.14}$$

$$H_{\mathrm{i}}(X,\gamma) \leq 0 \qquad \forall\, i \in \Psi_{\mathrm{ineq}} \tag{D.15}$$

$$G_{\mathrm{j}}(X,\gamma) = 0 \qquad \forall\, j \in \Psi_{\mathrm{eq}} \tag{D.16}$$

$$f(X,\gamma) \leq \Lambda_c \tag{D.17}$$

$$\Lambda_o = f_b(X,\gamma) + \delta_o |f_b(X,\gamma)| \qquad \gamma \in \Gamma \tag{D.18}$$

δ_o is the possible decrease from the base value and is set by the decision-maker. It can be viewed as the degree of profit maximization in the presence of uncertainties. The objective function value should be less than the opportunity value (Λ_o).

D.2 Distributional robust optimization (DRO)

Distributionally robust optimization (DRO) is a modeling system that overcomes the disadvantages of stochastic programming and robust modeling. In this modeling framework,

the unknown distribution of the uncertain variable is assumed to lie in an ambiguity set that has all the possible distributions of the uncertain variable. The probability distribution is formulated based on the partial information available. Hence it does not need a large dataset like probabilistic modeling to generate PDF. DRO optimizes the system for worst-case distribution in the ambiguity set. The solution and performance depend on the ambiguity set used. The ambiguity set should be formulated using data-driven methods. It contains true distribution, is small enough not to give any over-conservative results, requires fewer data to generate it, and gives a tractable formulation.

Ambiguity sets can be classified as moment-based, distance-based, structural, hypothesis-test-based, and likelihood-based. Out of these most commonly used ambiguity sets are moment-based. The distributions share moment information and are distance-based, in which distributions are selected that are close to a reference distribution with a predetermined probability discrepancy metric. The most commonly used metrics are Wasserstein-distance, phi-divergence, KL-divergence, and Prokhorov-metric. When dealing with a complex system, individual ambiguity sets are not sufficient as they have their disadvantages and convergence problems for the moment-based set. In such cases, ambiguity sets are combined such that disadvantages are compensated. Moment-based and Wasserstein-based are combined, which give a less conservative model and have a better convergence rate.

A data-driven Wasserstein-based ambiguity set was generated to model the wind power uncertainty for a rural microgrid to adjust economy and robustness, and DRO results are compared with SO and RO results [54]. EVCS siting and sizing problem was proposed in [57] to consider the load's uncertainty using a data-driven KL-divergence-based DRO. In [205], the wind power uncertainty was modeled using a moment-based ambiguity set for the energy management of an islanded microgrid. In terms of performance, it doesn't require large datasets to formulate PDF and gives less conservative results compared to RO. Even though DRO modeling addresses the technical challenge of stochastic and resilient optimization when applied to high-dimensional problems with a larger number of features than observations, it still needs to be improved. A general representation of ambiguity ser is shown in the Figure

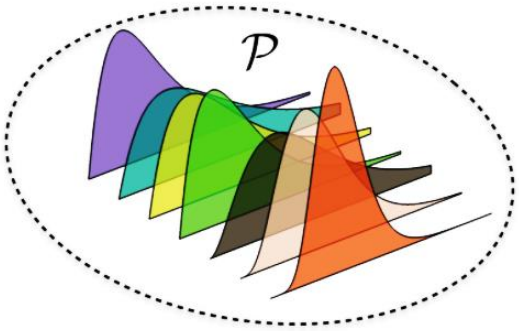

Figure D.1 Ambiguity set [156]

D.2.1 CVAR approximation of chance-constraint

The chance constraint needs to be in the general form [162,206]

$$\mathbb{P}_{\mathrm{t}}\left\{h^{0}(x_{\mathrm{t}})+h(x_{\mathrm{t}})\widetilde{P_{EV}}\leq 0\right\}\geq 1-\epsilon,\forall\mathbb{P}_{\mathrm{t}}\in \mathrm{P}_{t}^{2}\,,x_{\mathrm{t}}\in X \tag{D.19}$$

$\widetilde{P_{EV}}$ is the random variable of EV arrivals. For simplicity, the CVAR form is shown according to [162,206,207].

$$\inf_{\beta,\upsilon,\tau,z,s,\nu_{1},\nu_{2}}\beta+\frac{1}{\alpha_{\mathrm{aux}}}(\upsilon+s)\leq 0 \tag{D.20}$$

Subject to

$$\left\|\begin{matrix}\tau\\ h(x_{\mathrm{t}})\widetilde{\sigma_{EV}}\\ z-s\end{matrix}\right\|\leq z+s \tag{D.21}$$

$$z>0\;\;\upsilon>0 \tag{D.22}$$

$$\nu_{1}>0\;\;\nu_{2}>0 \tag{D.23}$$

$$h(x)=\;\nu_{1}-\nu_{2} \tag{D.24}$$

$$\upsilon-h^{0}(x)+\beta+\tau-\left(\nu_{1}\mu_{\mathrm{EV,up}}-\nu_{2}\mu_{\mathrm{EV,down}}\right)-z>0 \tag{D.25}$$

Here the $\beta,\upsilon,\tau,z,s,\nu_{1},\nu_{2}$ are the auxiliary variables.

E. Appendix: Results

E.1 Person distributions

Table E.1 Person distribution in the settlement

Dwelling	SFH	MFH1	MFH2	MFH3	MFH4	MFH5	MFH6
1	5	1	3	4	2	2	3
2	3	3	2	2	2	3	2
3	1	4	4	2	2	1	4
4	4	2	4	2	3	4	4
5	2	4	2	2	2	4	1
6		1	3	3	3	1	1
7		2	2	4	2	1	2
8		3	2	4	3	1	3
9		3	2	4	2	2	2
10		2	3	3	4	3	3
11		2	1	3	4	4	2
12		4	1	1	1	2	4
13				1	4	4	4
14				1	1	3	3
15				4	3	4	3
16				4	4	4	4

E.2 Heating load

Table E.2 DHW heating energy factor

Type	SFH	MFH
UWH	- 0.000133	0.000013284
UWB	- 0.0000682	0.0000043766
USH	0.000307	0.000004
USB	0.000359	0.000017
SWX	- 0.00021027	- 0.000053029
SSX	0.00014301	- 0.000044121
WWH	0.000073893	0.00002912
WWB	0.000023972	0.000028131
WSH	0.00074399	0.000021202
WSB	0.000398	0.000015

Table E.3 DHW energy demand in kWh per day type

Type	UWH	UWB	USH	USB	SWX	SSX	WWH	WWB	WSH	WSB
SFH	0.65	0.67	0.76	0.77	0.63	0.72	0.70	0.69	0.87	0.78
SFH	1.24	1.30	1.68	1.73	1.16	1.51	1.44	1.39	2.11	1.77
SFH	1.76	1.90	2.75	2.86	1.58	2.38	2.22	2.11	3.73	2.95
SFH	2.21	2.47	3.97	4.18	1.89	3.31	3.03	2.84	5.72	4.33
SFH	2.59	2.99	5.34	5.67	2.11	4.31	3.89	3.57	8.75	5.91
MFH	17.39	16.75	16.75	17.68	16.43	16.43	18.54	18.46	17.96	17.54

Type	UWH	UWB	USH	USB	SWX	SSX	WWH	WWB	WSH	WSB
MFH	23.61	22.47	22.48	24.12	21.91	21.92	25.65	25.52	24.63	23.87
CRE	40.10	37.09	37.09	41.44	35.61	35.62	45.46	45.12	42.78	40.77

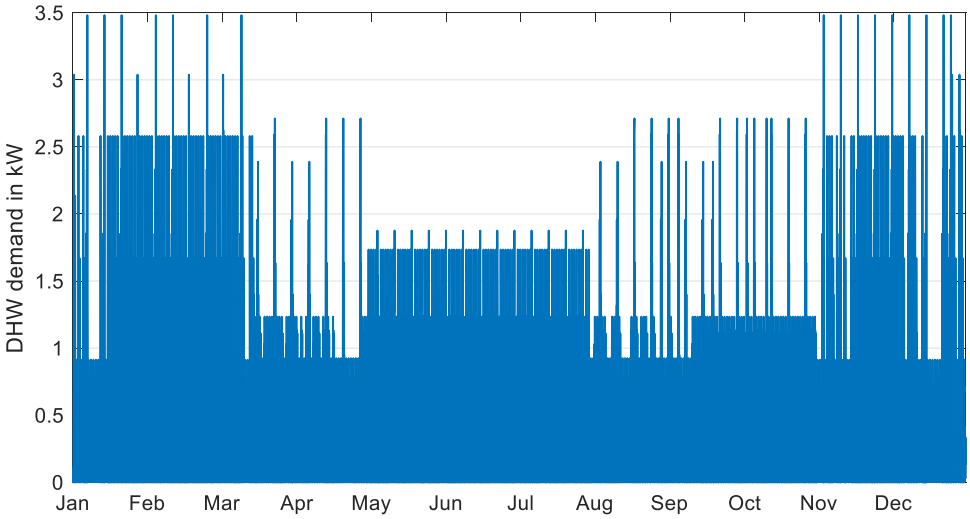

Figure E.1 Yearly DHW heating

E.3 Development in the e-mobility

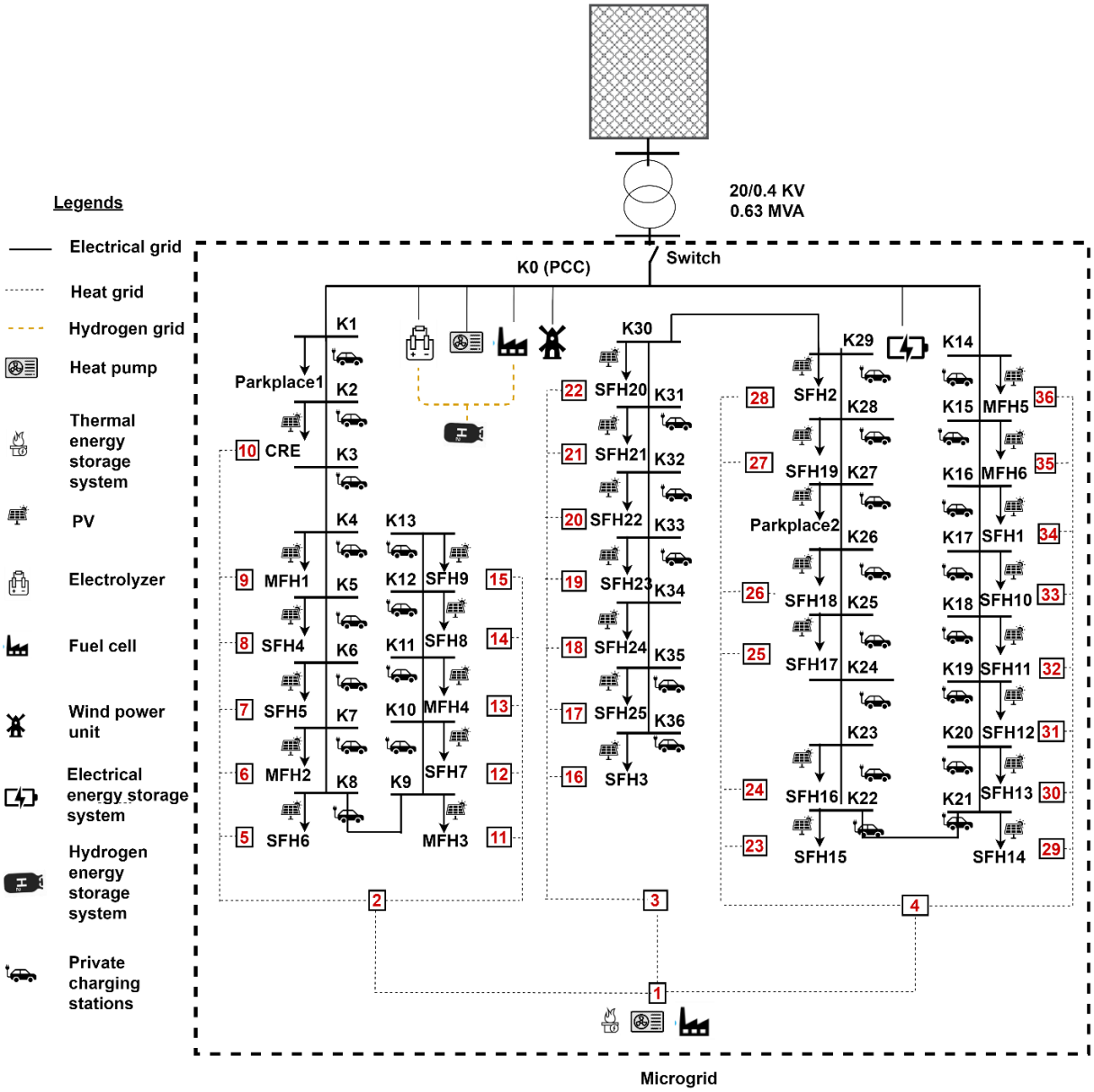

Figure E.2 Microgrid structure with private charging station in trend 2031

Table E.4 Share of EV in the settlement area in percentage

	Negative	Trend	Positve
2022	0.8	0.8	0.8
2023	1.7	1.6	1.6
2024	2.8	3.0	3.2
2025	3.9	4.6	5.3
2026	5.1	6.6	7.9
2027	6.4	9.1	11.2
2028	7.8	11.9	15.4
2029	9.2	15.4	20.7

2030	10.8	19.5	26.7
2031	12.4	24.5	32.7

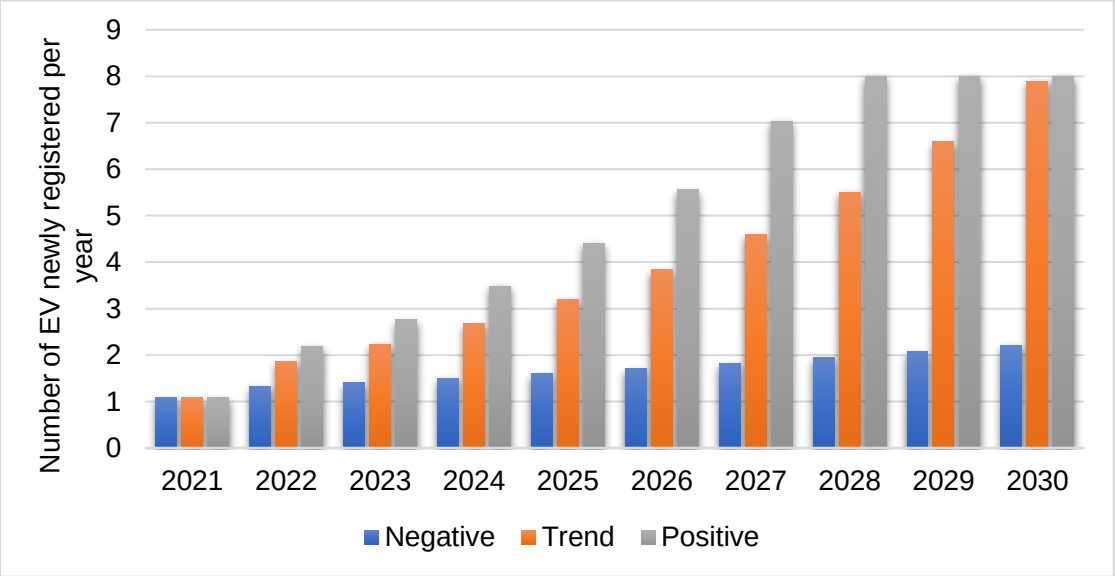

Figure E.3 Number of EVs replacing new registered conventional vehicles per year in the settlement area

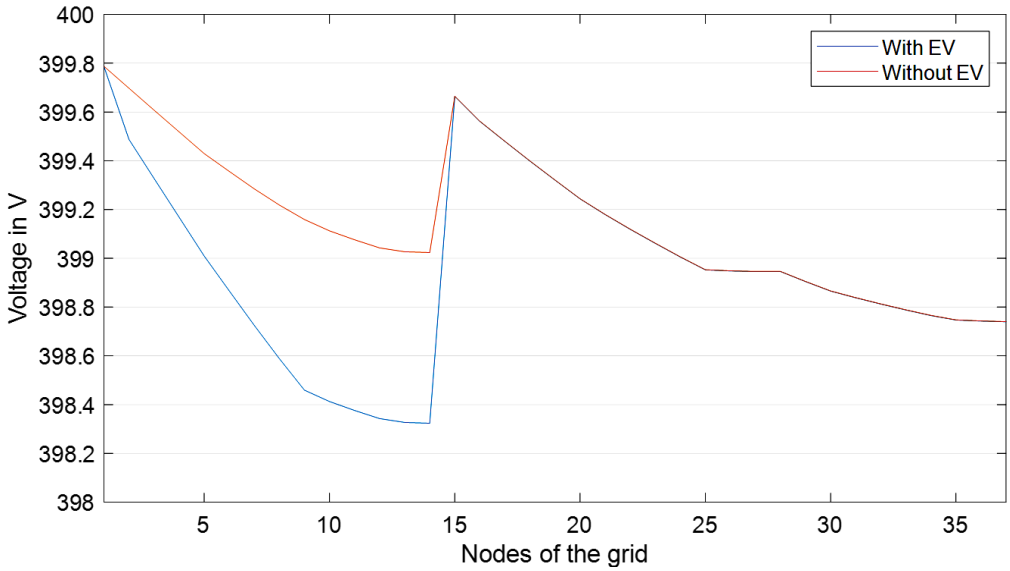

Figure E.4 Impact of a private charging station on string

E.4 Dimension of DERs in the settlement area

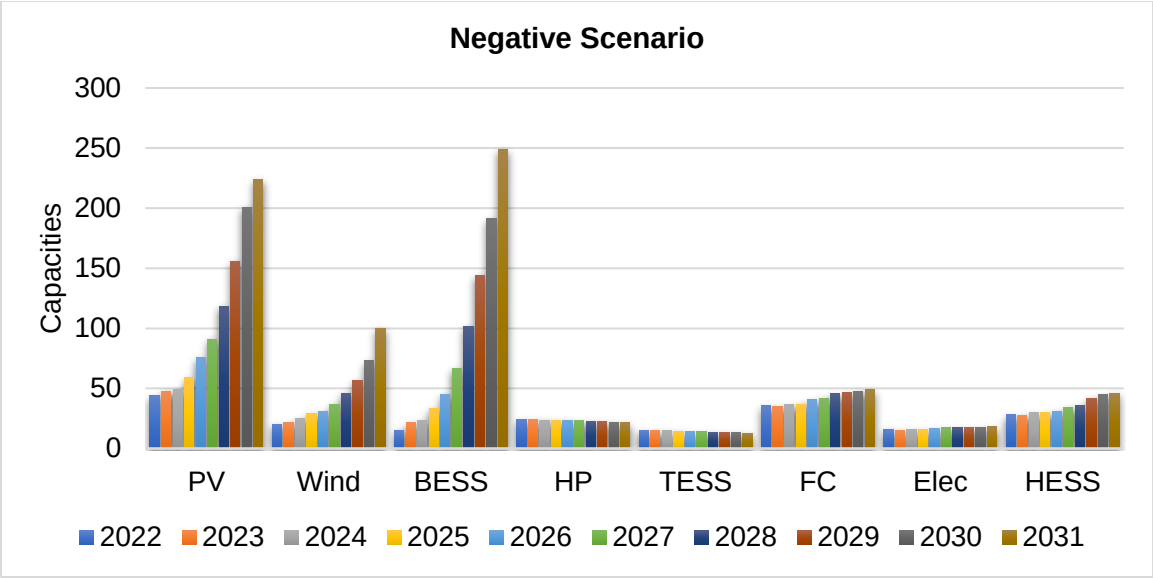

Figure E.5 Capacities of DERs in the negative scenario

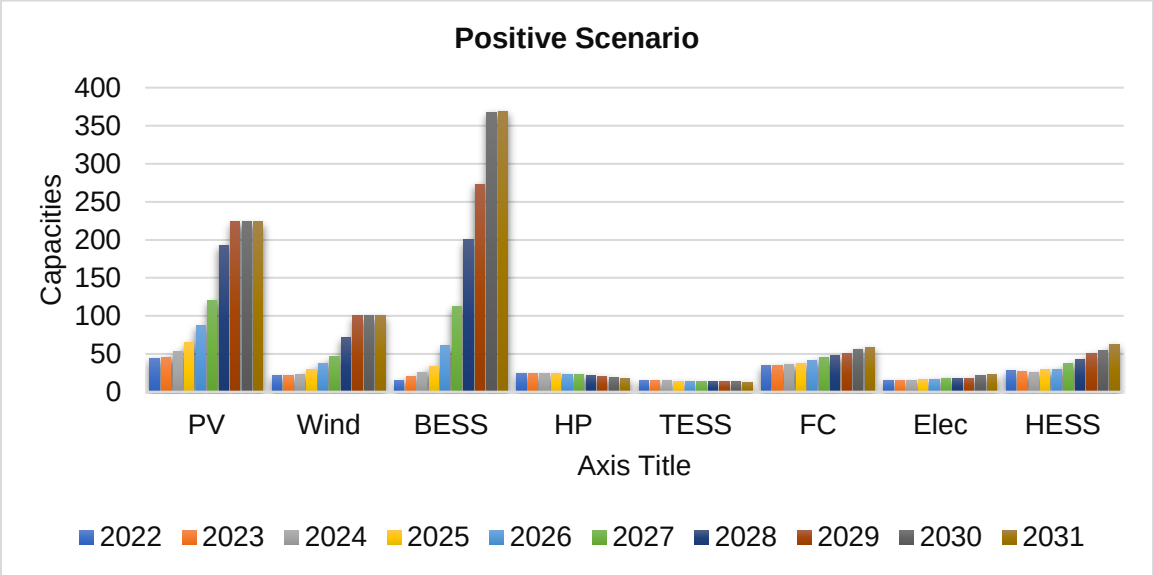

Figure E.6 Capacities of DERs in the positive scenario

E.5 Energy balance in summer

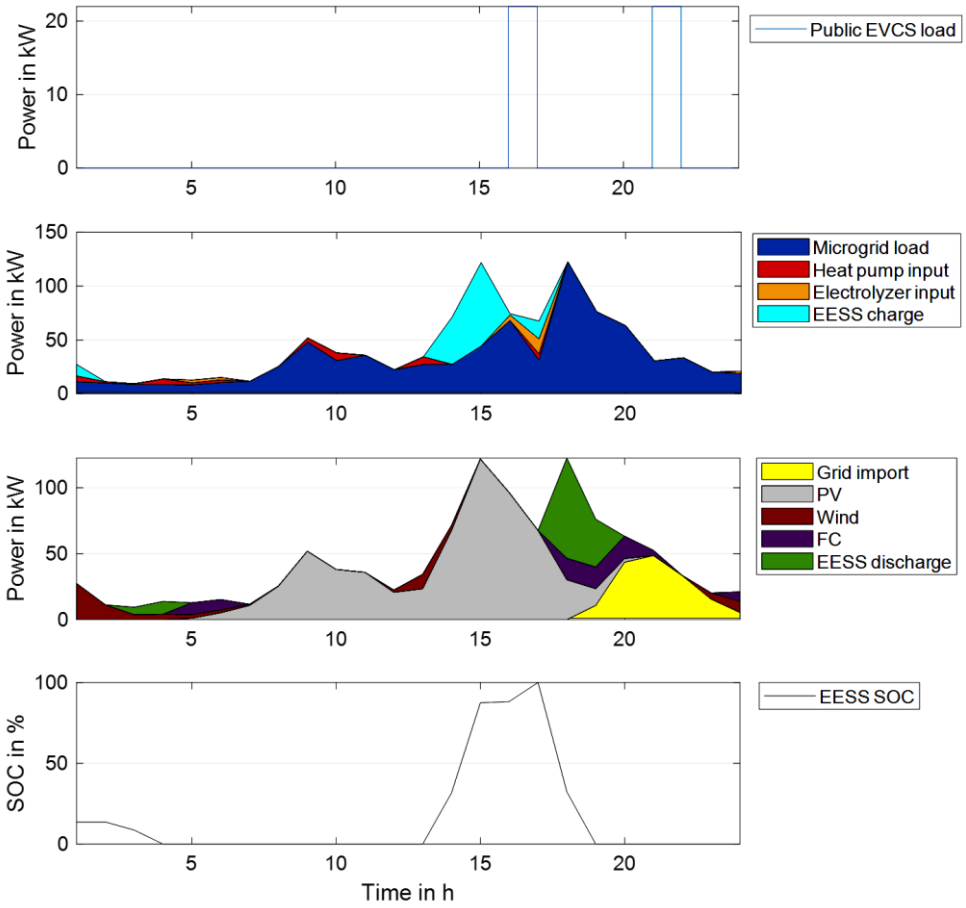

Figure E.7 Electrical energy balance in summer

E.6 Voltage in the settlement area

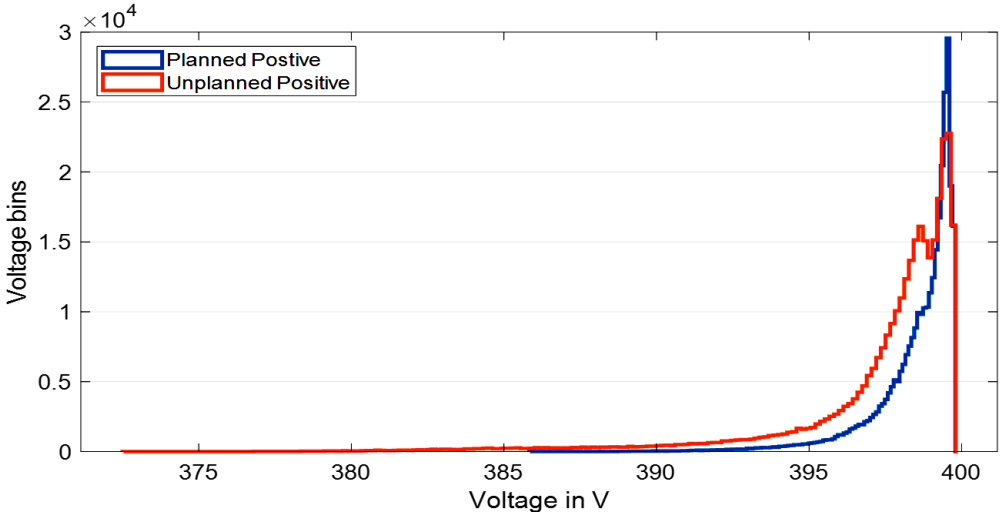

Figure E.8 Voltage distribution in the settlement area in trend 2030

E.7 Heating grid

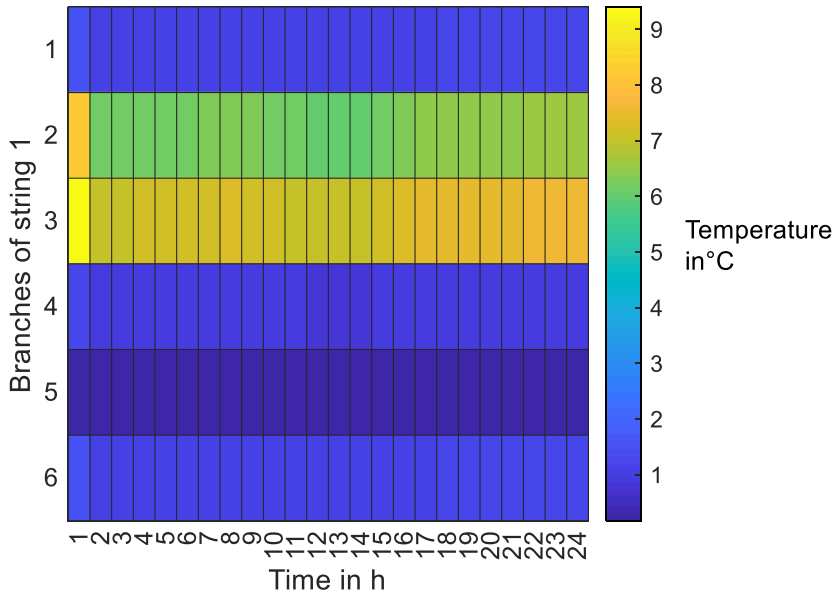

Figure E.9 Heating losses in string 1 of the heat grid

The heating losses are also considered on the mass flow rate. The nodes from 6 to 7 have higher losses because of the low mass flow rate.

E.8 Flexible tariff system

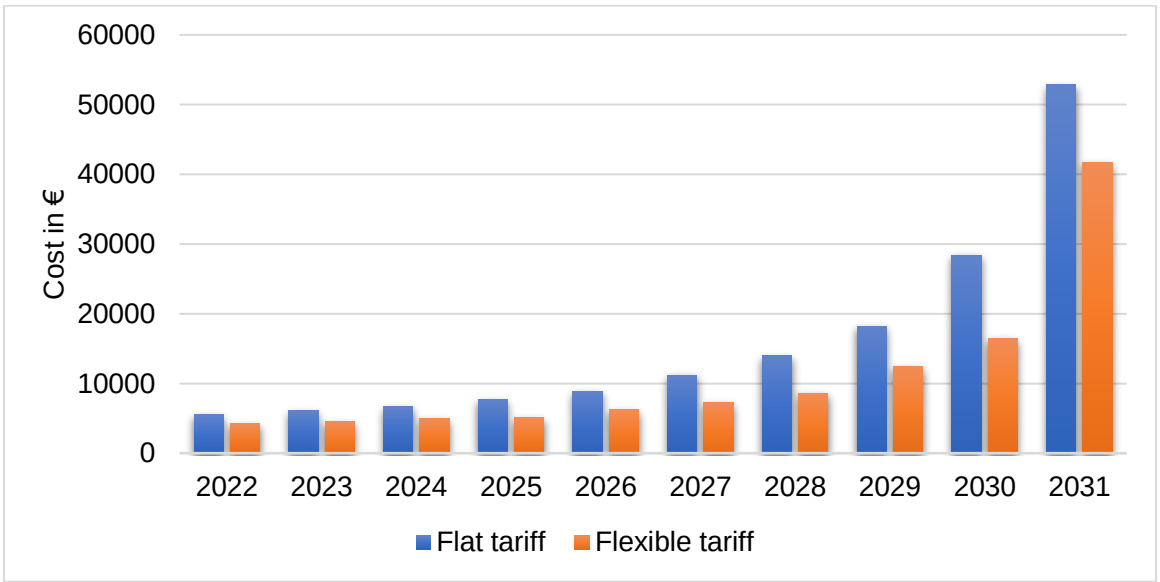

Figure E.10 Operation and CO_2 penalty cost comparison of flat and flexible tariffs

E.9 IGDM-DRO

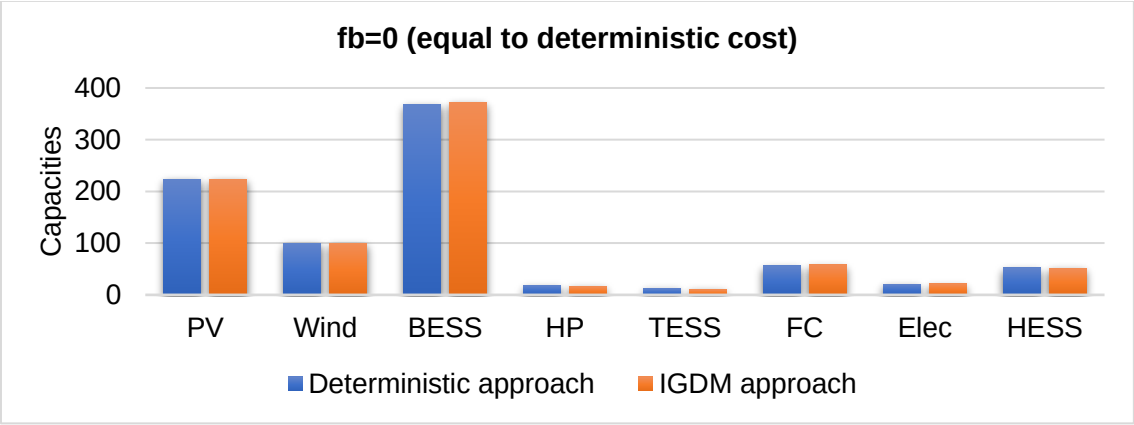

Figure E.11 Deterministic versus IGDM at allowable budget (fb=0)

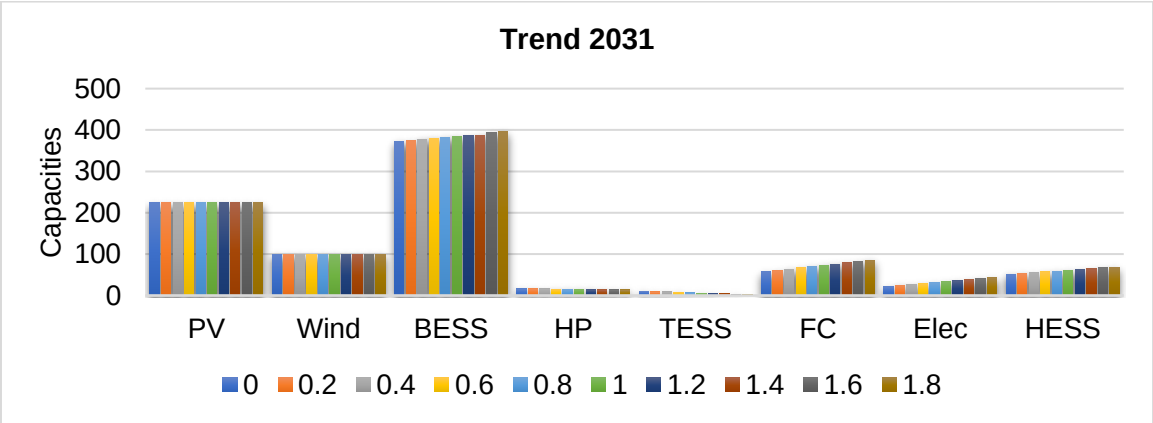

Figure E.12 Capacities of DERs for different allowable budget

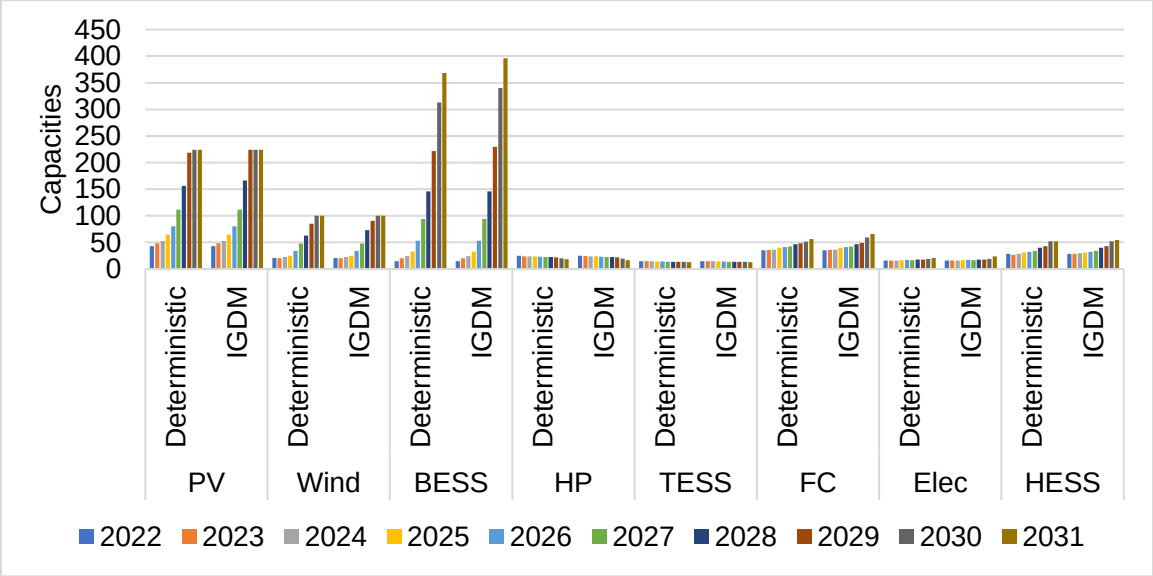

Figure E.13 Capacities comparison between deterministic and IGDM

PUBLISHED MAFO BOOKS

[1] A. Orths: Multikriterielle, optimale Planung von Verteilungsnetzen im liberalisierten Energiemarkt unter Verwendung von Spieltheoretischen Verfahren.
ISBN: 3-929757-57-5, 2003

[2] M. Purmann: Optimierung des Betriebsverhaltens von PEM-Brennstoffzellen unter Berücksichtigung von elektrischem und Gesamtwirkungsgrad bei unterschiedlichen Lastanforderungen und Betriebsparametern. ISBN: 3-929757-63-X, 2003

[3] M. Al-Hamid: Extraktion von höheren Moden TEM-Wellenleitern. ISBN: 3 929757-64-8, 2004

[4] H. Haase, J. Nitsch, T. Steinmetz: Transmission-Line Super Theory – A new Approach to an Effective Calculation of Electromagnetic Interference. ISBN: 3 929757-67-2, 2004

[5] A. Bachry: Power Quality Studies in Distribution Systems Involving Spectral Decomposition. ISBN: 3-929757-68-0, 2004

[6] Z. Styczynski (Editor): Power Network and Renewables – A Scientific Report- (5 Years Research). ISBN: 3-929757-69-9, 2004

[7] E. Blume: Numerische Analyse der Kopplung linearer Antennen innerhalb eines Resonators. ISBN: 3-929757-71-1, 2004

[8] E. Handschin, Z. Styczynski (Editors): Power System Application of the Modern Battery Storage. ISBN: 3-929757-75-3, 2004

[9] H. Haase: Full-Wave Field Interactions of Nonuniform Transmission Lines.
ISBN: 3-929757-78-8, 2005

[10] D. Nitsch: Die Wirkung eingekoppelter ultrabreitbandiger elektromagnetischer Impuls auf komplexe elektronische System. ISBN: 3-929757-79-6, 2005

[11] B. Hadzi-Kostova: Protection Concepts in Distribution Networks with Decentralised Energy Resources. ISBN: 3-929757-84-2, 2005

[12] T. Steinmetz: Ungleichförmige und zufällig geführte Mehrfachleitungen in komplexen, technischen Systemen. ISBN: 3-929757-98-2, 2006

[13] Z. Styczynski, J. Haubrock (Editors): Influence of Distributed and Renewable Generation on Power System Security. ISBN: 3-929757-99-0, 2006

[14] G. Heideck: Ein autonomes Brennstoffzellensystem: Optimierungsansätze.
ISBN: 3-929757-94-X, 2006

[15] Z. Styczynski, H. D. Musikowski (Editors): Dresdener Kreis Elektroenergieversorgung 7. ISBN: 3-929757-85-0, 2006

[16] F. Gronwald: Antenna Theory in Resonating Systems derived from Fundamental Electromagnetism. ISBN: 3-929757-93-1, 2006

[17] G. Krauthäuser: Grundlagen und Anwendungen von Modenverwirbelungs-kammern. ISBN: 978-3-929757-43-9, 2007

[18] C. Dzienis: Ersatzmodelle nichtlinearer Lasten in elektrischen Verteilungs-netzen. ISBN: 978-3-929757-07-1, 2007

[19] Z. Styczynski, J. Haubrock (Editors): Renewable and Dispersed Power Generation in Power Systems. ISBN: 978-3-929757-44-6, 2008

[20] J. Haubrock: Parametrierung elektrischer Äquivalentschaltbilder von PEM Brennstoffzellen. ISBN: 978-3-940961-02-0, 2008

[21] N. Angelov: Rechnergestütztes Lernen im Bereich der Regenerativen Energien (Ausgewählte Aspekte). ISBN: 978-3-940961-03-7, 2008

[22] P. Komarnicki: Anwendung hochgenauer, synchroner Messungen zur Verbesserung des Betriebs von Verteilungsnetzen. ISBN 978-3-940961-04-4, 2008

[23] C. Roggatz: Trainingssimulator für die Führung von elektrischen Systemen mit dezentralen Energieeinspeisungen - Trainingsszenarien und Umsetzung. ISBN: 978-3-940961-05-1, 2008

[24] K. Rudion: Aggregated Modelling of Wind Farms. ISBN: 978-3-940961-14-3, 2008

[25] M. R. Ganjavi: Protection System Coordination Using Expert System. ISBN: 978-3-940961-15-0, 2008

[26] S. Bofinger: Energieversorgungsnetze mit einem hohen Anteil an photovoltaischer Solarenergie: Standortbestimmung, Solarstromprognose, Netzintegration. ISBN: 978-3-940961-25-9, 2008

[27] Z. Styczynski, P. Komarnicki (Editorial Board): Distributed and Renewable Power Generation. ISBN: 978-3-940961-26-6, 2008

[28] S. Kochetov: Time- and frequency-domain modeling of passive interconnection structures in field and circuit analysis. ISBN: 978-3-940961-27-3, 2008

[29] M. Magdowski: Entwicklung und Validierung eines Werkzeugs zur Berechnung der elektromagnetischen Einkopplung von stochastischen Feldern in Leitungs-strukturen. ISBN: 978-940961-28-0, 2008

[30] F. Sonnemann: Elektromagnetische Effekte an elektrischen Zündmitteln (EED) mit angeschlossener Zündkreiselektronik (ZKE) bei impulsförmiger, breit-bandiger Bestrahlung. ISBN: 978-3-940961-32-7, 2009

[31] T. Smieja: Multikriterielle Planung interregionaler Elektrizitätsnetze im liberalisierten Energiemarkt. ISBN: 978-3-940961-35-8, 2009

[32] C. O. Heyde: Dynamic Voltage Security Assessment for On-Line Control Room Application. ISBN: 978-3-940961-40-2, 2010

[33] Z. A. Styczynski, N. I. Voropai (Editors): Renewable Energy Systems Fundamentals, Technologies, Techniques and Economics. ISBN: 978-3-940961-42-6, 2010

[34] Z. A. Styczynski, N. I. Voropai (Editors): Renewable Energy Systems Fundamentals, Technologies, Techniques and Economics. ISBN: 978-3-940961-44-0, (Russian Version), 2010

[35] Z. A. Styczynski, A. Lindemann (Editors): Integration of Renewable Energies into the Grid/ Proc. of the Power&Energy Student Summit 2010. ISBN: 978-3-940961-47-1, 2010

[36] Z. A. Styczynski, H.-D. Musikowski (Editors): Dresdener Kreis Elektroenergieversorgung 11, ISBN: 978-3-940961-51-8, 2010

[37] M. A. Gurbiel: Definition and Testing of a Digital Interface of a Power Substation. ISBN: 978-3-940961-54-9, 2011

[38] P. Lombardi: Multi criteria optimization of an autonomous virtual power plant. ISBN:978-3-940961-55-6, 2011

[39] M. Powalko: Beobachtbarkeit eines elektrischen Verteilungsnetzes. Ein Beitrag zum Smart Grid. ISBN:978-3-940961-62-4, 2011

[40] Z. A. Styczynski, K. Rudion, C. Nguyen-Mau (Editorial Board): Power System Dynamic Security Assessment. ISBN: 978-3-940961-61-7, 2011

[41] M. Käbisch: Optimale Dimensionierung und Betriebsführung einer brennstoffzellenbasierten Auxiliary Power Unit im Fahrzeug. ISBN 978-3-940961-67-9, 2011

[42] Z. A. Styczynski, N. I. Voropai (Editors): Special issue Grant 220 Russian Federation “Smart Grid for Efficient Energy Power System for the Future”, Proceedings Volume I. ISBN: 978-3-940961-74-7, 2012

[43] Z. A. Styczynski, P. Komarnicki, A. Naumann (Editors): Abschlussbericht Harz.ErneuerbareEnergien-mobility. ISBN: 978-3-940961-71-6, 2012

[44] M. Heuer: Diagnosetool für stationär betriebene PEM-Brennstoffzellensysteme. ISBN: 978-3-940961-77-8, 2012

[45] M. Stötzer: Demand Side Integration in elektrischen Verteilnetzen – Potenzialanalyse und Bewertung. ISBN: 978-3-940961-78-5 ,2012

[46] M. Magdowski: Vergleich der Einkopplung deterministischer und statistischer elektromagnetischer Felder in Leitungen. ISBN 978-3-940961-75-4, 2012

[47] A. Naumann: Leitwarte im Smart Grid. ISBN 978-3-940961-81-5, 2012

[48] K. Rudion: Offshore Power System Planning-Selected Aspects. ISBN 978-3-940961-82-2, 2012

[49] C. Nguyen Mau: Electric Power System Stability Enhancement by Voltage Source Converter based High Voltage Direct Current Technology. ISBN 978-3-940961-84-6, 2012

[50] H. Guo: Measurement-based-Load Modeling for Smart Grid Planning. ISBN 978-3-940961-86-0, 2012

[51] Z. A. Styczynski, N. Voropai, V. Stepanov, P. Lombardi (Editors): The power grid of the future. Proceedings No. 2 in the scope of Mega Grant Baikal. ISBN 978-3-940961-95-2, 2013

[52] Z. A. Styczynski, N. Voropai, V. Stepanov, P. Lombardi (Editors): The power grid of the future. Proceedings No. 3 in the scope of Mega Grant Baikal. ISBN: 978-3-940961-98-3, 2013

[53] Christoph Wenge: Optimaler Betrieb von mobilen Speichern im Smart Grid -Mobilitätsleitwarte-. Diss., Otto-von-Guericke-Universität Magdeburg, ISBN: 978-3-944722-01-6, 2014

[54] Christian Röhrig: Smart Distribution Planung unter Berücksichtigung von residualen Lasten. Diss., Otto-von-Guericke-Universität Magdeburg, ISBN: 978-3-944722-06-1, 2014

[55] Felix Middelstädt: Research of SEM Poles of Complex Wire Structures. ISBN: 978- 3-944722-07-8, 2014

[56] Zbigniew A. Styczynski (Editor): Power Network and Renewables - A Scientific Report-15 Years Research. ISBN: 978-3-944722-08-5, 2014

[57] N.N. Solonina, V.S. Stepanov, K.V. Suslov: Information technology in intelligent power networks. Monograph. ISBN: 978-3-944722-13-9, 2014

[58] Rainer Krebs: Fundamentals of Power System Protection. ISBN: 978-3-944722-15-3, 2014

[59] Natalia Moskalenko: Optimal Dynamic Energy Management System in Smart Homes. Diss., Otto-von-Guericke-Universität Magdeburg, ISBN: 978-3-944722-16-0, 2014

[60] Ines Hauer: Optimale Last- und Erzeugungsanpassung bei kritischen Netzzuständen - Algorithmen und deren Bewertung-. Diss., Otto-von-Guericke-Universität Magdeburg, ISBN: 978-3-944722-18-4, 2014

[61] Marc Richter: Dresdner Kreis Elektroenergieversorgung 15. Begleitband zum Workshop 2014. ISBN: 978-3-944722-21-4, 2014

[62] Z. A. Styczynski, A. Richter, P. Kühne (Editors): Second ELECON Workshop. Begleitband zum Workshop 2014. ISBN: 978-3-944722-23-8, 2014

[63] Paul Bernstein: Modellgestützte optimale Betriebsführung von PEM- Brennstoffzellen für autonome Anlagen. Diss., Otto-von-Guericke-Universität Magdeburg, ISBN: 978-3-944722-24-5, 2015

[64] Steffen Rabe: Betrieb einer Zweipunkt-Offshore-HGÜ-Verbindung Modelluntersuchungen. Diss., Otto-von-Guericke-Universität Magdeburg, ISBN: 978-3-944722-31-3, 2015

[65] Bartlomiej Arendarski: Reliability Assessment of Smart Grids. Diss., Otto-von-Guericke-Universität Magdeburg, ISBN: 978-3-944722-32-0, 2015

[66] Xiaofeng Pan: Numerisches EMV-Simulationsverfahren zur Berechnung der Störaussendung elektrischer Antriebssysteme in Hybridfahrzeugen. Diss., Otto-von-Guericke-Universität Magdeburg, ISBN: 978-3-944722-34-4, 2016

[67] Marc Richter: PMU-basierte Zustandsabschätzung in Smart Distribution. Diss., Otto-von-Guericke-Universität Magdeburg, ISBN: 978-3-944722-43-6, 2016

[68] Illia Bielchev: Adaptiver Distanzschutz im Standard IEC 61850. Diss., Otto-von-Guericke-Universität Magdeburg, ISBN: 978-3-944722-45-0, 2016

[69] Ahmed F. H. Hassan: Modeling of Single and Double-Shielded Cables for EMC Applications. Diss., Otto-von-Guericke-Universität Magdeburg, ISBN: 978-944722-41-2, 2016

[70] Xudan Liu: Control of Voltage Source Converter Based High Voltage Direct Current Transmission Systems for Grid Code Compliance. Diss., Otto-von-Guericke-Universität Magdeburg, ISBN: 978-3-944722-46-7, 2016

[71] Markus Kaiser: Fusion of Interventional Ultrasound & X-ray. Diss., Otto-von-Guericke-Universität Magdeburg, ISBN: 978-3-944722-51-1, 2016

[72] Folkhart Grieger: Ein Beitrag zur Bestimmung der Zuverlässigkeit von Leistungshalbleiterbauelementen unter Berücksichtigung der Anwendung. Diss., Otto-von-Guericke-Universität Magdeburg, ISBN: 978-3-944722-52-8, 2016

[73] Mengfei Li: Toward a Robust Electromagnetic Tracking System for Use in Medical Applications. Diss., Otto-von-Guericke-Universität Magdeburg, ISBN: 978-3-944722-66-5, 2018

[74] C. Klabunde, J. Dancker, N. Gast, T. Schröter, F. Schulz, J. Rossberg, A. Richter: Statusbericht der Otto-von-Guericke-Universität Magdeburg zum Verbundprojekt: Intelligentes Multi-Energie-System (SmartMES), ISBN: 987-3-944722-69-6, 2018

[75] Tamara Schröter: 19. Dresdner Kreis Elektroenergieversorgung, Begleitband zum Workshop 2018 in Magdeburg, ISBN: 978-3-944722-79-5

[76] C. Klabunde, J. Dancker, N. Gast, T. Schröter, F. Schulz, J. Rossberg: Intelligentes Multi-Energie-System (SmartMES). Statusbericht der Otto-von-Guericke-Universität Magdeburg zum Verbundprojekt; 2. Statusseminar 04. April 2019 in Magdeburg, ISBN: 987-3-944722-80-1, 2019

[77] S. Helm, J. Dancker, M. Fritsch, T. Schröter: Power and Energy Student Summit 2019, 09.-11. Juli 2019, Otto-von-Guericke-Universität Magdeburg, ISBN: 978-3-944722-84-9, 2019

[78] I. Chychykina: Comparison of Different Redispatch Optimization Strategies. Diss., Otto-von-Guericke-Universität Magdeburg, ISBN: 978-3-944722-89-4, 2019

[79] St. Balischewski: Multifunktionaler Einsatz von Batteriespeichern in elektrischen Verteilnetzen - Optimale Auslegung und Betrieb. Diss., Otto-von-Guericke-Universität Magdeburg, ISBN: 978-3-944722-92-4, 2020,

[80] J. Petzold: Analytische Beschreibung der Kopplung elektromagnetischer Felder durch Aperturen in Resonatoren. Diss., Otto-von-Guericke-Universität Magdeburg, ISBN: 978-3-944722-91-7, 2020

[81] L. Middelstädt: Transiente Effekte in leistungselektronischen Schaltungen mit schnellschaltenden Leistungshalbleitern unter besonderer Berücksichtigung der elektromagnetischen Verträglichkeit. Diss., Otto-von-Guericke-Universität Magdeburg, ISBN: 978-3-944722-95-5, 2020

[82] Y. Liu: Contribution to improve the EMI performance of electrical drive systems in vehicles with special consideration of power semiconductor modules. Diss., Otto-von-Guericke-Universität Magdeburg, ISBN: 978-3-948749-01-9, 2021

[83] A. Gerlach: Regelung von direktangetriebenen elektrischen Maschinen für Verbrennungsmotoren. Diss., Otto-von-Guericke-Universität Magdeburg, ISBN: 978-3-948749-03-3, 2021

[84] Y. Zhang: Analysis and Control of Resonances in HVDC Connected DFIG-Based Offshore Wind Farms. Diss., Otto-von-Guericke-Universität Magdeburg, ISBN: 978-3-948749-05-7, 2021

[85] E. Pannicke: Empfangsspulen für bildgeführte Eingriffe mittels Magnetresonanztomographie. Diss., Otto-von-Guericke-Universität Magdeburg, ISBN: 978-3-948749-12-5, 2021

[86] J. Kasper: Analysis of the Stochastic Electromagnetic Field Coupling to Single and Multiconductor Transmission Line Structures. Diss., Otto-von-Guericke-Universität Magdeburg, ISBN: 978-3-948749-13-2, 2021

[87] Hauer, I: Abschlussbericht zum Projekt InKola: Infrastrukturkopplung – Platzie- rung und Betrieb von Ladestationen aus Verkehrs- und Energienetzsicht, 2022. ISBN 978-3-948749- 15-6

[88] Raya, M: Circuit Models of Shielded Single and Multiconductor Cables for EMC Analyses, 2022. ISBN 978-3-948749-16-3

[89] Pribahsnik, F: GaN-Specific Mechanical Phenomena and Their Influence on Reliability in Power HEMT Operation, 2022. ISBN 978-3-948749-17-0.

[90] Willmann, B: Elektromagnetische Umweltverträglichkeit eines Elektrofahrzeugs mit kontaktlosem Ladesystem, 2022. ISBN 978-3-948749-19-4.

[91] Dancker, J: Sensitivity Factors for Integrated Energy Systems: A Joined Quasi- Steady-State Approach, 2022. ISBN 978-3-948749-24-8.